

**UNIVERSITÀ DEGLI STUDI DI NAPOLI**

**“FEDERICO II”**

FACOLTÀ DI INGEGNERIA



DIPARTIMENTO DI INGEGNERIA CHIMICA, DEI MATERIALI E DELLA PRODUZIONE  
INDUSTRIALE

DOTTORATO DI RICERCA IN

INGEGNERIA DEI MATERIALI E DELLE STRUTTURE

XV CICLO

**SYNTHESIS AND CHARACTERIZATION OF  
HYPERBRANCHED POLYESTERS FOR SPECIAL  
USES**

**Tutor:**

Ch.mo Prof. Cosimo Carfagna

Dott.ssa Veronica Ambroggi

**Candidata:**

Dott.ssa Laura Ascione

TRIENNIO 2010-2013

*A mia madre*

---

**Table of Contents**

Abstract	1
Chapter 1 - Hyperbranched (HB) polymers: synthesis, architecture, characterization and applications	4
1.1 Introduction	4
1.2 Classification of branched polymers	5
1.2.1 Regularly branched polymers	5
1.2.2 Statistically branched polymers	6
1.3 Synthesis of HB polymers: general aspects and methodologies	8
1.3.1 Step-growth approaches	8
$AB_x$ and $AB_x + B_y$	8
$A_2 + B_y$ and related approaches	9
1.3.2 Chain-growth approaches	10
Self-condensing vinyl polymerization (SCVP)	10
Ring-opening multi-branching polymerization (ROMBP)	11
Transfer concepts and other chain-growth mechanisms	11
1.3.3 Other synthetic approaches	12
1.4 Architectures with diluted branching and linear-hyperbranched hybrids	12
1.4.1 Copolymers	13
1.4.2 Dendrigraft and arborescent graft polymers, hyper-Macs	13
1.4.3 Linear-hyperbranched hybrid structures	13
Star-hyperbranched core structures	14
Linear-hyperbranched block copolymers	14
1.4.4 Core-shell structures, nanocapsules, self-assembly	14
1.5 Characterization of HB polymers	15
1.5.1 Structural characterization	16
Degree of branching (DB)	16
Branching ratio	17
Intermolecular hydrogen bonding	18
1.5.2 Solution characterization	19
Molar mass and molar mass distribution	19
1.5.3 Bulk characterization	21

## Table of Contents

---

Thermal properties	21
Melt rheology	22
1.6 Applications of HB polymers	23
References	25
Chapter 2 - Synthesis and characterization of HB polyesters	30
2.1 Introduction	30
2.2 Experimental section	31
2.2.1 Materials for HB polyesters synthesis	31
2.2.2 Synthesis of polyesters	32
Synthesis of linear telechelic PBA	32
Synthesis of linear-hyperbranched hybrid PBA copolymers	32
2.2.3 Characterization	35
Nuclear magnetic resonance spectroscopy (NMR)	35
Size exclusion chromatography (SEC)	35
Matrix-assisted laser desorption/ionization mass spectrometry (MALDI-TOF MS)	36
SEC/MALDI-TOF analysis	36
Thermogravimetric analysis (TGA)	37
Differential scanning calorimetry (DSC)	37
Wide angle X-ray diffraction (WAXD)	38
2.3 PBA and HB characterization: results and discussion	38
2.3.1 Synthesis and characterization of linear telechelic PBA	38
2.3.2 Linear-hyperbranched hybrid PBA copolymers (HB)	41
2.3.3 Nuclear magnetic resonance spectroscopy (NMR)	43
2.3.4 MALDI-TOF MS	46
2.3.5 SEC/MALDI-TOF characterization	56
2.3.6 Thermogravimetric analysis (TGA)	62
2.3.7 Differential scanning calorimetry (DSC)	64
2.3.8 Wide angle X-ray diffraction (WAXD)	69
References	72



---

Chapter 3 - HB polyesters as low migration plasticizers in flexible PVC	75
3.1 Introduction	75
3.2 Experimental section	77
3.2.1 Materials for PVC-based blends	77
3.2.2 Synthesis of HB polyester	78
3.2.3 Preparation of PVC-based blends	78
3.2.4 Characterization	79
Thermogravimetric analysis (TGA)	79
Wide angle X-ray diffraction (WAXD)	79
Dynamic mechanical thermal analysis (DMTA)	79
Mechanical properties	79
Migration tests	80
3.3 PVC-based blends characterization: results and discussion	81
3.3.1 Thermogravimetric analysis (TGA)	81
3.3.2 Wide angle X-ray diffraction (WAXD)	83
3.3.3 Dynamic mechanical thermal analysis (DMTA)	84
3.3.4 Mechanical properties	86
3.3.5 Migration tests	87
References	90
Chapter 4 - HB polyesters as toughening agents in epoxy resin	91
4.1 Introduction	91
4.2 Experimental section	92
4.2.1 Materials for epoxy resin-based blends	92
4.2.2 Synthesis of HB polyester	93
4.2.3 Preparation of epoxy resin-based blends	93
4.2.4 Characterization	94
Attenuated total reflectance spectroscopy (ATR)	94
Thermogravimetric analysis (TGA)	94
Differential scanning calorimetry (DSC)	94
Rheological characterization	94
Dynamic mechanical thermal analysis (DMTA)	95
Fracture toughness measurements	95
Morphological observation	96
	III

## Table of Contents

---

4.3	Epoxy resin-based blends characterization: results and discussion	96
4.3.1	Attenuated total reflectance spectroscopy (ATR)	96
4.3.2	Thermogravimetric analysis (TGA)	99
4.3.3	Differential scanning calorimetry (DSC)	100
4.3.4	Rheological characterization	102
4.3.5	Dynamic mechanical thermal analysis (DMTA)	105
4.3.6	Fracture toughness measurements	107
4.3.7	Morphological observations	109
	References	114
	Chapter 5 - HB polyesters in biomedical applications	116
5.1	Introduction	116
5.2	Experimental section	118
5.2.1	Materials for ART blends	118
5.2.2	Synthesis of HB polyesters	119
5.2.3	Preparation of ART blends	119
5.2.4	Characterization	120
	Attenuated total reflectance spectroscopy (ATR)	120
	Nuclear magnetic resonance spectroscopy (NMR)	120
	Thermogravimetric analysis (TGA)	120
	Differential scanning calorimetry (DSC)	120
	Wide angle X-ray diffraction (WAXD)	121
5.3	ART blends characterization: results and discussion	121
5.3.1	Attenuated total reflectance spectroscopy (ATR)	121
5.3.2	Nuclear magnetic resonance spectrometry (NMR)	124
5.3.3	Thermogravimetric analysis (TGA)	125
5.3.4	Differential scanning calorimetry (DSC)	127
5.3.5	Wide angle X-ray diffraction (WAXD)	129
5.3.6	Skin contact simulation	130
	References	133
	Chapter 6 - Conclusions	135
	List of Abbreviations	144

List of Equations	146
List of Figures	148
List of Tables	152
List of Schemes	154

---

**Abstract**

*“Life is branched”* was the motto of a special issue of Macromolecular Chemistry and Physics on “Branched Polymers”, indicating that branching is of similar importance in the world of synthetic macromolecules as it is in nature.

Dendrimers have been considered as perfect “nano-objects” with a great control on size and functionality, which is of high interest in nanotechnology and biomedicine. Hyperbranched (HB) polymers, instead, are a special type of dendritic polymers and have as a common feature a very high branching density with the potential of branching in each repeating unit. They are usually prepared in a one-pot synthesis, which limits the control on molar mass and branching accuracy and leads to “heterogeneous” products with a distribution in molar mass and branching. This distinguishes HB polymers from perfectly branched and monodisperse dendrimers. In the last 20 years, both classes of dendritic polymers, dendrimers as well as HB polymers, have attracted major attention because of their interesting properties resulting from the branched architecture as well as the high number of functional groups. HB polymers, however, were considered as products suitable for larger-scale application in typical polymer fields like coatings and resins, where a perfect structure is sacrificed for an easy and affordable synthetic route. More recently, unconventional synthetic methods have been adopted also for HB polymers and related structures.

This work is focus on the synthetic approaches used to prepare highly branched polymers, giving special attention to the new trends to dilute the branching with linear polymer chains by creating increasingly complex linear-branched hybrid structures. The irregular branched structure in HB polymers and highly branched derivatives leads also to significant and new challenges in the application of these materials.

Linear–hyperbranched hybrid polyesters were synthesized through a branching reaction between the tailored linear poly(butylene adipate) (PBA) pre-polymer ended with methyl ester groups and different molar percent (mol %) of 1,1,1-tris(hydroxy methyl)propane (TMP) used as branching agent. The progress of reaction was followed by  $^1\text{H}$  and solid-state  $^{13}\text{C}$ -NMR and MALDI-TOF mass spectrometry (MALDI-TOF MS) tools, to obtain reliable knowledge about structure and chemical composition of either telechelic PBA pre-polymer and final HB products, as a function of experimental parameters, such as time, temperature, and monomers molar ratio. The structure-to-thermal relationship was investigated through thermogravimetric analysis (TGA) and differential scanning

calorimetry (DSC) and put in connection with the degree of crystallization determined by wide angle X-ray diffraction (WAXD) analysis.

Thanks to a more complex architecture and compact structures, the absence of chain entanglements, and a large number of functional end-groups, in the recent years a growing interest has been shown for HB polymers as substitute of phthalate plasticizers (i.e., dioctyl phthalate, DOP) for flexible polyvinyl chloride, PVC. One of the major problem related to the use of low molecular weight plasticizers in flexible PVC compound is their migration from the plasticized material toward environment with consequent hardening of the artifact and undesired toxic effect when used in medical, food packaging and child care applications. We have investigated on the possibility to obtain tailored HB polymers characterized by highly branched structure diluted with linear polymer chains, as low migration polymeric plasticizers for flexible PVC compound.

Recently, HB polymers have been proposed as toughening agent for epoxy resin thanks to their compact structure and lack of restrictive inter-chain entanglements which result in low melt viscosities, even at high molecular weight. The high density of functional end-groups on HB polymers surface offers the potential for tailoring their compatibility with the epoxy resin through conversion of HB end-groups to chemically suitable moieties to form *in-situ* covalent bounds. As a result, HB polymers are promising candidates for modifying thermosets toughening properties with minimal decrease in processability, without affecting the thermal stability and storage modulus. We have investigated on the possibility to obtain tailored HB polyesters characterized by irregular and highly branched structure, with an external shell densely functionalized able to improve the miscibility and the interface adhesion with the epoxy matrix. The toughening effect produced by HB systems could be correlated to their intra-molecular defects, which give them the possibility to interpenetrate the epoxy network, absorbing much more energy while impacting.

In the last years, HB polymers are widely used as drug delivery systems in biomedical applications. The drugs are attached to HB structure through non-covalent bonding or are entrapped inside the nano-cavities of their complex architecture. These drug delivery systems offer several advantages, such as enhancing the aqueous solubility and bioavailability of drugs, prolonging the circulation time, inducing the preferential accumulation at the tumor sites through the enhanced permeability and retention effect, and reducing the systemic side effects. Since the discovery of the antimalarial properties of artemisinin (ART), much effort has been made to investigate the structure-activity

relationship in this molecule. Although ART has shown excellent permeability across the intestinal mucosa, it has low bioavailability due to poor aqueous solubility, which may lead to incomplete clearance of the malaria parasite, resulting in recurrence of malarial symptoms. Besides, ART is extensively metabolized by the liver, but oral bioavailability is low (32%). Transdermal drug delivery systems (TDDS) facilitates the passage of therapeutic drug substances through the skin into the general circulation, where they can have systemic effects, thus bypassing the hepatic first-pass effect. One of the major problem of ART is its crystallinity, which causes a reduction of solubility through the stratum corneum. To prevent the re-crystallization during the storage process, we have thought to use tailored HB systems as inhibitors or anti-nucleating agents. In fact, combining the drug with an amorphous or less crystalline polymer can change the degree of crystallinity and the polymorphic form of ART. As a result, it is possible to obtain less crystalline or more amorphous drug particles with enhanced solubility and increased bioavailability.

# Chapter 1

## Hyperbranched (HB) polymers: synthesis, architecture, characterization and applications

### 1.1 Introduction

The significance of branched macromolecules has evolved over the last 30 years from just being considered as a side reaction in polymerization or as a precursor step in the formation of networks. The concept of “polymer architectures” was very important for the change in the perception of branching, leading to new star- and graft-branched structures in the 1980s and then in the early 1990s to dendrimers and dendritic polymers. Today a very important aspect in the design of macromolecules and functional material is considered the possibility of controlling the branching.<sup>1</sup>

Dendrimers have been considered as perfect “nano-objects” with perfectly size and functionality, which is of high interest in nanotechnology and biomedicine. Hyperbranched (HB) polymers are a special type of dendritic polymers with high branching density with the potential of branching in each repeating unit. They are usually prepared in a one-pot synthesis, which limits the control on molar mass and branching accuracy and leads to “heterogeneous” products with a distribution in molar mass and branching. These peculiarities distinguish HB polymers from perfectly branched and mono-disperse dendrimers. In the last 20 years, both classes of dendritic polymers, dendrimers as well as HB polymers, have attracted major attention because of their interesting properties resulting from the branched architecture as well as the high number of functional groups,<sup>2</sup> where a perfect structure is sacrificed for an easy and affordable synthetic route.

In the last years, the major interest of researches was focalized on new trends to dilute the branching with linear polymer chains by creating increasingly complex linear-branched hybrid structures. The irregular branched structure in HB polymers and highly branched derivatives leads also to significant and new challenges in the characterization of these materials.

## 1.2 Classification of branched polymers

Polymers are traditionally classified, according to their macromolecular chain architecture, into three categories: linear, cross-linked and branched polymers. Further classification of branched macromolecules is very complex, because modern synthesis methods have enabled numerous different branching structures. Additionally, any unit on a linear chain is a potential branching point for another chain, which can also branch further more or less regularly. Therefore, it is possible to make difference between regularly and statistically branched polymers.<sup>3</sup>

### 1.2.1 Regularly branched polymers

There are three types of regularly branched polymers:

- *regular star polymers*, which contain three or more linear chains (arms) emanating from a single branch point (Figure 1.1). Arms of one star polymer can have identical constitution and degree of polymerization (uniform star polymers) or different monomeric units and different lengths (non-uniform star polymers). Because of their specific structure, the properties of star polymers deviate considerably from those of linear polymers.

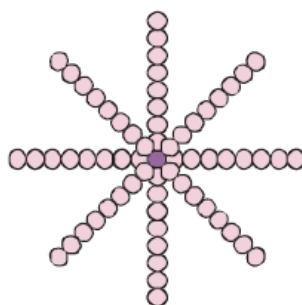


Figure 1.1: Regular star polymer.

- *regular comb polymers*, which consist of a linear flexible chain of known length (backbone) with multiple tri-functional branch points from each of which (uniformly or randomly) a linear side chain emanates (Figure 1.2). If the side chains are much shorter than the backbone, structure of comb polymer resembles a linear chain. On the other hand, if the backbone is shorter than the grafted long side chains, structure will approach the behavior of star molecules.



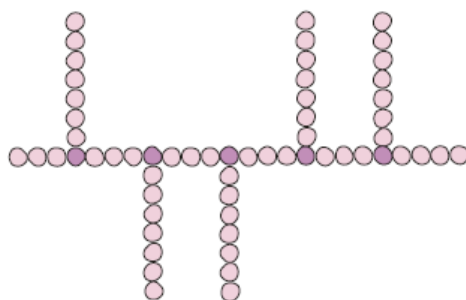


Figure 1.2: Regular comb polymer.

- *dendrimers* (from Greek, dendron = tree) are well-defined, regularly branched macromolecules comprised of  $AB_x$  type ( $x \geq 2$ ) monomers attached in concentric layers around a central  $B_y$  core (Figure 1.3). Each layer is called generation (G), where all B functional groups have reacted with A functional groups from the next layer. Unreacted B functional groups can be found at the surface of the molecule (last generation). Dendrimers possess highly branched, three-dimensional architecture, with a perfect symmetrical globular shape, and therefore, different properties from those of linear polymers of the same molar mass.

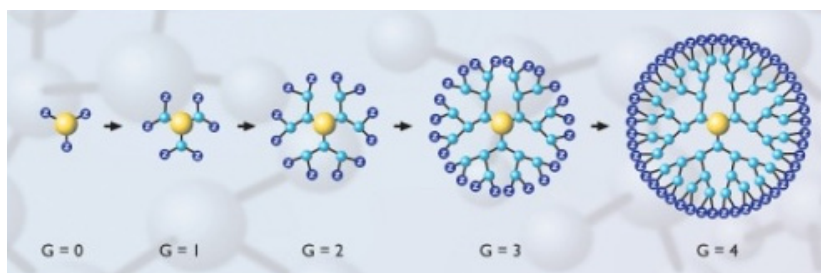


Figure 1.3: Dendrimer growth.

## 1.2.2 Statistically branched polymers

When regularity of branching is not the aim of the synthesis, statistically branched polymers can be obtained by simple mixing of multifunctional monomers in adequate reaction without any constraints. These kinds of polymers are in fact randomly branched systems, among whose it is supposed that reactivity of all functional groups is the same, and that the reaction between functional groups belonging to the same macromolecule is neglected (ring formation). Randomly branched systems can be studied by theories of random statistics, also known as the mean field theory, which is based on the extent of reaction,  $\alpha_A$ , defined by Flory<sup>4</sup> as:

$$\alpha_A = \frac{[A_t]}{[A_0]} \quad (1.1)$$

where  $[A_t]$  is the number of reacted functional groups and  $[A_0]$  is the number of all functional groups, while subscripts  $t$  and  $0$  denote the time of reaction and the starting time of reaction, respectively. Thus, the extent of reaction is actually a probability of reaction. However, randomly branched polymers represent an idealized model, since no real system is fully random. Particularly important influence in this case has the presence of excluded volume, because individual monomer units can approach each other only up to their diameter. Excluded volume can cause swelling of the branched structures and provoke the change in expected architectures.

On the other side, HB polymers represent a special group of branched structures, for which the mean field theory can be used. They are formed from  $AB_x$  monomers (like dendrimers), where only groups A can react with one of the B groups from another monomer unit to give bond AB. In principle, HB polymers have narrower molar mass distributions compared to randomly branched products. In contrast to dendrimers, HB polymers can have a certain number of unreacted B groups in their inner layers of molecules, which are therefore usually called pseudo generations (Figure 1.4). The reason for this is, that the extent of reaction  $\alpha_A$  of the A groups can have values from 0 to 1, while the extent of reaction  $\alpha_B$ , of the equally reactive B groups, cannot become larger than  $\alpha_B = \alpha_A/(x-1)$ . As a consequence of this, gelation can never occur, while a much higher branching density than by random polycondensation can be achieved. Although HB polymers are polydisperse and have less perfect globular shape than dendrimers, their properties are quite similar to dendrimers.

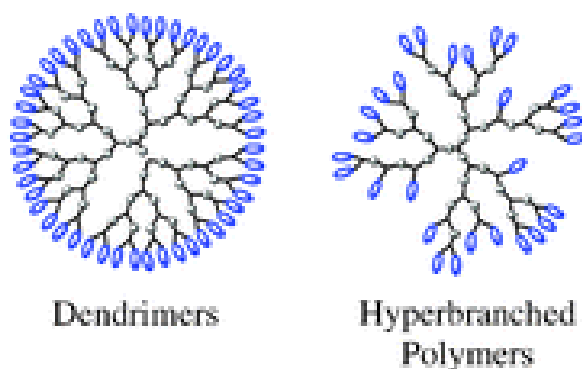


Figure 1.4: Difference between dendrimer and HB structures.

## 1.3 Synthesis of HB polymers: general aspects and methodologies

In the last 20 years,<sup>5,6</sup> very strong synthetic activity emerged on macromolecules that can be classified as “hyperbranched”.<sup>6</sup> This term now not only covers the “classical” products based on Flory’s  $AB_x$  approach<sup>4</sup> but is extended to various highly branched structures including those prepared by the  $A_2 + B_y$  monomer combination;<sup>4,7,8,9,10</sup> those prepared by self-condensing vinyl polymerization (SCVP),<sup>11</sup> or self-condensing ring-opening polymerization (SCROP), or proton transfer polymerization,<sup>12-15</sup> and those prepared by various co-polymerizations and methodology combinations including self-assembly aspects, which lead to linear-highly branched hybrids like dendronized polymers,<sup>16-18</sup> dendrigrafts,<sup>19-21</sup> and HB core star-branched structures<sup>22-23</sup> and nanocapsules.<sup>19,24</sup>

### 1.3.1 Step-growth approaches

#### $AB_x$ and $AB_x + B_y$

In the classical approach toward HB polymers, which goes back to Flory’s<sup>4</sup> early description as a special type of polycondensation,  $AB_x$  monomers with equal reactivity of the B functionalities are reacted (Figure 1.5). The reaction involves the typical features of a step-growth reaction of multifunctional monomers and the formed oligomers but without the possibility of cross-linking. The use of  $AB_2$  monomers dominates the synthetic approaches, leading to a very broad structural variety in HB products.

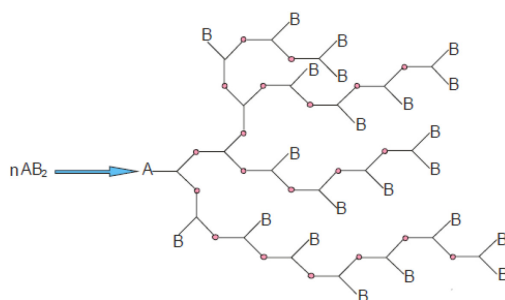
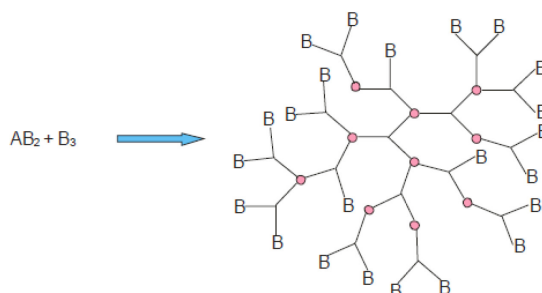


Figure 1.5: HB synthetic route (with focal unit, A) through polymerization of  $AB_2$  monomers.

For successful synthesis of classical HB polymers from  $AB_x$  monomers, the following requirements have to be fulfilled: A must react selectively with B without side reactions, the B functionalities must have equal reactivity, and there should be no internal cyclization reactions that limit the achievable molar mass. It was found that the occurrence of

cyclization reactions depends strongly on the monomer structure,<sup>25</sup> and their presence was first reported by Percec et al.<sup>26</sup> for liquid crystalline polyethers. Besides cyclization reactions, also other side-reactions can occur, e.g., ether formation during polyester synthesis,<sup>27</sup> which can lead to cross-linking since in this case B functions react with other B functions, occurring in an increasing of degree of branching (DB). These examples demonstrate that Flory's<sup>4</sup> theory of an equal reactivity of the B functions and absence of side-reactions might not be met in all synthetic examples.

Early on, the addition of a “core” molecule  $B_x$  ( $x \geq 2$ ) was explored (Figure 1.6), mainly for better control over molar mass but also for control of the resulting geometrical shape.<sup>28</sup> When a core molecule is used, the resulting products should no longer exhibit the focal unit A. This limits the molar mass buildup, and thus, the molar mass is controlled by the ratio  $AB_x$  to  $B_x$ .



**Figure 1.6: HB synthetic route (without focal unit) through copolymerization of  $AB_2$  monomers with  $B_3$  core molecule.**

### **$A_2 + B_y$ and related approaches**

The  $A_2 + B_y$  approach differs strongly from the classical  $AB_2$  approach, where gelation can never be reached under the Flory prerequisites, and actually, it has been questioned whether the resulting products can be termed as “hyperbranched”. Highly branched structures similar to HB materials are usually reached on the way toward networks just before the critical conversion (gel point) is reached. The growth and structure as well as the property profile of the  $A_2 + B_y$  products are not fully comparable to that of  $AB_x$  polymers.<sup>29</sup> This classical network formation approach, where  $A_2$  monomers are combined with  $B_y$ , has been known for a long time and has high technical relevance with a broad portfolio of suitable structures.<sup>4</sup> Gelation theories apply also for  $A_2 + B_y$  systems,<sup>30</sup> but early on, for practical considerations, the critical molar ratio of A/B groups was defined as the limiting molar ratio at which gelation took place at full conversion of the minority groups. Below this molar ratio or at lower conversion, the gel point could not be reached

and only soluble branched polymers were formed.<sup>31</sup> However, the gel formation in these condensations is dependent on many factors, e.g., the ratio of functionalities, monomer concentrations, purity of solvent and reagents, reaction time and temperature, and others,<sup>29</sup> and therefore, it is very difficult to fully control the reaction and to obtain HB polymers with high molar mass without the need for separation of the sol from the resulting gel fraction. For achieving reasonable molar masses as well as avoiding premature gelation, a functionality ratio A/B of 2:3 with functionality conversion below 87% provides generally favorable reaction conditions.<sup>4,32</sup> If a functionality ratio A/B of 1:2 is chosen, the system resembles an AB<sub>2</sub> approach with no danger of cross-linking. The structural variety of these systems is higher, since more variations regarding linear and branched units exist and certainly, the resulting polymer structures contain B as well as A functions in a significant amount, which depends on the ratio of A<sub>2</sub> to B<sub>y</sub> in the monomer mixture.<sup>29</sup>

### 1.3.2 Chain-growth approaches

The use of chain-growth mechanisms in the preparation of highly branched polymers has rapidly increased since self-condensing vinyl polymerization (SCVP) was initially reported by Freché et al.<sup>11</sup> in 1995 for the synthesis of HB polymers.

Chain-growth mechanisms are employed in SCVP, in self-condensing ring-opening polymerization (SCROP), also known as ring-opening multi-branching polymerization (ROMBP), or in proton transfer polymerizations,<sup>15</sup> as well as various copolymerizations.<sup>13</sup>

#### Self-condensing vinyl polymerization (SCVP)

SCVP is based on a vinyl monomer that additionally bears an initiating group (inimer = initiator + monomer<sup>33</sup>). These monomers allow propagation through the double bond (= chain growth) and addition of the initiating site to the double bond (= step growth) and thus lead to HB polymers in a one-pot reaction with possible branching in each repeating unit and, thus, with the potential to reach a degree of branching of 50% (Figure 1.7).

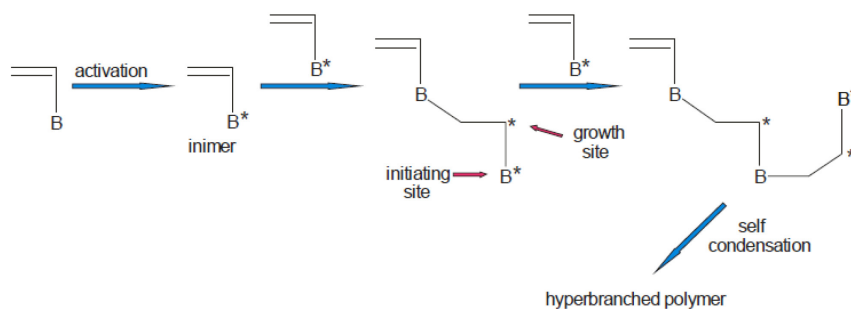


Figure 1.7: Mechanism of SCVP.

A general feature of SCVP is the unequal reactivity between chain growth of the vinyl group and step growth through the initiating site. Therefore, the DB can differ strongly from the value 50% of the random AB<sub>2</sub> condensation and depends on the reactivity ratio of the A\* or B\* end-groups. The danger of side-reactions (elimination, radical coupling) limits also the use of controlled radical processes. At longer reaction times, in particular, gel fractions cannot be avoided.

Often in SCVP it is not possible to determine the DB directly via NMR analysis. Therefore, indirect methods, e.g., viscosity measurements and light-scattering methods selective toward the more globular structure of a HB polymer, have to be used to indicate the branched architecture. The polydispersity is usually very high and represents the presumably non-living character of the reaction. However, the big advantage is the extension of the concept of HB polymers to vinyl monomers and chain-growth processes, which opens unexpected possibilities for new materials.

SCVP can readily be carried out as a copolymerization with conventional monomers, which is an easy way to prepare highly branched and high molar mass polymer architectures.<sup>13,34</sup> In the copolymerization, the molar mass distribution is reduced compared to the inimer homopolymerization, and the degree of branching can be adjusted to the desired property profiles.

### **Ring-opening multi-branching polymerization (ROMBP)**

ROMBP differs from SCVP in the fact that instead of a vinyl group a heterocyclic group is used as the monomer part of the inimer. In addition, whereas in SCVP usually irreversible reactions are involved, in ROMBP also reversible preconditions generally have to be considered. The ROMBP approaches have their origin in classical ring-opening reaction mechanism (ROP) toward linear polymers, especially polyethers and polyesters.

Interestingly, the molar mass still increases exponentially with conversion as observed for the classical HB polycondensations.<sup>30</sup> The authors stated that the polymerization mechanism is much more complicated than that of a classical polycondensation, especially due to the increased possibility of intramolecular cyclization, a problem which was addressed generally for all HB polymers by Dušek et al.<sup>25</sup>

### **Transfer concepts and other chain-growth mechanisms**

Various chain-transfer concepts have also been employed for the synthesis of HB polymers. One is the use of so-called “iniferter”, monomers which contain a chain-transfer

group like methacrylate and styrene derivatives with thiocarbamate groups<sup>35</sup> or a dithioester group.<sup>36</sup> Controlled transfer reactions are also the reason why soluble polymers are obtained in the free radical polymerization of monomers in the presence of cross-linkers (bi-functional monomers like bismethacrylates). Here, large amounts of chain-transfer agents are added to avoid gelation, but the resulting products exhibit extremely broad molar mass distributions and very multimodal size exclusion chromatography (SEC) traces and the transfer agents, e.g., alkanethiols, are incorporated into the macromolecules as end-groups.<sup>37</sup>

### 1.3.3 Other synthetic approaches

The above-described synthetic approaches cover most general methods to prepare HB or related highly branched structures. However, in order to further increase the structural variety and complexity of the designed macromolecular structures, increasingly, combinations of highly branched structures with linear units are described that lead to linear-dendritic block-copolymers, dendronized polymers, HB-core-star structures, dendri-grafts, and further complex architectures. Copolymerization of AB monomers with AB<sub>x</sub> monomers was described as early as by Flory<sup>30</sup> and has been used for commercial products,<sup>7</sup> but intentional “dilution” of the branching in HB polymers and the design of complex architectures are newer aspects of this concept.

## 1.4 Architectures with diluted branching and linear-hyperbranched hybrids

One drawback of “classical” HB polymers with branching sites in each repeating unit is the high branching density that prevents the formation of entanglements in the bulk material, and therefore, structural applications of plain HB polymers are not possible due to high brittleness and poor mechanical properties. In addition, the structural variety is limited since, in the one-pot AB<sub>x</sub> approach, only one polymerization type can be employed. Therefore, early in the development of HB polymers, the reduction of the DB and the branching density has been explored by various approaches, which led to a broad variety of linear-hyperbranched hybrids.<sup>38</sup>

### 1.4.1 Copolymers

Branching can be diluted easily by mixing  $AB_x$  monomers with AB monomers as it has been done in a few cases for the  $AB_x$  approach,<sup>5,39</sup> and which is rather standard in the area of SCVP leading to the broad field of self-condensing vinyl copolymerization (SCVCP).<sup>13</sup> As already outlined, Long et al.<sup>39</sup> discussed in detail how the long-chain branching induced into linear polyesters by adding branching units influences the material properties. When the linear chains between the chains are long enough, the good mechanical properties of linear polymers can be combined with enhanced solubility, lowered solution viscosity, and enhanced processing possibilities.

This method permits the combination of the positive properties of the linear polymers with improved melt and solution processing of HB polymers. In addition, very high molar mass branched products can be prepared that can be considered as nano-globules.

Branching is also diluted by increasing the distance between the branching points using oligomeric or polymeric branched starting material of  $AB_x$ <sup>40</sup> as well as in the  $A_2 + B_y$  approach<sup>41</sup> or by just using  $AB_x$  monomers of different molar masses and size.<sup>42</sup> This approach can also be considered a special case of arborescent polymers, which is classified as a macromonomer approach and which will be addressed below.

### 1.4.2 Dendrigrraft and arborescent graft polymers, hyper-Macs

Besides the regular dendrimers and HB polymers, a new class of dendritic polymers has emerged whose branching points are linked to each other by true polymeric chains. Different names appear in the literature describing those structures like com-burst polymers,<sup>19</sup> arborescent graft polymers,<sup>20</sup> dendrigrrafts,<sup>20</sup> polymers with dendritic branching,<sup>43</sup> and hyper-Macs.<sup>44</sup> These materials are generally obtained by combination of controlled polymerization techniques with selective branching reactions. A rapid increase in molar mass and in size is characteristic of the formation of the successive generations of these highly branched polymers.<sup>45</sup>

### 1.4.3 Linear-hyperbranched hybrid structures

The combination of linear chains and dendritic architectures was extensively studied early on for perfectly branched dendrons leading to complex architectures, e.g., dendron-linear block-copolymers<sup>46</sup> and dendronized or monodendron jacketed linear polymers,<sup>47-48</sup> and to star-polymers<sup>49</sup> with a dendritic core. Especially the attachment of monodendrons to a



linear polymer chain by post-modification or by polymerization of monodendron-containing macromonomers has attracted much attention due to the visualization of these stiffened polymer chains as single nanoscopic macromolecules by atomic force microscopy (AFM).<sup>47-48</sup>

### **Star-hyperbranched core structures**

Star-HB core structures leading to core-shell type materials. The preparation of more complex architectures using HB macromolecules, however, is a more recent trend. The field of star polymers with a HB core has been an area of particular interest.<sup>22,50</sup> Free radical, controlled radical, ring-opening, anionic, and cationic polymerizations have been applied using HB macro-initiators. The resulting polymers show typical behavior of star polymers, e.g., low solution viscosities nearly independent from molar mass. By combination of suitable core/arm combinations, structures with amphiphilic properties can be obtained.

### **Linear-hyperbranched block copolymers**

In comparison to the perfectly branched dendritic structures, where often dendrons are combined with linear polymer chains either as end “groups” (AB or ABA block-copolymers, nicely reviewed recently by Gitsov<sup>51</sup> and also Cho<sup>52</sup>) or in dendronized polymers,<sup>51</sup> only a few examples exist so far on linear-hyperbranched block-copolymer structures. The main reason for that is that the less controlled synthetic approaches toward HB structures easily can lead to undesired side reactions in block-copolymer formation, which reduces the control of the structure and can result in mixtures of products.

#### **1.4.4 Core-shell structures, nanocapsules, self-assembly**

As already indicated, polymer star-like architectures with HB cores can exhibit core-shell type topography, often with an amphiphilic character that allows consideration of these macromolecules as nanocontainers.<sup>24,53</sup>

A core-shell-like architecture can be achieved by considering the HB starting part as core and the grafted arms as shell provided that core and shell are immiscible and show different polarity character. Self-assembly can also be used to create even larger structures from preformed HB macromolecules. On the other hand, HB structures can also be further modified or functionalized through non-covalent interactions. By this process, e.g., a new

class of crystalline inclusion complexes of a multi-arm HB polyether combined with various cyclodextrins was successfully prepared.<sup>54</sup>

Compared to other materials used for functional nano-materials, like perfectly branched dendritic building blocks or well-defined amphiphilic block-copolymers, self-assembly concepts in combination with the irregular HB structures are still rarely and only very recently explored. Nevertheless, the first examples reported to date demonstrate well that this class of materials holds high promise.

## 1.5 Characterization of HB polymers

The enormous synthetic development in the field of HB polymers in the last two decades is based on the fact that these compounds possess new, particular characteristics that strongly influence material properties and open new application fields.<sup>7,38,55,56</sup> Therefore, simultaneously to the synthetic progress, strong efforts have been made to characterize, understand, and theoretically describe the properties of the HB polymers in order to obtain reliable knowledge about their structure-property relationships.

Considerable progress on the fundamental structure-property relationships in HB polymers has been achieved since the theoretical predictions made in the middle of the 20<sup>th</sup> century concerning polymers from  $AB_x$  monomers.<sup>4,30</sup> The increased availability of a wide variety of HB polymers, on the one hand, has enabled the verification of Flory's predictions but, on the other hand, has also revealed deviations in real systems from the assumptions that had been made by Flory for ideal  $AB_x$  systems. In addition, the complex branched HB polymer structures have presented an enormous challenge for full structure characterization and have shown limitations of current techniques.

On the basis of many detailed studies, we certainly have enhanced our knowledge about the characteristics of HB  $AB_x$  type as well as  $A_2 + B_y$  polymers, branched structures achieved by SCVP, and, in general, of different highly branched polymer architectures. All this work shows that HB polymers are very complex structures with multidimensional, broad distributions, e.g., in molar mass, DB, or chemical structure. An overview of the different methods for their structural, thermal, solution, and bulk characterization will be given and their potentials and limits will be discussed. Most of the analysis of the HB polymers is based on the property correlation to linear structures or to 100% branched molecules, in order to understand the differences and thus, the influence of the randomly branched architecture on the characteristics of these macromolecules.

## 1.5.1 Structural characterization

The imperfection of the structure of HB polymers originates from the fact that beside fully reacted (dendritic) and unreacted (terminal) units, HB polymers have also some linear units in their molecular structure. As can be seen from the Figure 1.8, in dendritic units all B groups have reacted, linear units have one unreacted B group, while terminal units possess two unreacted B groups. Linear segments in the structure of HB polymers are usually described as defects and their presence has big influence on physical properties of these macromolecules, such as glass temperature, melting point, crystallinity, etc.

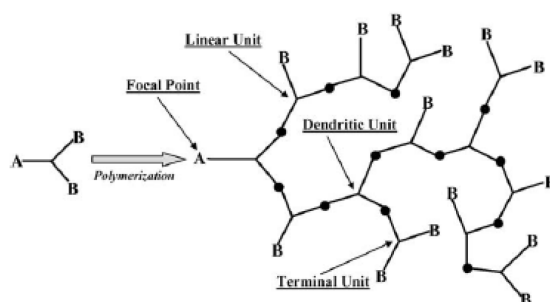


Figure 1.8: Different type of units in HB polymers.

### Degree of branching (DB)

The DB is one of the most important parameters of HB polymers, because of the fact that it is directly correlating with the density of the polymer structure and the number and location of the end-groups. In contrast to perfectly branched dendrimers, which possess only dendritic and terminal units, the HB polymers incorporate additionally linear units. To define and better understand structure of HB polymers, Fréchet and co-workers<sup>57</sup> introduced the average degree of branching,  $DB_{Fréchet}$ , for the HB polymers formed in the polycondensation of AB<sub>2</sub> monomers, which can be calculated from the Equation 1.2:

$$DB_{Fréchet} = \frac{D+T}{D+L+T} \quad (1.2)$$

where  $D$ ,  $T$  and  $L$  represent the numbers of dendritic, terminal and linear units, respectively. The core of the molecule is not counted as a unit because it is not taken into account. DB for the perfect dendrimers should be 1, for the linear structures 0 and consequently, DB for the HB polymers is between 0 and 1. However, according to the Fréchet definition, linear polymers based on AB<sub>2</sub> monomers would have  $DB > 0$ , because of the presence of terminal groups. Fréchet's definition of DB has one disadvantage; he did not consider the presence of unreacted monomer, which can bring to overestimate the DB.

In fact, this definition can indeed accurately describe DB for products with higher polymerization degrees, where the number of the dendritic units is approximating the number of the terminal units, but in the low molar mass region, another equation suggested by Frey et al.<sup>58</sup> and Yan et al.<sup>59</sup> is more suitable for the calculation of the DB:

$$DB_{Frey} = \frac{2D}{2D+L} \quad (1.3)$$

In this definition, the active number of growth directions for the polymer chain is compared to the maximum number of growth directions.

Most HB polymers, formed by the polymerization of AB<sub>2</sub> monomers or by copolymerization of the core molecule B<sub>y</sub> with AB<sub>2</sub> monomers, have a DB close to the 0.5, or in ideal case 0.5, when the reactivity of all functional groups is the same.

Experimentally DB can be calculated from <sup>13</sup>C-NMR spectra by comparing the integrals of the different units (D, T and L) in the HB polymer. Another method that can be used to calculate DB is the modification of end-groups and thence fully degradation of HB skeleton by hydrolysis.<sup>60</sup> Using capillary chromatography, degradation products can be identified. However, DB cannot give the full picture about the topology of HB polymers. One of the reasons for this is the possibility of forming isomeric structures due to the random adding of monomers during the polymerization.

### Branching ratio

Another alternative parameter that can be used to describe the molecular architecture of HB polymers is the branching ratio or “shrinking” factor (*g*) which can be calculated in the following manners:<sup>39</sup>

$$g = \frac{\langle R_g^2 \rangle_{branched}}{\langle R_g^2 \rangle_{linear}} \quad \text{or} \quad g' = \frac{[\eta]_{branched}}{[\eta]_{linear}} \quad (1.4)$$

where  $\langle R_g^2 \rangle_{branched}$  and  $\langle R_g^2 \rangle_{linear}$  represent the mean-square radius of gyration and  $[\eta]_{branched}$  and  $[\eta]_{linear}$  the limiting viscosity number of the given HB polymer and its linear analogue, respectively.

Theoretical as well as experimental investigations have been carried out in order to obtain a quantitative relationship between both contraction factors:

$$g' \approx g^b \quad (1.5)$$

Stockmeyer predicted theoretically  $b = 1.5$  for branched polymers according to the universal law.<sup>61</sup> Zimm<sup>62</sup> found that, for certain branching topologies,  $b$  should be 0.5. Empirically there were different values found for this parameter, lying between 0.5 and 1.5 for long-chain branched and star polymers. For HB polymers, however,  $b$  is strongly deviating from this regime. These strong deviations can be explained only by the non-constant draining factor for branched polymers, with strong dependence on  $g$ <sup>63</sup> due to varying compactness and interaction with the solvent, respectively. Different compactness of the molecules without solvent interactions can clearly be seen in the aromatic and in the aliphatic molecules. On the one hand, this is an effect of the size of the monomers defining the distance between the branching points; on the other hand, the rather stiff structure and steric hindrance do not allow the aliphatic-aromatic macromolecule to take a more compact shape. Interactions with a good solvent do not further influence the rather open structure even at higher molar masses. The opposite case was observed for the aliphatic polyester: interactions with a good solvent are leading to a more open molecular structure compared to the model in the solvent-free state as an effect of better flexibility, even though in total the branching point distance is much shorter and the macromolecules appear more compact. Hence, changes in molar mass may change the shape in solution of these HB polyesters. In other words, the chemical character of the polymer units, as well as end-groups, indeed plays an important role in the solution properties of the HB polymers and cannot be excluded when searching for explanations for their unusual solution behavior. However, the structure of HB polymers in solution is still not completely understood. It can be only concluded that they have more globular shape than analogue linear polymers. There are so many different parameters that have big influence on the structure of HB polymers, like the effect of monomer size on the molecule density or the influence of the nature of solvent.

### **Intermolecular hydrogen bonding**

Hydrogen bonding is a well-known phenomenon that plays a key role in biochemistry, defining the interactions of polar structures like proteins, nucleic acids, or polysaccharides. H-bonds have considerable importance in the area of synthetic polymers as well, since they can strongly influence solubility, crystallinity, rheology, blend formation, and, in general, processing of polymer mixtures. Because of the fact that HB polymers can possess a very large number of polar functional groups, they have a strong tendency to form H-bonds with neighboring molecules, solvent, water, or interactive surfaces.

Theoretically, the  $T_g$  should be reduced with increasing branching degree. However, the opposite effect was found,<sup>39</sup> increasing  $T_g$  with increasing degree of branching. The only possible explanation for this trend was the formation of an H-bond network, which becomes stronger with the increase in the number of end-groups and the degree of branching, respectively.

Thus, hydrogen bond formation in HB polymers with polar end-groups strongly influences properties like solubility, glass transition temperature, and, of course, melt rheology. From the practical point of view, one should also notice that an often observed strongly reduced solubility in HB polyesters or polyamides after heating (drying) might be the result of the formation of a strong hydrogen bond network and not necessarily that of the formation of a chemical network.

## 1.5.2 Solution characterization

### Molar mass and molar mass distribution

It is important to know the average molar mass and the molar mass distribution of polymers, because these parameters have a big influence on physical properties, processing behavior of polymers and consequently, on their application areas. By controlling both, molar mass and molar mass distribution, properties like melt viscosity, solubility, mechanical and thermal behavior can be regulated.<sup>64</sup> Depending on which method is used for measurements, the number average molar mass,  $M_n$ , or the weight average molar mass,  $M_w$ , can be obtained. The ratio between these two molar mass averages is called polydispersity index ( $PDI = M_w/M_n$ ) and can give more information about the breadth of the molar mass range in a polymer sample.

Discussing molar masses and molar mass distributions for HB polymers, first one has to note that the determination of the absolute molar mass of HB polymers is not a trivial task. Because of their densely branched structure, their overall molecular density is increased compared to their linear analogues in a good solvent, and the well-known method for the determination of the full molar mass distribution of polymers, size-exclusion chromatography (SEC) with differential refractive index detection (DRI) or UV-detection and subsequent calibration with a linear polymer standard, can lead to strong deviations from the actual values of molar mass. A comprehensive comparison between different interpretations of the SEC chromatograms of HB poly(etheramide) using polystyrene and poly(ethylene oxide) as a calibration standard, as well as the method of the universal

calibration,<sup>65</sup> has been carried out in order to find the best adequate method for processing the SEC results.<sup>66</sup> The comparison was made on the basis of the molar masses obtained by SEC coupled to DRI and static light-scattering detector (MALLS, multi-angle laser light scattering), the combination of which is known to give absolute molar mass values also for complex macromolecular architectures. The deviations between the values obtained by these three methods are extremely high.

However, at this point, we have to critically consider the benefits and limits of both, mostly applied absolute methods for molar mass characterization in dendritic systems, static light scattering and Matrix-assisted laser desorption/ionization time-of-flight mass spectrometry (MALDI-TOF MS). Static light scattering alone leads to reliable information about the weight-average molar mass of HB polymers, in the case that no aggregates are formed in the solution.<sup>67</sup> However, this information is not enough with respect to the broad polydispersities of HB polymers. In order to achieve complete information about the molar mass distribution of a HB polymer sample, the combination of SEC-DRI-MALLS is essential. The determination by MALLS of the lower molar mass region requires high contrast of the polymer solution to the solvent, i.e., a high refractive index increment,  $dn/dc$ , or high concentration, but the concentration used in SEC is limited. Even if these conditions are fulfilled, reliable MALLS molar mass determination is restricted to the high molar mass area. In order to overcome these problems, special interpretation methods could be applied for complete analysis of the molar masses.<sup>68</sup>

MALDI-TOF-MS is a powerful method for detection of molar masses of monodisperse samples. A limitation is due to the fact that, in broadly distributed samples, the lower molar mass species are preferably activated for desorption and, hence, the higher molar masses are not detectable or their intensity is so low that they are ignored. Therefore information about the complete polydispersity of the HB sample cannot be achieved. In order to apply this method for HB polymers, it is again reasonable first to separate the polymer in nearly monodisperse fractions and afterward to measure them using MALDI-TOF MS.<sup>69,70</sup> An additional advantage of MALDI-TOF MS is the access to information about specific structural properties. Nevertheless, this technique is limited not only to samples or fractions with low polydispersities but also in general to low molar mass polymers, which can be successfully detected quantitatively. For the purpose of analyzing high molar mass HB polymers, MALLS is definitely the better choice.

The usual way to conduct separation of polymers, SEC, is based on the well-balanced interactions between column material, solvent, and sample. In order to achieve complete



separation according to size and to determine reliable polydispersity values, interactions between sample and column material have to be excluded. This is not always possible in the case of HB polymers. As multifunctional materials, interactions with column material are guaranteed. It has been repeatedly observed that this problem is exacerbated for higher molar mass products. The explanation for this phenomenon cannot simply be that the absolute number of end groups per macromolecule increases with the molar mass since the molar amount of end groups in the sample keeps constant. The most reasonable explanation is an interplay between end group interactions and the change in molecular shape with molar. Several methods are employed to reduce these troublesome interactions, e.g., changing the solvent or the column material, or adding salts to the eluent.<sup>66,67</sup> However, these actions are often ineffective when it comes to multifunctional materials. A solution has been found for the separation of complex functional polymers using a column-free method the asymmetric flow field flow fractionation (A4F). This recently commercialized technique separates the molecules according to their size in a channel with a membrane using the forces of an eluent cross-flow.<sup>71,72</sup> Interactions with the channel material (regenerated cellulose) do not affect the analysis, and the only limitation is coming from the membrane, which is porous for molecules with molar mass lower than  $\sim 5\,000$  g/mol.

### 1.5.3 Bulk characterization

#### Thermal properties

The thermal properties of polymers like melting point and glass transition temperature are strongly influenced by branching. Usually branching reduces the crystallization ability, and the branching topology and length significantly determine the extent of this effect. HB polymers are usually formed by very short and dense branches, which completely prevent crystallization. There are only a couple of examples where crystallization has been observed either due to modification with long chains<sup>73</sup> or due to branching dilution,<sup>39</sup> where the length of the linear parts is sufficient for formation of crystalline domains and a very broad melting peak can be observed after characterization with differential scanning calorimetry (DSC). Another exception is the tendency of some HB polymers to assemble into liquid crystalline structures.<sup>74</sup> Glass transition temperature ( $T_g$ ) depends on the mobility of the polymer backbone, which in turn is sterically or chemically defined. In addition, the free volume of the molecules, which is reflected by the  $T_g$ , depends on the



end group interactions. From the topological point of view,  $T_g$  is decreasing with branching degree and branching density, due to limitations in the molecular mobility.

Nevertheless, direct comparison of linear, HB, and dendritic aromatic polyesters having identical repeating unit chemistry and number and nature of functional groups showed practically identical glass transition temperatures.<sup>75</sup> On the other hand, random copolymerization of two different  $AB_2$  monomers leading to pure HB structures were compared to linear random copolymers of similar chemical character and showed identical tendencies of  $T_g$  in complete agreement with the Fox equation.<sup>76</sup> This fact shows that the chemical character of the backbone is the primary consideration for  $T_g$ , and the branching topology plays a secondary role.<sup>77</sup>

The end-group effect on  $T_g$  in HB systems is very strong as well. In cases where the increasing number of polar end-groups can lead to strong interactions between the molecules with increasing DB, the opposite behavior has been observed as in the case of gradually branched polyesters by copolymerization of  $AB_2$  and AB monomers. For this type of polymer, H-bonding interactions have been confirmed by Fourier transform infrared (FTIR) measurements, and these strongly increase with increasing DB and end-group number. Amplification of the H-bonds effect on  $T_g$  could stem from the increasing flexibility of the backbone at higher contents of AB units in the polymer structure.

Longer linear parts in HB polymers are suspected to play the role of a plasticizer,<sup>73</sup> with strong decrease in  $T_g$  value and an additional melting peak due to linear chain length.

In summary, the effect of the dendritic branching on the glass transition cannot be explained simply by the particular branching topology, but it is defined by the combination of the monomer chemical character and the number and type of functional groups in the polymer and depends certainly on the combination of linear and branched units in one macromolecule.

## **Melt rheology**

One of the major advantages of HB polymers is their rheological behavior in the melt, which differs strongly from that of linear polymers and is extremely useful in applications, e.g., modifying the processing properties of linear polymers.<sup>78</sup> In order to take advantage of HB polymers for these applications, fundamental knowledge about the effect of the architecture on the rheological and processing properties is needed. And indeed, a number of experimental rheology investigations on HB polymers have been carried out showing strong deviations<sup>79</sup> from the theories developed for linear and star or HB-shaped polymers,

which have been the subject of theoretical and experimental investigations for several decades.<sup>80</sup> These deviations can be explained by the very high DB and the dense branching topology, which make it difficult for the HB molecules to entangle. For this reason, HB polymers should exhibit the properties of non-entangled macromolecules,<sup>81,82</sup> reflecting the behavior of Newtonian fluids, where the degree of branching, topology, and especially end groups have a strong influence on the rheology.

For the OH-terminated polymer, non-entangled elastic behavior can be observed, while typical behavior for a viscous melt with a plateau at low frequencies after 100% modification of the end-groups with C12 alkyl chains was found. These results are supported by the analysis of the complex modulus of both polymers.  $G'$  and  $G''$  for the OH-terminated polyester are completely identical even in the low-frequency region, showing equal viscous and elastic components. For C12-modified HB polymer, a strong reduction of both moduli has been observed and the relation between them corresponds to an increased viscous behavior.

The effect of end-groups is also related to the above-discussed tendency to formation of hydrogen bonds, which has been investigated in the work of McKee et al.<sup>83</sup>

## 1.6 Applications of HB polymers

HB polymers have received much industrial attention and have been commercialized for several applications or are presently in the advanced development stage. Their specific structure gives the possibility to use them in a large variety of industrial and medical areas. The commercial success of HB polymers is a result of the highly branched and dense but irregular structure that leads to excellent solubility, compared to linear polymers, low solution viscosity, modified melt rheology, and high level of terminal end group functionality.<sup>8,38,84,85</sup> HB polymers are mostly used in high solid or powder coatings, because of their low viscosity and high functionality and solubility,<sup>86</sup> which enables them to be used also as multifunctional cross-linkers.<sup>87,88</sup> Other potential applications include using these highly branched and highly functional polymers as polymer additives for improving the thermal stability and reducing the melt viscosity in linear polymers (i.e. as rheology modifiers for processing),<sup>89,90</sup> reducing the melt flow instabilities in film blowing<sup>91</sup> and as dye carriers.<sup>92</sup> Beside that, HB polymers are used as additives,<sup>6</sup> as components in non-linear optics,<sup>93</sup> in molecular imprinting,<sup>94</sup> in catalysis,<sup>95</sup> as thermoset resins,<sup>87</sup> as modifiers of metal surfaces,<sup>96</sup> as adhesive agents,<sup>97</sup> as compatibilizers,<sup>98</sup> as

dispersers,<sup>99</sup> for gas separation.<sup>100</sup> They can also be used to coat and functionalize carbon nanotubes.<sup>101</sup>

In addition to “traditional” applications of HB polymers, the unique dendritic structure opens up opportunities for new “nanotechnology” applications based on specific confinement of functional units and the formation of pores and cavities, e.g., as in thin films in sensor devices and diagnostics, as porogens for nanofoams.<sup>7,102-104</sup>

The most interesting and at the same time important application of dendrimers is as a controlled drug delivery system, because they can act as molecular encapsulants.<sup>105</sup> Since dendrimers possess controlled multivalency, several drug molecules, targeting groups and solubilizing groups can be attached to the periphery of the dendrimer in a well-defined manner. It is already proved that dendrimers can be used as anticancer drug carriers.<sup>106</sup> This property of dendrimers to encapsulate molecules is also used for protection against quenching.<sup>107</sup> Another important application of these polymers is that dendrimer-based polyanions can be used as inhibitors of HIV and other enveloped viruses.<sup>108</sup> HB polyesters have also been suggested as materials that can be used to control the drug concentration and delivery rate in the body.<sup>109,110</sup>

## References

1. Voit, B. I.; Lederer, A. *Chem Rev* 2009, 109, 5924–5973,
2. Voit, B. I., *C R Chimie* 2003, 6, 821-832;
3. Burchard, W., *Adv Polym Sci* 1999, 143, 113-194;
4. Flory, P. J., *J Am Chem Soc* 1952, 74, 2718-2723;
5. Kricheldorf, H. R.; Zang, Q.-Z.; Schwarz, G., *Polymer* 1982, 23, 1821-1826;
6. Kim, Y. H.; Webster, O. W., *J Am Chem Soc* 1990, 112, 4592-4593;
7. Gao, C.; Yan, D., *Prog Polym Sci* 2004, 29, 183-275;
8. Jikei, M.; Kakimoto, M., *J Polym Sci Part A: Polym Chem* 2004, 42, 1293-1309;
9. Jikei, M.; Chon, S.-H.; Kakimoto, M.; Kawauchi, S.; Imase, T.; Watanabe, J., *Macromolecules* 1999, 32, 2061-2064;
10. Emrick, T.; Chang, H.-T.; Fréchet, J. M. J., *Macromolecules* 1999, 32, 6380-6382;
11. Fréchet, J. M. J.; Henmi, H.; Gitsov, I.; Aoshima, S.; Leduc, M. R.; Grubbs, R. B., *Science* 1995, 269, 1080-1084;
12. Suzuki, M.; Ii, A.; Saegusa, T., *Macromolecules* 1992, 25, 7071-7072;
13. Mori, H.; Müller, A. H. E.; Simon, P. F. W. In *Macromolecular Engineering: Precise Synthesis, Materials, Properties, Applications*; Matyjaszewski, K., Gnanou, Y., Leibler, L., Eds.; Wiley-VCH: Weinheim, Germany, 2007; Vol. 2, p 973ff;
14. Sunder, A.; Hanselmann, R.; Frey, H.; Mülhaupt, R., *Macromolecules* 1999, 32, 4240-4246;
15. Kubisa, P., *J Polym Sci Part A: Polym Chem* 2003, 41, 457-468;
16. Freudenberg, R.; Claussen, W.; Schlüter, A. D., *Polymer* 1994, 35, 4496-4501;
17. Frauenrath, H., *Prog Polym Sci* 2005, 30, 325-384;
18. Schlüter, A. D., *Top Curr Chem* 2005, 245, 151-191;
19. Tomalia, A. D.; Hedstrand, D. M.; Ferrito, M. S., *Macromolecules* 1991, 24, 1435-1438;
20. Gauthier, M.; Möller, M., *Macromolecules* 1991, 24, 4548-4553;
21. Gauthier, M., *J Polym Sci Part A: Polym Chem* 2007, 45, 3803-3810;
22. Brenner, A. R.; Voit, B., *Macromol Chem Phys* 1996, 197, 2673-2689;
23. Liu, C.; Wang, G.; Zhang, Y.; Huang, J., *J Appl Polym Sci* 2008, 108, 777-784;
24. Xu, S.; Luo, Y.; Haag, R., *Macromol Biosci* 2007, 7, 968–974;
25. Dušek, K.; Šomvárský, J.; Smrcková, M.; Simonsick, W. J., Jr.; Wilczek, L., *Polym Bull* 1999, 42, 489-496;
26. Percec, V.; Chu, P.; Kawasumi, M. *Macromolecules* 1994, 27, 4441-4453;

27. Komber, H.; Ziemer, A.; Voit, B., *Macromolecules* 2002, 35, 3514-3519;
28. Kricheldorf, H. R.; Bolender, O.; Wollheim, T., *Macromolecules* 1999, 32, 3878-3882;
29. Monticelli, O.; Mariani, A.; Voit, B.; Komber, H.; Mendichi, R.; Pitto, V.; Tabuani, D.; Russo, S., *High Perform Polym* 2001, 13, 45-59;
30. Flory, P. J., *Principles in Polymer Chemistry*; Cornell University Press: Ithaca, NY, 1953;
31. Dušek, K.; Ilavsky, M.; Lunak, S., *J Polym Sci: Polym Symp.* 1975, 53, 29-44;
32. Schmaljohann, D.; Voit, B., *Macromol Theory Simul* 2003, 12, 679-689;
33. Müller, A. H. E.; Yan, D.; Wulkow, M., *Macromolecules* 1997, 30, 7015-7023;
34. Wurm, F.; López-Villanueva, F.-J.; Frey, H., *Macromol Chem. Phys* 2008, 209, 675-684;
35. Ishizu, K.; Ohta, Y.; Kawauchi, S. *Macromolecules* 2002, 35, 3781-3784;
36. Carter, S.; Rimmer, S.; Sturdy, A.; Webb, M., *Macromol Biosci* 2005, 5, 373-378;
37. Li, Y.; Armes, S. P. *Macromolecules* 2005, 38, 8155-8162;
38. Voit, B. I., *J Polym Sci Part A: Polym Chem* 2000, 38, 2505
39. McKee, M. G.; Unal, S.; Wilkes, G. L.; Long, T. E., *Prog Polym Sci* 2005, 30, 507-539;
40. Hong, L.; Cui, Y.; Wang, X.; Tang, X., *J Polym Sci Part A: Polym Chem* 2002, 40, 344-350;
41. Unal, S.; Yilgor, I.; Yilgor, E.; Sheth, J. P.; Wilkes, G. L.; Long, T. E., *Macromolecules* 2004, 37, 7081-7084;
42. Behera, G. C.; Ramakrishnan, S., *Macromolecules* 2004, 37, 9814-9820;
43. Knauss, D. M.; Huang, T., *Macromolecules* 2003, 36, 6036-6042;
44. Hutchings, L. R.; Roberts-Bleming, S. J., *Macromolecules* 2006, 39, 2144-2152;
45. Percec, V.; Barboiu, B.; Bera, T. K.; Grigoras, C., *Polym Prepr (ACS, Polymer Div)* 2002, 43, 173-181;
46. Gitsov, I.; Fréchet, J. M. J., *Macromolecules* 1993, 26, 6536-6546;
47. Schlüter, A.-D., *Top Curr Chem* 1998, 197, 165-192;
48. Prokhorova, S. A.; Sheiko, S. S.; Ahn, C.-H.; Percec, V.; Möller, M., *Macromolecules* 1999, 32, 2653-2660;
49. Hedrick, J. L.; Trollsås, M.; Hawker, C. J.; Atthoff, B.; Claesson, H.; Heise, A.; Miller, R. D.; Mecerreyes, D.; Jerome, R.; Dubois, P., *Macromolecules* 1998, 31, 8691-8705;
50. Knischka, R.; Lutz, P. J.; Sunder, A.; Mülhaupt, R.; Frey, H., *Macromolecules* 2000, 33, 315-320;

51. Gitsov, I., *J Polym Sci Part A: Polym Chem* 2008, 46, 5295-5314;
52. Cho, B.-K.; Chung, Y.-W.; Lee, B.-I.; Han, K.-H. *J. Inclusion Phenom. Macrocyclic Chem.* 2007, 58, 7;
53. Ternat, C.; Kreutzer, G.; Plummer, C. J. G.; Nguyen, T. Q.; Herrmann, A.; Ouali, L.; Sommer, H.; Fieber, W.; Velazco, M. I.; Klok, H.-A.; Månson, J.-A. E., *Macromol Chem Phys* 2007, 208, 131-145;
54. Zhu, X.; Chen, L.; Yan, D.; Chen, Q.; Yao, Y.; Xiao, Y.; Hou, J.; Li, J. *Langmuir* 2004, 20, 484-490;
55. Carlmark, A.; Hawker, C.; Hult, A.; Malkoch, M., *Chem Soc Rev* 2009, 38, 352-362;
56. Frey, H.; Haag, R., *Rev Mol Biotech* 2002, 90, 257-267;
57. Hawker, C. J.; Lee, R.; Fréchet, J. M. J., *J Am Chem Soc* 1996, 118, 5326-5327;
58. Hölter, D.; Burgath, A.; Frey, H., *Acta Polym.* 1997, 48, 30-35;
59. Yan, D.; Müller, A. H. E.; Matyjaszewski, K., *Macromolecules* 1997, 30, 7024-7033;
60. Kambouris, P.; Hawker, C. J., *J Chem Soc Perkin Tran* 1993, 1, 2717-2721;
61. Stockmayer, W. H.; Fixman, M., *Ann. N.Y. Acad. Sci.* 1953, 57, 334-352;
62. Zimm, B. H.; Kilb, R. W., *J Polym Sci* 1959, 37, 19-42;
63. De Luca, E.; Richards, R. W., *J Polym Sci Part B: Polym Phys* 2003, 41, 1339-1351;
64. Stevens, M. P., *Polymer chemistry* 1990, 2<sup>nd</sup> ed., Oxford University Press;
65. Grubisic, Z.; Rempp, P.; Benoit, H., *J Polym Sci Part B: Polym Phys* 1967, 5, 753-759;
66. Lederer, A.; Voigt, D.; Clausnitzer, C.; Voit, B., *J Chromatogr A* 2002, 976, 171-179;
67. Žagar, E.; Žigon, M., *Macromolecules* 2002, 35, 9913-9925;
68. Lederer, A.; Boye, S., *LCGC Ads* 2008, Nov/Dec, 24;
69. Chikh, L.; Tessier, M.; Fradet, A., *Macromolecules* 2008, 41, 9044-9050;
70. Montaudo, M. S., *J Am Soc Mass Spectrom* 2004, 15, 374-384;
71. Giddings, J. C., *Sep Sci* 1966, 1, 123-125;
72. Podzimek, S.; Vlcek, T.; Johann, C., *J Appl Polym Sci* 2001, 81, 1588-1594;
73. Schmaljohann, D.; Häußler, L.; Pötschke, P.; Voit, B. I.; Loontjens, T. J. A., *Macromol Chem Phys* 2000, 201, 49-57;
74. Marcos, M.; Martín-Rapún, R.; Omenat, A.; Serrano, J. L., *Chem Soc Rev* 2007, 36, 1889-1901;
75. Wooley, K. L.; Fréchet, J. M. J.; Hawker, C. J., *Polymer* 1994, 35, 4489-4495;
76. Fox, T. G., *Bull Am Phys Soc* 1956, 2, 123-124;
77. Behera, G. C.; Saha, A.; Ramakrishnan, S., *Macromolecules* 2005, 38, 7695-7701;
78. Voit, B., *J Polym Sci Part A: Polym Chem* 2005, 43, 2679-2699;

79. Kharchenko, S. B.; Kannan, R. M., *Macromolecules* 2003, 36, 399-406;
80. Pakula, T.; Vlasopoulos, D.; Fytas, G.; Roovers, J., *Macromolecules* 1998, 31, 8931-8940;
81. Farrington, P. J.; Hawker, C. J.; Fréchet, J. M. J.; Mackay, M. E., *Macromolecules* 1998, 31, 5043-5050;
82. Sendijarevic, I.; McHugh, A. J., *Macromolecules* 2000, 33, 590-596;
83. McKee, M. G.; Elkins, C. L.; Park, T.; Long, T. E., *Macromolecules* 2005, 38, 6015-6023;
84. Froehling, P., *J Polym Sci Part A: Polym Chem* 2004, 42, 3110-3115;
85. Hult, A.; Johansson, M.; Malmström, E., *Adv Polym Sci* 1999, 143, 1-34;
86. Johansson, M.; Hult, A., *J Coat Technol* 1995, 67, 35-39;
87. Johansson, M.; Malmström, E.; Hult, A., *J Pol Sci Part A: Polym Chem* 1993, 31, 619-624;
88. Hult, A.; Johansson, M.; Malmström, E., *Macromol Symp* 1995, 98, 1159-1161;
89. Massa, D. J.; Shriner, K. A.; Turner, S. R.; Voit, B. I., *Macromolecules* 1995, 28, 3214-3220;
90. Kim, H.; Webster, O.W., *Macromolecules* 1992, 25, 5561-5572;
91. Hong, JY.; Cooper-White, J. J.; Mackay, M. E.; Hawker, C. J.; Malmström, E.; Rehnberg, N., *J Rheol* 1999, 43, 781-793;
92. Schmaljohann, D.; Pötschke, P.; Hässler, R.; Voit, B. I.; Froehling, P. E.; Mostert, B.; Loontjens, J. A., *Macromolecules* 1999, 32, 6333-6339;
93. Zhang, Y.; Wang, L.; Wada, T.; Sasabe, H., *Macromol Chem Phys* 1996, 197, 667-676;
94. Griebel, T.; Maier, G., *Polym Prepr (ACS, Polymer Division)* 2000, 4, 89-90;
95. Persigehl, P.; West, N.; Zimmermann, B.; Nuyken, O., Presented at the Freiburger Makromolekularem Kolloquium, Freiburg, (2000);
96. Zhao, M.; Zhou, Y.; Bruening, M. L.; Bergbreiter, D. E.; Crooks, R. M., *Langmuir* 1997, 13, 1388-1391;
97. Emrick, T.; Chang, H.-T.; Fréchet, J. M. J.; Woods, J.; Baccei, L., *Polym Bull* 2000, 45, 1-7;
98. Jannerfeldt, G.; Boogh, L.; Månson, J.-A. E., *J Polym Sci Part A: Polym Chem* 1999, 37, 2069-2077;
99. Star, A.; Stoddart, J. F., *Macromolecules* 2002, 35, 7516-7520;
100. Fang, J.; Kita, H.; Okamoto, K.-I., *J Membr Sci* 2001, 182, 245-256;

101. Hong, C.-Y.; You, Y.-Z.; Wu, D.; Liu, Y.; Pan, C.-Y., *Macromolecules* 2005, 38, 2606-2611;
102. Yates, C. R.; Hayes, W., *Eur Polym J* 2004, 40, 1257-1281;
103. Inoue, K., *Prog Polym Sci* 2000, 25, 453-471;
104. Voit, B., *New J Chem* 2007, 31, 1139-1151;
105. Esfand, R.; Tomalia, D. A., *Drug Discovery Today* 2001, 6, 427-436;
106. Duncan, R.; Malik, N., *Proc Int Symp Control Release Bioact Mater* 1996, 23, 105-106;
107. Vinogradov, S. A.; Wilson, D. F., *Chem Eur J* 2000, 6, 2456-2461;
108. Gong, Y.; Matthews, B.; Cheung, D.; Tam, T.; Gadawski, I.; Leung, D.; Holan, G.; Raff, J.; Sacks, S., *Antiviral Res* 2002, 55, 319-329;
109. Uhrich, K., *Trends in Polym Sci* 1997, 5, 388-393;
110. Arce, E.; Nieto, P. M.; Diaz, V.; Castro, R. G.; Bernad, A.; Rojo, J., *Bioconjugate Chem* 2003, 14, 817-823.



## Chapter 2

# Synthesis and characterization of HB polyesters

## 2.1 Introduction

Hyperbranched (HB) polymers are a special category of dendritic polymers with a treelike structure, high branching density, and high density of terminal functional groups on their surface. The commercial success of HB polymers is a result of the highly branched and dense, but irregular structure that gives them unique physical and chemical properties and leads to excellent solubility, compared to linear polymers, low solution viscosity, modified melt rheology, and high level of terminal end-group functionality.<sup>1-5</sup>

They are usually prepared in a one-pot synthesis, which limits the control on molar mass (MM) and branching accuracy and leads to heterogeneous products with a distribution in MM, chemical composition, and branching, where a perfect structure is sacrificed for an easy and affordable synthetic route. Important commercial applications are as a reactive component in coating and resin formulations and as polymer additives in linear polymers for improving rheology and flow and for surface modification.<sup>1</sup> In addition to traditional applications, the unique structure of HB polymers makes them interesting matter for new “nanotechnology” applications as in thin films in sensor devices and diagnostics, as porogens for nanofoams, and as carriers for special additives, catalytic species, and therapeutics.<sup>6-9</sup> Recently, they found also application as polymeric plasticizers, in particular for polyvinyl chloride (PVC) in substitution of banned phthalate esters [DOP (dioctyl phthalate) or DEHP (di-2-ethyl hexyl phthalate)].<sup>9-11</sup> Within the different types of dendritic organic polymers, HB polyesters, in particular biodegradable type aliphatic HB polyesters, have attracted attention from both a scientific and a commercial point of view.<sup>1-5,12-35</sup> This is due to the relative easy procedure of synthesis and the availability of suitable monomer. One drawback of “classical” HB polymers with branching sites in each repeating unit is the high branching density that prevents the formation of entanglements in the bulk materials, and therefore, structural applications of plain HB polymers are not possible because of the high brittleness and poor mechanical properties. Therefore, early in the development of these polymers, the reduction of the degree of branching and the branching density has been explored, leading to a broad variety of linear–hyperbranched

hybrids.<sup>12,22–34</sup> Branching can be diluted by increasing the distance between the branching points using linear oligomeric starting materials. However, only a few examples exist so far on linear–hyperbranched block-copolymer structures.<sup>1</sup> The main reason for that is that less controlled synthetic approaches toward HB structures easily can lead to undesired side reactions in block-copolymer formation, which reduces the control of the structure and can result in mixtures of products.

The aim of this study was the synthesis of HB polyesters having different lengths of linear oligo(butylene adipate) (PBA) segments (blocks) incorporated in their branched chains, by a one-pot synthesis between tailored PBA samples terminated with methyl ester groups and 1,1,1-tris(hydroxy methyl)propane (TMP) used as branching agent, in the presence of titanium(IV)isopropoxide (TIP) as catalyst. The progress of reaction was followed by <sup>1</sup>H and solid-state <sup>13</sup>C-NMR and MALDI-TOF mass spectrometry (MALDI-TOF MS) tools, to obtain reliable knowledge about structure and chemical composition of either the telechelic PBA pre-polymer or the final HB products, as a function of reaction parameters, such as time, temperature, and monomers molar ratio. The average MMs ( $M_w$  and  $M_n$ ) of all PBA and HB samples were determined by SEC apparatus calibrated with absolute calibration curves obtained by the SEC/MALDI-TOF analysis of selected SEC fractions of representative PBA and HB samples. The calculated values were compared with those determined using the classical standard calibration curve for polystyrenes (PSs).

## 2.2 Experimental section

### 2.2.1 Materials for HB polyesters synthesis

1,4-Butanediol (BD; 99%), dimethyl ester of adipic acid (DMA;  $\geq 99\%$ ), titanium(IV)isopropoxide (TIP; 99.99%), as catalyst, and 1,1,1-tris(hydroxy methyl)propane (TMP;  $\geq 98\%$ ), as branching agent, were purchased from Sigma–Aldrich (Italy). In addition chloroform ( $\text{CHCl}_3$ ), tetrahydrofuran (THF), methanol ( $\text{CH}_3\text{OH}$ ), dimethyl sulphoxide (DMSO), N,N dimethylformamide (DMF), trifluoro acetic acid (TFA), deuterated chloroform ( $\text{CDCl}_3$ ), and deuterated dimethyl sulphoxide ( $\text{DMSO-d}_6$ ) solvents were also obtained from Sigma–Aldrich (Italy). The MALDI matrices, 2(-4-hydroxyphenylazo)-benzoic acid (HABA) and  $\alpha$ -cyano-4-hydroxycinnamic acid, were purchased from Sigma–Aldrich (Italy). All reagents and solvents were used without any further purification.

## 2.2.2 Synthesis of polyesters

### Synthesis of linear telechelic PBA

The linear tailored PBA polyesters terminated with methyl ester groups and with an average weight ranging from 4'000 to 9'500 g/mol (see Table 2.1) were synthesized through a polycondensation reaction between BD and DMA, using TIP as catalyst (see Scheme 2.1, step 1). Different PBA polymers were obtained by varying the DMA/BD molar ratios, the reaction temperatures and times, as summarized in Table 2.1.

Each PBA sample was obtained through two reaction steps: (i) the first one at atmospheric pressure and under nitrogen atmosphere and (ii) the second one under reduced pressure (~10 Torr), as sketched in Table 2.1. In particular, to synthesize PBA-9, in a two-necked round-bottom reaction vessel, BD ( $1.1100 \times 10^{-2}$  mol), DMA ( $1.1125 \times 10^{-2}$  mol), and TIP (0.2 mol %) were weighted. The reaction vessel was immersed in a silicon oil bath at 160 °C, where the reaction was continued for 1 h. After this phase, the temperature was raised up to 180 °C, and the reaction was continued for 2 h. The CH<sub>3</sub>OH formed in the reaction was continuously distilled out from the reaction mixture. Finally, the reaction was continued for 3 h at 180 °C under reduced pressure. As soon as the polymerization was completed, the reaction mixture was cooled down to room temperature ( $T_{\text{room}}$ ). The polyesters were dissolved in THF and removed from the reaction vessel. The polymers were precipitated into a large excess of CH<sub>3</sub>OH. The white polymer was finally filtrated and dried under vacuum at 40 °C for 24 h.

### Synthesis of linear-hyperbranched hybrid PBA copolymers

Linear-hyperbranched PBA copolymers (referred here as HB samples) were synthesized by one-pot synthesis performed in two steps, according to Scheme 2.1, in a three-necked round bottom flask equipped with a magnetic stirrer and connected with a gas inlet and outlet adapters. In the first step, the tailored PBA methyl ester ended pre-polymers were synthesized using a DMA/BD molar ratio of 1.0025/1 as described before and using the experimental parameters reported for the PBA-9 sample. In the second step, different molar amounts (1.5, 3, 5, 7, and 10 mol % with respect to the initial moles of DMA and BD) of TMP as branching agents were added, and the reaction was carried out at 180 °C for 2 h at 1 atm, under nitrogen flow and under stirring. Then, the reaction was continued under vacuum for different times as reported in Table 2.1, to obtain HB hybrid polyesters with linear PBA blocks along the chains.

**Table 2.1: Experimental synthesis condition, molar mass distributions and yields of synthesized tailored PBA pre-polymers and HB polyesters samples.**

Samples	Experimental Parameters				$M_n^a$ (g/mol)	$M_w^a$ (g/mol)	$M_n^b$ (g/mol)	$M_w^b$ (g/mol)	$M_n^c$ (g/mol)	Yield (%)
	DMA/BD Molar ratio	TMP (mol%)	T (°C)	Reaction Time (min)						
PBA-1	1.05/1	----	130	60	4'350	4'900	4'900	6'100	5'200	55
			150	60						
			170	60						
			180	80 <sup>d</sup>						
PBA-2	1.02/1	----	150	60	4'250	5'100	4'800	6'600	4'200	67
			160	60						
			180	60						
			180	80 <sup>d</sup>						
PBA-3	1.02/1	----	130	60	4'800	5'300	5'650	6'800	4'500	57
			150	120						
			150	80 <sup>d</sup>						
PBA-4	1.02/1	----	130	60	4'600	5'000	5'400	6'500	4'200	25
			150	60						
			170	60						
			170	80 <sup>d</sup>						
PBA-5	1.02/1	----	130	60	5'300	9'400	6'400	14'400	6'400	64
			160	120						
			160	120 <sup>d</sup>						
PBA-6	1.01/1	----	130	60	5'200	9'500	6'200	13'750	3'800	54
			160	120						
			160	120 <sup>d</sup>						
PBA-7	1.005/1	----	130	60	4'450	5'550	5'150	7'400	4'400	70
			160	120						
			160	180 <sup>d</sup>						
PBA-8	1.0025/1	----	130	60	3'700	4'650	5'300	6'650	3'800	66
			160	120						
			160	120 <sup>d</sup>						
PBA-9	1.0025/1	----	160	60	4'150	5'500	4'600	7'200	4'800	83
			180	120						
			180	180 <sup>d</sup>						
PBA-10	1.001/1	----	160	60	4'100	5'500	4'550	7'100	4'900	81
			180	120						
			180	180 <sup>d</sup>						
1.5HB16	1.0025/1	1.5	180 <sup>e</sup>	16 <sup>e</sup>	6'700	12'000	11'370	19'000	---	91
1.5HB24	1.0025/1	1.5	180 <sup>e</sup>	24 <sup>e</sup>	10'300	32'000	17'000	49'800	---	93
1.5HB16§	1.001/1	1.5	180 <sup>e</sup>	16 <sup>e</sup>	8'900	16'900	14'850	26'300	---	93
1.5HB24§	1.001/1	1.5	180 <sup>e</sup>	24 <sup>e</sup>	11'000	28'000	18'100	43'400	---	92
1.5HB30§	1.001/1	1.5	180 <sup>e</sup>	30 <sup>e</sup>	14'500	54'700	24'100	85'300	---	95
3HB16	1.0025/1	3	180 <sup>e</sup>	16 <sup>e</sup>	6'400	24'200	10'500	37'100	---	90
3HB24	1.0025/1	3	180 <sup>e</sup>	24 <sup>e</sup>	6'950	27'000	12'300	42'400	---	90
3HB24§	1.0025/1	3	170 <sup>e</sup>	24 <sup>e</sup>	4'400	7'700	7'200	12'000	---	91
5HB16	1.0025/1	5	180 <sup>e</sup>	16 <sup>e</sup>	6'300	9'550	10'300	15'100	---	91
5HB24	1.0025/1	5	180 <sup>e</sup>	24 <sup>e</sup>	9'850	16'400	15'800	25'400	---	93
5HB30	1.0025/1	5	180 <sup>e</sup>	30 <sup>e</sup>	17'900	37'700	29'500	58'700	---	93
5HB44	1.0025/1	5	180 <sup>e</sup>	44 <sup>e</sup>	---	---	---	---	---	---
7HB8	1.0025/1	7	180 <sup>e</sup>	8 <sup>e</sup>	9'500	28'000	18'600	38'000	---	92
7HB16	1.0025/1	7	180 <sup>e</sup>	16 <sup>e</sup>	17'400	97'600	25'600	136'700	---	95
10HB8	1.0025/1	10	180 <sup>e</sup>	8 <sup>e</sup>	4'600	9'600	7'600	1'380	---	89
10HB16	1.0025/1	10	180 <sup>e</sup>	16 <sup>e</sup>	9'300	32'500	15'000	43'600	---	91

<sup>a</sup> Data were calculated using appropriate SEC curve calibrations built by SEC/MALDI-TOF MS analysis of PBA-9 and 3HB16 for PBA and HB samples, respectively;

<sup>b</sup> Calculated by SEC calibrated with the polystyrene (PS) narrow standards;

<sup>c</sup> Calculated by <sup>1</sup>H-NMR; <sup>d</sup> step carried out under vacuum (~10 Torr);

<sup>e</sup> Indicate the temperature and the reaction time of the last step carried out under vacuum.

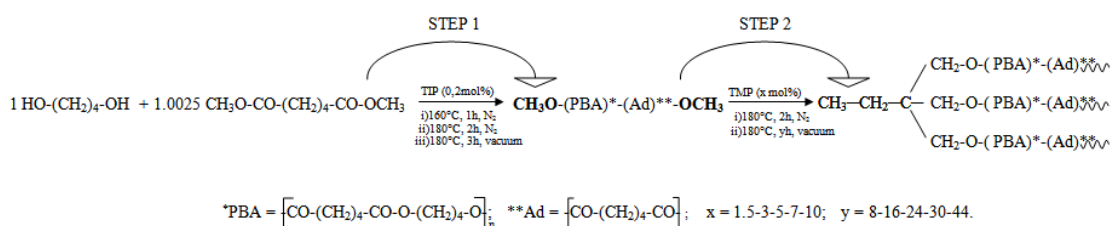
After the reaction, 50 mL of CHCl<sub>3</sub> was added into the flask and stirred for 2 h. The solution was filtered to remove the insoluble part of the material (1–2 wt % for each HB sample). The filtrate was precipitated into CH<sub>3</sub>OH in excess to obtain a white powdery polymer. The filtered polymer was washed with CH<sub>3</sub>OH and dried at 25 °C for 24 h in a vacuum oven.

The HB samples synthesized with 5, 7, and 10 molar percent of TMP were partially soluble in CHCl<sub>3</sub> and totally soluble in TFA at T<sub>room</sub>, and either in DMF or in DMSO at about 30–35 °C, and also in THF at a concentration of about 2 mg/mL. Therefore, these samples were purified by dissolving in DMSO at 40 °C (with a concentration of 10 mg/mL) and precipitated into a large excess (fivefold) of CH<sub>3</sub>OH.

The sample synthesized with 5 molar percent of TMP for 44 h resulted only partially soluble in these same solvents, probably due to the presence of a cross-linked portion, as widely confirmed in literature for polymers with highly branched structure.<sup>12,17</sup> In order to separate the insoluble cross-linked portion, soxhlet extraction technique was employed using CHCl<sub>3</sub> at 70 °C for 24 h. The extraction thimble containing the CHCl<sub>3</sub>-insoluble polymer fraction was then dried in an oven at 40 °C for 24 h under vacuum. The weight percentage of insoluble part, named 5HB44 onwards, was calculated gravimetrically<sup>36</sup> according to the Equation 2.1:

$$\text{Insoluble fraction wt. \%} = \frac{(W_{tg} - W_t)}{W_s} * 100 \quad (2.1)$$

where W<sub>tg</sub> is the thimble weight containing the insoluble fraction; W<sub>t</sub> is the thimble weight; W<sub>s</sub> is the sample weight. The insoluble content of the sample was calculated to be 90 wt. %.



**Scheme 2.1: Synthesis route of HB polyester samples.**

## 2.2.3 Characterization

### Nuclear magnetic resonance spectroscopy (NMR)

$^1\text{H}$ -NMR spectra were recorded using a Bruker 200 MHz. The samples were dissolved in deuterated solvents without any internal standard at  $T_{\text{room}}$ .  $\text{CDCl}_3$  was used to analyze all linear PBA and HB samples prepared using 1.5 and 3 molar percent of TMP, whereas  $\text{DMSO-d}_6$  was utilized for the other HB samples synthesized using 5, 7, and 10 molar percent of TMP. The data were elaborated with 1D Win-NMR software applying the Lorentz–Gauss enhance function using appropriate Line broadening and Gaussian broadening parameters to improve the resolution of peaks. The concentration of polymers is about 10 mg/mL for the proton analysis.

Solid-state  $^{13}\text{C}$ -NMR was used to analyze 5HB44 sample since it appears insoluble in most solvents commonly used to dissolve the other HB polymers. Solid-state  $^{13}\text{C}$  cross-polarization, magic angle spinning (CP-MAS) NMR spectra were collected at 100.47 MHz on a Bruker Avance II 400 spectrometer operating at a static field of 9.4 T, equipped with a 4 mm MAS probe. The  $1\text{H}$   $\pi/2$  pulse width was 3.4  $\mu\text{s}$ , and the CP contact time was 2 ms. The materials were packed into 4 mm zirconia rotors and sealed with Kel-F caps. The spinning speed was set to 8 kHz.

### Size exclusion chromatography (SEC)

SEC analyses carried out by means of a Waters 515 apparatus, equipped with four Ultrastyrigel HR columns (7.8–300 mm; in the order HR-4, HR-3, HR-2, and HR-1) connected in series, and a Waters R401 differential refractometer (RI) detector. The SEC curves were recorded and processed using a Clarity-GPC software provided by DataApex.

In a typical analysis, 100  $\mu\text{L}$  of a polymer solution in THF (2–3 mg/mL) was injected and eluted at a flow rate of 1 mL/min using THF as eluent and *o*-dichlorobenzene (1  $\mu\text{L}$ ) as flow marker. The average MMs of all polymer samples were calculated using the calibration curves built by SEC analyses of linear PS narrow standards and by SEC/MALDI-TOF data obtained by MALDI analysis of polymer SEC fractions.

Fractionations by SEC of two PBA samples (PBA-1 and PBA-9) and two HB samples (3HB16 and 3HB24§) were performed using THF as eluent (1 mL/min). 100  $\mu\text{L}$  of a polymer solution in THF (4–5 mg/mL) was injected, and fractions were taken every 25 s (0.25 mL) using a Waters fraction collector, positioned at the outlet of the RI detector. For each sample, 40–50 fractions were collected. Polystyrene standards (Polymer Laboratories)

were first used to calibrate the system. The solvent of SEC fractions was reduced at 30–50  $\mu\text{L}$ , and the absolute MMs of selected fractions were determined by MALDI-TOF mass spectrometry (see next section). The fractions were afterward reinjected in the SEC apparatus as standards for absolute MM calibration for PBA and HB samples.

### **Matrix-assisted laser desorption/ionization mass spectrometry (MALDI-TOF MS)**

The MALDI-TOF mass spectra were recorded in reflectron or linear delayed extraction mode, using a Voyager-DE STR instrument (Perseptive Biosystem) mass spectrometer, equipped with a nitrogen laser ( $\lambda = 337 \text{ nm}$ , pulse width = 3 ns), working in a positive ion mode. The accelerating voltage was 20 kV, grid voltage and delay time (delayed extraction, time lag) were optimized for each sample to achieve the higher mass resolution (M/DM). Laser irradiance was maintained slightly above threshold. HABA (0.1 M in THF) and  $\alpha$ -cyano-4-hydroxycinnamic acid (0.1 M in THF) were used as matrices. Samples of linear PBA and HB polyesters used for the MALDI analyses were prepared as follows: 10  $\mu\text{L}$  of polymer solution (5 mg/mL in THF or DMSO) was mixed with 10  $\mu\text{L}$  or 30  $\mu\text{L}$  of a matrix solution (0.1 M in THF). Then, 1  $\mu\text{L}$  of each analyte/matrix mixture was spotted on the MALDI sample holder and slowly dried to allow analyte/matrix co-crystallization. The better spectra were recorded using  $\alpha$ -cyano-4-hydroxycinnamic acid, obtaining a mass resolution of about 800–1'000 in linear mode and 5'000–7'000 in reflectron mode, in the mass range from  $m/z$  1'000 to 4'000. For the analysis of polymer SEC fractions, 1  $\mu\text{L}$  of each selected concentrated SEC solution was mixed with 1 or 3  $\mu\text{L}$  of the matrix solution ( $\alpha$ -cyano-4-hydroxycinnamic acid in THF). The same procedure was used for the MALDI analyses of all samples analyzed. The MALDI spectra of the SEC fractions recorded in linear mode were processed by the PGRAMS program provided by Perseptive Biosystem, which use mass-spectral intensities to compute the quantities known as most-probable molecular weight ( $M_p$ ), number-average molar mass ( $M_n$ ), weight-average molar mass ( $M_w$ ), and polydispersity index ( $\text{PDI} = M_w/M_n$ ). The  $M_w$  values were used to build absolute MM calibration of SEC traces of PBA and HB samples.

### **SEC/MALDI-TOF analysis**

MALDI-TOF MS is a powerful technique giving information about different structural formations and repeating units in complex polymer systems,<sup>37–43</sup> and has been successfully applied to the characterization of HB polyesters.<sup>13,20,28,30,34</sup> However, it often fails in the



analysis of polymers with PDI higher than 1.1,<sup>37-43</sup> because it gives mass peaks in the range 1'000–15'000 Da that may not be representative of high MM polymers. In such cases, the polydispersed polymers should be fractionated into several fractions of narrow MM distribution (PDI < 1.05), which are then analyzed by MALDI-TOF MS and used to calibrate the SEC curves against absolute MMs (self-calibration). This method, referred to as SEC/MALDI-TOF MS, was applied to the characterization of linear polymers, such as poly(dimethylsiloxane), polyesters, and copolyesters,<sup>37,43</sup> and recently for the characterization of HB polyester based on 2,2-bis(hydroxymethyl)propanoic acid.<sup>13</sup> Therefore, in this paper, the average MMs ( $M_w$  and  $M_n$ ) of all PBA and HB samples were determined by SEC apparatus calibrated with absolute calibration curves obtained by the SEC/MALDI-TOF analysis of the selected SEC fractions of representative PBA and HB samples.

### **Thermogravimetric analysis (TGA)**

TGA measurements were performed in duplicate by TA Q5000 analyzer in order to investigate the thermal stabilities of PBA-9 pre-polymer and all HB samples. Samples size was about 5-10 mg and test procedure involved a ramp from 40 °C up to 600 °C at heating rate of 10 °C/min in nitrogen atmosphere.

### **Differential scanning calorimetry (DSC)**

The thermal properties of PBA-9 pre-polymer and all HB samples were determined under nitrogen atmosphere (flow rate of 50 ml/min) by TA Instrument Q20 DSC held in sealed aluminium crucibles.

A dynamic heating rate of 10 °C/min was used for the preliminary thermal analysis of 1.5HB16 sample. This sample was heated up to 120 °C, held at this temperature for 5 min, then cooled down to 10 °C and heated again to 120 °C.

For isothermal crystallization, about 6 mg of 1.5HB16 sample were first heated to 75 °C, which is about 20 °C above its melting temperature, held at this temperature for 5 min, then quenched to three selected temperature  $T_c$  (27, 29, 32 °C), and held at these temperature for 30 min. After completion of crystallization, 1.5HB16 sample was heated directly from  $T_c$  to 100 °C at a rate of 10 °C/min.

PBA-9 pre-polymer and all HB samples were analyzed following the same runs: a first heating scan at 10 °C/min from 40 °C up to 100 °C, then equilibrated to -75 °C and held



isothermally at this temperature for 5 min, finally heating at 10 °C/min from -75 °C up to 100 °C and cooling at 10 °C/min from 100 °C to -10 °C.

## Wide angle X-ray diffraction (WAXD)

WAXD measurements were conducted using a Philips XPW diffractometer with Cu Ka radiation (1.542 Å ) filtered by nickel. The scanning rate was 0.02 °/s, and the scanning angle was from 2 to 60°. The ratio of the area under the crystalline peaks and the total area multiplied by 100 was taken as the crystalline percentage degree (DC).

## 2.3 PBA and HB characterization: results and discussion

### 2.3.1 Synthesis and characterization of linear telechelic PBA

In a preliminary study, linear telechelic PBA chains terminated with methyl ester groups were synthesized. A series of polymerization experiments were carried out to evaluate the influence of the DMA/BD molar ratios, the temperature, the reaction times, and the pressure on the composition of the synthesized PBA polymers.

The experimental conditions used are summarized in Table 2.1. It shows that as the polycondensation conditions changed, linear PBA polymers with different average MMs ( $M_w$  and  $M_n$ ) and a PDI within 1.1 and 1.5, except for the PBA-5 and PBA-6 samples, were obtained. All PBA samples were characterized by  $^1\text{H-NMR}$  and thoroughly by MALDI-TOF MS to identify their end-groups and characterize their composition.  $M_n$  values were calculated from the corresponding  $^1\text{H-NMR}$  spectra applying Equations 2.2 and Equation 2.3, using the integrated area of the signals (singlet) at 3.67 ppm due to the resonances of the three protons belonging to the methyl ester end-groups (protons  $\text{H}^e$  in Table 2.3, and Figure 2.3a), and the integrated area of the unresolved triplet at 4.09 ppm due to the resonance of the four methylene protons belonging to the adipate units in  $\alpha$  to the ester groups (protons  $\text{H}^a$  in Table 2.3, and Figure 2.3a).

$$X_n = (I_{4.09}/4)/(I_{3.67}/6) + 1 \quad (2.2)$$

$$M_n = X_n \cdot 200.2 \quad (2.3)$$

where 200.2 is the mass of PBA repetitive units.

All linear PBAs were analyzed by MALDI-TOF MS either in the linear mode for its greater range (up to  $m/z$  10'000) or in the reflectron mode (up to  $m/z$  7'000) for its better resolution and mass accuracy. All spectra show clusters of homologous peaks separated by 200.2 Da corresponding to the mass of the PBA repeating units. Each cluster can be assigned to linear PBA chains bearing different end-groups, as reported in Table 2.2.

**Table 2.2: Structural assignments of peaks displayed in the MALDI-TOF mass spectra of PBA samples as reported in Figure 2.1.**

Species	Structures <sup>a</sup>	$[M+Na]^+(n)$ <sup>(b)</sup>
$A_n$	$CH_3O-(PBA)_n-Ad-OCH_3$ $(M_{A_n} + Na^+) = n \cdot 200.2 + 174.1 + 23$	1798.7(8); 1998.9(9); 2199.1(10); 2399.3(11); etc
$B_n$	$CH_3O-(PBA)_n-H$ $(M_{B_n} + Na^+) = n \cdot 200.2 + 32 + 23$	1656.6(8); 1856.8(9); 2057.0(10); 2257.2(11); etc
$C_n$	$HO-(CH_2)_4-O-(PBA)_n-H$ $(M_{C_n} + Na^+) = n \cdot 200.2 + 90 + 23$	1714.6(8); 1914.8(9); 2115.0(10); 2315.2(11); etc
$D_n$	$CH_3O-Ad-(PBA)_n-O-(PBA)_n-Ad-OCH_3$ $(M_{D_n} + Na^+) = n \cdot 200.2 + 302.1 + 23$	1926.7(8); 2126.9(9); 2327.1(10); 2527.3(11); etc
$A'_n$	$HO-(PBA)_n-Ad-OCH_3$ $(M_{A'_n} + Na^+) = n \cdot 200.2 + 160.1 + 23$	1784.7(8); 1984.9(9); 2185.1(10); 2385.3(11); etc

<sup>a</sup>  $(-PBA-)_n = -CO-(CH_2)_4-CO-O-(CH_2)_4-O-$ ;  $(-Ad-)_n = -CO-(CH_2)_4-CO-$ ;

<sup>b</sup> The experimental mass were measured with an accuracy of  $\pm (0.5 \div 0.6)$  Da.

As an example, in Figure 2.1, the MALDI mass spectra of PBA-9 (Figure 2.1a) and PBA-1 (Figure 2.1b) samples recorded in reflectron mode are reported; and the assigned peaks are listed in Table 2.2. In Figure 2.1a, as expected on the basis of synthesis procedure, the main peak series correspond to the sodiated ions of the linear PBA chains terminated with methyl ester groups at both ends (oligomers  $A_n$ ), accompanied by the corresponding potassiated ions characterized by  $m/z$  values of 16 mass units higher than sodiated  $A_n$  species. The less intense peaks are due to sodiated and potassiated ions of  $B_n$  type oligomers. In Figure 2.1b, weak peaks labeled as  $D_n$  correspond to the sodiated and potassiated ions of linear PBA oligomers terminated with methyl esters at both ends and containing one anhydride unit in the backbone are recognized. These unexpected macromolecules resulted from the side reactions between the carboxyl acid end-groups of two different PBA chains (Scheme 2.2). PBA oligomers terminated with carboxyl acid groups are also identified in the spectrum in Figure 2.1a and Figure 2.1b corresponding to the weak peaks labeled as  $A'_n$ . These oligomers were formed through polycondensation of

butanediol terminal units with monomethyl ester of adipic acid present as impurity (less 1%) in the used DMA reagent, or by hydrolysis of methyl ester groups owing to eventual trace of water present in polymerization step carried out at atmospheric pressure. MALDI mass spectrum of PBA-1, synthesized with an excess of 5 molar percent of DMA, shows another family of peaks related to  $C_n$  species.

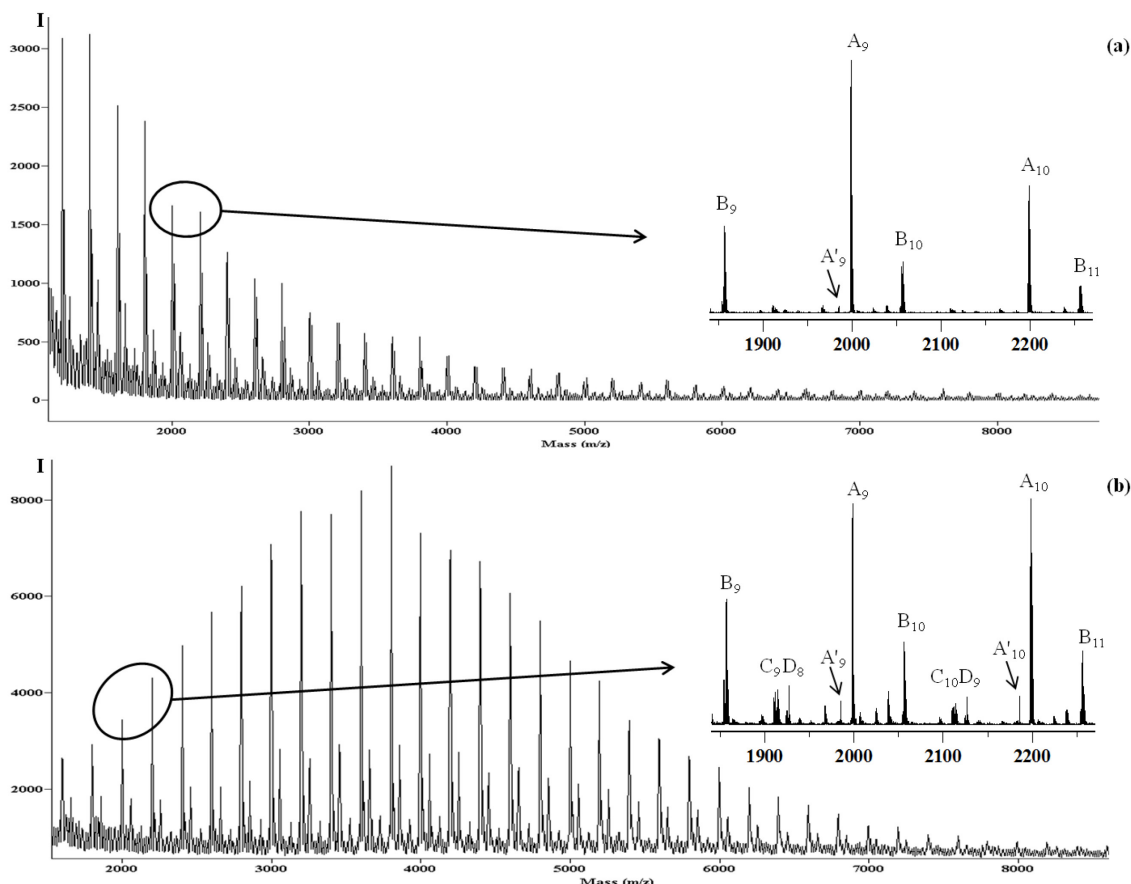
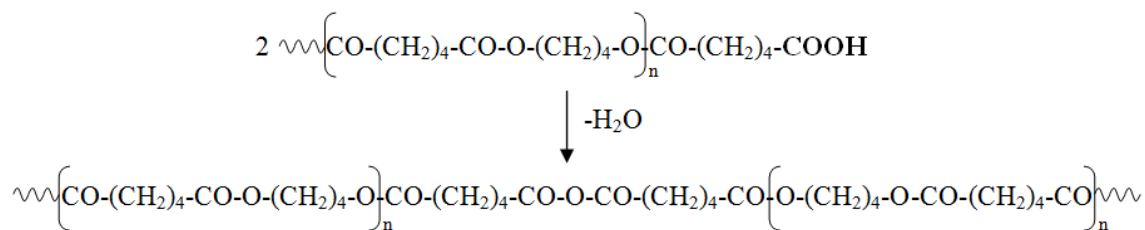


Figure 2.1: MALDI-TOF mass spectra of PBA-9 (a) and PBA-1 (b) samples.

Comparing both spectra, we can observe that in the MALDI mass spectrum of PBA-1 the relative intensity of  $D_n$  peak increases compared to that of the peak series  $A_n$ , suggesting that the formation of the family of oligomers  $D_n$  is favored by increasing the molar amount of the DMA in the feed.



Scheme 2.2: Formation of anhydride groups,  $D_n$ .

Assuming that the molar ratio of each individual species is proportional to the MS detector response, the relative % of end-groups from the mass spectrum was calculated. This assumption is reasonable for MALDI spectra of polymers with a narrow MM distribution. However, it is also realistic, if the analysis is limited to a portion of the spectrum. Using the intensity of each peak series in the mass range from  $m/z$  1'500 to  $m/z$  2'500 and Equations 2.4 and Equation 2.5, we have calculated that PBA-9 and PBA-1 are terminated with 90% and 72% of methyl ester groups, respectively:

$$\%mol_{(-OCH_3)} = (I_A + I_D + 1/2I_B)/(I_A + I_B + I_C + I_D) \quad (2.4)$$

$$\%mol_{(-OH)} = (I_C + 1/2I_B)/(I_A + I_B + I_C + I_D) \quad (2.5)$$

The  $M_w$  and  $M_n$  values of all PBA samples were also determined by SEC analysis using the absolute calibration curves derived from MALDI-TOF MS analysis of selected narrow PBA-9 and PBA-1 SEC fractions. Both absolute calibration curves agree with Equation 2.6, which, therefore, was used to calculate the  $M_n$  and  $M_w$  values of all synthesized PBA samples.

$$\log M_w = 8.005 - 0.147V_e + 3.213 \cdot 10^{-4}(V_e)^2 \quad (2.6)$$

The  $M_n$  values calculated by absolute self-calibration method are statistically in agreement with those calculated by  $^1\text{H-NMR}$  analysis, as can be seen in Table 2.1. On the other hand, using SEC calibration curve built with linear PS standards, the calculated average MMs are 25–30% higher than those calculated by absolute SEC/MALDI-TOF calibration curve. The discrepancy increases in the case of the samples PBA-5 and PBA-6, which have a PDI higher than 2. This result was expected, because SEC analysis calibrated with linear narrow standards [PS and polymethyl methacrylate (PMMA)] cannot account for the shape of branched macromolecules.<sup>14</sup>

### 2.3.2 Linear-hyperbranched hybrid PBA copolymers (HB)

MALDI-TOF MS analyses revealed that tailored linear PBA samples with high amount of methyl ester end-groups were obtained using a DMA/BD molar ratio of 1.0025/1 (and of 1.001/1), and a final temperature reaction of 180 °C for 3 h under vacuum. Following these findings, HBs were then synthesized in one-pot synthesis according to a two-step procedure as reported in Scheme 2.1, using in the first step a DMA/BD molar ratio of

1.0025/1 (or of 1.001/1) and in the second step 1.5, 3, 5, 7, and 10 molar percent of TMP as branching agent. The experimental conditions used for the synthesis of HB samples are summarized in Table 2.1. All HB samples were purified using appropriate solvent/nonsolvent mixture as reported in “Experimental” section and were analyzed by SEC using THF as a solvent at a flow of 1 mL/min and a polymer concentration of 2–3 mg/mL of THF. Their average MMs were calculated by SEC calibration curves built by the SEC/MALDI-TOF analysis of 3HB16 or 3HB24§ samples (see *infra*), and also with the common linear PS narrow standards. The calculated values are reported in Table 2.1. The average MMs calculated by SEC calibrated with PS standards are overestimated (about 50–60% higher than those calculated by absolute SEC/MALDI self-calibration) indicating that the hydrodynamic volume of the HB polymers is higher than that of the linear PSs with similar MMs. Table 2.1 also shows that the average MMs of the prepared HBs using the same DMA/BD molar ratio and the same amount of TMP (i.e., homologous samples: (i) 1.5HB16 and 1.5HB24; (ii) 1.5HB16§, 1.5HB24§, 1.5HB30§) increase with the reaction time under vacuum, maybe owing to the progress of the reactions.

All synthesized HB samples exhibit average MMs higher than the corresponding linear PBA pre-polymer as can be observed in Figure 2.2, in which the SEC curves of PBA-9 and synthesized HBs using a DMA/DB molar ratio of 1.0025/1 and 1.5 molar percent of TMP (samples 1.5HB16 and 1.5HB24 in Table 2.1) are shown.

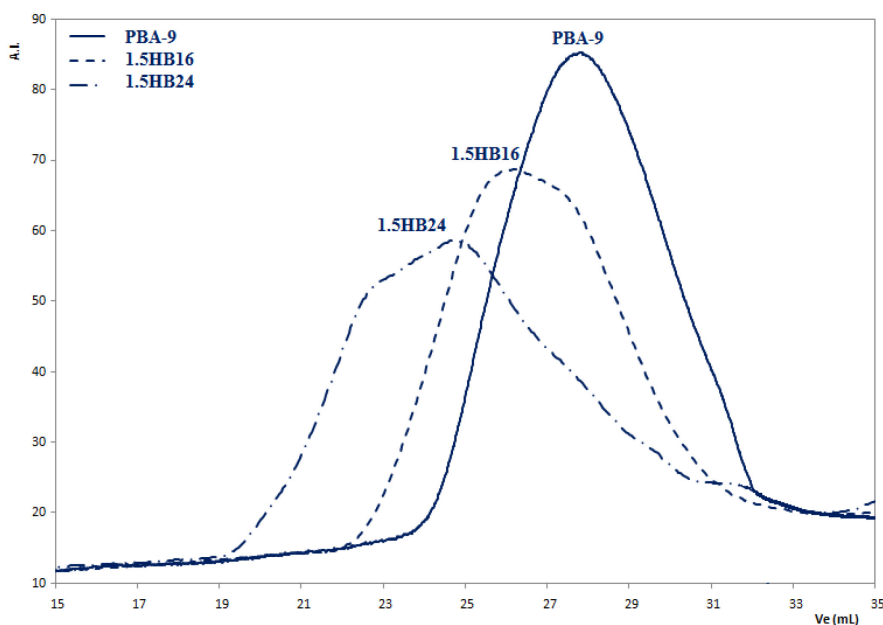


Figure 2.2: SEC traces of PBA-9, 1.5HB16, and 1.5HB24 samples.

### 2.3.3 Nuclear magnetic resonance spectroscopy (NMR)

Each HB polyesters was characterized by  $^1\text{H}$ -NMR analysis using  $\text{CDCl}_3$  and  $\text{DMSO-d}_6$  as solvents at 25 and 60 °C, respectively. From the comparison between  $^1\text{H}$ - NMR spectra of PBA-9 pre-polymer and HB samples, it is evident that HB polymers contain a molar fraction of TMP units close to that in the feed, indicating the complete conversion of the TMP moles used. As an example, in Figure 2.3, the  $^1\text{H}$ -NMR spectra of PBA-9, 1.5HB16, 3HB16, 5HB16, 7HB16, and 10HB16 are portrayed; the peak values are reported in Table 2.3 and are in agreement with the chemical shifts of the PBA and the TMP model compounds.

**Table 2.3: Assignments of proton signals due to PBA oligomers and their end-groups, TMP unit, and TMP unit linked to PBA sequences as observed in  $^1\text{H}$ -NMR spectra.**

Structures	H	Chemical Shift (ppm)
a) $\left( \begin{array}{c} \text{O} \\ \parallel \\ \text{CH}_2 - (\text{CH}_2)_2 - \text{CH}_2 - \text{O} - \text{C} - \text{O} - \text{CH}_2 - (\text{CH}_2)_2 - \text{CH}_2 - \text{O} \end{array} \right)_n$	<b>a</b>	4.09
	<b>b</b>	1.69
	<b>c</b>	2.33
$\text{CH}_3\text{O}-$	<b>c'</b>	3.40
$-\text{CH}_2-(\text{CH}_2)_2-\text{CH}_2-\text{OH}$	<b>d</b>	1.65
	<b>e</b>	3.67
b) $\begin{array}{c} \chi \quad \gamma \\ \text{CH}_2-\text{OH} \\ \alpha \quad \beta \\ \text{CH}_3-\text{CH}_2-\text{C} \\ \chi \quad \gamma \\ \text{CH}_2-\text{OH} \\ \chi \quad \gamma \\ \text{CH}_2-\text{OH} \\ \gamma \end{array}$	<b><math>\alpha</math></b>	0.84
	<b><math>\beta</math></b>	1.25
	<b><math>\chi</math></b>	3.73
	<b><math>\gamma</math></b>	2.74
c) $\begin{array}{c} \chi \quad \gamma \\ \text{CH}_2-\text{OH} \\ \alpha \quad \beta \\ \text{CH}_3-\text{CH}_2-\text{C} \\ \text{CH}_2-\text{O}\sim\sim\sim \\ \text{CH}_2-\text{O}-\text{CO}-(\text{CH}_2)_4-\text{CO}\sim\sim\sim \\ \delta \end{array}$	<b><math>\alpha</math></b>	0.87
	<b><math>\beta</math></b>	1.46
	<b><math>\chi</math></b>	3.73
	<b><math>\gamma</math></b>	2.74
	<b><math>\delta</math></b>	4.06

Protons belonging to TMP units within the HB copolymer chains resonate at 0.87 ppm (triplet,  $\text{H}^\alpha$ ), 1.46 ppm (quartet,  $\text{H}^\beta$ ), 3.73 ppm (triplet,  $\text{H}^\chi$ ), and 4.06 ppm (triplet,  $\text{H}^\delta$ ); in particular, the signals at 3.73 ppm reveal the unreacted methylol groups ( $-\text{CH}_2-\text{OH}$ ) belonging to TMP units, whereas the signal at 4.06 ppm is related to the corresponding groups linked to PBA sequences.

All  $^1\text{H}$ -NMR spectra of HB samples display the same signals pattern (with a little variation of the relative signal intensities).

Only 5HB44 sample was analyzed by solid-state  $^{13}\text{C}$ -NMR since it appears insoluble in most commonly solvents used to dissolve the other HB species. As an example, in Figure 2.4, the  $^{13}\text{C}$ -NMR spectra of 5HB44 sample is portrayed; the peak values are reported in details in Table 2.4. It is interesting to note the absence of signals related to  $-\text{OCH}_3$  end-groups in accordance to the data obtained by MALDI-TOF characterization on 5HB30 sample (the last soluble sample synthesized using 5 molar percent of TMP).

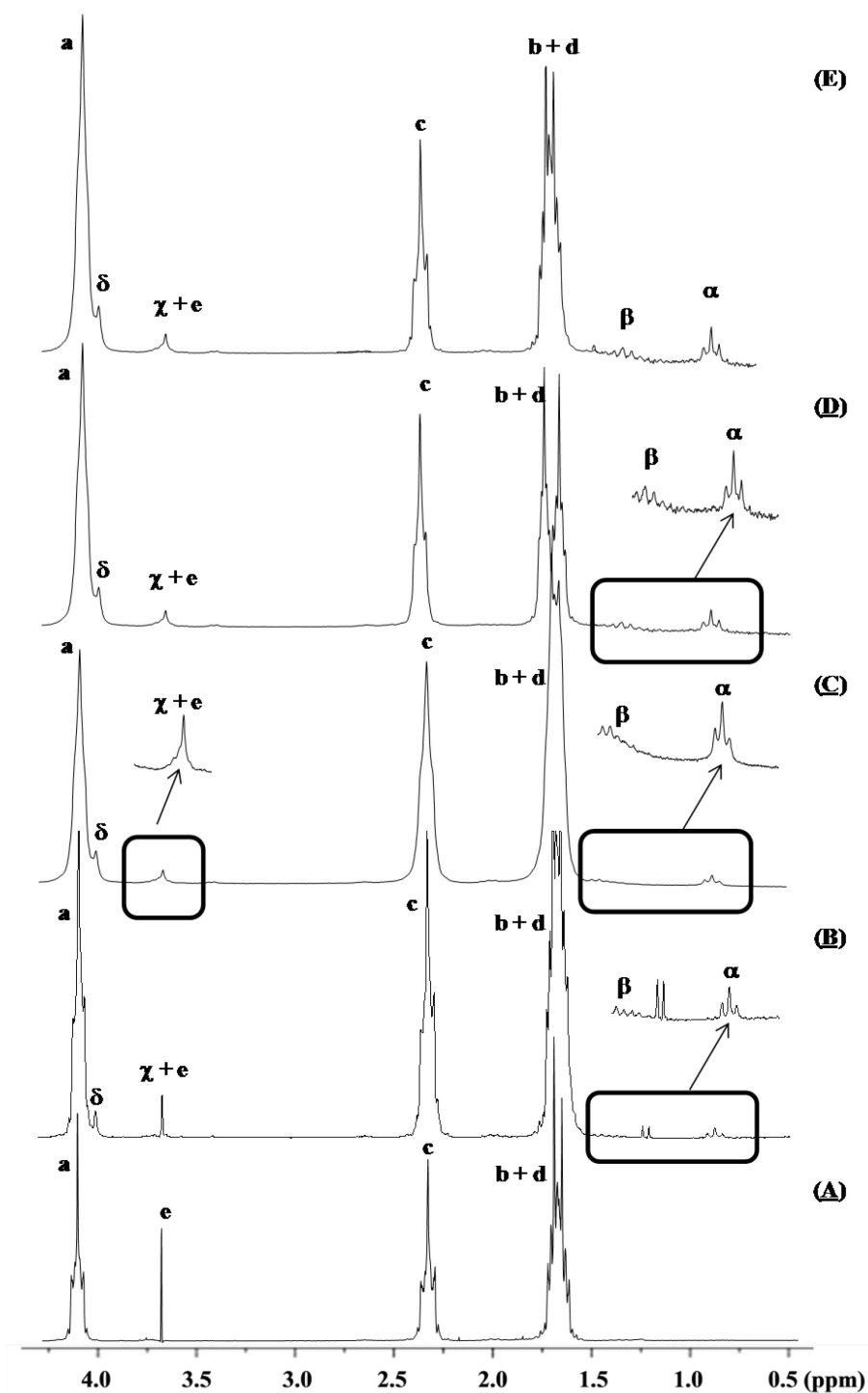
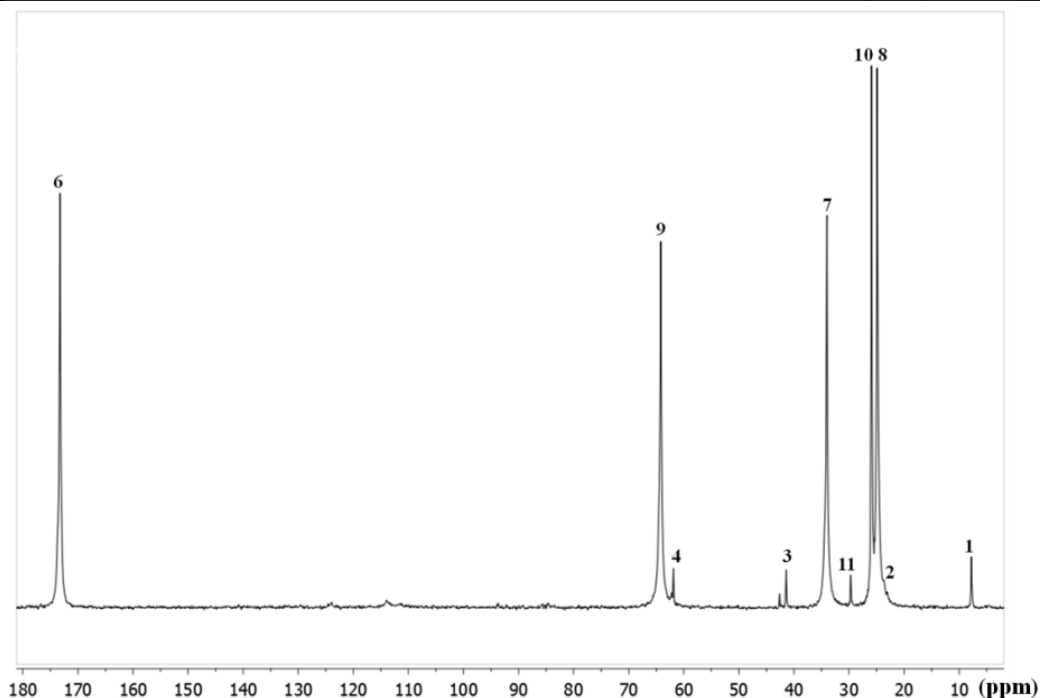


Figure 2.3: Sections of the  $^1\text{H}$ -NMR spectra of PBA-9 (A), 1.5HB16 (B), 3HB16 (C), 7HB16 (D), and 10HB16 (E) samples.

**Table 2.4: Assignments of carbon signals due to HB species as observed in  $^{13}\text{C}$ -NMR spectrum of 5HB44 sample.**

Structures	C	Chemical Shift (ppm)
	6	172.2
	5	66.2
	9	64.6
	4	63.1
	12	51.7
	3	43.3
	7	34.7
	11	29.1
	10	25.4
	8	24.7
	2	22.2
	1	7.8



**Figure 2.4: Solid-state  $^{13}\text{C}$ -NMR spectrum of 5HB44 sample.**

According to the literature, NMR spectra can be used to determine the DB in HB polymers,<sup>1-5,13-15,17,20,34,35,37-39</sup> which is a needful prerequisite to describe their structural features and correlate the structure with their properties.<sup>31</sup> The average degree of branching, first proposed by Fréchet and coworkers,<sup>32</sup> is commonly calculated as the sum of the terminal and dendritic units divided by the total sum of all repeating units as previously reported in Equation 1.2:



$$DB_{Fréchet} = \frac{D+T}{D+L+T} \quad (1.2)$$

where D, T and L are the number of dendritically, terminally, and linearly incorporated monomer units in the HB polymer. Determination of DB is usually limited to the cases, in which the fractions of each component (D, L, and T) are distinguishable, mostly observable with the spectroscopic methods such as NMR and FT-IR. However, for our HB samples, it was not possible to calculate their DB from  $^1\text{H-NMR}$  spectra, because the signals corresponding to the dendritic, linear, and terminal units cannot be assigned unequivocally. The NMR analysis provided qualitative information on the formation of the HB samples, however, it was not possible to identify the structure and composition of their components.

### 2.3.4 MALDI-TOF MS

To further investigate on the structural features of all synthesized HB samples, MALDI-TOF MS analysis in positive mode using the  $\alpha$ -cyano-4-hydroxycinnamic acid as a matrix was carried out, because comprehensive investigation via MALDI-TOF MS could lead to quantitative information on the structure of the components of the synthesized HBs. The MALDI mass spectra of 1.5HB16 and 1.5HB24 samples show a series of mass peaks in the mass range  $m/z$  1'000–8'000 (see Figure 2.5). In Figure 2.5a, related to 1.5HB16 sample, besides the peaks belonging to HB chains, three mass peak series corresponding to the linear unreacted PBA macromolecules  $A_n$ ,  $B_n$ , and  $C_n$  are visible (see Table 2.2). Their relative intensity changes as the reaction time increases but in a different way respect to the corresponding PBA-9 pre-polymer, displayed in Figure 2.1a. In particular, in the range higher than  $m/z$  2'500, the intensity of peaks  $A_n$  decreases drastically in the mass spectrum of 1.5HB24 sample (Figure 2.5b) obtained at 24 h, whereas the intensity of the peaks associated with the  $C_n$  species increases. This result suggests that, as expected, with low concentration of TMP (1.5 mol %), its reactive hydroxyl groups mainly react with the methyl ester end-groups of the PBA pre-polymer leading to the formation of HB species:  $IP_{A_n}$ ,  $IP_{B_n}$ ,  $IP_{C_n}$ , and  $IP_2A_n$  (see Table 2.5 and Table 2.6), which are terminated with methyl esters, and in lower extent with the PBA chains terminated with -OH groups (species  $B_n$  and  $C_n$ ). As the reaction time increases and the amount of the methyl ester end-groups decreases, the transesterification reactions, involving the ester inner groups, occur more significantly generating HB chains with more TMP units (i.e., species  $IP_2A_n$ ,  $IP_2B_n$ ,

IP<sub>2</sub>C<sub>n</sub>, IP<sub>2</sub>D<sub>n</sub>, IP<sub>3</sub>B<sub>n</sub>, etc. in Table 2.6) and causing the decrease of PBA linear macromolecules.

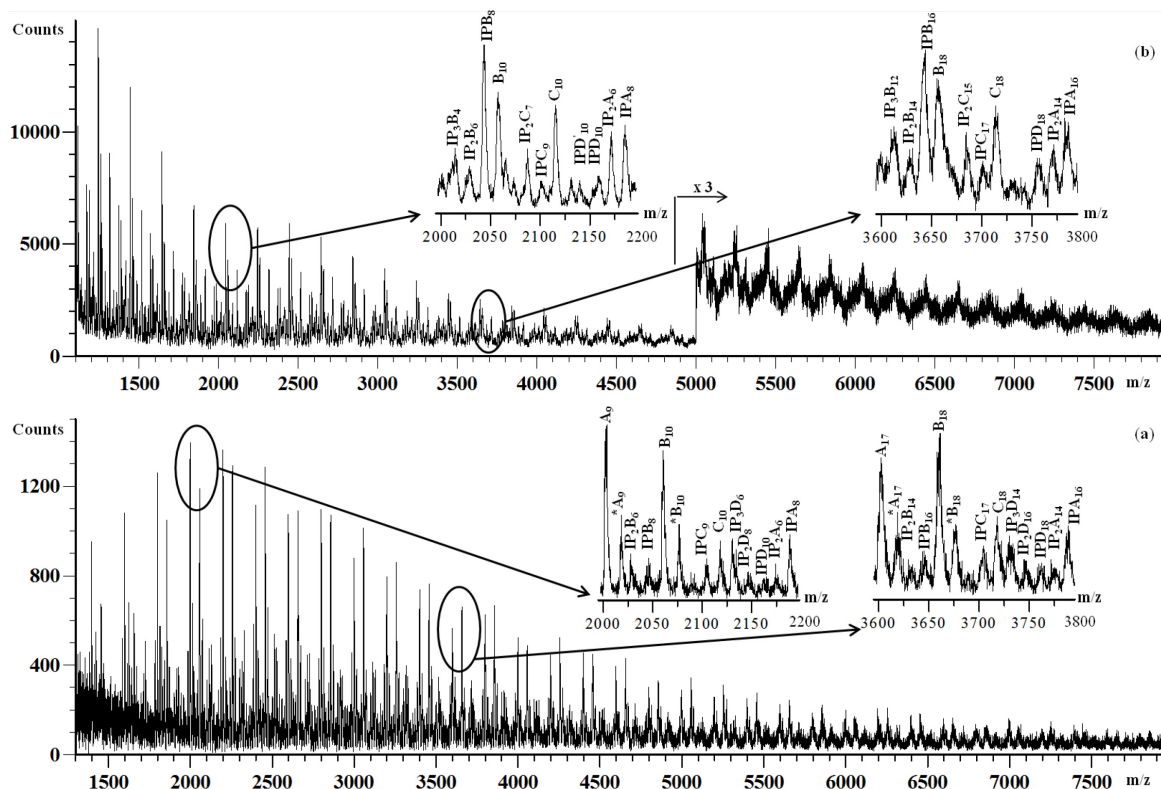
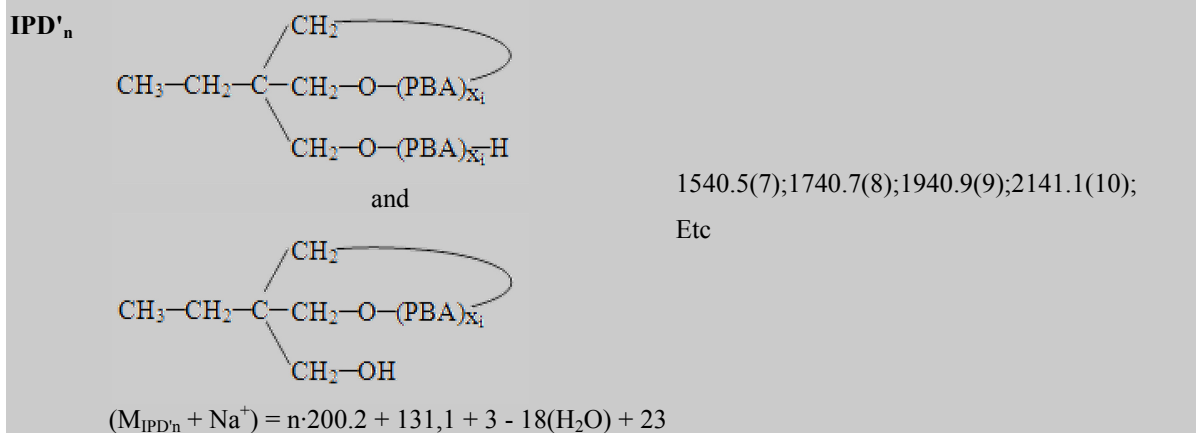
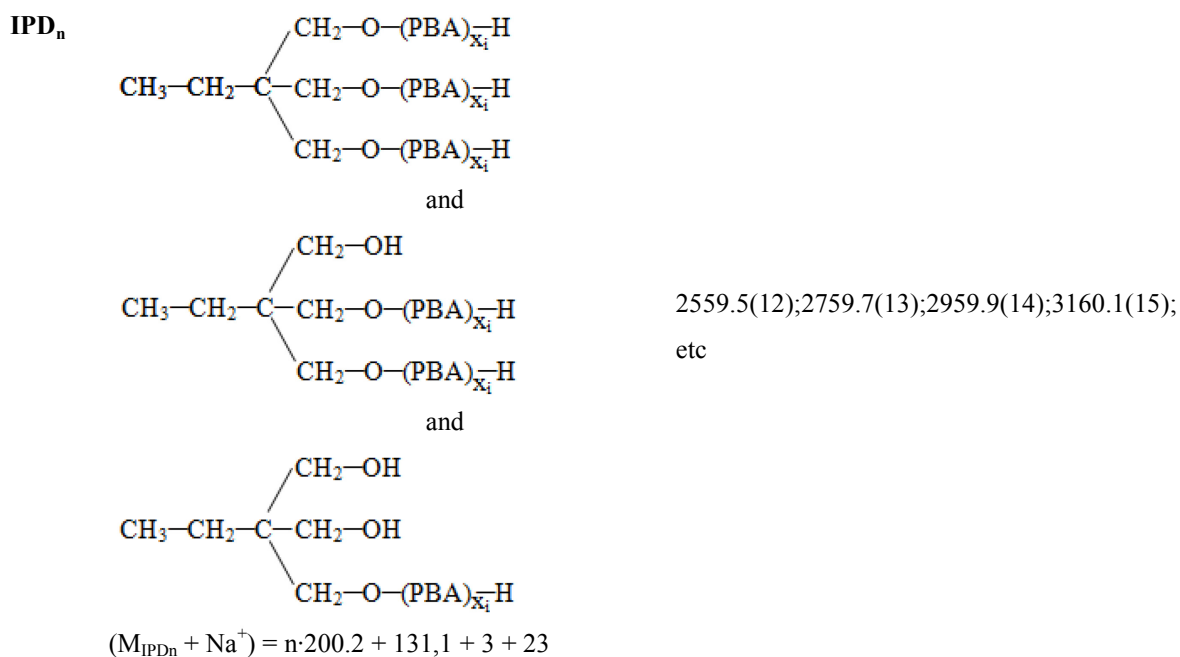
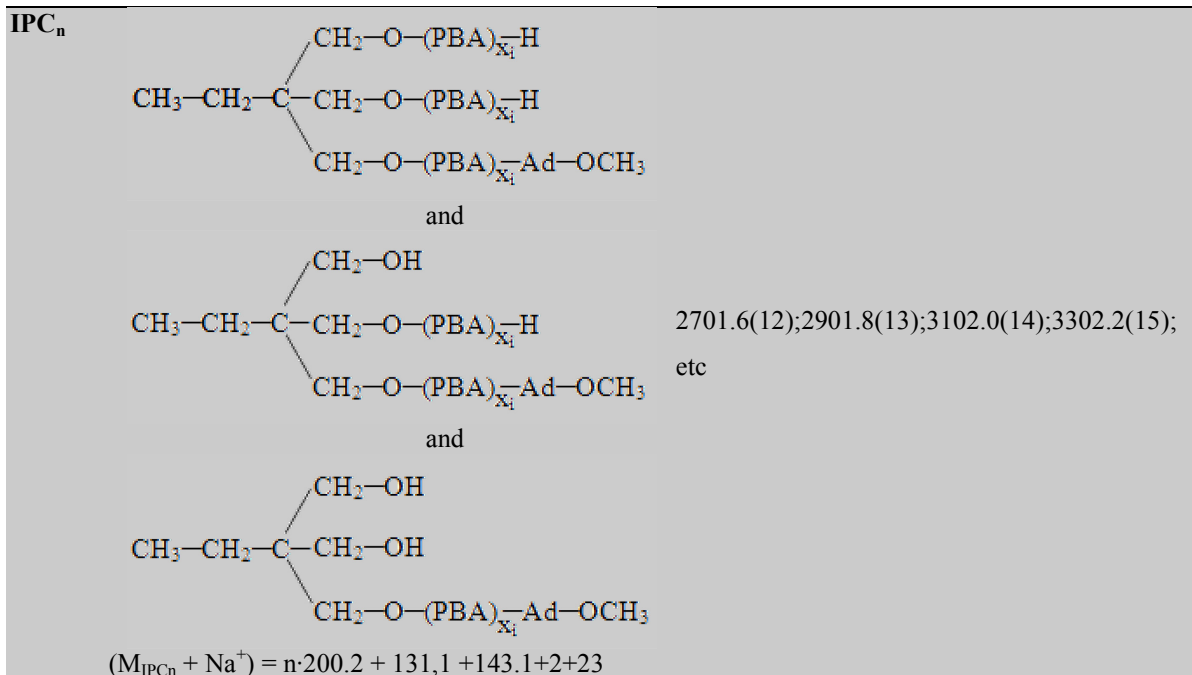


Figure 2.5: MALDI-TOF mass spectra of 1.5HB16 (a) and 1.5HB24 (b) samples. In the insets some enlarged sections of these spectra are reported.

Table 2.5: Structural assignments of peaks displayed in the MALDI mass spectra of HB samples.

Species	Structures <sup>a,b,c</sup>	[M+Na] <sup>+</sup> (n) <sup>d</sup>
IPAn	$\begin{array}{l} \text{CH}_2\text{-O-(PBA)}_{X_1}\text{-Ad-OCH}_3 \\ \text{CH}_3\text{-CH}_2\text{-C} \begin{cases} \text{CH}_2\text{-O-(PBA)}_{X_1}\text{-Ad-OCH}_3 \\ \text{CH}_2\text{-O-(PBA)}_{X_1}\text{-Ad-OCH}_3 \end{cases} \end{array}$	2785.6(11);2985.8(12);3186.0(13);3386.2(14); etc
	$(M_{IPAn} + Na^+) = n \cdot 200.2 + 131.1 + 3 \cdot 143.1 + 23$	
IPBn	$\begin{array}{l} \text{CH}_2\text{-O-(PBA)}_{X_1}\text{-H} \\ \text{CH}_3\text{-CH}_2\text{-C} \begin{cases} \text{CH}_2\text{-O-(PBA)}_{X_1}\text{-Ad-OCH}_3 \\ \text{CH}_2\text{-O-(PBA)}_{X_1}\text{-Ad-OCH}_3 \end{cases} \end{array}$ <p style="text-align: center;">and</p> $\begin{array}{l} \text{CH}_2\text{-OH} \\ \text{CH}_3\text{-CH}_2\text{-C} \begin{cases} \text{CH}_2\text{-O-(PBA)}_{X_1}\text{-Ad-OCH}_3 \\ \text{CH}_2\text{-O-(PBA)}_{X_1}\text{-Ad-OCH}_3 \end{cases} \end{array}$	2643.5(11);2843.7(12);3043.9(13);3244.1(14); etc
	$(M_{IPBn} + Na^+) = n \cdot 200.2 + 131.1 + 2 \cdot 143.1 + 1 + 23$	



<sup>a</sup>  $(-PBA-)_n = -CO-(CH_2)_4-CO-O-(CH_2)_4-O-$ ;  $-Ad- = -CO-(CH_2)_4-CO-$ ;

<sup>b</sup> For HB species terminated with hydroxyl groups correspond several isobar structures as highlighted for the families IPB, IPC and IPD;

<sup>c</sup>  $n = \sum X_i$ ;

<sup>d</sup> The experimental mass was measured with an accuracy of  $\pm (0.5 \div 0.6)$  Da.

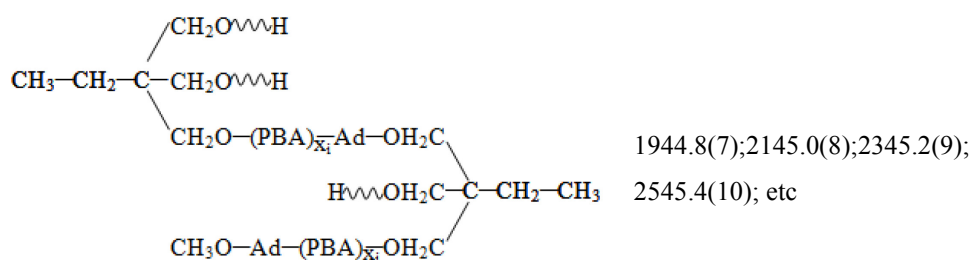
The mass spectrum of 1.5HB24, see Figure 2.5b, shows also weak peaks corresponding to HB chains containing ether units (i.e., species IPD'<sub>n</sub> in Table 2.5). This species may be formed by intramolecular transesterification reactions of the HB chains having hydroxyl end-groups, as sketched in Scheme 2.3a.

A similar behavior was observed for 1.5HB16§, 1.5HB24§, and 1.5HB30§ samples, which were prepared using a DMA/BD molar ratio of 1.001/1 and 1.5 molar percent of TMP (see Table 2.1).

**Table 2.6: Structural assignments of peaks displayed in the MALDI mass spectra of HB families, ether and cyclic units.**

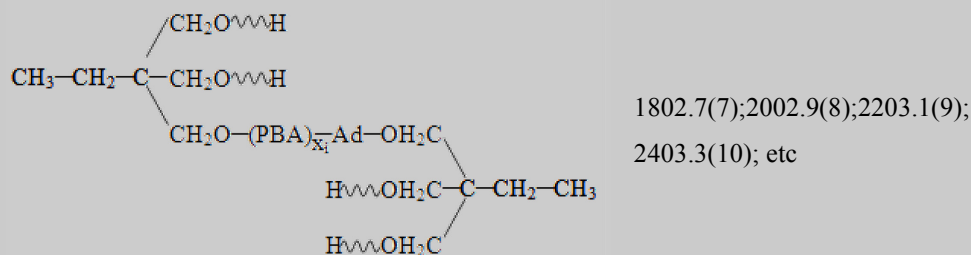
Species	Structures <sup>a,b</sup>	$[M+Na]^+(n)^c$	
<b>(IP<sub>2</sub>A)<sub>n</sub></b>	$CH_3-CH_2-C \begin{cases} CH_2O-(PBA)_{X_1}-Ad-OCH_3 \\ CH_2O-(PBA)_{X_1}-Ad-OCH_3 \\ CH_2O-(PBA)_{X_1}-Ad-OH_2C \\ CH_3O-Ad-(PBA)_{X_1}-OH_2C \\ CH_3O-Ad-(PBA)_{X_1}-OH_2C \end{cases}$	2371.1(7); 2571.3(8); 2771.5(9); 2971.7(10); etc	
	$(M_{(IP_2A)n} + Na^+) = n \cdot 200.2 + 2 \cdot 131.1 + 4 \cdot 143.1 + 112.1 + 23$		
	<b>(IP<sub>2</sub>B)<sub>n</sub></b>	$CH_3-CH_2-C \begin{cases} CH_2O \rightsquigarrow H \\ CH_2O-(PBA)_{X_1}-Ad-OCH_3 \\ CH_2O-(PBA)_{X_1}-Ad-OH_2C \\ CH_3O-Ad-(PBA)_{X_1}-OH_2C \\ CH_3O-Ad-(PBA)_{X_1}-OH_2C \end{cases}$	2229.0(7); 2429.2(8); 2629.4(9); 2829.6(10); etc
		$(M_{(IP_2B)n} + Na^+) = n \cdot 200.2 + 2 \cdot 131.1 + 3 \cdot 143.1 + 112.1 + 1 + 23$	
		<b>(IP<sub>2</sub>C)<sub>n</sub></b>	$CH_3-CH_2-C \begin{cases} CH_2O-(PBA)_{X_1}-Ad-OCH_3 \\ CH_2O \rightsquigarrow H \\ CH_2O-(PBA)_{X_1}-Ad-OH_2C \\ H \rightsquigarrow OH_2C \\ CH_3O-Ad-(PBA)_{X_1}-OH_2C \end{cases}$
$(M_{(IP_2C)n} + Na^+) = n \cdot 200.2 + 2 \cdot 131.1 + 2 \cdot 143.1 + 112.1 + 2 + 23$			

(IP<sub>2</sub>D)<sub>n</sub>



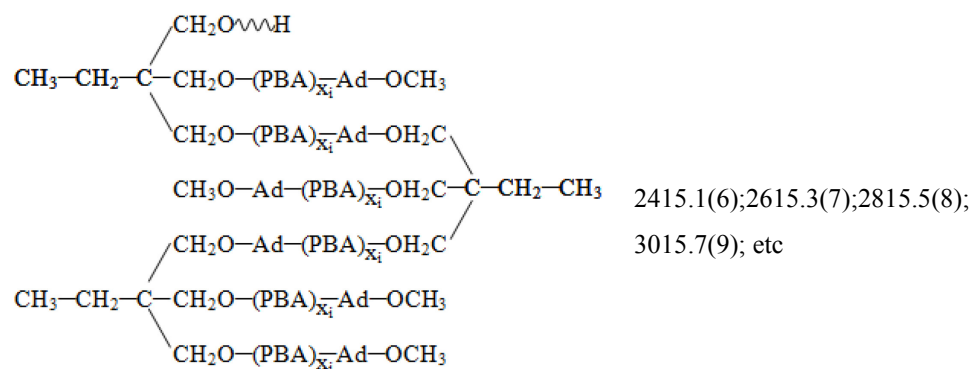
$$(M_{(\text{IP}_2\text{D})_n} + \text{Na}^+) = n \cdot 200.2 + 2 \cdot 131.1 + 143.1 + 112.1 + 3 + 23$$

(IP<sub>2</sub>E)<sub>n</sub>



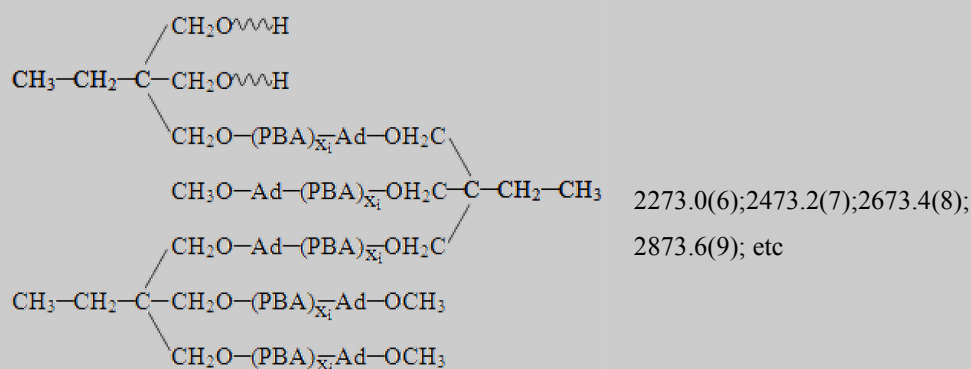
$$(M_{(\text{IP}_2\text{E})_n} + \text{Na}^+) = n \cdot 200.2 + 2 \cdot 131.1 + 112.1 + 4 + 23$$

(IP<sub>3</sub>B)<sub>n</sub>

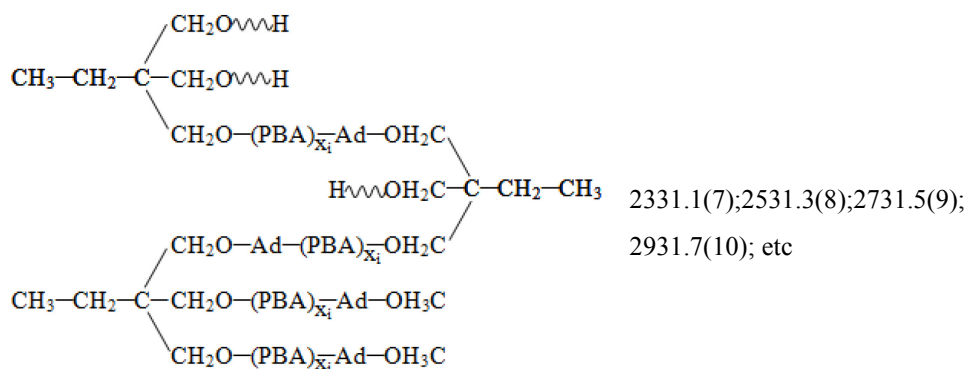


$$(M_{(\text{IP}_3\text{B})_n} + \text{Na}^+) = n \cdot 200.2 + 3 \cdot 131.1 + 4 \cdot 143.1 + 2 \cdot 112.1 + 1 + 23$$

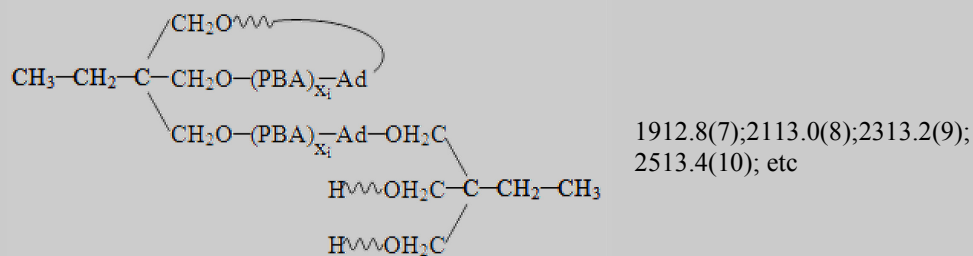
(IP<sub>3</sub>C)<sub>n</sub>



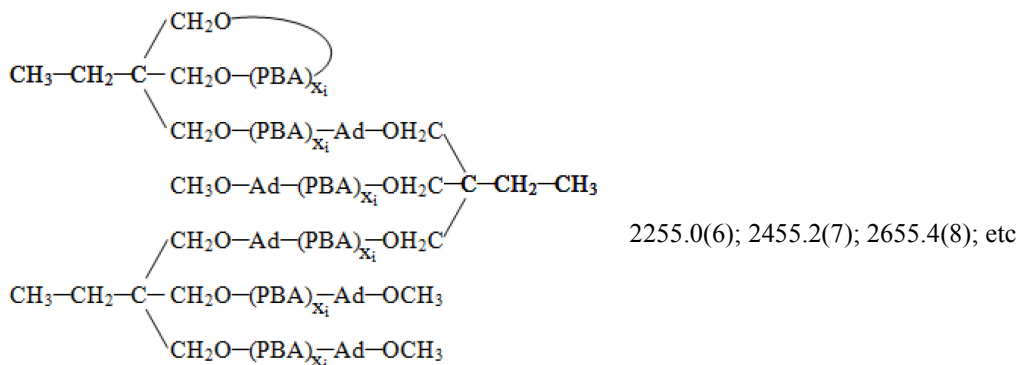
$$(M_{(\text{IP}_3\text{C})_n} + \text{Na}^+) = n \cdot 200.2 + 3 \cdot 131.1 + 3 \cdot 143.1 + 2 \cdot 112.1 + 2 + 23$$

$(IP_3D)_n$ 


$$(M_{(IP_3D)_n} + Na^+) = n \cdot 200.2 + 3 \cdot 131.1 + 2 \cdot 143.1 + 2 \cdot 112.1 + 3 + 23$$

 $(IP_2Ec)_n$ 


$$(M_{(IP_2Ec)_n} + Na^+) = n \cdot 200.2 + 2 \cdot 131.1 + 2 \cdot 112.1 + 2 + 23$$

 $(IP_3C')_n$ 


$$(M_{(IP_3C')_n} + Na^+) = n \cdot 200.2 + 3 \cdot 131.1 + 3 \cdot 143.1 + 2 \cdot 112.1 + 2 - 18 + 23$$

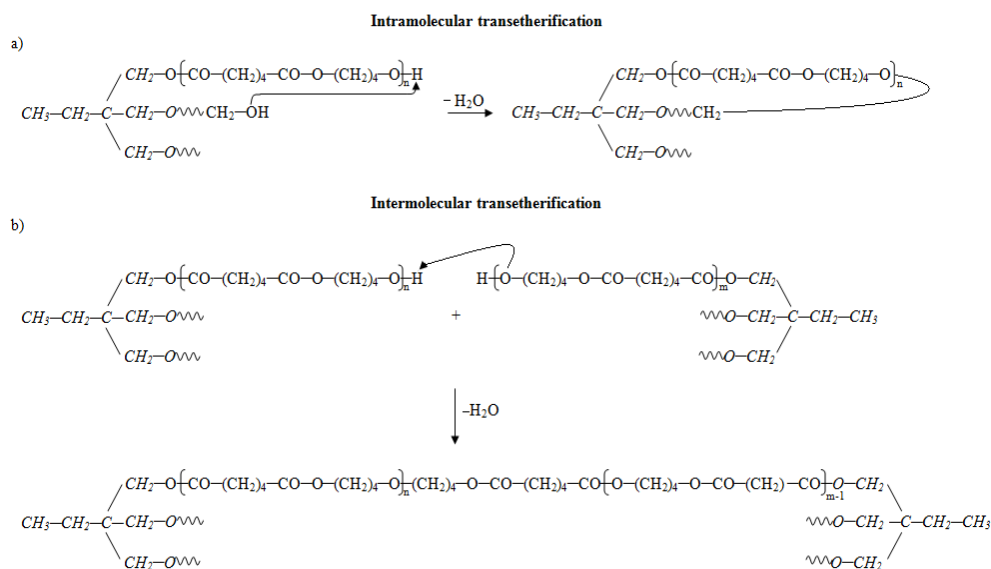
<sup>a</sup>  $(-PBA-)_n = -CO-(CH_2)_4-CO-O-(CH_2)_4-O-$ ;  $-(Ad)- = -CO-(CH_2)_4-CO-$ ;

<sup>b</sup>  $n = \sum x_i$

<sup>c</sup> The experimental mass was measured with an accuracy of  $\pm (0.5 \div 0.6)$  Da.

In the case of 3HB16 sample, see Figure 2.6, the PBA oligomers belonging to the families  $A_n$  disappear in the MALDI mass spectrum, suggesting that the transesterification reactions between the methyl end-groups of the PBA pre-polymer and the hydroxyl groups of the TMP units reach the completion at reaction time higher than 24 h, at 180 °C under vacuum. However, the mass spectrum of this sample shows again the presence of the linear PBA oligomers  $B_n$  and  $C_n$ , besides the peaks series due to sodiated ions of the HB chains. The PBA oligomers  $B_n$  and  $C_n$  could be formed by the transesterification reactions, which

involve the ester inner groups of PBA units within the HB macromolecules and the hydroxyl groups belonging to TMP units or to the PBA chains, as schematized in Scheme 2.4. As an example, in Figure 2.6, the MALDI mass spectrum recorded in reflectron mode of 3HB16 sample is shown. It shows a series of peaks due to linear PBA chains belonging to the families of  $B_n$  and  $C_n$  oligomers, and HB chains containing different TMP units, as highlighted in the inset in Figure 2.6 .



**Scheme 2.3: Transesterification reactions.**

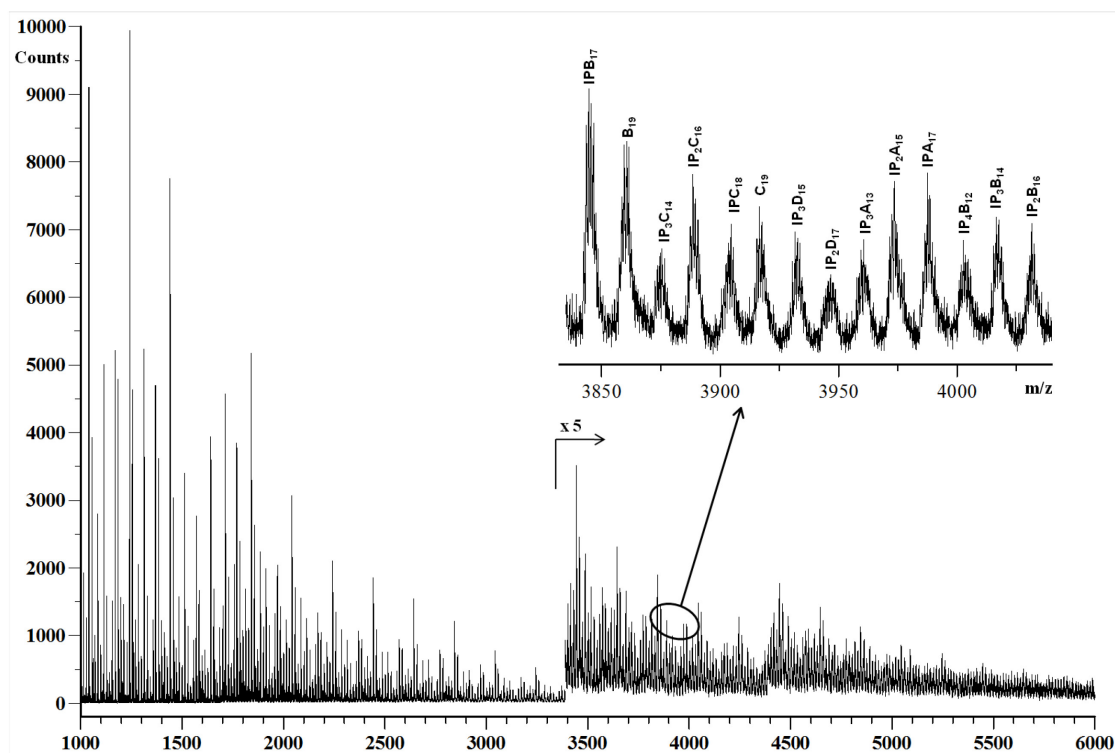
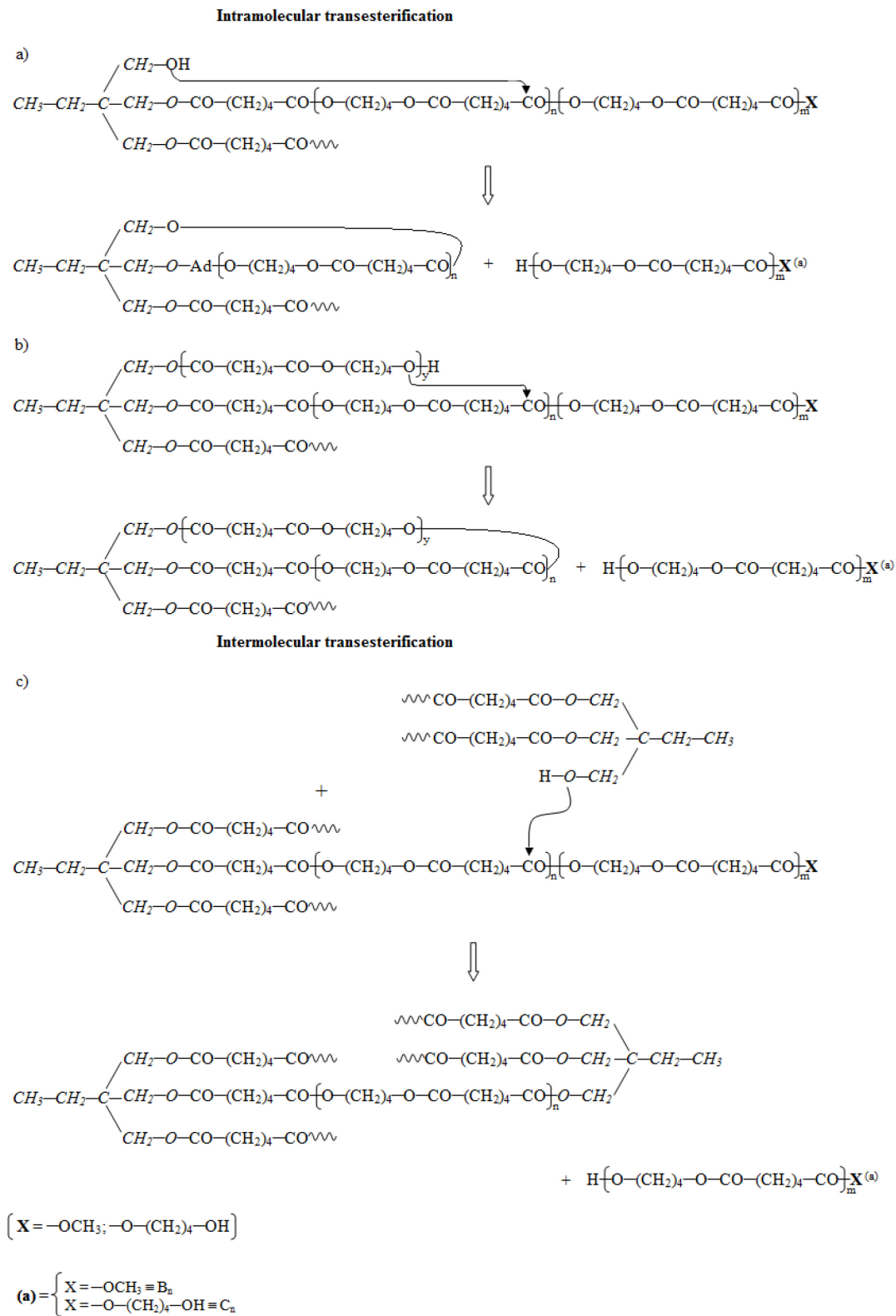


**Figure 2.6: MALDI-TOF mass spectrum of 3HB16 sample.**

Similar results were obtained for HB samples prepared using 3, 5, 7, and 10 molar percent of TMP. MALDI spectra of these samples do not show peaks corresponding to families  $A_n$ , but appear enriched of the HB families containing three or more TMP units (i.e., species  $IP_3A_n$ ,  $IP_3B_n$ ,  $IP_3C_n$ ,  $IP_3D_n$ ,  $IP_4B_n$ , etc.).



Scheme 2.4: Transesterification reactions.



The MALDI mass spectra of the synthesized HBs using an amount of TMP higher than 3 molar percent and longer reaction time also show intense peaks because of HB macromolecules containing cyclic branches (i.e., species  $IP_2Ec_n$ ), which may be formed through the intramolecular transesterification mechanism, as well as families of peaks containing ether units formed by (inter and intra)-molecular.

For more details, in Figure 2.7, the HB structure variation of the species obtained using 5 molar percent of TMP for different reaction time (16 – 24 – 30 h) is reported compared to linear PBA-9 pre-polymer. In this figure, the MALDI mass spectra of PBA-9 (a), 5HB16 (b), 5HB24 (c), 5HB30 (d) samples and the enlarged section of these spectra are reported in the mass range  $m/z$  of 1'000-8'000.

The MALDI mass spectrum of 5HB16 sample, Figure 2.7b, shows both mass peaks related to free oligomers  $A_n$ ,  $B_n$ ,  $C_n$  and peaks belonging to HB chains. The relative intensity of free oligomers changes as the reaction time increases. In particular, the intensity of  $A_n$  family in the mass range higher than 2'400  $m/z$  decreases drastically, whereas the intensity of the peaks associated with  $B_n$  and  $C_n$  species increases. This is due to the condensation between the reactive hydroxyl groups of TMP and the methyl ester end-groups of the pre-polymer, leading to the formation of the HB species  $IPA_n$ ,  $IPB_n$ ,  $IPC_n$ ,  $IPD_n$ . In this mass spectrum, the presence of two families,  $IP_2C_n$  and  $IP_2D_n$ , (see Table 2.6) is also visible. These families are made by two TMP units linked together, and are characterized by signals with a rather short intensity, being in the early stage of formation.

The MALDI mass spectrum of 5HB24 sample, Figure 2.7c, shows only peaks related to  $B_n$ ,  $C_n$  free oligomers and peaks belonging to HB chains. The disappearance of  $A_n$  family indicates the consumption of linear  $-OCH_3$  oligomeric starting species. As the reaction time increases from 16 h to 24 h, the amount of the methyl ester end-groups decreases. Consequently, the transesterification reactions involving the ester inner groups occur more significantly, generating HB chains with more TMP units linked together, such as  $IP_2A_n$ ,  $IP_2B_n$ ,  $IP_2C_n$ ,  $IP_2D_n$ ,  $IP_2E_n$ ,  $IP_3B_n$ ,  $IP_3C_n$ ,  $IP_3D_n$  species.

The MALDI mass spectrum of 5HB30 sample, Figure 2.7d, shows only peaks related to HB chains. In particular, it is worth noting the presence of peaks corresponding to HB chains containing ether units (species  $IP_3C'_n$ ), formed by (intra e inter)-molecular transesterification reactions and cyclic branches (species  $IP_2Ec_n$ ) due to intra-molecular transesterification.

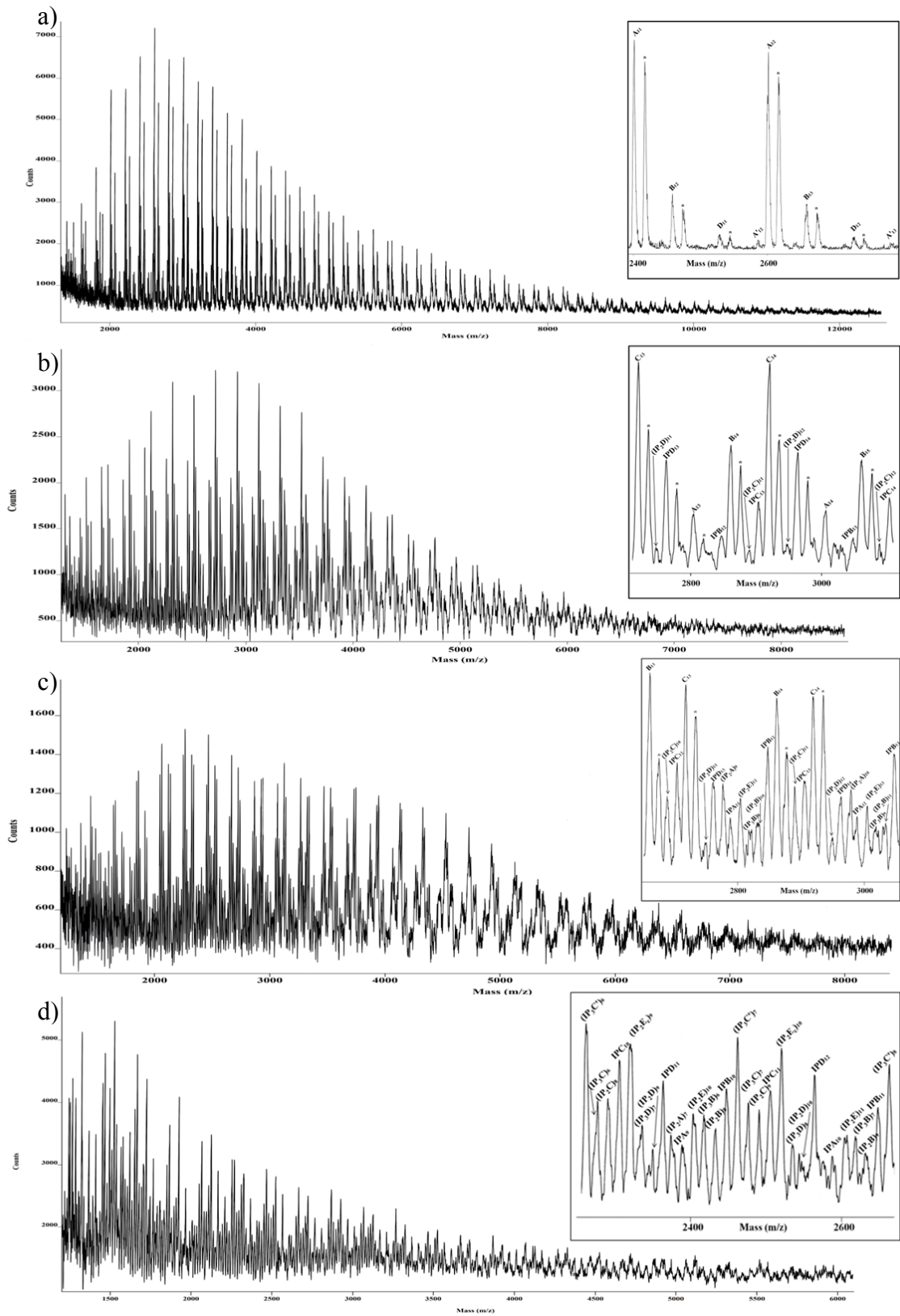


Figure 2.7: MALDI-TOF mass spectra of PBA-9 (a), 5HB16 (b), 5HB24 (c), 5HB30 (d) samples.

5HB44 sample was not characterized by MALDI-TOF since it is not soluble. The reason of this insolubility is linked to the formation of cross-linked portion.<sup>12,17</sup>

The recorded MALDI-TOF mass spectra contributed to provide interesting information about the composition of HBs and indicated that the synthetic procedure used in this work could lead to the formation of HB samples containing either HB or linear PBA macromolecules. The molar percent of linear PBA chains decreases as the amount of TMP in the feed and the reaction time increase. Mass spectra provided unequivocally information on the TMP units and also on the end-groups present in the synthesized HB macromolecules. MALDI-TOF mass spectra of HB samples synthesized using 5, 7, and 10 molar percent of TMP reveal that HB chains terminated with hydroxyl groups were preferentially formed (i.e., species  $IPD_n$ ,  $IP_2D_n$ ). These families of HB macromolecules can give (inter and intra)-molecular transesterification as the reaction time increases, and the corresponding mass spectra show families of peaks due to HB chains containing ether units. The relative intensities of the last peaks series increase with the reaction time and the molar percent of TMP. In these mass spectra, the relative intensities of the peaks corresponding to HB macromolecules containing cyclic branches (i.e., mass series  $IP_2Ec_n$ ) also increase.

### 2.3.5 SEC/MALDI-TOF characterization

SEC curves of the HBs calibrated with linear PS standards provide a large distribution of MMs ( $PDI > 2$ ). Moreover, they show that their macromolecular components have molecular masses ranging from about 1'000 to 30'000 g/mol or higher.

Therefore, the corresponding MALDI-TOF mass spectra discussed above could be scarcely representative of the real and total composition of the polydispersed HB polyesters analyzed, because low molecular mass species may be more easily desorbed than high molecular mass ones. In fact, they show peaks only in the mass range  $m/z$  1'000–9'000. We believe that HB polyester chains dominate in the MM range higher than 10'000 g/mol and therefore, are not detected in the MALDI mass spectra of the neat HBs. To overcome this problem, some representative HB samples were fractionated by the SEC apparatus, and then, the narrowly distributed SEC fractions were analyzed by MALDI-TOF MS to obtain reliable information on the composition as a function of the elution volume ( $V_e$ ). Furthermore, as for samples with narrow MM distribution ( $PDI < 1.05$ ), the MALDI-TOF technique provides their absolute MMs ( $M_w$  and  $M_n$ ),<sup>33,34,39</sup> from the MALDI spectrum of each SEC fractions, we can calculate its absolute average MMs and then, calibrate the SEC curves again using these values as a function of the  $V_e$  of each fraction (self-calibration). Then, by the refereed absolute SEC/MALDI-TOF calibration,

we have calculated the reliable average MMs of all HB samples, and the results are reported in Table 2.1. The calibration curves obtained for the fractionated HBs agreed with Equation 2.7, which was applied to calculate the  $M_w$  and  $M_n$  of HB samples synthesized.

$$\log M_w = 18.18 - 1.0817V_e + 0.01308 (V_e)^2 \quad (2.7)$$

The SEC/MALDI-TOF results obtained for 3HB16 and 3HB24§ samples are discussed below. In Figure 2.8, an illustrative example of the SEC trace of 3HB16 sample, together with the MALDI spectra of fractions eluted at 22.625 (F15), 23.375 (F18), 26.125 (F29), 27.125 (F33), 28.625 (F39), and 29.375 mL (F42), is reported.

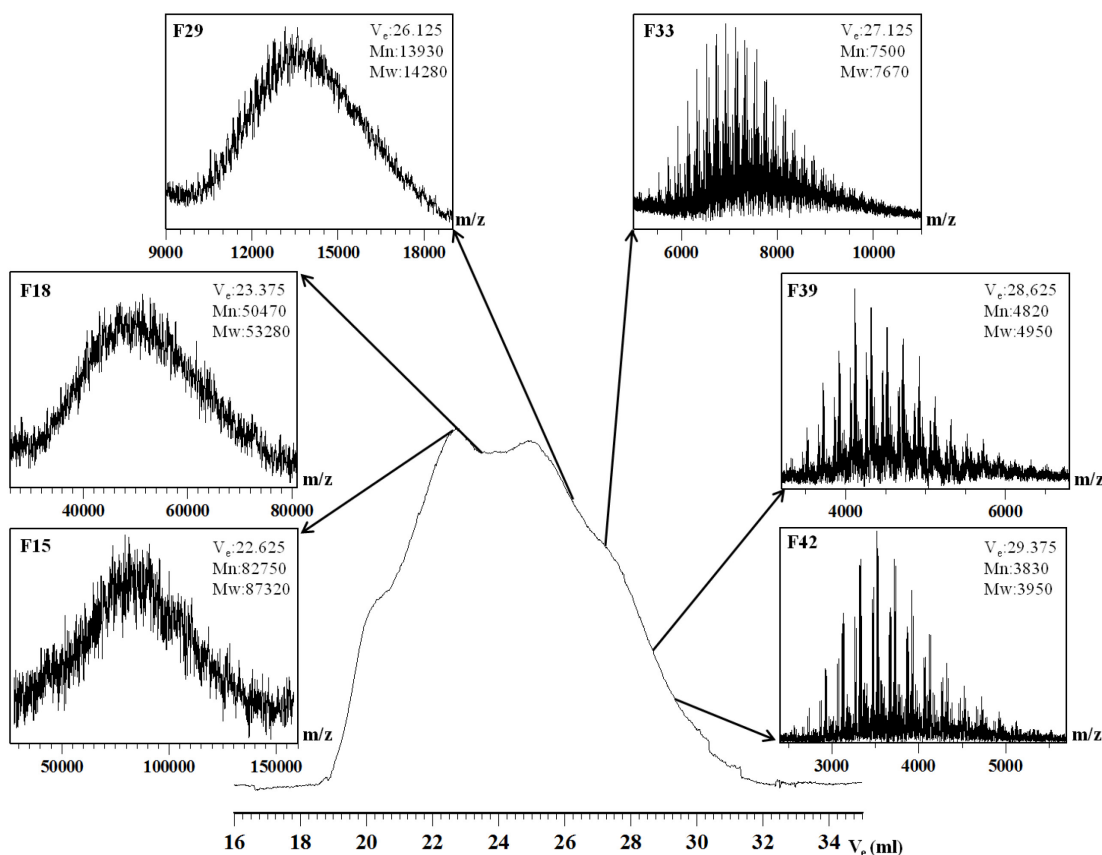


Figure 2.8: SEC chromatogram and MALDI-TOF mass spectra of some fractions of 3HB16 sample.

All MALDI-TOF mass spectra confirmed a narrow distribution ( $PDI < 1.06$ ) for samples obtained by SEC fractionation. As shown in Figure 2.8, the MALDI mass spectra of the SEC fractions display well-resolved peaks from 1'000 to 10'000-12'000  $m/z$ , allowing the assignment of each peak to the corresponding oligomers and also the identification of the end-groups, and consequently of the most-probable structures of the formed HB macromolecules. Therefore, the mass spectra allow the identification of the branching units (TMP) present in the formed HB chains.

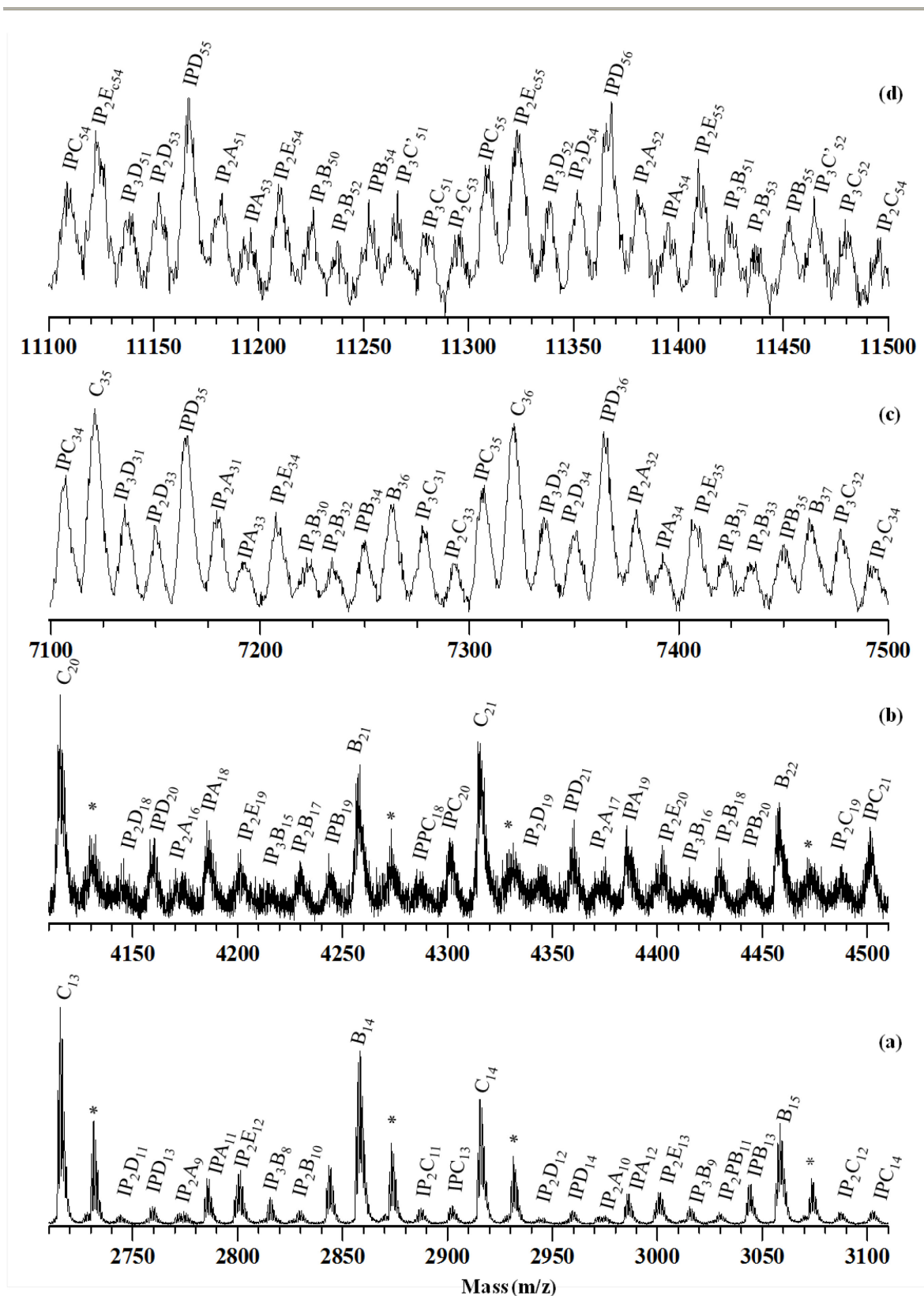


Figure 2.9: Enlarged sections of MALDI-TOF mass spectra of some fractions of 3HB16 sample: F45 (a), F39 (b), F33(c), F29 (d).

The MALDI spectra of the SEC fractions taken at higher  $V_e$  show most intense peaks because of linear PBA oligomers  $B_n$  and  $C_n$ , and weak signals corresponding to the HB

macromolecules. The relative intensity of the peaks due to HB macromolecules increase in the mass spectra of SEC fractions taken at  $V_e < 27.125$  mL, which contains higher molecular mass species. In these mass spectra, the intensity of the linear PBA oligomers  $B_n$  and  $C_n$  decreased. Resolved MALDI spectra of the SEC fractions taken at  $V_e < 26.0$  mL show peak series belonging only to the HB macromolecules, as can be observed in Figure 2.9, which displays enlarged sections of the mass spectra of fractions F29, F33, F39, and F42 of 3HB16 sample, taken at different elution times (26.125, 27.125, 28.625, and 29.375 mL, respectively). In the spectra of the fractions eluted at  $V_e$  lower than 26.0 mL (i.e., F29 in Figure 2.9d), only family peaks corresponding to the sodiated ions of the HB macromolecules containing different TMP units (i.e., species  $IPB_n$ ,  $IP_2B_n$ ,  $IPC_n$ ,  $IP_2C_n$ , etc.) are observed. In this mass spectrum, intense peaks due to HB macromolecules containing a cyclic branch (species  $IP_2Ec_n$ ) and HB chains containing ether bonds (species  $IP_3C'_n$ ) are also present. These species that appear at  $-18$  m/z with respect to the analogous HB species (i.e.,  $IP_3C_n$ ) were probably formed through (inter and intra)-molecular transesterification. Their presence in the SEC fractions eluted at lower  $V_e$  suggests that intermolecular transesterification mechanisms lead to the formation of HB macromolecules of higher MMs. SEC fractions eluted at  $V_e$  lower than 25.5 mL give unresolved MALDI spectra, as it can be seen in Figure 2.9; however, on the basis of the spectrum of the fraction F29 displayed in Figure 2.9d, we can hypothesize that they contain only HB macromolecules.

The same results were obtained for 3HB24 sample obtained at 24 h of reaction at 180 °C, using the same molar ratio of reactants used for the sample 3HB16 discussed above.

Data in Table 2.1 show that the average MMs of 3HB24 are higher than 3HB16 owing to the occurrence of intermolecular reactions. However, when the synthesis of the polymer was carried out at about 170 °C for 24 h, sample 3HB24§, the SEC analysis reveals average MMs lower than 3HB24 sample. Figure 2.10 displays the SEC curve of the 3HB24§, together with the MALDI mass spectra of some selected fractions eluted at 24.875 (F4), 28.625 (F19), 29.375 (F22), 30.125 (F25), and 31.625 mL (F31). SEC/MALDI-TOF analysis on 3HB24§ sample confirms that this sample contains macromolecular species with MMs ranging from 800 to about 33'000 g/mol. In this case, linear PBA oligomers are observed only in the mass spectra of the fractions eluted at  $V_e$  higher than 28.5 mL.

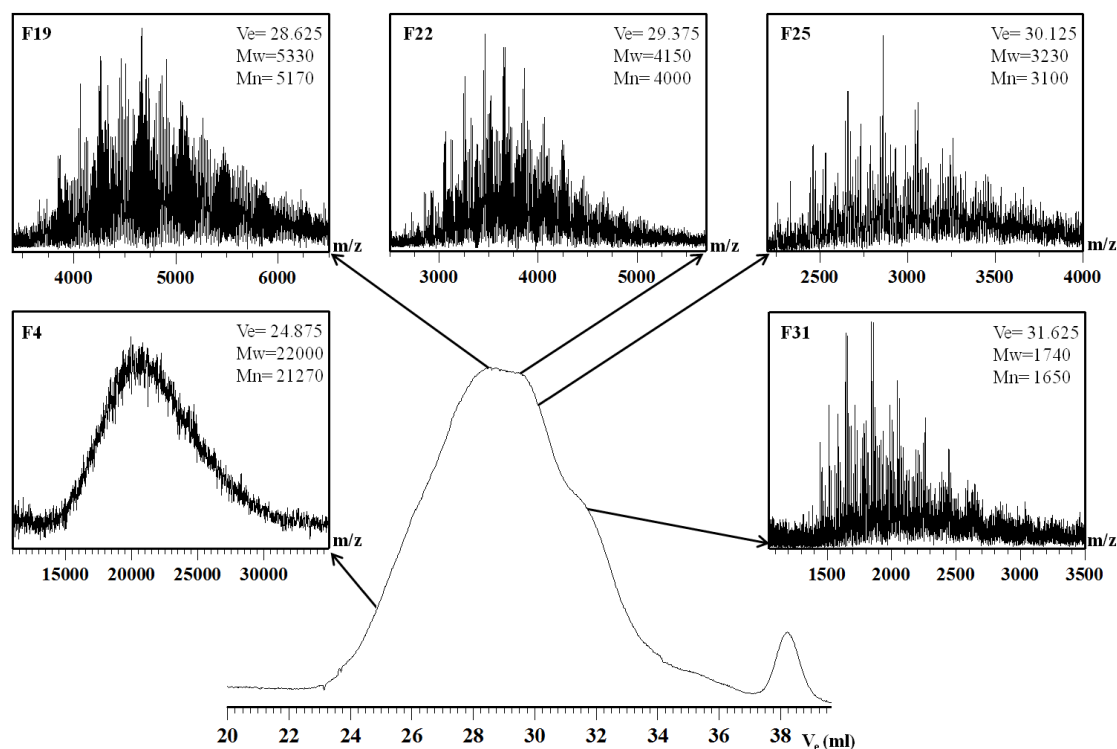


Figure 2.10: SEC chromatogram and MALDI-TOF mass spectra of some fractions of 3HB24§ sample.

Also, these fractions contain HB macromolecules having from 1 to 3 TMP units. The formation of HB molecule with short PBA blocks suggests that inner transesterification reactions prevail at 24 h reaction carried out at 170 °C.

The mass spectra of the unfractionated 3HB24§, as well as those of its SEC fractions (see Figure 2.11), show no signal due to HB macromolecules containing ether units, suggesting that at this temperature the transesterification reactions do not occur or are undetectable.



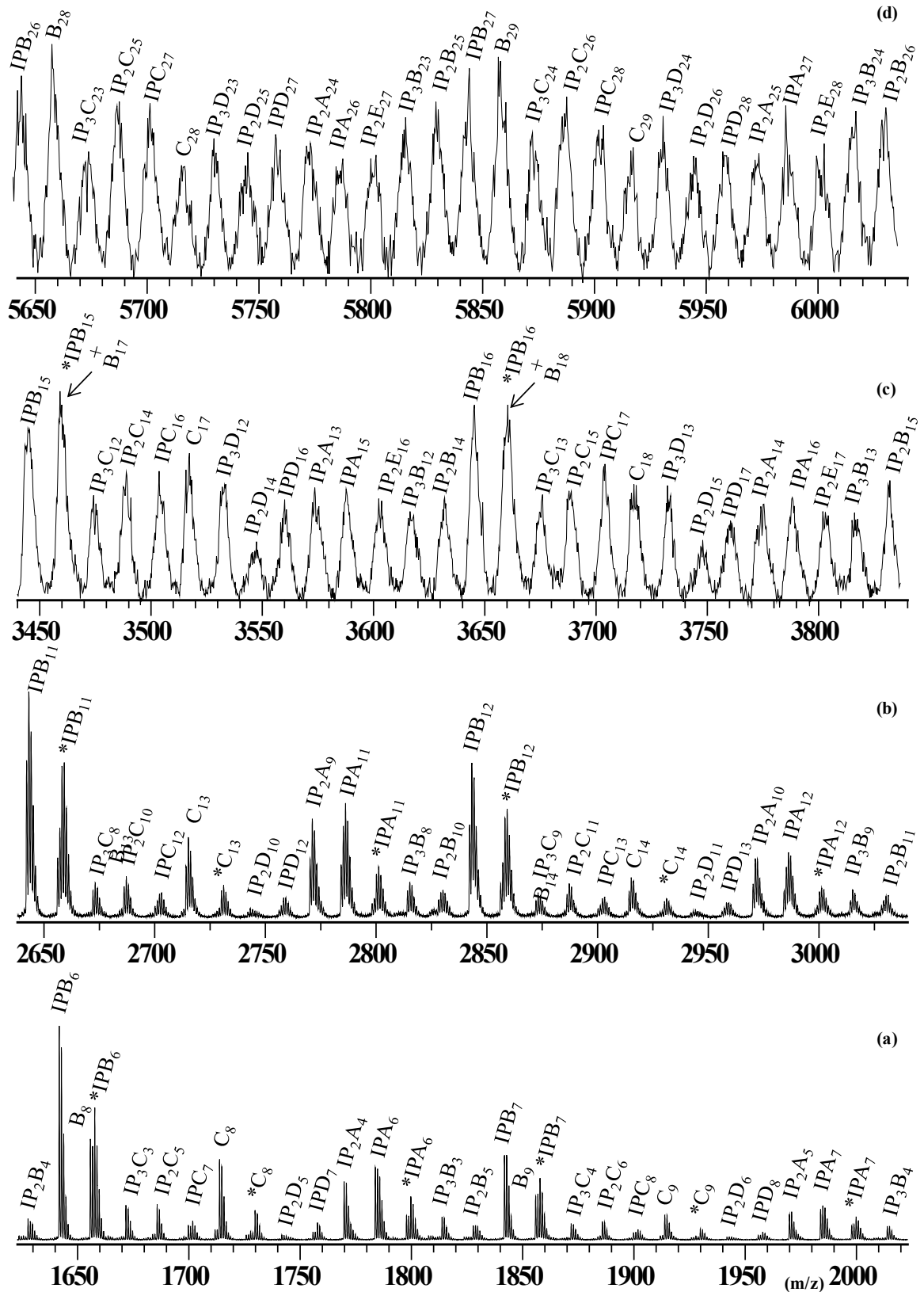


Figure 2.11: Enlarged sections of MALDI-TOF mass spectra of some fractions of 3HB24 sample: F31 (a), F25 (b), F22(c), F16 (d).



### 2.3.6 Thermogravimetric analysis (TGA)

The structure-to-thermal stability relationship was investigated through thermogravimetric analysis (TGA). In Table 2.7 the onset temperature ( $T_{\text{onset}}$ ), the temperature at 5 % weight loss ( $T_{5\% \text{wt. loss}}$ ) and the temperature at maximum degradation rate (defined as the maximum of the weight loss derivative curves) ( $T_{\text{max. deg. rate}}$ ) are reported for all HB samples and PBA-9 pre-polymer, used as reference.

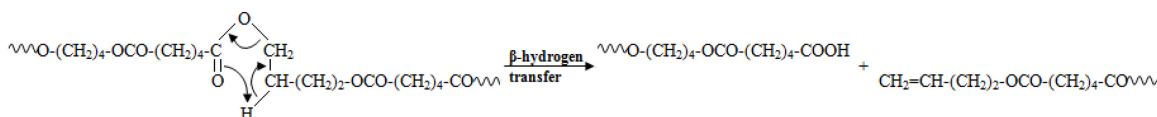
**Table 2.7:  $T_{\text{onset}}$ ,  $T_{5\% \text{wt. loss}}$  and  $T_{\text{max. deg. rate}}$  of PBA-9 and HB samples.**

<b>Samples</b>	<b><math>T_{\text{onset}}</math> (°C)</b>	<b><math>T_{5\% \text{wt. loss}}</math> (°C)</b>	<b><math>T_{\text{max. deg. rate}}</math> (°C)</b>
<b>PBA-9</b>	292	329	402
<b>1.5HB16</b>	290	322	401
<b>1.5HB24</b>	279	303	366
<b>1.5HB16§</b>	285	310	370
<b>1.5HB24§</b>	290	310	363
<b>1.5HB30§</b>	288	310	366
<b>3HB16</b>	290	314	376
<b>3HB24</b>	257	291	360
<b>3HB24§</b>	244	272	352
<b>5HB16</b>	248	291	364
<b>5HB24</b>	205	271	382
<b>5HB30</b>	238	265	391
<b>5HB44</b>	285	326	394
<b>7HB8</b>	272	294	349
<b>7HB16</b>	275	298	359
<b>10HB8</b>	254	290	358
<b>10HB16</b>	283	307	364

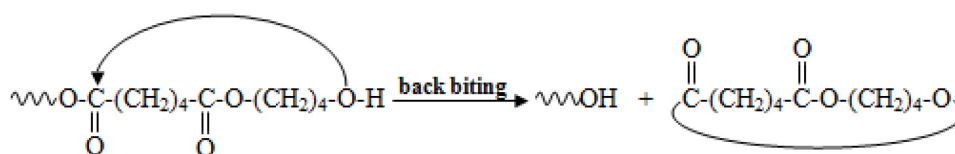
From Table 2.7, it can be observed that, depending on the experimental conditions used during the synthesis and thus on the chemical structure of the obtained systems, the thermal behavior changes significantly. In particular, the most stable samples are the linear -OCH<sub>3</sub> terminated PBA as well as the HB systems 1.5HB16 and 3HB16 obtained with low amount of TMP (i.e. 1.5 and 3 mol %), which are mainly characterized by the presence of linear -OCH<sub>3</sub> terminated oligomers. The same systems reacted for 24h (i.e. 1.5HB24 and 3HB24) show a lower thermal stability, due to the change in their chemical structures, exhibiting a significant amount of -OH terminated free oligomers. The abundance of these species may be related to the fact that longer reaction of times promoted the formation of branched structures as a consequence of side intermolecular reactions between -OCH<sub>3</sub>

terminated oligomers and the residual -OH end-groups of TMP. Previous results obtained from MALDI-TOF mass spectra confirmed these experimental findings.

A better insight of this behavior may be achieved considering the general degradation mechanism of polyesters. This latter occurs typically through two main degradation processes: a chain scission through a  $\beta$ -hydrogen transfer reaction, leading to vinyl ester and acid end-groups, as described in Scheme 2.5, and an intramolecular back-biting, leading to cyclic oligomers of up to three units in size, as depicted in Scheme 2.6.<sup>44-49</sup>



**Scheme 2.5:  $\beta$ -hydrogen transfer mechanism.**



**Scheme 2.6: Back-biting mechanism.**

Most probably, the primary cleavage process in poorly HB systems, such as 1.5HB16 and 3HB16, is a  $\beta$ -hydrogen transfer reaction, which generates a series of open-chain oligomers. As soon as the time of reaction increases, more complex and HB systems (i.e. 1.5HB24 and 3HB24) form, leading to short hydroxyl terminated branches. These structures are thought to be the initiation site for easier degradation, as they would allow for back-biting on the main-chain and formation of cyclic oligomers.<sup>46</sup> This explains why, increasing the reaction time, the HB systems are more prone to degradation than the less reacted ones. This behavior is also evident in the particular case of HB samples obtained using 5 molar percent of TMP, from 5HB16 to 5HB30 samples (see Table 2.7 and Figure 2.12), whose degradation temperatures decrease of about 30 degrees due to the abundance of HB moieties -OH terminated, as evidenced by MALDI-TOF analysis. Finally, 5HB44 sample exhibits higher degradation temperature ( $T_{5\%wt.loss} = 326^{\circ}C$ ) since longer reaction time are related to more stable systems.

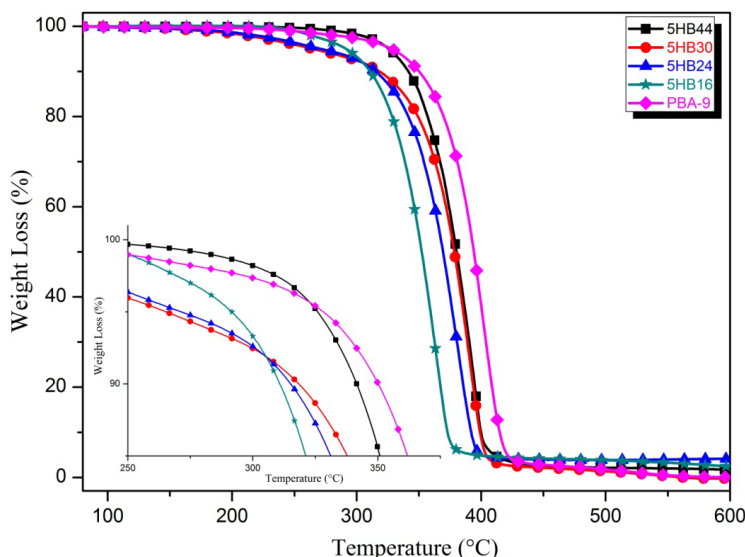


**Figure 2.12: TG traces of PBA-9, 5HB16, 5HB24, 5HB30, and 5HB44 samples. Inset: Detailed view of the curves in the temperature range between 250 and 400 °C.**

Most probably for prolonged reaction times ether units, cyclic branches and cross-linked portions are generated, which conferred very high thermal stability to the HB system. The presence of cross-linked portion<sup>12,17</sup> is confirmed by the fact that this sample is not soluble in numerous solvents, especially in  $\text{CHCl}_3$  and THF that are typically used to dissolve HBs.

For systems with TMP amounts higher than 5 molar percent, a similar effect is observed, leading to the formation of interconnected TMP units which are responsible for the higher thermal stability of the HB systems with increasing the reaction time.

### 2.3.7 Differential scanning calorimetry (DSC)

In order to evaluate the thermal behavior of HB systems, the linear PBA-9 pre-polymer was considered as reference sample. The melting behavior of 1.5HB16 sample was investigated by differential scanning calorimetry (DSC) and reported in detail in Figure 2.13. In the first heating scan a wide shape melting peak is observable, whose maximum is associated to a melting temperature of 53 °C. Furthermore, a side shoulder is visible around 50 °C. When the sample is cooled down a single crystallization temperature of 29 °C is found. However, in the second heating scan, two melting peaks at 50 and 56 °C are found.

As reported in literature,<sup>50,51</sup> the polymorphism phenomena usually has been observed in linear poly(butylene adipate). PBA is characterized by a rather complex melting behavior.

Temperature is an important factor in favoring a specific type of crystal formation in polymorphic polymers.

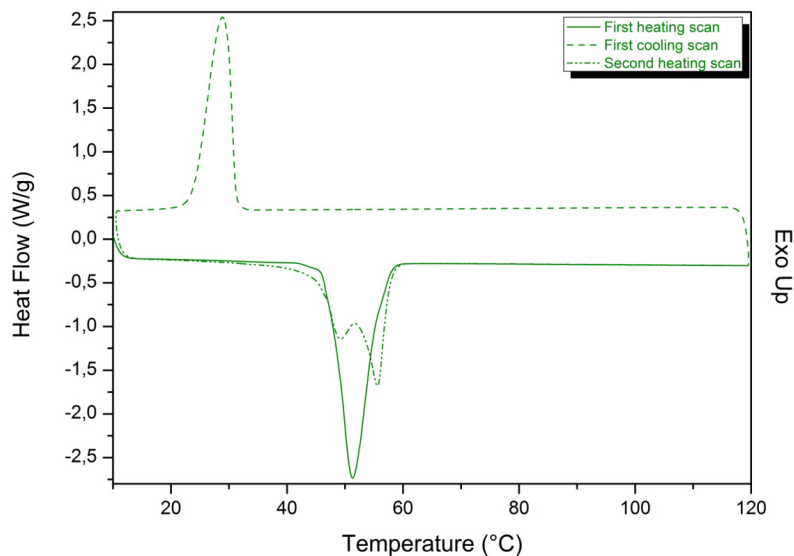


Figure 2.13: DSC curve of 1.5HB16 sample.

PBA shows two types of polymorphic crystals: a more stable  $\alpha$ -form, which is normally favored for crystallization from melt at higher temperatures (31–35 °C), or upon slow cooling from the melt, and a  $\beta$ -form that forms from crystallization at low temperatures (25–28 °C). These forms are clearly evident during heating scan rate because each one is characterized by two melting peaks. PBA packed with both crystal forms can display up to four melting peaks (see Figure 2.14).<sup>50,51</sup>

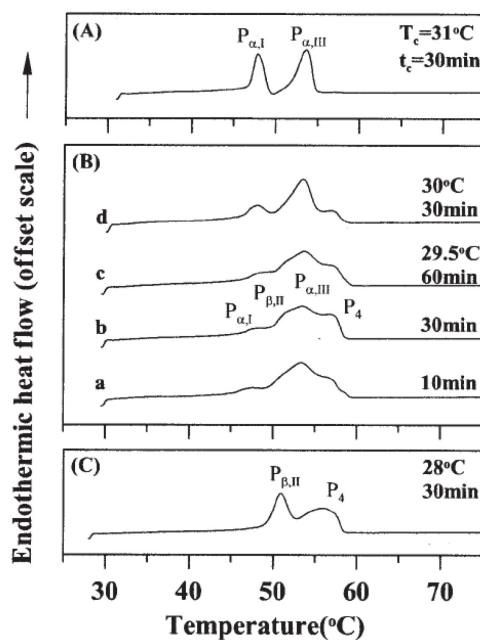


Figure 2.14: DSC curves of PBA sample crystallized at three temperature regimes: (A) high-T, (B) intermediate-T, and (C) low-T.<sup>51</sup>

Drawing on the work on PBA, three different temperatures, 27, 29 and 32 °C, were chosen for DSC isothermal crystallization run (also see section "Characterization") in order to investigate the polymorphism of 1.5HB16 sample.

The DSC curves, obtained after melt-crystallized in the temperature ranges from 27 to 32 °C, are reported. After isothermal crystallization at 27 °C, Figure 2.15, two melting peaks appear at 50 and 56 °C, which could correspond to the  $\beta$ -crystalline form.

After isothermal crystallization at 32 °C, Figure 2.16, two melting peaks appear at 48 and 53 °C, which could correspond to the  $\alpha$ -crystalline form.

In the last isothermal crystallization run at 29 °C, Figure 2.17, a wide melting peak is located at 54 °C showing also two shoulders centered at 46 and 51 °C, respectively.

This result is due to the coexistence of both  $\alpha$  and  $\beta$  forms in the 1.5HB16 sample. It is likely to state that polymorphism phenomena of this HB sample is related to the presence of long linear PBA chains, as free units or linked to the branching agent, making this HB sample much similar to linear systems for thermal behavior.

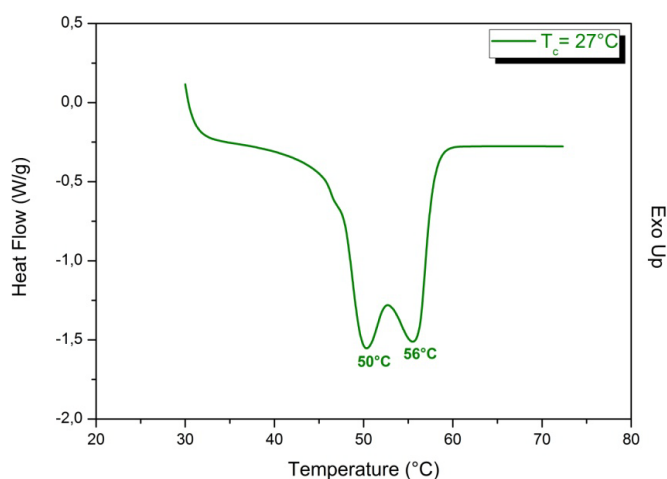


Figure 2.15: DSC curve of 1.5HB16 sample obtained after melt-crystallized at 27 °C.

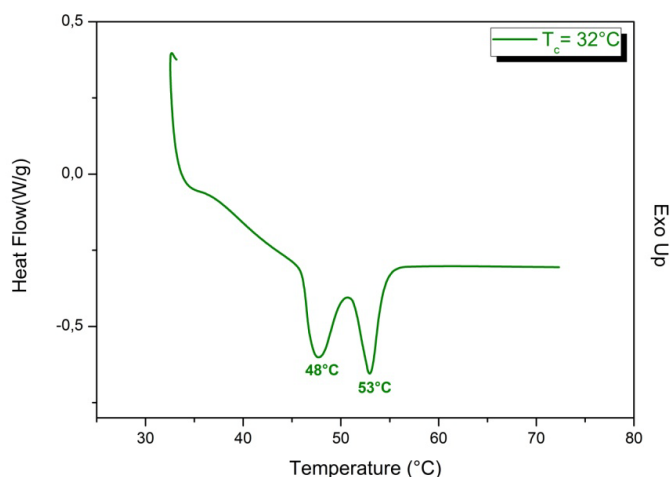


Figure 2.16: DSC curve of 1.5HB16 sample obtained after melt-crystallized at 32 °C.

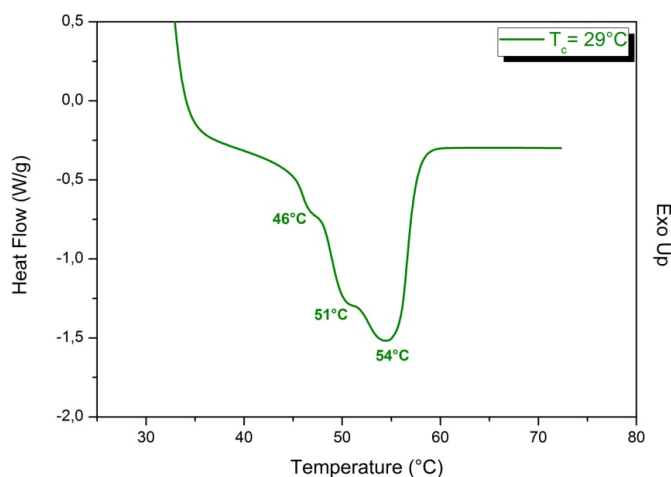


Figure 2.17: DSC curve of 1.5HB16 sample obtained after melt-crystallized at 29 °C.

In Table 2.8, the melting temperature ( $T_m$ ) and heat of fusion ( $\Delta H_m$ ) measured from the second heating scan, the glass transition temperature ( $T_g$ ), the crystallization temperature ( $T_c$ ) and heat of crystallization ( $\Delta H_c$ ) calculated from the first cooling scan are listed.

Table 2.8:  $T_m$ ,  $T_g$ ,  $T_c$ ,  $\Delta H_m$  and  $\Delta H_c$  of PBA-9 and HB samples.

Samples	$T_m^*$ (°C)	$T_g$ (°C)	$T_c^{**}$ (°C)	$\Delta H_m^*$ (J/g)	$\Delta H_c^{**}$ (J/g)
PBA-9	50-56-60	-57	28	64.4	64.4
1.5HB16	50-57	-55	25	50.8	53.7
1.5HB24	48-55	-57	20	56.1	57.9
1.5HB16§	50-56	-57	19	71.5	68.8
1.5HB24§	49-56	-56	22	64.7	65.9
1.5HB30§	48-55	-55	18	52.4	55.7
3HB16	47-54	-55	19	53.1	56.7
3HB24	41-49	-57	15	48.8	52.3
3HB24§	40-48	-56	14	56.5	51.9
5HB16	42-50	-54	18	64.0	64.1
5HB24	34-46	-52	8	49.8	52.4
5HB30	31-42	-50	-6	37.0	42.4
5HB44	26-37	-50	-13	33.2	31.6
7HB8	50-57	-55	22	61.4	61.9
7HB16	48-55	-55	20	52.2	56.2
10HB8	39-46	-55	18	53.8	55.4
10HB16	37-44	-55	14	41.1	45.8

\*values measured from the second heating scan; \*\*values measured from the first cooling scan.

The thermal behavior of 1.5HB16 and 1.5HB24 samples (and 1.5HB16§, 1.5HB24§, 1.5HB30§), similarly to PBA, is characterized by two melting points associated to the two different crystalline forms. This is due to the particular branched structure of these

systems, characterized by few branching points and long linear chains with a mobility comparable to that of PBA. These branching units somehow hinder the achievement of an ordered structure, causing a decrease of  $\Delta H$  values.

Crystallization is further inhibited when 3 molar percent of TMP is used. Comparing 1.5HB16 and 3HB16 samples, it can be noted that  $T_m$  values decrease due to the growing extent of branching as well as to the reduction of linear PBA length linking to TMP units. This effect is even more evident in 3HB24 sample obtained employing higher reaction times. As for HB samples containing 5 molar percent of TMP, it is worth noticing that the thermal behavior is closely related to the evolution of chain architecture. From data reported in Table 2.8 it can be inferred that melting temperatures and  $\Delta H$  values decrease by increasing the reaction time. These results indicate that the formation of even more complex branched structures, such as cyclic and cross-linked moieties, affect the extent of ordered portions, leading to an increment of amorphous phase. In Figure 2.18 the traces of second heating scan of PBA and HBs obtained using 5 molar percent of TMP are reported.

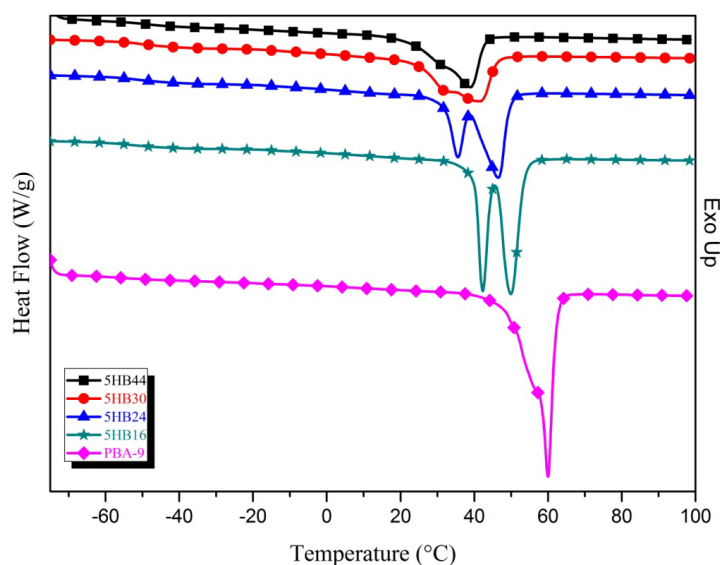


**Figure 2.18: DSC traces of PBA-9, 5HB16, 5HB24, 5HB30, and 5HB44 samples measured from the second heating scan.**

As evidenced also by the trend of the DSC traces, moving from PBA to HB samples, it seems that as the branching reaction evolves, the branched fraction having a behavior similar to that of PBA is reduced, generating a HB structure less prone to crystallize.

The same trend is evident in HB samples obtained with 7 and 10 molar percent of TMP, for which the enthalpy of fusion decreased due to the formation of complex branched architectures as a consequence of the high amounts of branching agent.<sup>12,52</sup>

Summarizing, both reaction times and molar amounts of branching agent are key factors in determining the structural features of HB systems and thus their thermal behavior. As matter of fact, the  $T_m$  values of the HB samples obtained after 16 h of reaction (i.e. 1.5HB24, 3HB24, 5HB24), decrease as the molar percent of TMP increases due to the growing extent of branching together with the reduction of linear PBA length linking to TMP units. The same behavior is observed in Figure 2.19 where the traces of first cooling scan of PBA and HB samples obtained using 5 molar percent of TMP are reported. From data in Table 2.8 is also visible that  $\Delta H_c$  values decrease with increasing the reaction time.

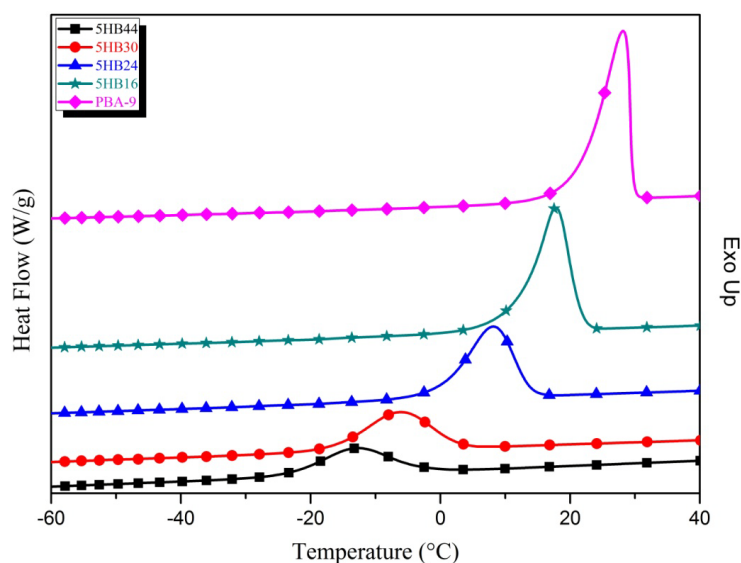


Figure 2.19: DSC traces of PBA-9, 5HB16, 5HB24, 5HB30, and 5HB44 measured from the first cooling scan.

### 2.3.8 Wide angle X-ray diffraction (WAXD)

The crystallization, such as melting behaviors of HB polymers, are closely related to their chain architecture. All samples were characterized by WAXD technique to determine the degree of crystallinity (DC), reported in Table 2.9, and correlate it to thermal analysis data. To understand the complex behavior of HB species, linear PBA was used as reference sample. The crystal structures of PBA were investigated by WAXD analysis in a temperature range from 25 to 35 °C by Doi et al.<sup>50</sup> Two types of polymorphic crystals of PBA were identified. The  $\alpha$ -form crystal is characterized as monoclinic unit cell with dimensions of  $a = 6.73 \text{ \AA}$ ,  $b = 7.94 \text{ \AA}$ ,  $c = 14.20 \text{ \AA}$  (fiber axis), and  $\beta = 45.5^\circ$ . While for another  $\beta$ -form, the PBA chains are packed in an orthorhombic unit cell with dimensions of  $a = 5.06 \text{ \AA}$ ,  $b = 7.35 \text{ \AA}$ , and  $c = 14.67 \text{ \AA}$  (fiber axis). The  $\beta$ -form crystals are formed at temperatures below 31 °C, while the  $\alpha$ -form crystals are formed above 29 °C. When the crystallization temperature is  $30 \pm 1 \text{ }^\circ\text{C}$ , a mixture of  $\alpha$ -form and  $\beta$ -form crystals has been



formed, see Figure 2.20. Therefore, the monoclinic  $\alpha$ -form crystals are the more stable ones.

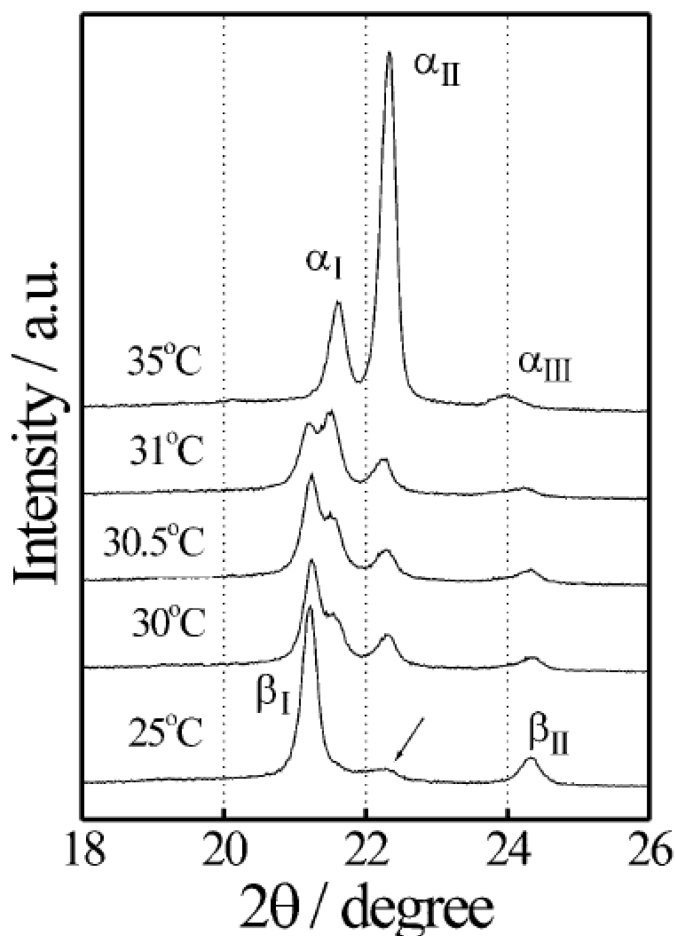


Figure 2.20: XRD patterns of poly(butylene adipate) films after melt-crystallized at different temperatures.<sup>50</sup>

As described in literature,<sup>52,54</sup> all HB samples display peaks at 21.35 and 24.55° which are identical to the peak positions observed for the linear PBA-9, but at lower intensities. As expected, this reflects lower degree of crystallinity in HB samples with increasing HB structure. These results are in excellent agreement with their thermal properties determined by DSC and TGA analyses, previously discussed.

Table 2.9: DC measured by X-ray diffractogram of PBA-9 and HB samples.

<b>Samples</b>	<b>DC (%)</b>
<b>PBA-9</b>	30
<b>1.5HB16</b>	27
<b>1.5HB24</b>	24
<b>1.5HB16§</b>	30
<b>1.5HB24§</b>	28
<b>1.5HB30§</b>	26
<b>3HB16</b>	25
<b>3HB24</b>	23
<b>3HB24§</b>	28
<b>5HB16</b>	24
<b>5HB24</b>	22
<b>5HB30</b>	20
<b>5HB44</b>	16
<b>7HB8</b>	22
<b>7HB16</b>	17
<b>10HB8</b>	19
<b>10HB16</b>	13

## References

1. Voit, B. I.; Lederer, A. *Chem Rev* 2009, 109, 5924–5973;
2. Percec, V.; Chu, P.; Kawasumi, M., *Macromolecules* 1994, 27, 4441–4453;
3. Wurm, F.; Frey, H., *Prog Polym Sci* 2011, 36, 1–52;
4. Žagar, E.; Žigom, M., *Polym Sci* 2011, 36, 53–58;
5. Johansson, M.; Malmoström, E.; Hult, A., *TRIP* 196, 4, 398–403;
6. Gao, C.; Yan, D., *Prog Polym Sci* 2004, 29, 183–275;
7. Yates, C. R.; Hayes, W., *Eur Polym J* 2004, 40, 1257–1281;
8. Inoue, K., *Prog Polym Sci* 2000, 25, 453–571;
9. Lindström, A.; Hakkarainen, M., *J Appl Polym Sci* 2006, 100, 2180–2188;
10. Ascione, L.; Ambrogi, V.; Battiato, S.; Carfagna, C.; Persico, P., *Funct Mater Lett* 2011, 4, 361–364;
11. Lindström, A.; Hakkarainen, M., *J Appl Polym Sci* 2007, 104, 2458–2467;
12. Han, Y.-K.; Um, I. W.; Im, S. S.; Kim, B. C., *J Polym Sci Part A: Polym Chem* 2001, 39, 2143–2150;
13. Chikh, L.; Tessier, M.; Fradet, A., *Macromolecules* 2008, 41, 9044–9050;
14. Malmoström, E.; Johansson, M.; Hult, A., *Macromolecules* 1995, 28, 1698–1703;
15. Murillo, E. A.; Vallejo, P. P.; Sierra, L.; López B. L., *J App Polym Sci* 2009, 112, 200–207;
16. Chick, L.; Arnaud, X.; Guillermain, C.; Tessier, M.; Fradet, A., *Macromol Symp* 2003, 199, 209–221;
17. Stumbé, J.-F.; Bruchmann, B., *Macromol Rapid Comm* 2004, 25, 921–924;
18. Chu, F.; Hawker, C. J.; Powery, P. J.; Hill, D. J. T., *J Polym Sci Part A: Polym Chem* 1997, 35, 1627–1633;
19. Kricheldorf, H. R.; Behnken, G., *J Polym Sci Part A: Polym Chem* 2009, 47, 231–238;
20. Žagar, E.; Žigom, M.; Podzimek, S., *Polymer* 2006, 47, 166–175;
21. Voit, B. I., *J Polym Sci Part A: Polym Chem* 2000, 38, 2505–2525;
22. Taton, D.; Feng, X.; Gnanou, Y., *New J Chem* 2007, 31, 1097–1110;
23. Terestra, S. J.; Gauthier, M., *Prog Polym Sci* 2004, 29, 277–283;
24. Khalyavina, A.; Schallausky, F.; Komber, H.; Al Samman, M.; Radke, W.; Lederer, A., *Macromolecules* 2010, 43, 3268–3276;
25. Yamagushi, N.; Wang, J.-S.; Hewitt, M.; Lenhart, W. C.; Mourey, T. H., *J Polym Sci Part A: Polym Chem* 2002, 40, 2855–2867;
26. Voit, B. I., *J Polym Sci Part A: Polym Chem* 2005, 43, 2679–2699;

27. Erber, M.; Boye, S.; Hartmann, T.; Voit, B. I.; Lederer, A., *J Polym Sci Part A: Polym Chem* 2009, 47, 5158–5168;
28. Fischer, A. M.; Fey, H., *Macromolecules* 2010, 43, 8539–8548;
29. Stumbé, J.-F.; Bruchmann, B., *Macromol Rapid Commun* 2004, 25, 921–924;
30. Chikh, L.; Tessier, M.; Fradet, A., *Polymer* 2007, 48, 1884–1892;
31. Kwak, S.-Y.; Lee, H. Y., *Macromolecules* 2000; 33, 5536–5543;
32. Hawker, C. J.; Lee, R.; Fréchet, J. M. J., *J Am Chem Soc* 1991, 113, 4583–4588;
33. Gray-Weale, A.; Gilbert, R. G., *J Polym Sci Part A: Polym Chem* 2009, 47, 3914–3930;
34. Choi, J.; Kwak, S.-Y., *Macromolecules* 2003; 36, 8630–8637;
35. Lederer, A.; Voigt, D.; Clausnitzer, C.; Voit, B., *J Chromatogr A* 2002, 976, 171–179;
36. Arias, A.; Benavides, R.; Castillo Garza, E.L.; Téllez Rosas, M. M., *J Vinyl Addit Tech* 2006, 12, 49-54;
37. Montaudo, G.; Montaudo, M. S.; Samperi, F., In *Matrix-Assisted Laser Desorption Ionisation/Mass Spectrometry of Polymers*; Montaudo, G.; Lattimer, R. P., Eds.; CRC Press: Boca Raton, FL, 2002; Vol 1, pp 419–521;
38. Montaudo, G.; Samperi, F.; Montaudo, M. S., *Prog Polym Sci* 2006, 31, 277–357;
39. Räder, H. J.; Schrepp, W., *Acta Polym* 1998, 49, 272–293;
40. Pasch, H.; Schrepp, W., *MALDI-TOF Mass Spectrometry of Polymers*; Springer: Berlin, 2003; p 298;
41. Nielen, M. W. F., *Mass Spectrom Rev* 1999, 18, 309–344;
42. Montaudo, G.; Garozzo, D.; Montaudo, M. S.; Puglisi, C.; Samperi, F., *Macromolecules* 1995, 28, 7983–7989;
43. Zimm, B. H.; Stockmayer, W. H., *J Chem Phys* 1949, 17, 1301–1314;
44. Holland, B.J.; Hay, J.N., *Polymer* 2002, 43, 1835-1847;
45. Rizzarelli, P.; Carroccio, S., *Polymer Degradation and Stability* 2009, 94, 1825–1838;
46. Montaudo, G.; Puglisi, C.; Samperi, F., *Polymer Degradation and Stability* 1993, 42, 13-28;
47. Wachsen, O.; Reichert, K.H.; Kruger, R.P.; Much, H.; Schulz, G., *Polym Degrad Stab* 1997, 55, 225–231;
48. Kim, D.J.; Kim, W.S.; Lee, D.H.; Min, K.E.; Park, L.S.; Kang, I.K., *J Appl Polym Sci* 2001, 81, 1115–1124;
49. Persenaire, O.; Alexandre, M.; Degée, P.; Dubois P., *Biomacromolecules* 2001, 2, 288-294;

50. Gan, Z.; Abe, H.; Doi, Y., *Macromol Chem Phys* 2002, 203, 2369–2374;
51. Woo, E. M.; Wu, M. C., *J Polym Sci Part B: Polym Phys* 2005, 43, 1662–1672;
52. Zhu, X.; Zhou, Y.; Yan, D., *J. Polym Sci Part B: Polym Phys* 2011, 49, 1277-1286;
53. Ouchi, T.; Ichimura, S.; Ohya, Y., *Polymer* 2006, 47, 429–434;
54. Baeka J.-B.; Tanb L.-S., *Polymer* 2003, 44, 3451–3459.

## Chapter 3

# HB polyesters as low migration plasticizers in flexible PVC

### 3.1 Introduction

Poly(vinyl chloride) (PVC) is one of the most important plastic materials since the 1950s.<sup>1</sup> It exhibits a broad collection of applications in different areas, owing to its good flame and weather resistance, low permeability, thermal, electrical and acoustic insulation, high transparency, high price/performance ratio, good processability and versatility assured through compounding. Flexible PVC grades are obtained by compounding PVC with plasticizers. Most of the plasticizers used for PVC are low molecular weight compounds.<sup>2</sup> The most diffused monomeric plasticizers are esters derived from phthalic acids. They constitute the 97% of total amount of plasticizers used and they can be added in a content up to 50% of the final weight of products. In particular, the most investigated phthalate was dioctyl phthalate (DOP). Phosphates, trimellitates, citrates, sebacates and adipates were also used.<sup>3</sup> One of the main problems related to the use of low molecular weight plasticizers is their migration from flexible PVC toward environment. This phenomenon leads to a hardening of the material.<sup>4</sup> Moreover, for some of them, the use in medical and food packaging applications is severely restricted due to their toxicity. In vitro tests have demonstrated that phthalate esters can have adverse effects in many organs, are irritants and harmful to human fertility and reproduction. In particular, DOP has been classified as “an agent possibly carcinogenic to humans” by the International Agency for Research on Cancer.<sup>2</sup> Moreover, the recent European regulation for Chemicals, REACH, foresees a restriction process in order to regulate the manufacture, placing on the market or use of certain substances if they pose an unacceptable risk to health and/or environment. This restriction, designed as a “safety net” to manage risks, forces producers and sellers worldwide to employ carefully DOP.

Migration of harmful substances from PVC can be avoided by substituting the unsafe plasticizer or by preventing its mass transfer from polymer matrix by surface modification. Among the substitutive low-molecular plasticizers evaluated, citrates, adipates and phosphates have been found to be less toxic than phthalates, though often at the expense of

original application performance.<sup>3</sup> Reducing mass transfer by surface modification such as surface coating,<sup>5</sup> chemical<sup>6</sup> and radiation cross-linking, covalent linkage of the additive to polymer chains<sup>7</sup> may be considered promising alternatives but at the cost of other properties, such as flexibility, thermal stability, surface properties and appearance.

On the other hand, an advantageous strategy is also to replace the typical plasticizers by compatible and nontoxic polymers.<sup>8,9</sup> Among them, linear saturated polyesters have been used in flexible PVC formulations, as they are characterized by a reduced migration because of their high molecular weight. Moreover, they exhibit good miscibility with PVC, improving its mechanical properties, such as abrasion and fatigue resistance. However, they could make in many cases PVC blends difficult to process.<sup>8-10</sup> Therefore, a manufacturing dilemma is determining the plasticizer molecular weight that should be used to satisfy the conflicting requirements of increased plasticizer retention and decreased manufacturing compatibility and processability.

In recent years, a growing interest has been shown also for hyperbranched (HB) polymers<sup>11</sup> characterized by a globular, compact structure with a large number of peripheral terminal functional groups.<sup>12,13</sup> The functionality of HB polymers allows for the tailoring of their chemical, thermal, rheological and solution properties, thus proving a powerful tool to design polymers for a wide variety of applications. Several works have been written dealing with the study of blends with HB polymers used as polymeric thermoplastics with regard to compatibility and change in mechanical properties.<sup>14-17</sup> In their work,<sup>9</sup> Lindström and her colleagues have used HB poly(butylene adipate) as migration resistant polymeric plasticizer for PVC.

In order to reduce the extent of plasticizer migration from the flexible PVC matrix, new formulations of flexible PVC were obtained by replacing low-molecular weight DOP with poly(butylene adipate)-based plasticizers, with both linear (PBA) and HB structures.

The work was carried out in two stages:

- The synthesis and characterization of a tailored HB poly(butylene adipate) polyester, 1.5HB16 sample.
- The preparation and characterization of flexible PVC blends with three different plasticizers: DOP, commercial linear poly(butylene adipate), PBA, and synthesized HB poly(butylene adipate), 1.5HB16.

According to the characterization of HB polyesters previously synthesized (reported in detail in Chapter 2), 1.5HB16 sample was selected as polymeric HB plasticizer for PVC blends. The choice of this sample was done considering that it is the only HB sample,

having a high content of linear PBA, as free chains or linked to the branching units. For our studies it is very important to obtain new formulation of flexible PVC with increased plasticizer migration stability together with comparable technical requirements than classical PVC formulation. For this reason as references for our studies two standard formulations of plasticized PVC, one with DOP and the other with commercial PBA, Palamoll, were used. The key issue was to obtain a material with low plasticizers migration, workable in conventional processing equipments and conditions, matching the technical requirements such as degree of flexibility, thermal and mechanical resistance, and manufactured at a comparable cost of usual flexible PVC.

## **3.2 Experimental section**

### **3.2.1 Materials for PVC-based blends**

Rigid PVC sheets were prepared using PVC pellets BENVICVIC® IH007W025AA (Solvay Benvic, Italy). The base polymer used for flexible samples (PVC) was PVC Lacovyl® S7015 PVC (Arkema, France).

(Ca + Zn)-based powder Reapak B-NT/7060 (Ca + Zn 0.5-0.8 phr) (Ca/Zn- Reagens, Italy), as heat stabilizer, and epoxy soybean oil (ESBO- Shangai Yanan Oil and Grease Co.), as co-thermal stabilizer, were selected.

Low-molecular weight commercial plasticizer was used as reference for our studies; dioctyl phtalate (DOP) DIPLAST® 0 (purity > 95%) was received from Lonza S.p.A., Italy.

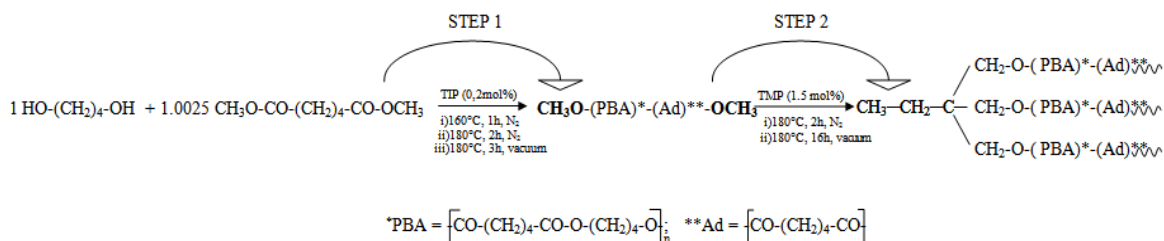
A linear, viscous polyester Palamoll® 654 (Palamoll) (BASF Corporation, USA) (Mw = 5200 g/mol, density at 25 °C = 1.0761 g/mL) was selected as a commercial linear polymeric plasticizer for PVC.

A synthesized HB polyester was also used as low migration polymeric plasticizer. For the synthesis of this sample 1,4-butanediol (BD) (99%), dimethyl ester of adipic acid (DMA) ( $\geq 99\%$ ), titanium(IV)isopropoxide (TIP) (99.99%), as catalyst, 1,1,1-tris(hydroxy methyl)propane (TMP) ( $\geq 98.0\%$ ), as branching agent, chloroform (CHCl<sub>3</sub>) and methanol (CH<sub>3</sub>OH), as solvents, were also purchased from Sigma-Aldrich (Italy) and used without any purification.



### 3.2.2 Synthesis of HB polyester

1.5HB16 sample, chosen as HB polymeric plasticizer for flexible PVC, was synthesized in one-pot synthesis performed in two steps, according to the Scheme 3.1.



**Scheme 3.1: Synthesis route of 1.5HB16 sample.**

In the first step, a tailored PBA methyl ester ended pre-polymer was synthesized using a DMA/BD molar ratio of 1.0025/1 as described before in Chapter 2. In the second step, 1.5 molar percent (with respect to the initial moles of monomer reagents) of TMP as branching agent was added and the reaction was carried out at 180 °C for 2 h at 1 atm, under nitrogen flow and under stirring. Then the reaction was continued under vacuum for 16 h, in order to obtain HB hybrid polyesters with linear PBA blocks along the chains.

For more details, see Table 2.1 in Chapter 2, in which experimental parameters (i.e. DMA/BD molar ratio, temperature, and reaction time) and molar mass distribution are described.

### 3.2.3 Preparation of PVC-based blends

All samples were prepared by mixing PVC, Ca/Zn, ESBO and plasticizers in a roll-milled plasticorder at 40 rpm, T = 120°C for 15 min. The formulations of all flexible PVC-based blends are reported in detail in Table 3.1.

**Table 3.1: Flexible PVC-based formulations.**

Components	R70	L50	L60	L70	L80	H50	H60	H70	H80
PVC (phr)	100	100	100	100	100	100	100	100	100
ESBO (phr)	2	2	2	2	2	2	2	2	2
Ca/Zn (phr)	1	1	1	1	1	1	1	1	1
<b>Plasticizers</b>									
DOP (phr)	70								
PBA (phr)		50	60	70	80				
HB (phr)						50	60	70	80

The flexible sheets with a thickness of 1 mm were obtained using a hot press (lab-scale Collin P 200 E) at 150 °C and 200 bar for 7 min.

Rigid PVC sheets with a thickness of 2 mm were prepared by press-molding the polymer pellets at 190 °C and 200 bar for 7 min.

### **3.2.4 Characterization**

#### **Thermogravimetric analysis (TGA)**

TGA measurements of all plasticizers and PVC-based blends were carried out in duplicate at 10 °C/min heating rate from 25 °C to 600 °C under nitrogen flow using a Q5000 (TA Instruments) thermo balance.

#### **Wide angle X-ray diffraction (WAXD)**

WAXD measurements were conducted on 1.5HB16 and PVC-based blends using a Philips XPW diffractometer with Cu K $\alpha$  radiation (1.542 Å ) filtered by nickel. The scanning rate was 0.02 °/s, and the scanning angle was from 2 to 60°.

#### **Dynamic mechanical thermal analysis (DMTA)**

DMTA measurements were carried out using a Triton Technology mod. Tritec 2000 testing machine. Tests were performed in single cantilever bending mode, using a constant frequency of 1 Hz and an amplitude of oscillation of 0.01 mm. Samples were heated from -80 °C up to different temperatures (40, 60, 80 °C), depending on the sample, at 5 °C/min heating rate. The glass transition temperature,  $T_g$ , was taken as the peak temperature of  $\tan\delta$  curve.

#### **Mechanical properties**

The Young's modulus ( $E$ ), ultimate tensile strength ( $\sigma_b$ ), and elongation at break ( $\epsilon_b$ ) were determined from a traction test in an universal dynamometer INSTRON mod.5564 at  $T_{room}$  using 1 KN load cell, at a crosshead speed of 10 mm/min. The dog bone shaped mini tensile bars were characterized by a thickness of 2 mm, width of 4 mm and length of 28 mm. For each sample a batch of five specimens was tested and the average values were reported.

## Migration tests

Plasticizer migration was determined by monitoring weight changes of PVC blends according to UNI EN ISO 177. Small rectangular sheets of flexible PVC-based samples with approximately 1 mm thickness were placed between two rigid PVC layers with 2 mm thickness and kept under 5.0 kg weight in an oven at 60 °C between two glass plates in order to force the migration of plasticizers to the contacting rigid substrates (also see Figure 3.1 as explicative setup).

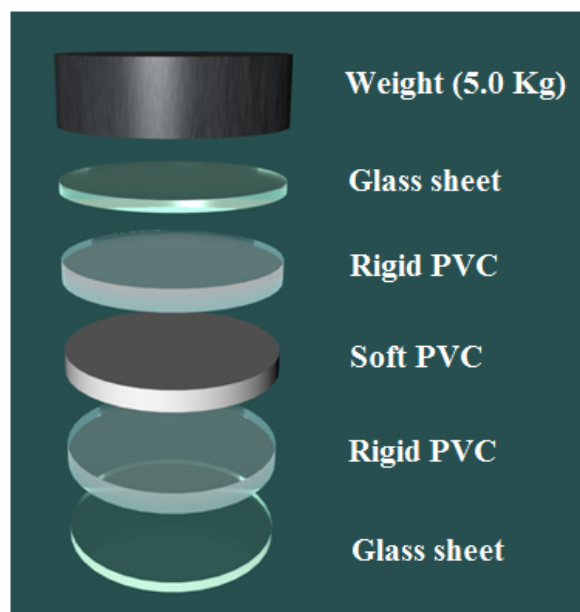


Figure 3.1: Migration test setup.

The specimens removed from the oven at different aging times (i.e. 1, 4, 8, 15, 25, 30 days) were immediately weighted. The weight loss of the exudable flexible component was determined by measuring the samples weight according to equation 3.1:<sup>16</sup>

$$\text{Extent of migration (\%)} = \frac{W_i - W_t}{W_i * y} * 100 \quad (3.1)$$

where  $W_i$  is the initial weight of soft part,  $W_t$  is the weight of the soft part at the selected times and  $y$  is a factor related to the amount of the exudable plasticizer present in the blends ( $y = 50/153, 60/163, 70/173, 80/183$  for H50-L50, H60-L60, H70-L70, H80-L80, respectively).

### 3.3 PVC-based blends characterization: results and discussion

#### 3.3.1 Thermogravimetric analysis (TGA)

Even if the thermal stability of 1.5HB16 sample was studied and reported in detail in the Chapter 2, in Figure 3.2 the TG curves of DOP, PBA and 1.5HB16 are overlapped for comparison.

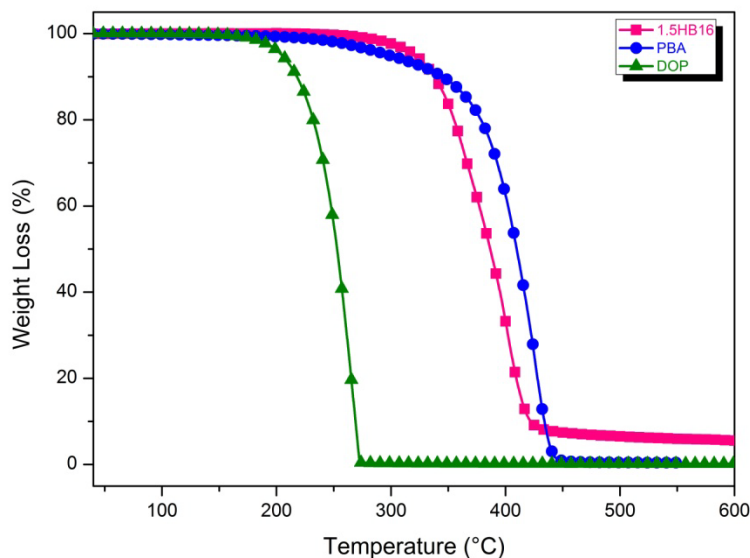


Figure 3.2: TG curves of DOP, PBA and 1.5HB16 plasticizers.

In Table 3.2 the temperature at 5 % weight loss ( $T_{5\%wt.loss}$ ), and the temperature at maximum degradation rate (defined as the maximum of the weight loss derivative curves) ( $T_{max.deg.rate}$ ) for all plasticizers are listed.

Table 3.2:  $T_{5\%wt.loss}$  and  $T_{max.deg.rate}$  of plasticizers.

	1.5HB16	PBA	DOP
$T_{5\%wt.loss}$ (°C)	320	298	204
$T_{max.deg.rate}$ (°C)	401	426	267

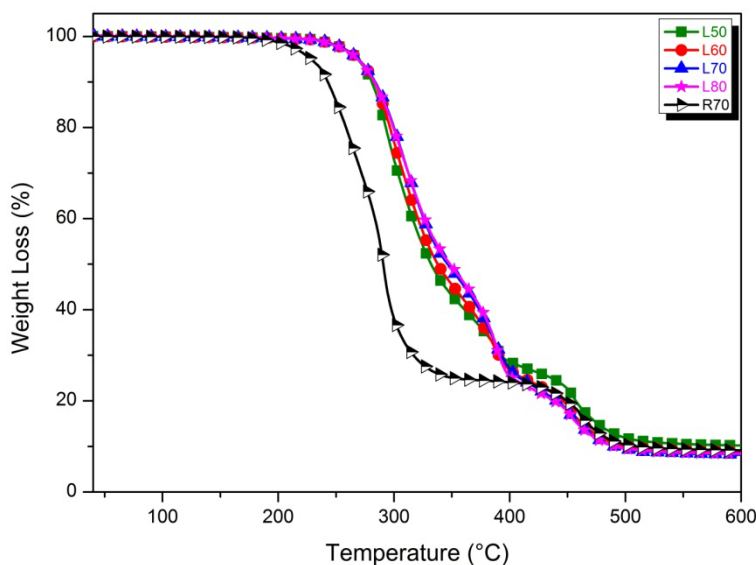
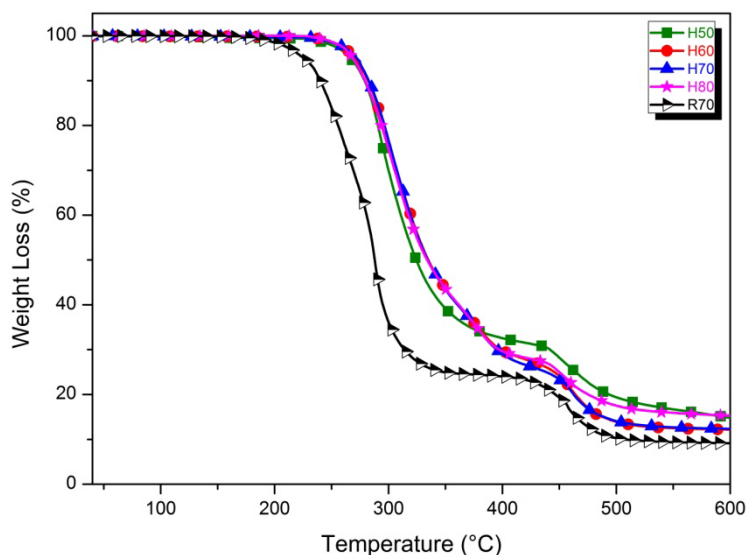
It can be noticed that 1.5HB16, PBA and DOP are thermally stable up to 320, 298 and 204 °C, respectively. Above this temperature interval, the plasticizers undergo the thermal degradation. PBA is characterized by the highest  $T_{max}$  value while faster degradation occur for DOP sample.

The  $T_{5\%wt.loss}$  and  $T_{max.deg.rate}$  for all PVC-based blends are reported in Table 3.3.

**Table 3.3:  $T_{5\%wt.loss}$  and  $T_{max.deg.rate}$  of PVC-based blends.**

	R70	L50	L60	L70	L80	H50	H60	H70	H80
$T_{5\%wt.loss}$ (°C)	225	268	269	269	268	265	270	272	268
$T_{max.deg.rate}$ (°C)	289	294	298	308	305	299	298	300	292

The TG curves of PVC/PBA and PVC/HB blends are reported in Figure 3.3 and in Figure 3.4, respectively. The TG curve of PVC/DOP blend is also overlapped in both figures for comparison.

**Figure 3.3: TG curves of PVC/DOP and PVC/PBA blends.****Figure 3.4: TG curves of PVC/DOP and PVC/HB blends.**

The PVC thermal degradation process proceeds in two basic stages. Within the range of 200 – 400 °C mainly dehydrochlorination (DHCl) of PVC takes place.<sup>18</sup> This phenomenon is clearly observed in our blends at  $T = 289$  °C. The second degradative stage at  $T > 400$

°C corresponds to scission of covalent bonds in PVC chains. In this step all samples exhibit the same behavior.

Since 1.5HB16 and PBA are basically more stable at heating, their presence in PVC increased blends thermal stability. The  $T_{5\%wt.loss}$  is increased by 40 °C when the polymeric plasticizers are employed, regardless of the polyesters amount used. This greater thermal stability was also proved by higher  $T_{max.deg.rate}$  values (in the first degradation step) indicating that the PVC dehydrochlorination reaction was slowed down.

### 3.3.2 Wide angle X-ray diffraction (WAXD)

The morphology of 1.5HB16 sample was studied by X-ray technique and reported in Figure 3.5.

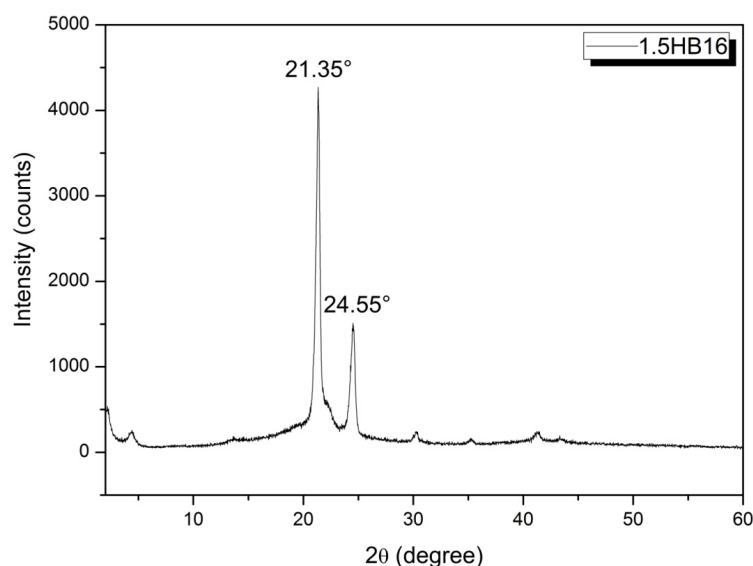


Figure 3.5: XRD pattern of 1.5HB16 sample.

The Figure 3.5 shows the X-ray diffraction (XRD) pattern of 1.5HB16 sample. Two diffraction peaks located at 21.35 ° and 24.55 ° are observed thus confirming the semi-crystalline structure of the synthesized polymer. The ratio of the area under the crystalline peaks and the total area multiplied by 100 was taken as the crystalline percentage degree (DC), equal to 27% for this sample (for more details see Chapter 2).

WAXD technique was also used to investigate the morphology of PVC/HB blends. We chose to report only the WAXD pattern of H70 (Figure 3.6) since it contains high amount of polymeric plasticizer. In spite of the high percentage of semi-crystalline structure of 1.5HB16 sample, used in H70 blend as plasticizer, this latter is amorphous at X-ray diffraction analysis, see Figure 3.6, suggesting that PVC hinders the formation of

plasticizer crystalline phase. This result may be considered as an indirect indication of good miscibility between PVC and highly branched polyester.

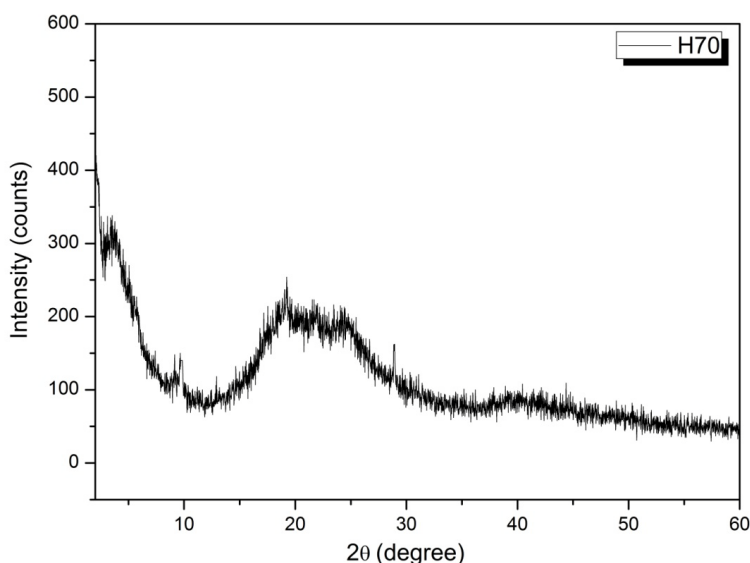


Figure 3.6: XRD pattern of H70 blend.

### 3.3.3 Dynamic mechanical thermal analysis (DMTA)

The dynamic-mechanical analysis was performed to determine the glass transition temperature ( $T_g$ ) of the PVC-based blends. The trend of  $T_g$ s was used as an indirect tool to evaluate the extent of compatibility between PVC matrix and polymeric plasticizers.

In Table 3.4 the  $T_g$  values (at the maximum of  $\tan\delta$  curves) of all PVC-based blends are reported. The PVC/PBA (Figure 3.7) and PVC/HB(Figure 3.8)  $\tan\delta$  traces are shown as a function of temperature.

Table 3.4:  $T_g$  values of PVC-based blends.

	R70	L50	L60	L70	L80	H50	H60	H70	H80
$T_g$ (°C)	11	30	18	15	7	39	29	23	18

A single glass transition temperature was observed at each composition indicating miscibility between the two polymer components. Monotonic shift of transition temperatures toward low values were observed with increasing the amount of polymeric plasticizers. This compositional dependence of single  $T_g$  indicates that PVC/poly(butylene adipate)s are miscible. The good miscibility between polyester and PVC can be ascribed to the hydrogen bonding existing between the carbonyl groups of the ester and the  $\alpha$ -hydrogen next to the chlorine atoms in PVC.<sup>10</sup>

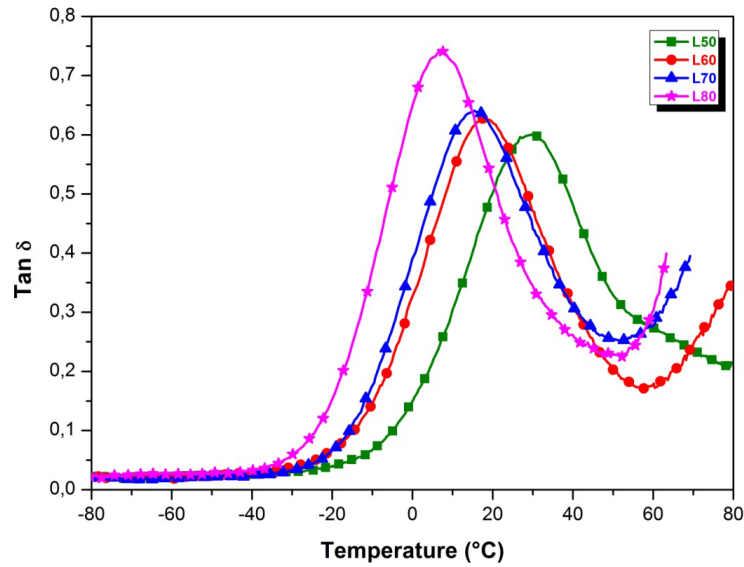


Figure 3.7: DMTA curves of PVC/DOP and PVC/PBA blends.

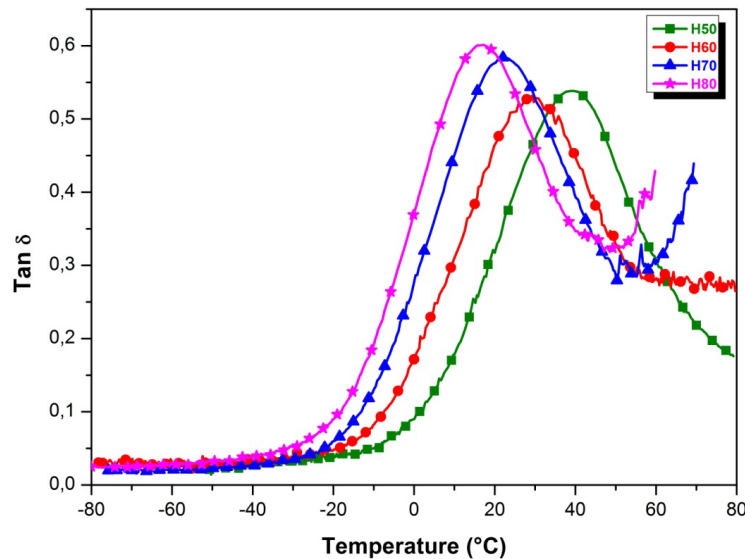


Figure 3.8: DMTA curves of PVC/DOP and PVC/HB blends.

The effect of the complex molecular architecture of HB plasticizer on  $T_g$  values of samples containing the same amount of plasticizer was also estimated. For example, H70 blend exhibits a  $T_g$  of about 10 degrees higher than L70 and R70 samples, providing evidence of a correlation between the high molecular weight of 1.5HB16 plasticizer and the restriction on macromolecule mobility. Instead, a low molecular weight plasticizer shows easily mixed with the polymer resin and its high chain ends density induces much free volume in the material.



### 3.3.4 Mechanical properties

The tensile properties of flexible PVC blends were measured on mini tensile bars. The Young's modulus ( $E$ ), ultimate tensile strength ( $\sigma_b$ ) and elongation at break ( $\epsilon_b$ ) of PVC/PBA (Table 3.5) and PVC/HB (Table 3.6) blends are reported and compared with flexible PVC plasticized with DOP (R70).

Table 3.5: Mechanical properties of PVC/PBA blends.

	R70	L50	L60	L70	L80
<b>E (MPa)</b>	$7.1 \pm 0.6$	$10.4 \pm 0.8$	$7.8 \pm 0.6$	$6.5 \pm 0.6$	$4.6 \pm 0.5$
<b><math>\sigma_b</math> (MPa)</b>	$9.4 \pm 2.1$	$17.1 \pm 0.7$	$12.6 \pm 2.0$	$12.5 \pm 0.9$	$8.5 \pm 0.8$
<b><math>\epsilon_b</math> (%)</b>	$287.8 \pm 21.2$	$289.8 \pm 22.0$	$296.5 \pm 48.8$	$343.2 \pm 24.5$	$353.7 \pm 33.0$

Table 3.6: Mechanical properties of PVC/HB blends.

	R70	H50	H60	H70	H80
<b>E (MPa)</b>	$7.1 \pm 0.6$	$17.4 \pm 1.8$	$10.9 \pm 0.9$	$7.3 \pm 0.6$	$5.4 \pm 0.5$
<b><math>\sigma_b</math> (MPa)</b>	$9.4 \pm 2.1$	$19.5 \pm 0.4$	$18.4 \pm 0.5$	$14.3 \pm 0.4$	$13.3 \pm 0.8$
<b><math>\epsilon_b</math> (%)</b>	$287.8 \pm 21.2$	$314.2 \pm 5.1$	$316.3 \pm 16.1$	$314.5 \pm 8.8$	$378.2 \pm 16.8$

Plasticizer contents is the most important parameter for the evaluation of plasticizing effects on PVC systems. Monotonic shift of the tensile modulus toward low values was observed with increasing the amount of both polymeric plasticizers. This finding attests the good plasticizing efficiency of the polyesters which can be used as alternative plasticizers in flexible PVC formulations.

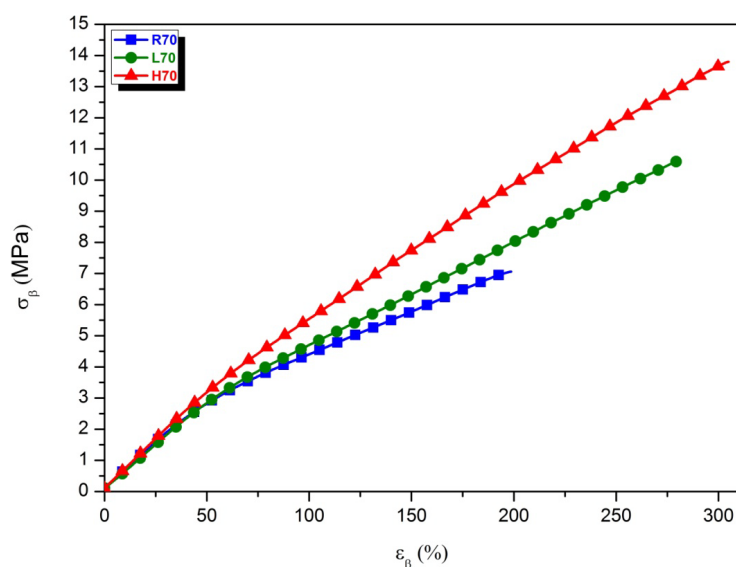


Figure 3.9: Stress-strain curves of R70 (-■-), L70 (-●-), and H70 (-▲-) blends.

In addition, polymeric plasticizers produced tougher materials with rather similar ductility as systems containing DOP. Higher stress values observed for materials containing the HB polymer may be ascribed to a good interfacial tension between PVC and PBA phases.

In Figure 3.9 the stress-strain curves of R70, L70, H70 are shown. Higher stress values were observed for blends containing polymeric plasticizers indicating the superior interphase adhesion and the interfacial tension between the PVC and poly(butylene adipate) phase.

### 3.3.5 Migration tests

Since the polymeric plasticizers were expected to have better migration stability compared to the monomeric one (DOP), migration tests were performed according to UNI EN ISO 177. The weight loss of the exudable flexible component was determined by measuring the weights of the samples according to Equation 3.1, at different aging times, i.e  $t = 1, 4, 8, 15, 25$  and 30 days.

Figure 3.10 and Figure 3.11 show the curves of extent of migration (%) for PVC/PBA and PVC/HB blends, respectively. A reduced migration of polymeric plasticizers compared to DOP is evident in both polymeric systems. There are three relevant plasticizer molecular properties that control plasticizer retention: molecular weight, polarity and linearity. Plasticizer mobility is one of the main factors governing plasticizer the diffusion out of the polymer structure. It is common to relate plasticizer mobility with plasticizer molecular weight. The smaller the plasticizer molecular weight, the greater plasticizer volatility and diffusivity. The superior migration stability of the PVC/polymeric plasticizers is anticipated to their much higher molecular weights in comparison with monomeric DOP.<sup>9,10</sup> Wilson also showed that the migration can be potentially reduced increasing the plasticizer molecular weight and decreasing the linearity of plasticizer. As a matter of fact, PVC/HB blends exhibit a reduced exudation compared to PVC/PBA and PVC/DOP (see Figure 3.12). The polymer's high molar mass and bulkiness significantly reduces its volatility and diffusivity compared to low molar mass plasticizers.<sup>16</sup> Moreover, the high miscibility between polyester and PVC could be responsible for the reduced migration tendency.<sup>10</sup> Since HB polymers have a higher density of functionality compared to linear polymers of the same molar mass, they can give rise to effective molecular interactions with PVC leading to higher migration stability systems.

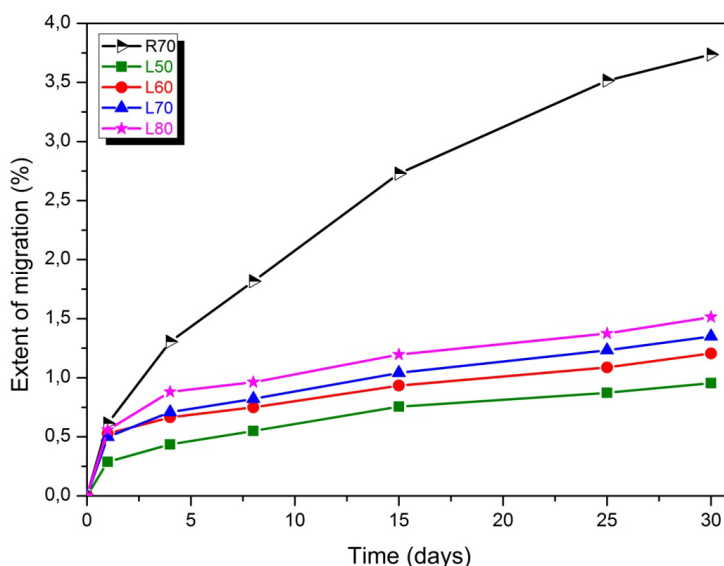


Figure 3.10: Extent of migration (%) from flexible PVC sheets for PVC/DOP and PVC/PBA blends.

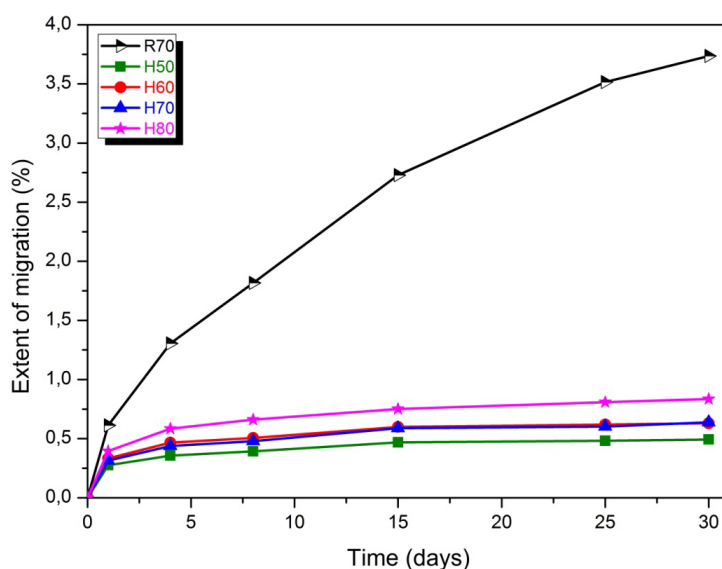


Figure 3.11: Extent of migration (%) from flexible PVC sheets for PVC/DOP and PVC/HB blends.

As expected, 1.5HB16 containing system exhibits the lowest values of weight loss, which remain constant with the aging time, meaning that an efficient plasticizer retention was achieved by the use of highly branched poly(butylene adipate).

According to obtained results, 1.5HB16 sample can be considered as a useful plasticizer aiming to reduce the potential health risk related to migration of phthalates from PVC matrix. Loss of plasticizer was limited by their polymeric nature and the presence of branched chains, which increased steric hindrance and reduced mobility of HB polyester, without affecting the properties of flexible PVC products.

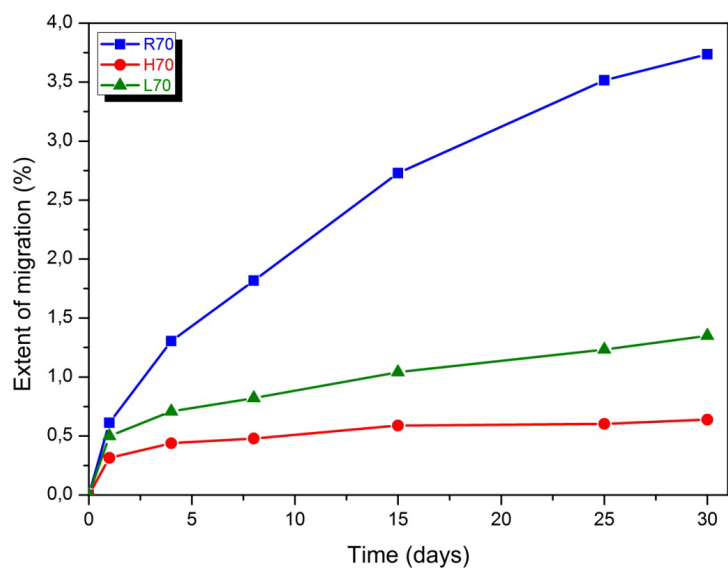


Figure 3.12: Extent of migration (%) for R70 (-■-), H70 (-●-), L70 (-▲-) blends.

## References

1. Smallwood, P. V., Concise Encyclopedia of Polymer Science and Engineering ed. J. I. Kroschwitz (John Wiley and Sons, New York, 1990);
2. Howick, C. J., Plasticizers Plastic Additives: An AZ Reference, ed. Pritchard (Chapman & Hall, London, 1998), pp. 499-513;
3. Persico, P.; Ambrogi, V.; Acierno, D.; Carfagna, C., *J Vinyl Add Technol* 2009, 15, 139-146;
4. Peña, J. R.; Hidalgo, M.; Mijangos, C., *J Appl Polym Sci* 2000, 75, 1303-1312;
5. Messori, M.; Toselli, M.; Pilati, F.; Fabbri, E.; Fabbri, P.; Pasquali, L.; Nannarone, S., *Polymer* 2004, 45, 805-813;
6. Romero Tendero, P. M.; Jimenez, A.; Greco, A.; Maffezzoli, A., *Eur Polym J* 2006, 42, 961-969;
7. Navarro, R.; Perrino, M. P.; Tardajos, M. G.; Reinecke, H., *Macromolecules* 2010, 43, 2377-2381;
8. Pita, V. J. R. R.; Sampaio, E. E. M.; Monteiro, E. E. C., *Polym Test* 2002, 21, 545-550;
9. Lindström, A.; Hakkarainen, M., *J Appl Polym Sci* 2007, 104, 2458-2467;
10. Lindström, A.; Hakkarainen, M., *J Appl Polym Sci* 2006, 100, 2180-2188;
11. Lindström, A.; Hakkarainen, M., *Biomacromolecules* 2007, 8, 1187-1194;
12. Sunder, A.; Mülhaupt, R.; Haag, R.; Frey, H., *Adv Mater* 2000, 12, 235-239;
13. Gao, C.; Yan, D., *Prog Polym Sci* 2004, 29, 183-275;
14. Kim, Y. H.; Webster, O. W., *Macromolecules* 1992, 25, 5561-5572;
15. Schmaljohann, D.; Potschke, P.; Hassler, R.; Voit, B. I.; Froehling, P. E.; Mostert, B.; Loontjens, J. A., *Macromolecules* 1999, 32, 6333-6339;
16. Choi, J.; Kwak, S. Y., *Environ Sci Technol* 2007, 41, 3763-3768;
17. Choi, J.; Kwak, S. Y., *Macromolecules* 2004, 37, 3745-3754;
18. Hidalgo, M.; Beltràn, M. I.; Reinecke, H.; Mijangos, C., *J Appl Polym Sci* 1998, 70, 865-872.

## Chapter 4

# HB polyesters as toughening agents in epoxy resin

### 4.1 Introduction

Thermoset epoxy resins are widely used in coatings, adhesives, electrical and electronic materials, moulding compounds, polymer composites, and structural applications due to their superior thermo-mechanical properties as high strength, adhesion, good dimensional, thermal and environmental stabilities. They also exhibit good electrical properties and excellent processability.<sup>1</sup>

However, the main disadvantage associated with their application is related to their inherent brittleness because of their highly crosslinked structure, which affect the durability.<sup>1-4</sup>

In this respect, many efforts have been made to improve the toughness of cured epoxy resins by introducing rigid particles, reactive rubbers, interpenetrating polymer networks (IPNs), and engineering polyesters within the matrix. However, they can affect the resin glass transition temperature ( $T_g$ ) to various degrees, sacrifice the thermal stability and storage modulus, and always limit the processability such as unwanted great increase of viscosity.<sup>1-4</sup>

Hyperbranched (HB) polymers, because of their unique structure, are known to exhibit lower melt and solution viscosities, high peripheral functionality, and smaller dimensions of the HB polymer molecules compared to their molecular weight than linear polymers of the same molar mass.<sup>5-11</sup> They are now commercially available to be used as processing aids, branching agents, compatibilizers, and tougheners for conventional polyesters and thermosets.<sup>9-11</sup> HB polymers have also been explored as novel, high potential, low viscosity additives for epoxy resins that increase fracture toughness properties without deleterious effects on other properties.<sup>12-17</sup>

Varying the shell surface chemistry of HB macromolecules, a very powerful tool for designing final properties of HBP/diglycidyl ether of bisphenol A (DGEBA) blends was created.<sup>13-16</sup>

In order to enhance the toughness of a commercial one-part liquid epoxy resin system (Cycom), new formulations of epoxy resin-based blends were obtained using commercial dendrimer and synthesized HB polyesters.

The work was carried out in two stages:

- The synthesis and characterization of HB poly(butylene adipate) polyester, 5HB30 sample.
- The preparation and characterization of epoxy resin-based blends with two different toughening additives: commercial dendritic (Boltorn), and synthesized HB (5HB30) polyesters.

The properties of epoxy resin-based systems toughened with Boltorn and 5HB30 were determined, using the neat Cycom as reference.

According to the characterization of HB polyesters previously synthesized (reported in detail in Chapter 2), 5HB30 sample was selected as HB toughening agent for epoxy resin-based blends. The choice of this sample was done considering that it represents the most HB species of a family of samples synthesized using 5 molar percent of branching agent (TMP). It appears soluble in most solvents commonly used for these type of HB polymers, chloroform (CHCl<sub>3</sub>), tetrahydrofuran (THF), dimeyhl sulphoxide (DMSO), N,N dimethylformamide (DMF), trifluoro acetic acid (TFA), and for this reason fully characterized by means of <sup>1</sup>H-NMR and ATR spectroscopy, MALDI-TOF mass spectrometry, SEC chromatography, WAXD diffraction, DSC and TGA thermal analyses. The MALDI mass spectrum of 5HB30 sample, reported in Chapter 2, shows only peaks related to HB macromolecules, in particular chains containing ether units and cyclic branches formed by (intra e inter)-molecular trans-etherification and intra-molecular trans-esterification reactions, respectively.

The key issue of this work was to obtain an epoxy resin-based material with an increased toughness, workable in conventional processing equipments and conditions, and matching the technical requirements such as thermal and mechanical resistance.

## 4.2 Experimental section

### 4.2.1 Materials for epoxy resin-based blends

Epoxy resin-based blends were prepared using a commercial one-part liquid epoxy resin system Cycom® 890 RTM (Cycom), produced by Cytec Industries (density at 25 °C = 1.22 g/cm<sup>3</sup>).

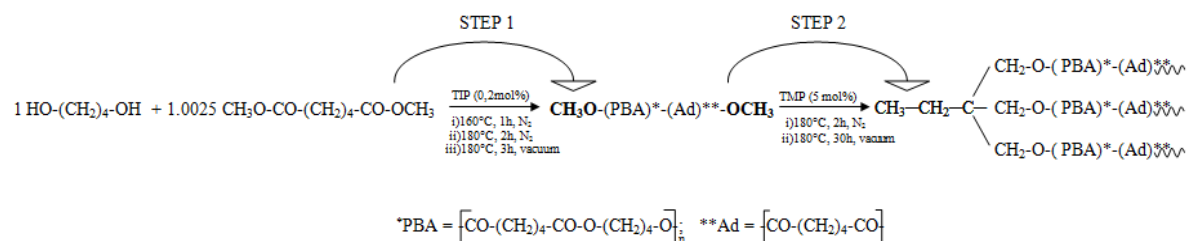
Boltorn® H311 (Boltorn) is a dendritic polyester polyol with high hydroxyl functionality ( $M_w = 5700$  g/mol, hydroxyl number = 230-260 mg KOH/g), used in this work as

toughening agent. It contains 10 % of water and is a viscous liquid at  $T_{\text{room}}$ ; it presents excellent solubility in polyether, polyols, glycols, and polyalcohol's.

As toughening agent a tailored synthesized HB polyester, 5HB30 sample, was also selected and used. For the synthesis of this polymer 1,4-butanediol (BD) (99%), dimethyl ester of adipic acid (DMA) ( $\geq 99\%$ ), titanium(IV)isopropoxide (TIP) (99.99%), as catalyst, 1,1,1-tris(hydroxy methyl)propane (TMP) ( $\geq 98.0\%$ ), as branching agent, chloroform ( $\text{CHCl}_3$ ) and methanol ( $\text{CH}_3\text{OH}$ ), as solvents, were also purchased from Sigma-Aldrich (Italy) and used without any purification.

## 4.2.2 Synthesis of HB polyester

5HB30 sample, chosen as HB toughener for epoxy resin-based blends, was synthesized in one-pot synthesis performed in two steps, according to the Scheme 4.1.



**Scheme 4.1: Synthesis route of 5HB30 sample.**

In the first step, a tailored PBA methyl ester ended pre-polymer was synthesized using a DMA/BD molar ratio of 1.0025/1 as described before in Chapter 2. In the second step, 5 molar percent (with respect to the initial moles of monomer reagents) of TMP as branching agent was added and the reaction was carried out at 180 °C for 2 h at 1 atm, under nitrogen flow and under stirring. Then the reaction was continued under vacuum for 30 h, in order to obtain HB species.

For more details, see Table 2.1 in Chapter 2, in which experimental parameters (i.e. DMA/BD molar ratio, temperature, and reaction time) and molar mass distribution are described.

## 4.2.3 Preparation of epoxy resin-based blends

The blends were prepared by mixing dendritic and HB polymers with the epoxy resin. The mixture was heated at 90 °C for 1 h under stirring. The cure was carried out at 180 °C for 2 h under vacuum. The formulations of all epoxy resin-based blends are reported in detail in Table 4.1.



Table 4.1: Epoxy resin-based blends.

Polymer content (wt. %)	Boltorn blend	5HB30 blend
1	C1B	C1H
3	C3B	C3H
5	C5B	C5H
10	C10B	C10H

The sheets with a thickness of 4 mm were obtained using a silicon frame between two glass plates. The cure on the samples was conducted at 180 °C for 2 h as specified in the Cycom's data sheets.

#### 4.2.4 Characterization

##### Attenuated total reflectance spectroscopy (ATR)

The structural properties of cured and uncured neat Cycom and Cycom-based blends were studied by means of ATR spectroscopy using a Nicolet 6700 FT-IR (Thermo Fischer Scientific). The ATR spectra were obtained at a resolution of 4 cm<sup>-1</sup> and 16 scans were averaged for each spectrum in a range between 4000-650 cm<sup>-1</sup>.

##### Thermogravimetric analysis (TGA)

The thermal stability of toughening polymers, neat Cycom, and the epoxy resin-based blends after cure at 180 °C for 2 h was studied by means of TGA analysis. TGAs were performed in duplicate and carried out at heating rate of 10 °C/min from 25 °C to 700 °C under nitrogen flow using a thermo balance (Q5000 by TA Instruments).

##### Differential scanning calorimetry (DSC)

The dynamical cure behavior of neat Cycom and epoxy resin-based blends was investigated using a differential scanning calorimeter (Q2000 by TA Instruments). A dynamic heating rate of 10 °C/ min was used. The blends were heated from 40 to 310 °C, cooled from 310 to 40 °C and heated again to 250 °C.

##### Rheological characterization

The rheological behavior were studied on a rotational rheometer (AR-G2 by TA Instruments), equipped with steel parallel plates of 25mm diameter.

Steady-state flow experiments were performed within the linear visco-elastic region for the two toughening agents and PBA pre-polymer, used as reference, at frequencies between 0.1 and 100 s<sup>-1</sup>. The sample temperature was set at 80 °C, and controlled to within 1 °C of the set point. Nitrogen gas was used to force convection within the rheometer oven and to prevent thermal oxidation of the samples.

Neat Cycom and epoxy resin-based blends were analyzed isothermally at 80 and 100 °C, at a frequency of 1 rad/s, for a period of 60 minutes.

### **Dynamic mechanical thermal analysis (DMTA)**

DMTA measurements were carried out for cured neat Cycom and epoxy resin-based blends by using a Tritec 2000 DMA testing machine by Triton Technology, UK. Tests were performed in single cantilever bending mode on samples with dimensions of (30 x 6 x 4)mm, using a constant frequency of 1 Hz and an amplitude of oscillation of 0.01 mm. Samples were heated from -80 °C to 260 °C, at a heating rate of 3 °C/min.

### **Fracture toughness measurements**

Fracture toughness tests of cured neat Cycom and epoxy resin-based blends were performed by using the single-edge-notch bending (SENB) method according to ASTM D 5045-99 using an Instron 4505 universal tester machine. The sample dimensions are (60 x 6 x 4) mm. A cross-head speed of 1 mm/min was used for testing. The critical stress-intensity factor,  $K_{Ic}$ , was calculated by the following equation (4.1):

$$K_{Ic} = \left( \frac{P}{BW^{3/2}} \right) f(x) \quad (4.1)$$

where  $P$  is the maximum load,  $B$  and  $W$  are the specimen thickness and width, respectively, and  $f(x)$  is expressed as follows:

$$f(x) = 6x^{1/2} \frac{[1.99 - x(1-x)(2.15 - 3.93x + 2.7x^2)]}{(1+2x)(1-x)^{3/2}} \quad (4.2)$$

where  $x = a/W$ , in which  $a$  is the crack length. The critical strain energy release rate,  $G_{Ic}$ , was calculated by the following equation (4.3):

$$G_{Ic} = \frac{(1-\nu^2)K_{Ic}^2}{E} \quad (4.3)$$

where  $\nu$  is the Poisson's coefficient equal to 0.3 for epoxy resin and  $E$  is Young's modulus determined by flexural three point bend test. To determine the  $K_{Ic}$  and  $G_{Ic}$  values, five samples were tested for each material.

For a result to be considered valid, the following size criteria has been verified:

$$B, a, (W-a) > 2.5 (K_Q/\sigma_y)^2 \quad (4.4)$$

where  $K_Q$  is the conditional or trial  $K_{Ic}$  value and  $\sigma_y$  is the yield stress of the material for the temperature and loading rate of the test. The criteria require that  $B$  must be sufficient to ensure plane strain and that  $(W-a)$  be sufficient to avoid excessive plasticity in the ligament

### **Morphological observation**

The fractography of the failed SENB samples was observed to examine the fracture characteristics of the cured neat Cycom and epoxy resin-based blends. A Quanta 200 Feg scanning electron microscope (by FEI Company) was used for observation, before which the surface were coated with gold/palladium of the thickness of about 13 nm.

## **4.3 Epoxy resin-based blends characterization: results and discussion**

### **4.3.1 Attenuated total reflectance spectroscopy (ATR)**

Being a commercial product, Cycom® 890 RTM formulation is not known. However, it may be hypothesized that it includes more than one component because it is an one-part liquid epoxy resin system.

The constituent for epoxy resin is always an epoxy monomer. The main feature of the epoxy monomer is the oxirane functional group, which is a three member ring formed between two carbon atoms and an oxygen. This atomic arrangement shows enhanced reactivity when compared with common ethers because of its high strain. Due to the different electronegativity of carbon and oxygen, the carbon atoms of the ring are electrophilic. Thus, epoxies can undergo ring opening reactions towards nucleophiles. The polarity of the oxirane ring makes possible detection by IR spectroscopy.

The cure of the neat epoxy resin, displayed in Figure 4.1, was monitored by the disappearance of the epoxy vibration, which occurs at about  $909\text{ cm}^{-1}$ , attributed to the C-O deformation of the oxirane group, and the appearance of C-N stretch at approximately  $3300\text{ cm}^{-1}$ . These bands can also indicate whether the cure process has been completed

satisfactorily and are an indication of either non-stoichiometric of the reactants or insufficient reaction occurring during the cure process. The second band is located at approximately  $3050\text{ cm}^{-1}$  and is attributed to the C-H tension of the methylene group of the epoxy ring. This band is not very useful since its intensity is low and it is also very close to the strong O-H absorptions.<sup>18</sup> It is found a broad, ill resolved absorption with a maximum at  $3380\text{ cm}^{-1}$ , due to the O-H stretching absorption. These are extensively H-bonded, as witnessed by the band's breadth. The multicomponent shape of the O-H band indicates a complex system where multiple H-bonding species coexist, together with a non negligible fraction of non-interacting groups.<sup>19</sup>

In Table 4.2 the peak frequencies and tentative assignments for the spectrum of cured neat Cycom, displayed in Figure 4.1, are reported according to the litterature.<sup>19,20</sup>

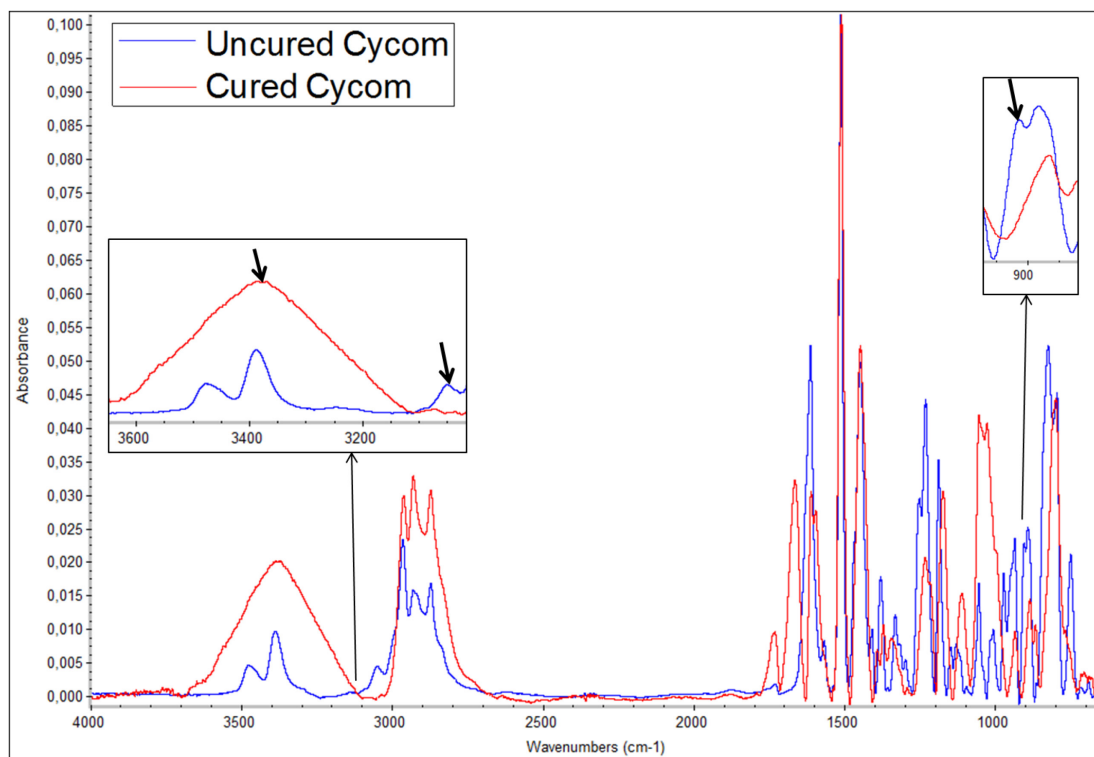


**Figure 4.1: ATR spectra of cured and uncured neat Cycom.**

The ATR spectra of Boltorn, cured neat Cycom, and Cycom/Boltorn blends are shown in Figure 4.2; instead, the ATR spectra of 5HB30, cured neat Cycom, and Cycom/HB blends are illustrated in Figure 4.3. In these pictures the presence of the peak related to the stretching of carbonyl group ( $\text{C}=\text{O}$ ), typical of polyester species, is visible. In both insets, the signal at  $1735\text{ cm}^{-1}$  increases with increasing the content of polymers in the epoxy resin-based blends. The broad band at  $\sim 3500\text{ cm}^{-1}$  reveals the presence of hydroxyl end-groups ( $-\text{OH}$ ) in Boltorn sample. From the Figure 4.2 and Figure 4.3 it is also clear that the signals of ATR spectra of neat Cycom and its blends are very similar, suggesting the

existence of only physical and not chemical bonds between epoxy resin matrix and polyesters added.

**Table 4.2: Peak frequencies and tentative assignments for the spectrum of cured neat Cycom.**

Peak position (cm <sup>-1</sup> )	Tentative assignment
3380 m	$\nu$ (O-H); Hydrogen bonded
2944 m	$\nu_{as}$ (CH <sub>3</sub> )
2930 m	$\nu_{as}$ (CH <sub>2</sub> )
2872 m	$\nu_s$ (CH <sub>2</sub> )
1735 w	$\nu_s$ (C=O)
1593 m	Ring quadrant stretching I
1509 s	Ring semicircle stretching I
1460 m	$\delta_{as}$ (CH <sub>2</sub> )
1384 w	$\delta_{as}$ (CH <sub>3</sub> )
1362 w	$\delta_s$ (CH <sub>3</sub> )
1294 m	-
1246 m	$\nu$ (Ar-O-CH <sub>2</sub> -)
1182 w	(CH <sub>3</sub> -C-CH <sub>3</sub> ) skeletal
1038 m	$\nu$ (Ar-O-CH <sub>2</sub> -)
1012 w	$\delta$ (Ar-H) in-plane
882 w	$\gamma$ (Ar-H) out-of-plane
795 m	$\rho$ rocking (CH <sub>2</sub> )

$\nu_{as}$  = asymmetrical stretching;  $\nu_s$  = symmetrical stretching;  $\delta$  = in-plane deformation;  $\gamma$  = out-of-plane deformation;  $\rho$  = rocking vibration. s = strong; m = medium; w = weak.

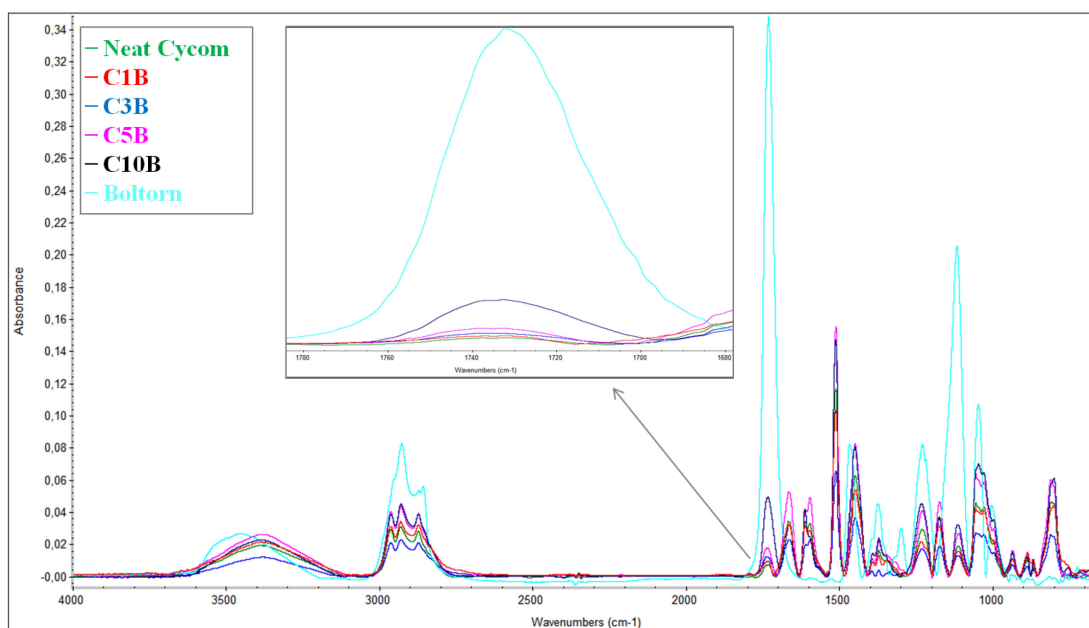


**Figure 4.2: ATR spectra of Boltorn, cured neat Cycom, and Cycom/Boltorn blends.**

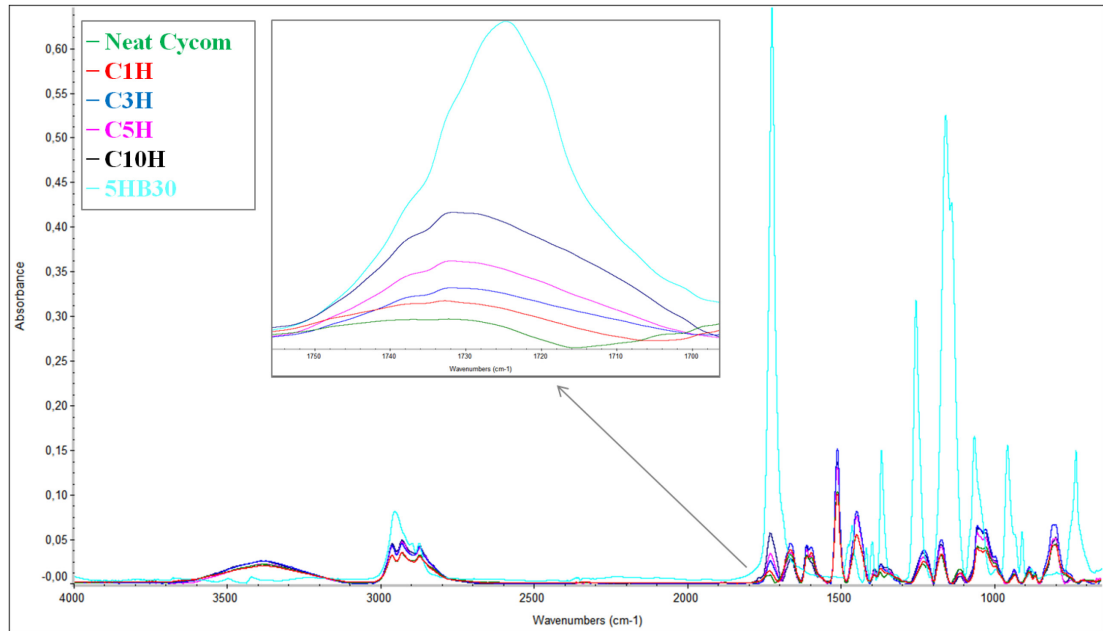


Figure 4.3: ATR spectra of 5HB30, cured neat Cycom, and Cycom/HB blends.

### 4.3.2 Thermogravimetric analysis (TGA)

In Table 4.3, the onset temperature ( $T_{\text{onset}}$ ), the temperature at 5 % weight loss ( $T_{5\% \text{wt. loss}}$ ), the temperature at maximum degradation rate ( $T_{\text{max. deg. rate}}$ ), and the char yield at 700 °C are listed for neat Cycom, two toughening polymers, and all epoxy resin-based blends.

Table 4.3:  $T_{\text{onset}}$ ,  $T_{5\% \text{wt. loss}}$ ,  $T_{\text{max. deg. rate}}$  and char yield for neat Cycom, Boltorn, 5HB30, and epoxy resin-based blends.

	Neat Cycom	Boltorn	C1B	C3B	C5B	C10B	5HB30	C1H	C3H	C5H	C10H
$T_{\text{onset}}$ (°C)	326.2	263.4	318.8	321.0	322.9	316.0	275.9	314.2	316.8	322.8	317.3
$T_{5\% \text{wt. loss}}$ (°C)	347.9	287.6	345.9	344.4	343.5	340.4	313.5	345.0	346.2	350.0	345.5
$T_{\text{max. deg. rate}}$ (°C)	391.4	338.0	393.4	395.3	396.0	398.0	387.3	396.3	395.1	393.3	390.0
Char Yield (%)	21.2	0.9	19.5	19.5	20.2	19.6	0.2	17.5	17.5	17.6	17.6

Figure 4.4 shows the TG curves of Boltorn, neat Cycom, and Cycom/Boltorn blends; instead Figure 4.5 illustrates the TG curves of 5HB30, neat Cycom, and Cycom/HB blends. From both TG pictures, it is evident that all epoxy resin-based blends show a thermal degradation behavior very similar to neat Cycom despite the lower thermal stability of both toughening polymers.

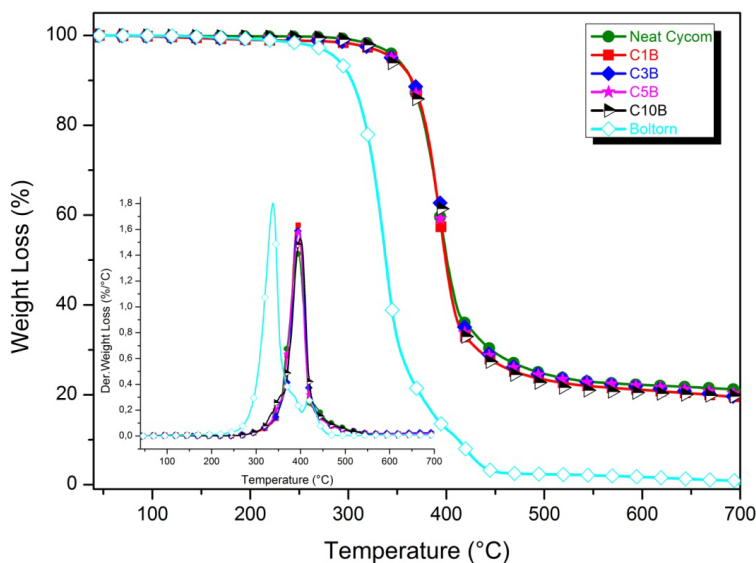


Figure 4.4: TG curves of Boltorn, neat Cycom, and Cycom/Boltorn blends.

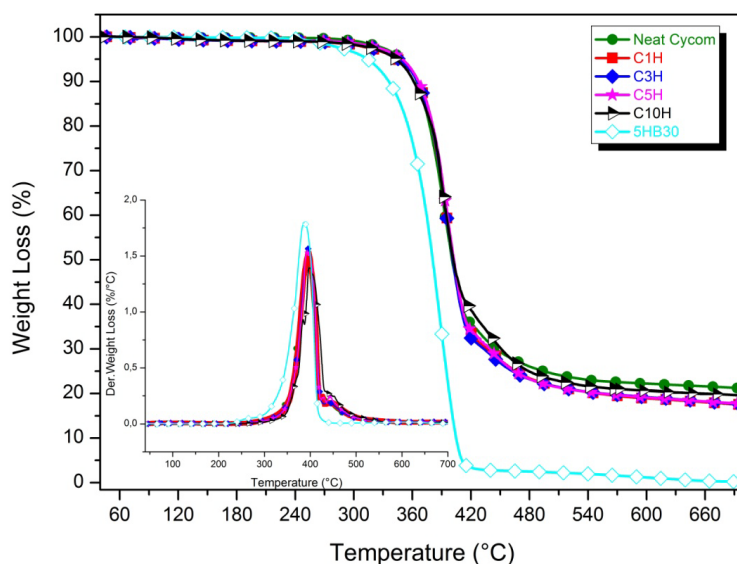


Figure 4.5: TG curves of 5HB30, neat Cycom, and Cycom/HB blends.

This is also visible in the value of the temperature at maximum degradation rate. These results suggest that the increment in toughening content does not influence the stability of blends. The neat Cycom shows a char content of 21.2 % at 700 °C under nitrogen atmosphere, and this residue is also present in all blends but, independently from the content and type of toughening agent used, this value decreases.

### 4.3.3 Differential scanning calorimetry (DSC)

In Table 4.4, the onset curing temperature ( $T_{\text{onset}}$ ), the exothermic peak temperature ( $T_{\text{max}}$ ), the heat of cure process in terms of the enthalpy of reaction ( $\Delta H$ ) and normalized enthalpy

of reaction ( $\Delta H_{\text{norm}}$ , normalized for the effective weight of the epoxide in the blends) are reported for neat Cycom and epoxy resin-based blends.

**Table 4.4:**  $T_{\text{onset}}$ ,  $T_{\text{max}}$ ,  $\Delta H$ ,  $\Delta H^*_{\text{norm}}$  for neat Cycom and epoxy resin-based blends.

	Neat Cycom	C1B	C3B	C5B	C10B	C1H	C3H	C5H	C10H
$T_{\text{onset}}$ (°C)	242	238	232	230	220	241	241	241	242
$T_{\text{max}}$ (°C)	276	275	273	270	265	277	278	278	281
$\Delta H$ (J/g)	433.9	416.0	423.9	417.2	397.7	412.3	410.5	422.3	413.1
$\Delta H^*_{\text{norm.}}$ (J/g)	433.9	420.2	437.0	439.2	441.9	416.5	423.2	444.5	459.0

$\Delta H^*_{\text{norm.}}$  were measured from  $\Delta H$  blends considering the polymers wt. % content added.

Figure 4.6 shows the Boltorn loading effect on the cure reaction for Cycom/Boltorn blends. It is clear from the Figure 4.6 that Boltorn induces a shift of the curing peak to lower temperatures (see also  $T_{\text{onset}}$  and  $T_{\text{max}}$  values reported in Table 4.4) with increasing the content of dendrimer in the blends.

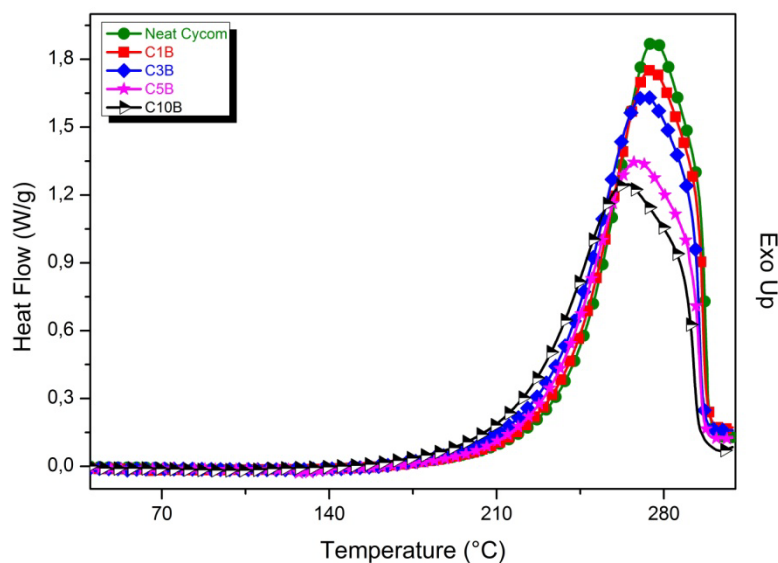


**Figure 4.6:** Dynamical cure analysis for neat Cycom and Cycom/Boltorn blends.

The addition of Boltorn, having a highly branched flexible backbone with numerous primary hydroxyl groups, enhances the reactivity of epoxy, resulting in a high degree of epoxy conversion.<sup>21</sup> This can be interpreted in terms of intermolecular transition state.<sup>22</sup> According to this mechanism, the strong hydrogen-bonding species, such as alcohol groups, stabilize the transition state, thus encouraging the nucleophilic attack of the amine.<sup>7,23,24</sup>



Figure 4.7 shows the 5HB30 loading effect on the cure reaction of Cycom/HB blends. It is evident that the addition of 5HB30 sample does not affect the cure kinetics of epoxy resin, suggesting that this polyester does not behave as cure catalyst.

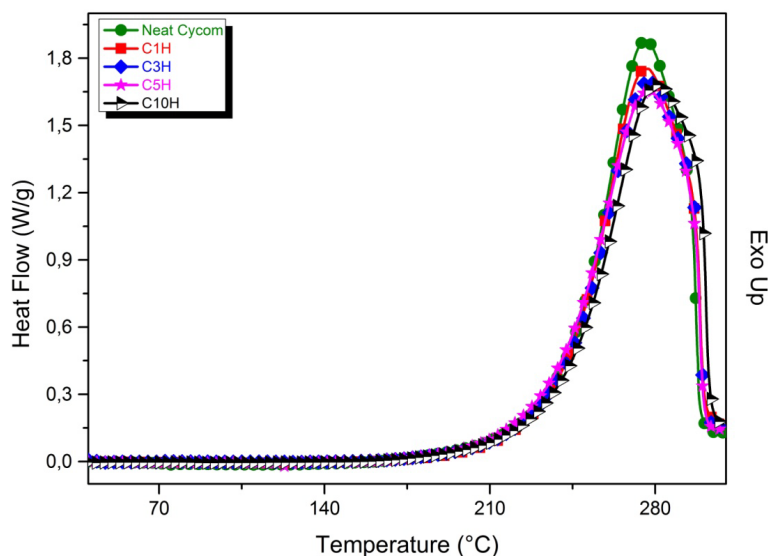


Figure 4.7: Dynamical cure analysis for neat Cycom and Cycom/HB blends.

Besides, it is interesting to note the absence of 5HB30 melting peak in the DSC thermograms of Cycom/HB blends. This behavior could be explained according to the blends preparation which involves temperature above the  $T_m$  of HB sample, inducing the amorphization of the polyester additive. After mixed, the epoxide chains avoid the recrystallization of 5HB30 sample.

From data reported in Table 4.4, it is evident that the heat of reaction is influenced by the presence of Boltorn and 5HB30 samples, since it increases with increasing the polymers content. Considering that the energy measured is related to the epoxy rings opening, the increment in the value of  $\Delta H_{\text{norm}}^*$  could be attributed to the polymers addition. The presence of these polyesters in the epoxy matrix prevent the cure reaction caused by viscosity effect, hindering the motion of the reactive chain segments and requiring a larger amount of energy to complete the cure reaction.<sup>25,26</sup>

#### 4.3.4 Rheological characterization

In order to understand the effect of the addition of toughening agents on epoxy matrix, the two polymers, Boltorn and 5HB30, were analyzed rheologically by means of a steady-state flow experiments.

Figure 4.8 shows steady-state flow curves of Boltorn, 5HB30 and PBA pre-polymer, used as reference. Rheological tests show that both Boltorn and PBA pre-polymer exhibit

Newtonian behavior in the melt state, while 5HB30 shows shear thinning behavior. First of all, it is of interest to note that Boltorn exhibits a lower viscosity (about an order of magnitude) than the linear PBA pre-polymer with similar molar mass, as widely confirmed in literature, due to its globular shape, followed by low hydrodynamic volume and melt viscosity.<sup>27</sup>

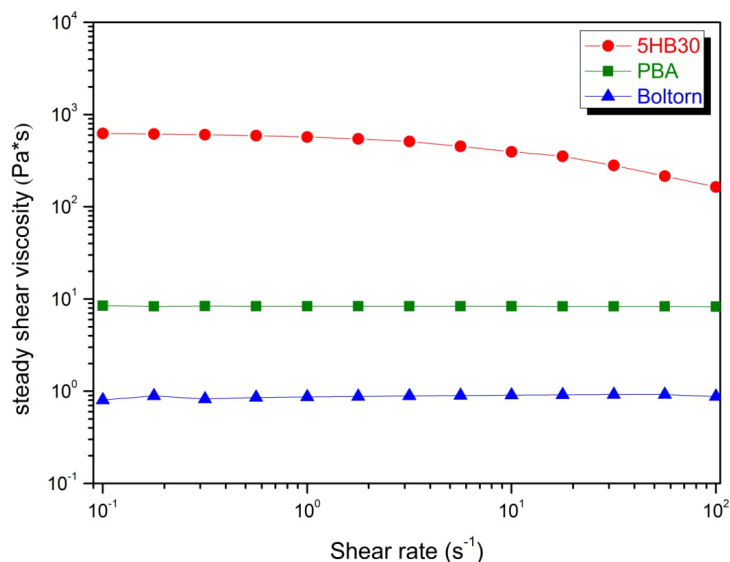


**Figure 4.8: Steady shear viscosity of 5HB30, Boltorn, and PBA pre-polymer, used as reference, at 80 °C.**

The Newtonian behavior in the melt state is typical of dendritic polymers and it is justified by the absence of entanglement points for such globular structures.<sup>28,29</sup> In the case of 5HB30 sample, the presence of shear thinning behavior has to be ascribed to the presence of some sort of interaction between the molecules, in particular hydrogen bonding due to hydroxyl end-groups of HB macromolecules with consequent shear thinning. In the case of Boltorn, the dendritic arms became more flexible and can fold back into the HB molecule, thus leaving less polar end-groups exposed to the other molecules.

The first requirement for a RTM resin is the attainment of low viscosity during the injection phase. In order to understand the effect of the addition of toughening additives in epoxy resin, the uncured neat Cycom and epoxy resin-based blends, were studied in a parallel plate rheometer for 1 h. In Figure 4.9a the viscosity traces of uncured Cycom/Boltorn versus time are reported; instead, in Figure 4.9b the viscosity traces of uncured Cycom/HB blends versus time are displayed to study the stability of epoxy resin-based blends in time at 80 °C. From the viscosity graphs of the neat Cycom and their blends, we can observe that both polymeric systems, Boltorn and 5HB30, show a decrease

in viscosity blends. But Cycom/Boltorn blends always exhibit viscosity values higher than Cycom/HB blends at the same polymeric additive content as reported in Table 4.5.

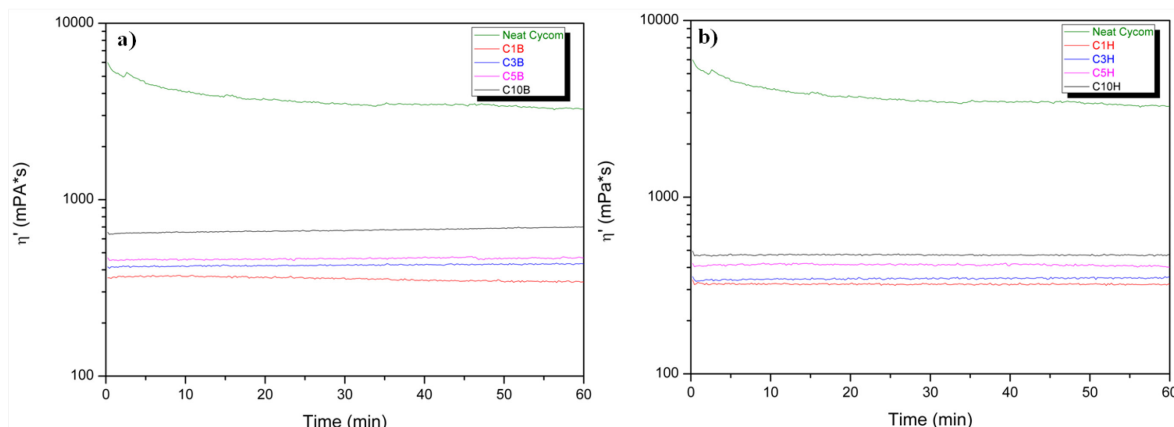


Figure 4.9: Time sweep test for Cycom/Boltorn (a) and Cycom/HB (b) blends at 80 °C.

The same behavior is also visible at 100 °C, as displayed in Figure 4.10

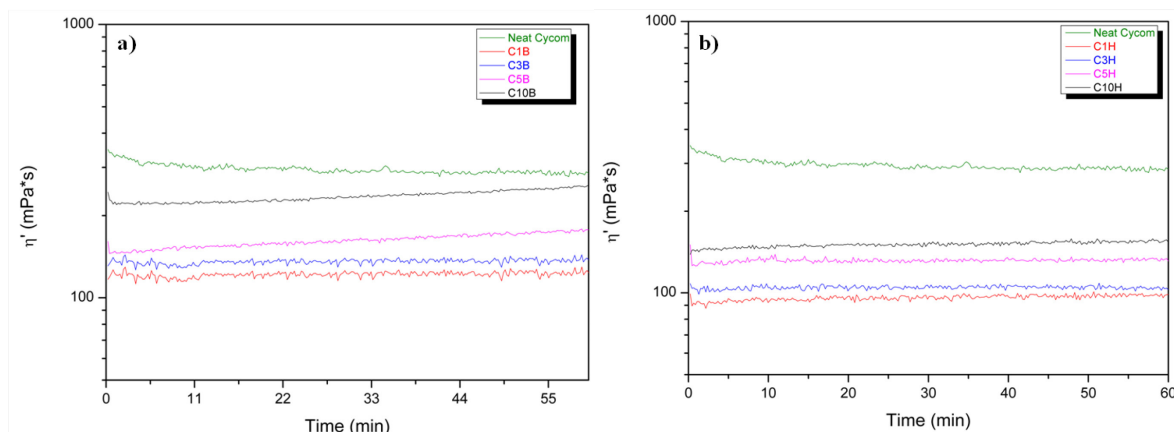


Figure 4.10: Time sweep test for Cycom/Boltorn (a) and Cycom/HB (b) blends at 100 °C.

Table 4.5: Viscosity values of neat Cycom and epoxy resin-based blends.

	Neat Cycom	C1B	C3B	C5B	C10B	C1H	C3H	C5H	C10H
$\eta'_{(T=80\text{ }^{\circ}\text{C})}$	3432	353	429	477	670	320	348	418	482
$\eta'_{(T=100\text{ }^{\circ}\text{C})}$	295	122	138	160	232	97	106	132	153

Both toughening agents possess spherical structures which cause a lower viscosity than linear polymers for equivalent molecular weight.<sup>30</sup> This decrease in viscosity blends is due to finely phase separation which causes a sort of slipping of the epoxy macromolecules on the toughening particles. Increasing the polymers content, the polyester particles aggregate to each other generating agglomerates firmly attached to the epoxy matrix by hydrogen bonding causing the increment of viscosity blends.<sup>31</sup>

Boltorn, unlike to 5HB30 sample, has high concentration of polar groups (-OH) on the dendritic shell that could give rise to hydrogen bonding able to catalyze the epoxy reaction, also increasing the reaction rate.<sup>32</sup> This is the reason for which, at the same polymeric content, Cycom/Boltorn blends have higher viscosity values than Cycom/HB blends.

### 4.3.5 Dynamic mechanical thermal analysis (DMTA)

The dynamic mechanical thermal analysis was performed to determine the glass transition temperature ( $T_g$ ) and storage modulus ( $E'$ ) for neat Cycom and epoxy resin-based blends. The trend of  $T_g$ s was used as an indirect tool to evaluate the extent of compatibility between epoxy resin matrix and polymeric tougheners.

In Table 4.6 the  $T_g^{\text{DMA}}$  (measured at the maximum of  $\tan\delta$  curves), the  $T_g^{\text{DSC}}$  derived from DSC analysis and the theoretically  $T_g^{\text{Fox Eq.}}$  values calculated from the Fox equation (as reported in Equation 4.5) of all samples are reported,

$$1/T_{gb} = w_1/T_{g1} + w_2/T_{g2} \quad (4.5)$$

where  $w_1$  and  $w_2$  are the weight fraction and  $T_{g1}$ ,  $T_{g2}$  and  $T_{gb}$  are the glass transition temperatures of individual polyesters (i.e. Boltorn and 5HB30) and the neat Cycom, respectively. The  $T_g$ s of neat Cycom, Boltorn and 5HB30 samples are 220, -20, and -50 °C, respectively. All blends show a single  $T_g$  and this value gradually shifted to lower temperature with increasing concentration of polyester content. The decrease in  $\tan\delta$  peak temperature at higher concentration of HB polymer is related to the dissolution of some tougheners into the epoxy resin matrix.<sup>7</sup>

The clearly lower  $T_g^{\text{DMA}}$  values observed for dynamically scanned blends compared to those polymerized with the cure schedule, outline the importance of the control of cure temperature. Thus, the difference in  $T_g$  values, quoted in Table 4.6 for the blends cured by the above referred ways, would be connected to distinct levels of segregation through phase separation during the dynamic curing, and during polymerization with the cure schedule. In the case of dynamic scan, the HB polymers does not get sufficient time to undergo phase separation completely.<sup>7</sup>

The experimental  $T_g^{\text{DMA}}$  values are higher than that calculated from Fox Equation. This indicates very strong interaction between tougheners and epoxy resin matrix possible due to extensive hydrogen bonding.<sup>33-34</sup>

Table 4.6: DMTA values in terms of  $E'$ ,  $T_g^{DMA}$ ,  $T_g^{DSC}$  and  $T_g^{Fox Eq.}$  for neat Cycom and epoxy resin-based blends.

	Neat Cycom	C1B	C3B	C5B	C10B	C1H	C3H	C5H	C10H
$E'$ (GPa)	1.89	2.02	2.03	2.10	1.90	1.94	2.04	2.09	1.74
$T_g^{DMA}$ (°C)	220	216	213	208	193	217	208	204	182
$T_g^{DSC}$ (°C)	148	141	140	140	128	149	138	130	120
$T_g^{Fox Eq.}$ (°C)	-	215	206	198	177	214	202	192	167

The  $\tan\delta$  traces of Cycom/Boltorn and Cycom/HB blends are reported as a function of temperature in Figure 4.11 and Figure 4.12, respectively.

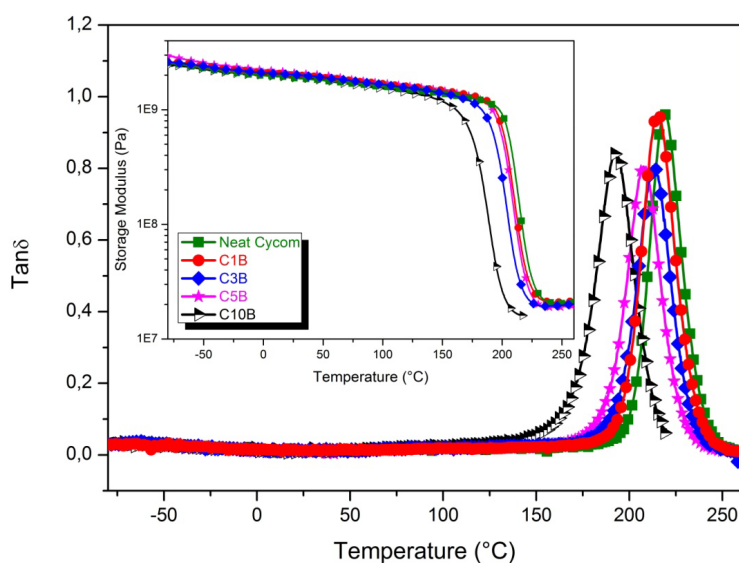


Figure 4.11: DMTA curves of neat Cycom and Cycom/Boltorn blends.

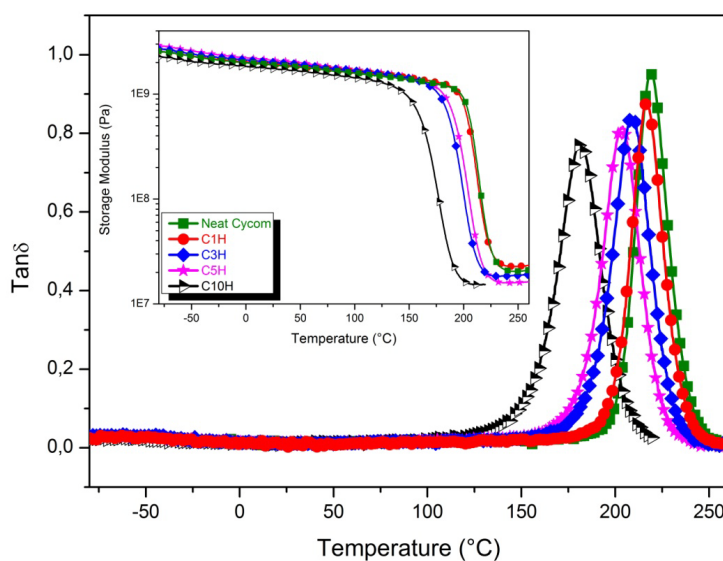


Figure 4.12: DMTA curves of neat Cycom and Cycom/HB blends.

It is well known that  $T_g$  depends on the mobility of the chain segments of macromolecules in the network structure. As temperature is increased, it is observed that the damping goes through a maximum in the transition region and then decreases in the rubbery region. The damping is low below  $T_g$  as the chain segment in that region is frozen. Below  $T_g$  the deformations are thus primarily elastic, and the molecular slips resulting in viscous flow are low. Also above  $T_g$ , in the rubbery region, the damping is low because the molecular segments are free to move, and consequently there is little resistance to flow. In the transition region, on the other hand, the damping is high because of the initiation of micro-Brownian motion of the molecular chain segments and their stress relaxation.<sup>35</sup>

For both systems, a single glass transition temperature was observed at each composition indicating miscibility between epoxy resin matrix and toughening polymers. The good miscibility can be ascribed to the hydrogen bonding existing between the carbonyl groups ( $-C=O$ ) of the esters and the hydroxyl groups ( $-OH$ ) of the epoxy matrix. Low  $T_g$  is also related to the reduction of cross-linking density as a result of the dilution effect of the un-cross-linked, HB molecules.<sup>32</sup>

From the dynamic spectra, values of storage moduli ( $E'$ ) at 25 °C are obtained and listed in Table 4.6. The storage modulus at room temperature increases with increasing in HB concentration up to 5 wt. % than decreases for 10 wt. %. The increment in the storage moduli can be attributed to the presence of entangled networks and a very high level of interaction between epoxy resin matrix and HB polymers.<sup>20</sup>

### 4.3.6 Fracture toughness measurements

In Table 4.7 the  $K_{Ic}$  and  $G_{Ic}$  values for neat Cycom and epoxy resin-base blends are reported.

**Table 4.7:  $K_{Ic}$  and  $G_{Ic}$  for neat Cycom and epoxy resin-based blends.**

	Neat Cycom	C1B	C3B	C5B	C10B	C1H	C3H	C5H	C10H
$K_{Ic}$ ( $MPa \cdot m^{1/2}$ )	0.318± 0.027	0.455± 0.033	0.439± 0.045	0.348± 0.027	0.350± 0.023	0.470± 0.047	0.495± 0.048	0.609± 0.045	0.275± 0.023
$G_{Ic}$ ( $KJ/m^2$ )	0.037± 0.004	0.075± 0.011	0.071± 0.014	0.043± 0.005	0.047± 0.006	0.086± 0.011	0.091± 0.012	0.149± 0.010	0.027± 0.005

The effect of toughening polymers content for Cycom/Boltorn and Cycom/HB blends on the  $K_{Ic}$  and  $G_{Ic}$  values is reported in Figure 4.13 and Figure 4.14, respectively.

The neat cycom resin is a very brittle material, with a  $K_{Ic}$  value of  $0.318 MPa \cdot m^{1/2}$ . If we consider Cycom/Boltorn blends, only a small improvement in the impact strength was

achieved. C1B blend increases  $K_{Ic}$  value of 43% than neat Cycom. Instead, if we consider the Cycom/HB blends, the  $K_{Ic}$  and  $G_{Ic}$  values gradually increase with increasing the content of 5HB30 up to 5 wt. % but then rapidly drop down for 10 wt. %. The  $K_{Ic}$  value of C5H blends reach  $0.609 \text{ MPa}\cdot\text{m}^{1/2}$  with an improvement of 90% than neat Cycom. It is interesting to note that all Cycom/Boltorn blends always improve the toughness of neat Cycom even if of low extent unlike to Cycom /HB blends.

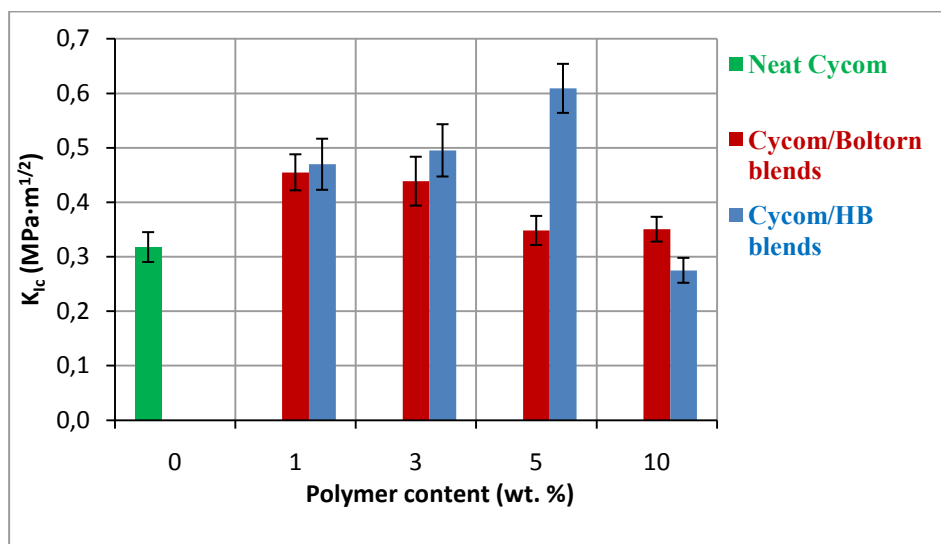


Figure 4.13: Effect of polymers loading on the  $K_{Ic}$  for the neat Cycom and the epoxy resin-based blends.

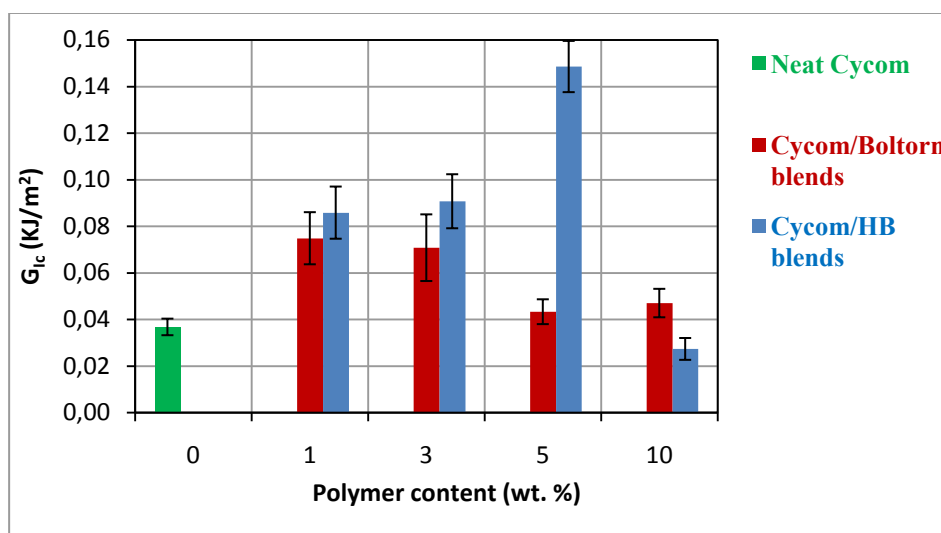


Figure 4.14: Effect of polymers loading on the  $G_{Ic}$  for the neat Cycom and the epoxy resin-based blends.

The addition of HB polymers can remarkably improve the toughness of the epoxy resin because of the intramolecular defect of HB polymers, which can absorb much more energy while impacting.



### 4.3.7 Morphological observations

In conclusion, the addition of 5HB30 and Boltorn samples can effectively improve the toughness of epoxy matrix, as widely reported in other literature.<sup>7,20,21,36</sup> The toughness behaviors of epoxy resin-based blends can be explained in terms of morphology with scanning electron microscopy (SEM). The fracture surface of these blends after impact tests were investigated with SEM and the results are shown in figures below.

Figure 4.15 shows a micrographs of the fracture morphologies of the neat Cycom. The epoxy network clearly appears as a smooth, glassy, fractured surface with cracks in different planes and without any sign of plastic deformation, and this accounts for its poor impact strength.

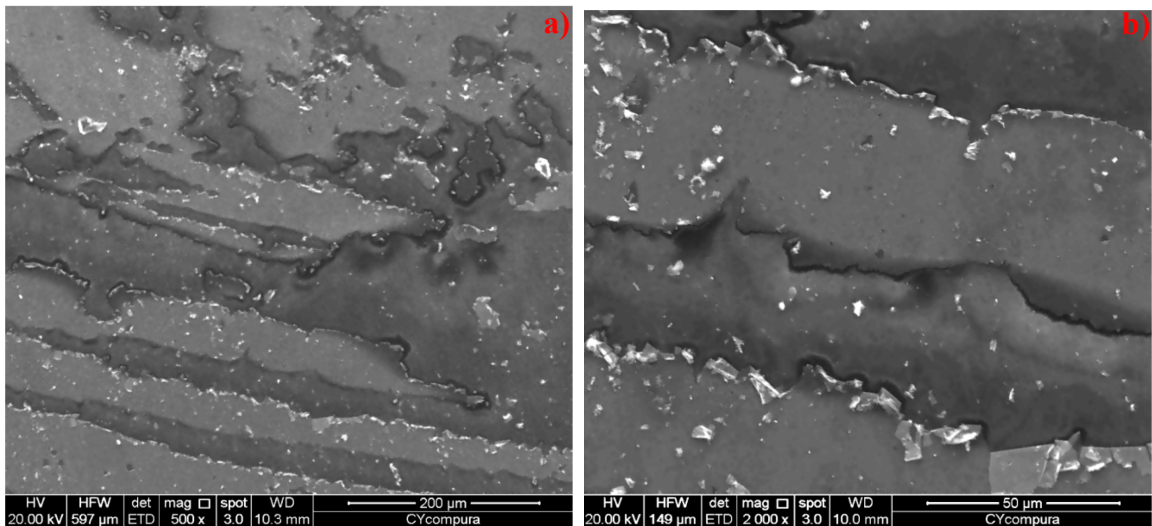


**Figure 4.15: SEM images of the fracture surface under impact of the neat Cycom at 500X (a), and 2000X (b).**

Figure 4.16 displays the SEM images of C1H (a) and C3H (b) samples in which we can note that increasing the 5HB30 content, a particulate morphology in which the discrete HB-rich phases are dispersed in a continuous matrix of epoxy resin is obtained.<sup>24,37</sup> In other words, the fracture surface of the modified networks consist of two phases: a globular HB particles phase dispersed in a continuous matrix of epoxy resin. Inclusion of 3 wt. % of 5HB30 produces a HB-rich phase with larger particle size distribution due to aggregation which causes increased adhesion to the epoxy matrix with an improved toughening effect.

The SEM images of C5H sample show “sea-island” structures (see Figure 4.17 and Figure 4.18a), “dimple-like” structures and macroscopically sized stress-whitened zones surround the crack which are generally the characteristics of rubber-modified epoxy resins and called “toughness dimples” (also see Figure 4.18b).



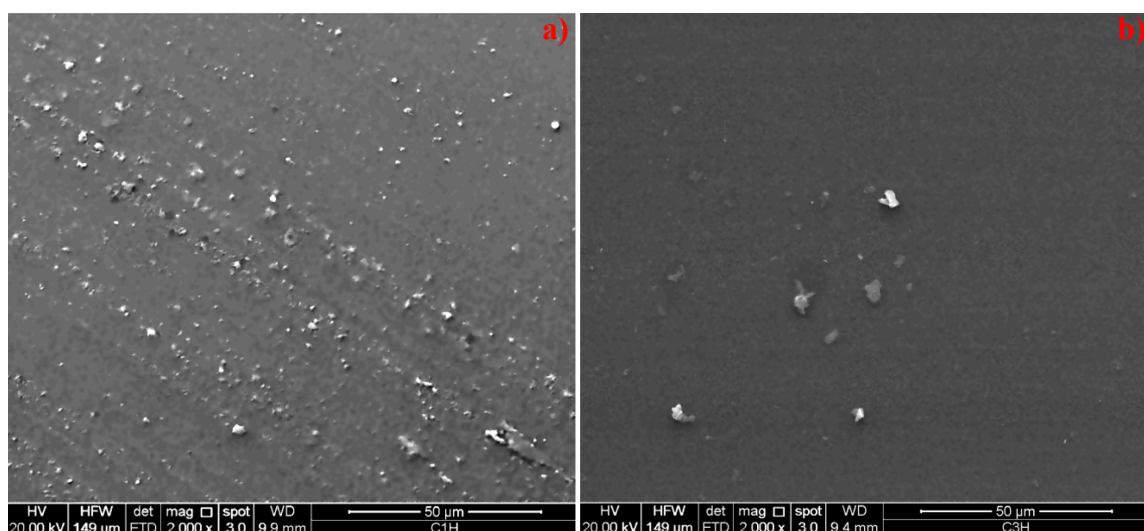


Figure 4.16: SEM images of fracture surface under impact of the C1H (a) and C3H (b) samples.

When phase separation occurs, the particles disperse efficiently as a fine structure and the HB systems interpenetrate the epoxy networks improving the miscibility and the interface adhesion between HB polymers and epoxy matrix; therefore the toughness is improved.<sup>20</sup> Stress whitening is due to the scattering of visible light from the layer of the scattering centers, which in this case are voids. The generation of the voids is due to the cavitations of rubbery HB particles and is an important aspect of the dissipation of energy in rubber toughened epoxies,<sup>38,39</sup> both because cavitations absorb energy, and importantly because it encourages the yielding of the polymer matrix, a process favored by the uniform distribution of the rubber particles throughout the matrix.<sup>4,40,41</sup>

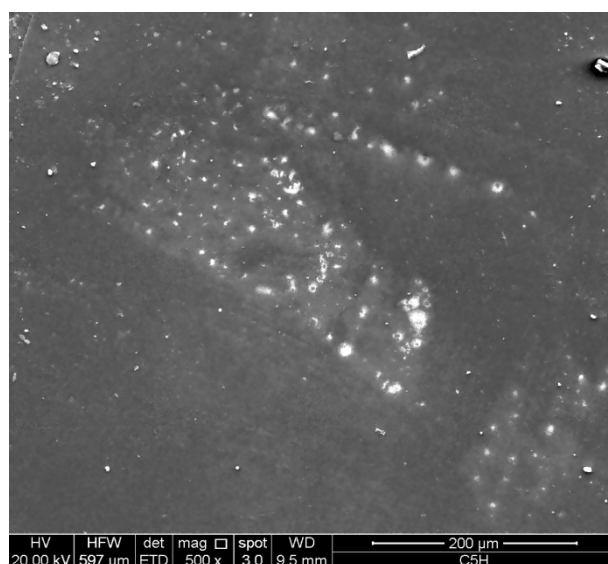
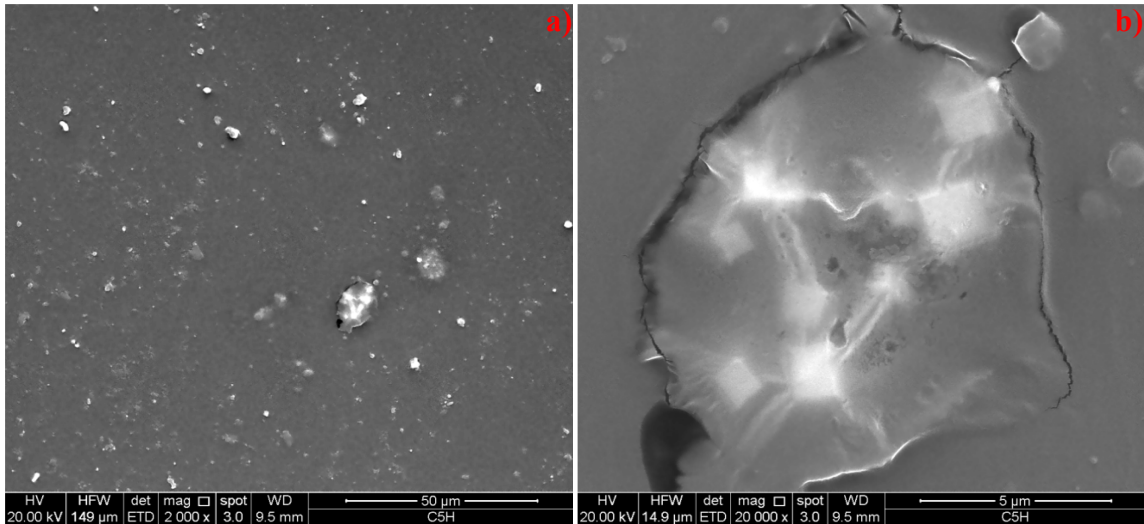


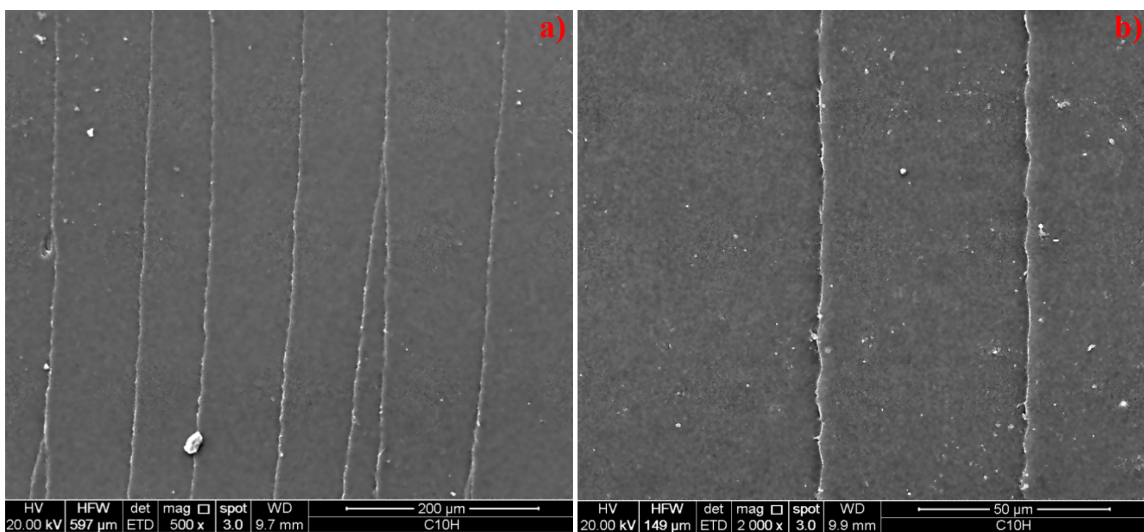
Figure 4.17: SEM image of the fracture surface under impact of C5H sample.



**Figure 4.18: Particular of SEM images of C5H sample at 2000X (a) and 20000X (b).**

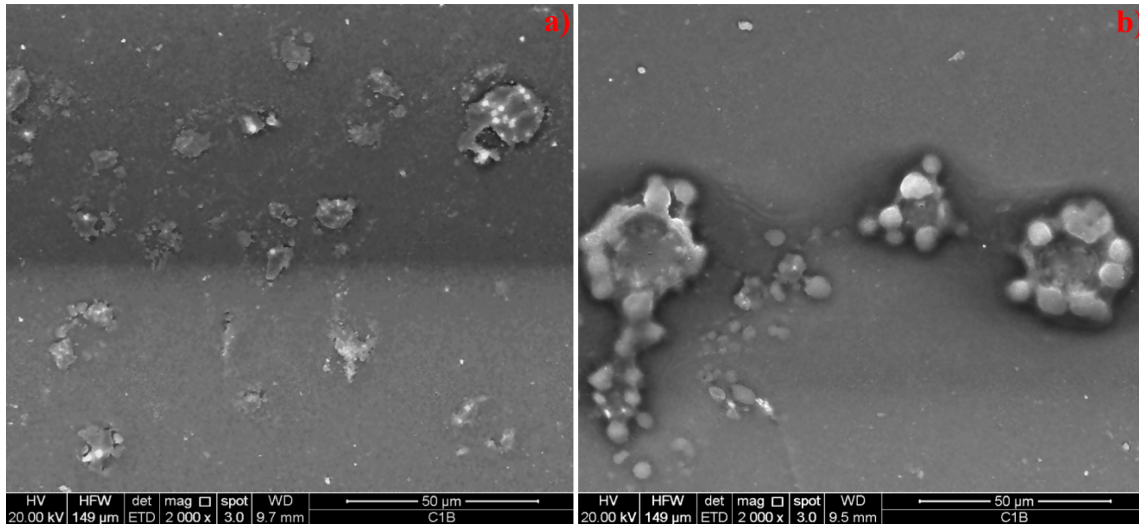
This explains why the Cycom/HB blends exhibits higher impact strength compared to the neat Cycom. These cavities represent the initial position of the rubber particles, which are pulled out or broken during the fracture process. These cavities are firmly attached to the matrix, resulting in a good adhesion and a strong interface between synthesized HB sample and epoxy phase.

In the case of C10H blend (Figure 4.19a and Figure 4.19b) the elevated density of polyester charges promotes the craze propagation, because the continuity of the epoxy network is interrupted and the particles appear as many points of discontinuity. In this case the toughening behavior is worse than neat Cycom, inducing brittle surface fracture under impact.



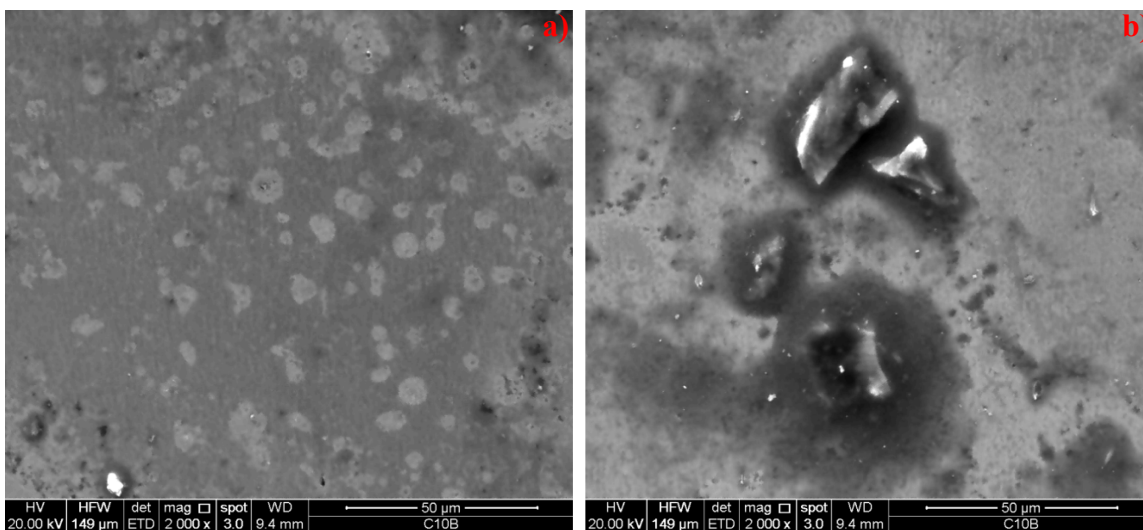
**Figure 4.19: SEM images of fracture surface under impact of C10H sample at 500 X (a) and 2000X (b).**

In Figure 4.20 the SEM images of fracture surface under impact of C1B sample is reported. It is worth noticeable that the dimension of globular Boltorn dispersed particles in epoxy matrix is much larger than 5HB30. Boltorn creates big spherical agglomerates in epoxy matrix due to the particles aggregation.<sup>21</sup>



**Figure 4.20: SEM images of fracture surface under impact of C1B sample at 2000X.**

The aggregation of Boltorn particles increases with increasing polymer content in epoxy matrix, see Figure 4.21. This aggregation cannot undergo plastic deformation, which result in a low impact strength. Moreover, also see Figure 4.21c, there are no cavitations because Boltorn particles are tightly enwrapped into epoxy matrix. This indicates that the good interfacial adhesion between Cycom matrix and Boltorn particles occurs due to the strong hydrogen bonding.<sup>21</sup>



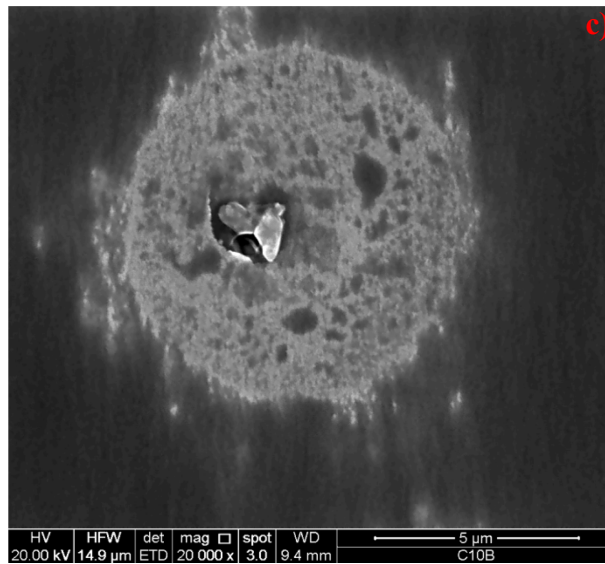


Figure 4.21: SEM images of the fracture surface under impact of C10B sample at 2000X (a and b) and 20000X (c).

## References

1. Batog, A. E. ; Pet'ko, I. P.; Penczek, P., Aliphatic-cycloaliphatic epoxy compounds and polymers. *Polymer Latexes - Epoxide Resins – Polyampholytes*. *Adv Polym Sci* 1999, 144, 49–113;
2. Iijima, T.; Miura, S.; Fujimaki, M.; Taguchi, T.; Fukuda, W.; Tomoi, M., *J Appl Polym Sci* 1996, 61, 163–175;
3. Lowe, A.; Kwon, O. H.; Mai, Y. W., *Polymer* 1996, 37, 565–572;
4. Hodgkin, J. H.; Simon, G. P.; Varley, R. J., *Polym Adv Technol* 1998, 9, 3–10;
5. Boogh, L.; Pettersson, B.; Kaiser, P.; Manson, J. A., *Sampe J* 1997, 33, 45–49;
6. Guo, Q. P.; Habrard, A.; Park, Y.; Halley, P. J.; Simon, G. P., *J Polym Sci Part B: Polym Phys* 2006, 44, 889–899;
7. Ratna, D.; Simon, G. P., *Polymer* 2001, 42, 8833–8839;
8. Ratna, D.; Varley, R.; Raman, R. K. S.; Simon, G. P., *J Mater Sci* 2003, 38, 147–154;
9. Varley, R. J., *Polym Int* 2004, 53, 78–84;
10. Zhang, D. H.; Jia, D. M., *J Appl Polym Sci* 2006, 101, 2504–2511;
11. Hult, A.; Johansson, M.; Malmström, E., *Hyperbranched Polymers. Branched Polymers II*. *Adv Polym Sci Volume* 1999, 143, 1-34;
12. DeCarli, M.; Kozielski, K.; Tian, W.; Varley, R., *Compos Sci Technol* 2005, 65, 2156–2166;
13. Mezzenga, R.; Boogh, L.; Pettersson, B.; Manson, J. A. E., *Macro Symp* 2000, 149, 17–22;
14. Mezzenga, R.; Manson, J. A. E., *J Mater Sci* 2001, 36, 4883–4891;
15. Mezzenga, R.; Boogh, L.; Manson, J. A. E., *Compos Sci Technol* 2001, 61, 787–795;
16. Mezzenga, R.; Plummer, C. J. G.; Boogh, L.; Manson, J. A. E., *Polymer* 2001, 42, 305–317;
17. Luciani, A.; Plummer, C. J. G.; Nguyen, T.; Garamszegi, L.; Manson, J. A. E., *J Polym Sci Part B: Polym Phys* 2004, 42, 1218–1225;
18. Campbell, D.; Pethrick, R. A.; White, J. R., *Polymer Characterization: Physical techniques*, Second Edition 2000, Stanley Thornes (Publishers) Ltd, Delta Place, United Kingdom;
19. Musto, P.; Abbate, M.; Pannico, M.; Scarinzi, G.; Ragosta, G; *Polym* 2012, 53, 5016-5036;
20. Fu, J.-F.; Shi, L.-Y.; Yuan, S.; Zhong, Q.-D.; Zhang, D.-S.; Chen, Y.; Wu, J., *Polym Adv Technol* 2008, 19, 1597–1607;



21. Xu, G.; Shi, W.; Gong, M.; Yu, F.; Feng, J., *Polym Adv Technol* 2004, 15, 639-644;
22. Smith, I. T., *Polymer* 1961, 2, 95-108;
23. Jin, F. L.; Park, S. J., *J Polym Sci Part B: Polym Phys* 2006, 42, 3348–3356;
24. Zhang, J.; Guo, Q.; Fox, B., *J Polym Sci Part B: Polym Phys* 2010, 48, 417–424;
25. Martinez, I.; Martin, M. D.; Eceiza, A.; Oyanguren, P.; Mondragon, I., *Polymer* 2000, 41, 1027-1035;
26. Verchere, D.; Sautereau, H.; Pascault, J. P.; Moschair, S. M.; Riccardi, C. C.; Williams, R. J. J., *J Polym Sci* 1991, 42, 467-480;
27. Li, X.; Zhang, S.; Wang, H.; Zhang, C.; Pang, J.; Mu, J.; Ma, G.; Wang, G.; Jiang, Z., *Polym Int* 2011, 60, 607–612;
28. Hawker, C. J.; Farrington, P. J.; Mackay M. E.; Wooley K. L.; Fréchet, J. M. J., *J Am Chem Soc* 1995, 117, 4409-4410;
29. Hsieh, T. T.; Tiu, C.; Simon, G. P., *Polymer* 2001, 42, 1931-1939;
30. Pettersson, B.; Sörensen K., *Proceedings of the 21<sup>st</sup> Waterborne, Higher-Solids and powder coatings Symposium, New Orleans, Louisiana, 1994, 2, 753-764;*
31. Boogh, L.; Pettersson, B.; Månson J.-A. E., *Polymer* 1999, 40, 2249-2261;
32. Cicala, G.; Recca, A.; Restuccia, C., *Polym Eng Sci* 2005, 42, 225-237;
33. Muliken, T. J.; Bech Tan N. C., *Polymer* 2000, 41, 1027-1035;
34. Xu, J.; Wu, H.; Mills, O. P.; Heiden, P.A., *J Appl Polym Sci* 1999, 72, 1065;
35. Ratna, D.; Simon, G. P., *Polym Eng Sci* 2001, 41, 1815–1822;
36. Zhang, D.; Cheng, X.; Zhang, A.; Ji, D., *Funct Mater Lett* 2011, 4, 351-355;
37. Guo, Q.; Huang, J.; Ge, L.; Feng, Z., *Polym J* 1992, 28, 405-409;
38. Bagheri, R.; Pearson, R. A., *Polymer* 1996, 37, 4529–4538;
39. Cardwell, B. J.; Yee, A. F., *J Mater Sci* 1998, 33, 5473–5484;
40. Lowe, A.; Kwon, O. H.; Mai, Y. W., *Polymer* 1996, 37, 565–572;
41. Schröder, N.; Könczöl, L.; Döll, W.; Mülhaupt, R., *J Appl Polym Sci* 1998, 70, 785–796.

## Chapter 5

# HB polyesters in biomedical applications

### 5.1 Introduction

The resistance to conventional antimalarial drugs has led to changes in malaria control policies globally in favor of Artemisinin (ART). ART is a parent compound of a novel family of antimalarials extracted from the Chinese traditional plant, *Artemisia annua* L. Asteraceae. It has been reported that ART is very effective against malaria parasites, including the multidrug-resistant strains of *Plasmodium falciparum* malaria.<sup>1,2</sup> It was first isolated and characterized as an active compound by Chinese scientist and since then has been successfully utilized as an antimalarial drug.<sup>3</sup> ART is a sesquiterpene lactone with an endo-peroxide bridge, that is thought to be responsible for its antimalarial activity, since either blocks the polymerization to hemozoin of the free heme released by the *Plasmodium falciparum* parasite<sup>4-6</sup> or acts on key proteins causing the parasite death<sup>7,8</sup>. In fact, the interaction of the trioxanic ring of ART with the Fe(II)-heme complex by means of the peroxide group leads to the formation of carbon-centered free radicals which are extremely damaging for the parasites.<sup>9,10</sup> ART is a poorly water-soluble drug. This could cause a number of negative clinical effects, such as high local drug concentrations at the sites of aggregate deposition, which could be associated with local toxic effects, and decreased systemic bioavailability. Besides, ART has short half-life of 2-3 h and it is extensively metabolized by the liver, but oral bioavailability is low (32%).<sup>1,11,12</sup> Although ART has shown excellent permeability across the intestinal mucosa, it has low bioavailability due to poor aqueous solubility, which may lead to incomplete clearance of the malaria parasite, resulting in recurrence of malarial symptoms.<sup>13</sup> An additional problem in pharmacokinetic studies with ART is the fact that the absolute bioavailability of ART is not known because of the lack of an intravenous formulation for human use. Nevertheless, a few pharmacokinetic studies indicate that ART is incompletely absorbed after oral intake. The relative bioavailability in comparison with an intramuscular injection of a suspension in oil is estimated to be about 32%.<sup>14</sup> A study carried out by Ashton et al.<sup>15</sup> showed high interindividual variability in plasma concentrations after both oral and rectal administration. The low bioavailability after oral intake can be due to a low transepithelial

transport across the intestinal mucosa and to the poor dissolution characteristics of ART in the intestinal fluids.

To overcome this limitation transdermal drug delivery systems (TDDS) have been studied. TDDS facilitates the passage of therapeutic quantities of drug substances through the skin into the general circulation where they can have systemic effects, thus bypassing the hepatic first-pass effect. Drug delivery through the cutaneous route has several advantages over other routes but faces a major problem presented by the barrier function of the skin, in which the stratum corneum plays a vital role.<sup>16</sup> Physical and chemical methods are widely used to overcome this passive barrier. The physical enhancement techniques currently in use, for example iontophoresis and sonophoresis, require complex equipment.<sup>17</sup> Alternatively, chemical permeation enhancers are extensively used, which temporarily lower the impermeability of skin and facilitate the absorption of drug through the skin. Various techniques have been used previously to improve the solubility and in turn the dissolution of drugs poorly soluble in water. Drug-polymer complexation using a hydrophilic polymer is quite a popular technique and involves formation of solid dispersions using either solvent evaporation or a freeze drying method.<sup>18-20</sup>

The good permeability of ART provides a potential application in TDDS,<sup>21</sup> also known as patches. They are dosage forms designed to deliver therapeutic dose of drugs through patients' skins. Usually, model drugs are mostly dissolved in the adhesive matrix of TDDS forming a solid dispersion. As a matter of fact, these systems are thermodynamically unstable and the drugs frequently re-crystallize during the storage process.<sup>22-23</sup> The growth of drug crystals in TDDS often causes a reduction in the drug flux through the stratum corneum,<sup>24</sup> a decreasing of solubility and an incomplete clearance of the parasites resulting in recrudescence.<sup>25</sup> Therefore, inhibition of ART crystallization is imperative to maintain its efficiency and prolongs the shelf-life of this active ingredient. To prevent model drugs from separating crystals out of TDDS, some crystallization inhibitors or anti-nucleating agents are mixed in the adhesive matrix.<sup>26</sup> However, these methods may not be effective in some situations.<sup>27</sup> Many works had tried to encapsulate ART into micro-particles, but these techniques could not prevent ART crystallization effectively.<sup>28,29</sup>

In order to inhibit the crystallization of a potent antimalarial drug, artemisinin (ART), commercial dendrimer (Boltorn), and two synthesized HB polyesters were used to prepare blends with ART.

The experimental part was carried out in two stages:



- The synthesis and characterization of HB poly(butylene adipate) polyesters, 1.5HB16 and 5HB30 samples.
- The preparation and characterization of ART blends with two different synthesized HB polymers, 1.5HB16 and 5HB30, and commercial dendritic polyester, Boltorn.

In this work, the properties of ART blends with Boltorn and HB polyesters were studied, using the neat ART as reference. The key issue was to obtain a system in which the re-crystallization of this potent antimalarial drug was inhibited, by “encapsulating” it in a HB or dendritic system, characterized by unique topological structure and interesting physical/chemical properties. These type of polymers could entrapped ART molecules in their branches, preventing the subsequent re-crystallization. The crucial point of this proceeding is to obtain blends in which the chemical activity of ART is preserved. For this reason our studies were finalized to the analysis of thermal behavior of ART blends and structural measurements to be sure that peroxide bridge is not broken during our treatment. Finally a preliminary study on the possibilities of the release of ART from these blends to human skin were examined. A sebum formulation was reproduced and subsequently the amount of ART released in it was assessed by mean of ATR spectroscopy.

## 5.2 Experimental section

### 5.2.1 Materials for ART blends

Artemisinin (ART) ( $M_w = 282.33$  g/mol) was purchased from Chemical Point.

Boltorn® H311 (Boltorn) is a dendritic polymer polyol with high hydroxyl functionality ( $M_w = 5700$  g/mol, hydroxyl number = 230-260 mg KOH/g), used in this work as commercial crystallization inhibitor. It contains 10 % water and is a viscous liquid at  $T_{room}$ ; it presents excellent solubility in polyether, polyols, glycols and polyalcohol's. It is an amorphous dendritic polyester with a transition temperature ( $T_g$ ) of  $-20$  °C.

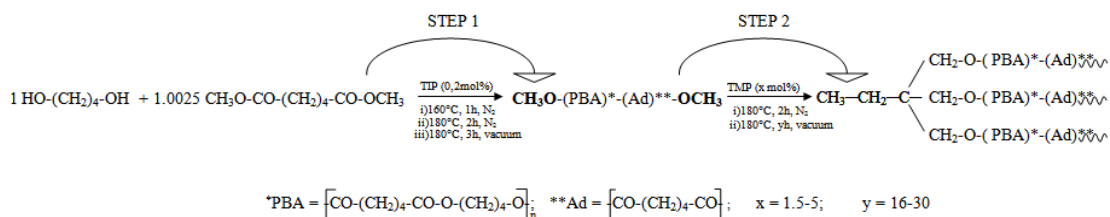
As crystallization inhibitors two synthesized HB polymers were also used. For the synthesis of these polyesters 1,4-butanediol (BD) (99%), dimethyl ester of adipic acid (DMA) ( $\geq 99\%$ ), titanium(IV)isopropoxide (TIP) (99.99%), as catalyst, 1,1,1-tris(hydroxy methyl)propane (TMP) ( $\geq 98.0\%$ ), as branching agent, chloroform ( $CHCl_3$ ) and methanol ( $CH_3OH$ ), as solvents, were also purchased from Sigma-Aldrich (Italy) and used without any purification.

N,N-Dimethyl acetamide (DMAc), acetone (Ac), were supplied from Sigma-Aldrich (Italy) and used as received.

Squalene, tripalmitine, oleic acid, palmitic acid, myristic acid, cholesterol, and glycerol, to reproduce sebum formulation, were also obtained from Sigma-Aldrich (Italy) and used as received.

## 5.2.2 Synthesis of HB polyesters

1.5HB16 and 5HB30 samples, chosen as HB tougheners for ART blends, were synthesized in one-pot synthesis performed in two steps, according to the Scheme 5.1.



**Scheme 5.1: Synthesis route of HB samples.**

In the first step, a tailored PBA methyl ester ended pre-polymer was synthesized using a DMA/BD molar ratio of 1.0025/1 as described before in Chapter 2. In the second step, 1.5 and 5 molar percent (with respect to the initial moles of monomer reagents) of TMP as branching agent was added and the reaction was carried out at 180 °C for 2 h at 1 atm, under nitrogen flow and under stirring. Then the reaction was continued under vacuum for 16 or 30 h, respectively, in order to obtain HB samples, 1.5HB16 and 5HB30.

For more details, see Table 2.1 in Chapter 2, in which experimental parameters (i.e. DMA/BD molar ratio, temperature, and reaction time) and molar mass distribution are described.

## 5.2.3 Preparation of ART blends

The three blends were prepared by mixing each crystallization inhibitor (1.5HB16, 5HB30, and Boltorn) with ART in a proportion of 1/0.4 wt. % in a binary solution of Ac/DMAc 50/50 in volume. Previously, Boltorn was held in a vacuum oven at 100 °C for 24 h to remove all water content. The mixture was held under stirring for 1 h at  $T_{\text{room}}$ , then for 1 h at 60 °C to facilitate the polymers and ART dissolution. The blends were obtained by evaporation of the solvent (Ac/DMAc) under vacuum using a rotary evaporator and, finally, were kept drying in a oven at 50 °C over night under vacuum. The formulations of ART blends are reported in detail in Table 5.1.

Table 5.1: ART blends

Crystallization Inhibitors	Blend Name
1.5HB16	HB1A
5HB30	HB2A
Boltorn	BA

## 5.2.4 Characterization

### Attenuated total reflectance spectroscopy (ATR)

The structural properties of neat ART and ART blends were studied by means of ATR spectroscopy, using a Nicolet 6700 FT-IR (Thermo Fischer Scientific). The ATR spectra were obtained at a resolution of  $4\text{ cm}^{-1}$  and 16 scans were averaged for each spectrum in a range between  $4000\text{-}650\text{ cm}^{-1}$ .

### Nuclear magnetic resonance spectroscopy (NMR)

Solid-state  $^{13}\text{C}$ -NMR was used to analyze the chemical structures of neat ART and ART blends. Solid-state  $^{13}\text{C}$  cross-polarization, magic angle spinning (CP-MAS) NMR spectra were collected at 100.47 MHz on a Bruker Avance II 400 spectrometer operating at a static field of 9.4 T, equipped with a 4 mm MAS probe. The  $^1\text{H}$   $\pi/2$  pulse width was  $3.4\ \mu\text{s}$ , and the CP contact time was 2 ms. The materials were packed into 4 mm zirconia rotors and sealed with Kel-F caps. The spinning speed was set to 8 kHz for all the experiments.

### Thermogravimetric analysis (TGA)

The thermal stability of ART and ART blends, were studied by means of TGA equipment. TGAs were performed in duplicate and carried out at  $10\text{ }^\circ\text{C}/\text{min}$  heating rate from  $25\text{ }^\circ\text{C}$  to  $700\text{ }^\circ\text{C}$  under nitrogen flow using a thermo balance (Q5000 by TA Instruments).

### Differential scanning calorimetry (DSC)

The melting behavior of neat ART and ART blends were investigated using a DSC, TA Instruments (mod Q2000). A dynamic heating rate of  $10\text{ }^\circ\text{C}/\text{min}$  was used for all analyses. The sample was heated from room temperature to  $180\text{ }^\circ\text{C}$ , cooled down to  $40\text{ }^\circ\text{C}$  and heated again to  $180\text{ }^\circ\text{C}$ .

For isothermal crystallization of ART blends, the samples were first heated to  $140\text{ }^\circ\text{C}$ , temperature close to the ART melting point, and held at this temperature for 1 h to allow

the ART to reorganize into its crystalline forms, cooled down to 40 °C, heated again to 180 °C, and finally chilled to 40 °C.

### Wide angle X-ray diffraction (WAXD)

WAXD measurements were conducted on neat ART and ART blends using a Philips XPW diffractometer with Cu K $\alpha$  radiation (1.542 Å) filtered by nickel. The scanning rate was 0.02 °/s, and the scanning angle was from 2 to 60°.

## 5.3 ART blends characterization: results and discussion

### 5.3.1 Attenuated total reflectance spectroscopy (ATR)

In Figure 5.1 the molecular structure of ART with atomic numbering and the molecular units which compose ART structure are reported.

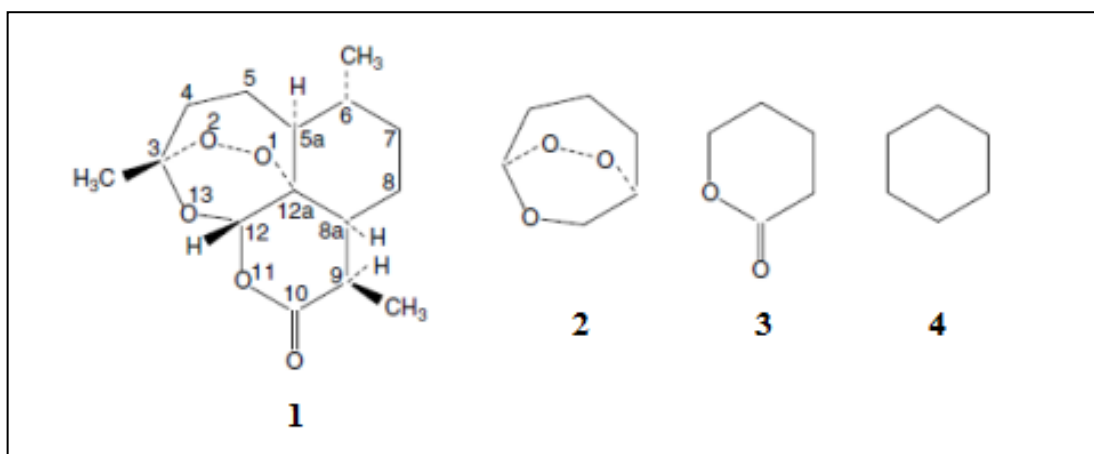


**Figure 5.1: Molecular structures of ART (1) with atomic numbering, 1,2,4-trioxane (2), v-valerolactone (3) and cyclohexane (4).**

In Table 5.2, the vibrational assignment of ART is discussed in terms of ring modes and, in particular, of modes directly related to the endo-peroxide group. We have not considered the local modes relative to the CH<sub>3</sub>, CH<sub>2</sub> and CH alkyl groups. These modes can, however, be easily associated to the infrared bands in the range  $\sim(1200\text{--}1500)\text{ cm}^{-1}$ .<sup>30,31</sup>

Among ring vibrations, those relative to the endo-peroxide bridge have been considered in more detail owing to the essential role of this chemical structure for the antimalarial activity of ART.

**Table 5.2: Experimental ATR wavenumbers (cm<sup>-1</sup>) and vibrational assignment. In the assignment column, 2,3,4 refer to the molecular units as shown in Figure 5.1.**

<b>ATR wave number (cm<sup>-1</sup>)</b>	<b>Assignment for neat ART molecule</b>
<b>700</b>	2, 3, 4; C <sub>12</sub> -C <sub>12a</sub> , C <sub>8a</sub> -C <sub>12a</sub>
<b>725</b>	2; C <sub>3</sub> -O <sub>13</sub> , C <sub>3</sub> -C <sub>4</sub>
<b>771</b>	2, 3; C <sub>8a</sub> C <sub>9</sub> C <sub>10</sub> , C <sub>9</sub> C <sub>10</sub> C <sub>11</sub> , C <sub>5</sub> C <sub>5a</sub> C <sub>12a</sub>
<b>793</b>	3; C <sub>10</sub> -O <sub>11</sub> , C <sub>10</sub> -O <sub>9</sub>
<b>817</b>	2, 4; CH <sub>2</sub> rocking
<b>832</b>	ring breathing, CH <sub>2</sub> rocking
<b>840</b>	2, 4; C <sub>6</sub> -C <sub>7</sub> , CH <sub>2</sub> rocking
<b>858</b>	2, 4; C <sub>3</sub> -O <sub>2</sub> , C <sub>12a</sub> -O <sub>1</sub> , C <sub>3</sub> -O <sub>13</sub> , CH <sub>3</sub> rocking
<b>870</b>	2, 3, 4; C <sub>8a</sub> -C <sub>9</sub> , CH <sub>3</sub> , CH <sub>2</sub> rocking
<b>883</b>	2; O <sub>1</sub> -O <sub>2</sub> stretch, C <sub>4</sub> C <sub>5</sub> C <sub>5a</sub> , CH <sub>3</sub> rocking
<b>917</b>	2; C <sub>3</sub> -O <sub>2</sub> , 3-CH <sub>3</sub> rocking
<b>928</b>	2, 4; O <sub>1</sub> -O <sub>2</sub> , ring bending
<b>940</b>	4; CH <sub>3</sub> rocking
<b>962</b>	2, 3, 4; ring stretch, CH <sub>3</sub> rocking
<b>993</b>	2, 3, 4; C <sub>12</sub> -O <sub>11</sub> , C <sub>12</sub> -O <sub>13</sub> , C <sub>7</sub> -C <sub>8</sub>
<b>1012</b>	3; C <sub>12</sub> -O <sub>11</sub> , CH <sub>3</sub> rocking
<b>1027</b>	3; C <sub>12</sub> -O <sub>11</sub> , C <sub>10</sub> -O <sub>11</sub> , CH <sub>2</sub> rocking
<b>1033</b>	4; C <sub>7</sub> -C <sub>8</sub>
<b>1053</b>	2; C <sub>4</sub> -C <sub>5</sub> , C <sub>5</sub> -C <sub>5a</sub>
<b>1061</b>	4; ring stretch, CH <sub>2</sub> rocking
<b>1077</b>	2, 4; C <sub>6</sub> -CH <sub>3</sub> , C <sub>4</sub> -C <sub>5</sub> , C <sub>5</sub> -C <sub>5a</sub>
<b>1101</b>	2, 3, 4; C <sub>12</sub> -O <sub>11</sub> , C <sub>6</sub> -CH <sub>3</sub>
<b>1118</b>	2; C <sub>5a</sub> -C <sub>12a</sub> , O <sub>13</sub> -C <sub>12</sub>
<b>1137</b>	2, 3; C <sub>12</sub> -O <sub>13</sub>
<b>1150</b>	2, 4; C <sub>5a</sub> -C <sub>12a</sub> , C <sub>5</sub> -C <sub>5a</sub> , C <sub>5a</sub> -C <sub>6</sub>
<b>1173</b>	2, 3; C <sub>3</sub> -O <sub>13</sub> , C <sub>9</sub> -C <sub>8a</sub> , CH <sub>2</sub> , CH <sub>3</sub> rocking
<b>1183</b>	2, 3, 4; C <sub>10</sub> -O <sub>11</sub> , C <sub>3</sub> -O <sub>2</sub> , C <sub>8a</sub> -C <sub>9</sub>
<b>1202</b>	3; C <sub>10</sub> -O <sub>11</sub> , C <sub>9</sub> -O <sub>10</sub>
<b>1735</b>	3; C=O stretching
<b>2850-2906-3000</b>	Fermi resonance of the symmetric CH <sub>3</sub> stretch with overtones of the methyl bending modes

In Figure 5.2 the ATR spectra of neat ART (a), HB1A blend (b), and synthesized HB polyester, 1.5HB16, (c) are reported. It is interesting to note the presence of characteristic peaks related to the ART endo-peroxide bridge in HB1A blend (858, 883, 917, 928 cm<sup>-1</sup>), index of the good blend preparation which not altered the ART chemical structure. This is a crucial point for these blends because if peroxide bridge was broken, the chemical activity of ART would be invalidated.

The ATR spectra of neat ART, HB2A blend and the relative synthesized HB polyester, 5HB30, also show the same pattern displayed below for the other synthesized sample.

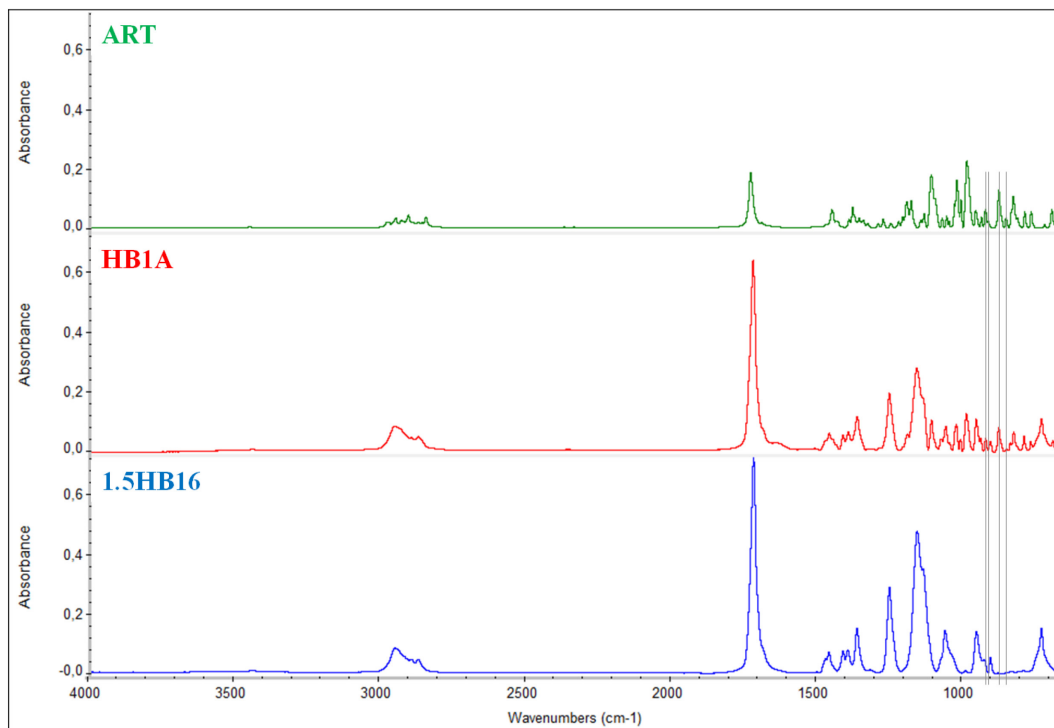


**Figure 5.2:** ATR spectra of neat ART, HB1A blend, and 1.5HB16 sample.

In Figure 5.3, instead, the ATR spectra of neat ART (a), BA blend (b), and Boltorn (c) are shown.

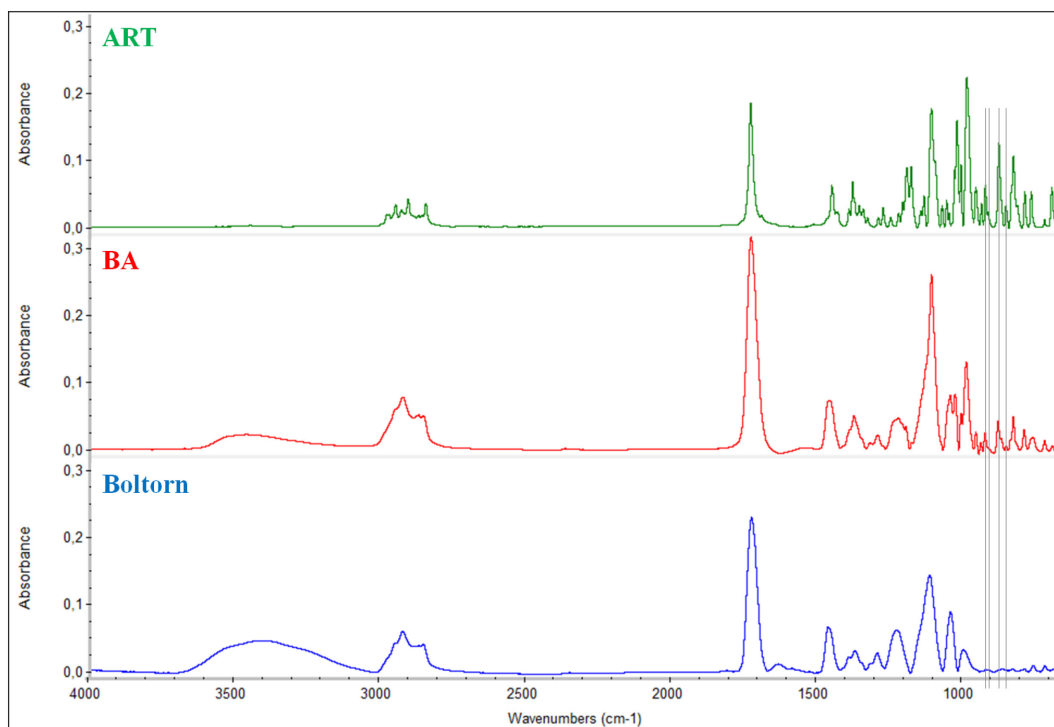


**Figure 5.3:** ATR spectra of neat ART, BA blend, and Boltorn sample.

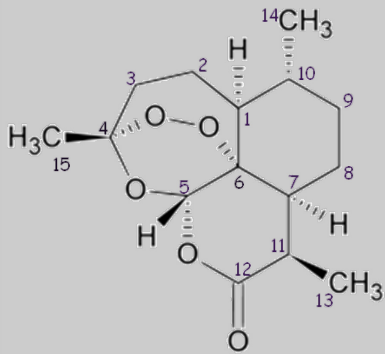
Also in ART blend with commercial dendrimer, reported in Figure 5.3, the specific signals of ART endo-peroxide bridge remain unchanged.

It is important to note the presence in the ATR spectrum of Boltorn, and relative BA blend, of a broad band in the range  $\sim(3400\text{--}3500)\text{ cm}^{-1}$ , despite the sample was put overnight in a oven to remove all water content. This band is related to  $\text{--OH}$  end-groups belonging to Boltorn structure.

### 5.3.2 Nuclear magnetic resonance spectrometry (NMR)

To analyze the chemical structure of neat ART and to be sure that its endo-peroxide bridge is present in its blends with synthesized and commercial dendritic polyesters, the blends were studied by means of solid-state  $^{13}\text{C}$ -NMR. The peak values are reported in Table 5.3 and are in agreement with the chemical shifts provided in literature.<sup>32,33</sup>

**Table 5.3: Assignments of carbon signals belonging to ART molecule as observed in solid-state  $^{13}\text{C}$ -NMR spectrum.**

ART Structure	C	Chemical Shift (ppm)
	12	172.4
	4	106.6
	5	93.8
	6	80.8
	1	47.4
	7	42.6
	10	39.4
	3	36.4
	9	34.5
	11	33.7
	8	25.4
	15	24.3
	14	20.5
	13	12.4

It is worthy noticing that in ART blends with synthesized HB polyesters, HB1A (Figure 5.4b) and HB2A (Figure 5.4c), the signals belonging to the endo-peroxide bridge of neat ART (106.6, 80.8, 24.3 ppm) are visible together with that due to HB structure. This confirms that the chemical structure of ART remains unchanged in ART blends. To better interpret the NMR spectra of the ART blends, we refer to the Chapter 2 in which a solid state  $^{13}\text{C}$ -NMR of synthesized HB sample is reported and analyzed.

The Figure 5.4d concerns to ART blend with Boltorn, BA. The spectrum of this blend shows only the signals related to ART chemical structure since dendrimer polymer is a viscous liquid and the signals connected to polyester structure does not resonate with this type of analysis.

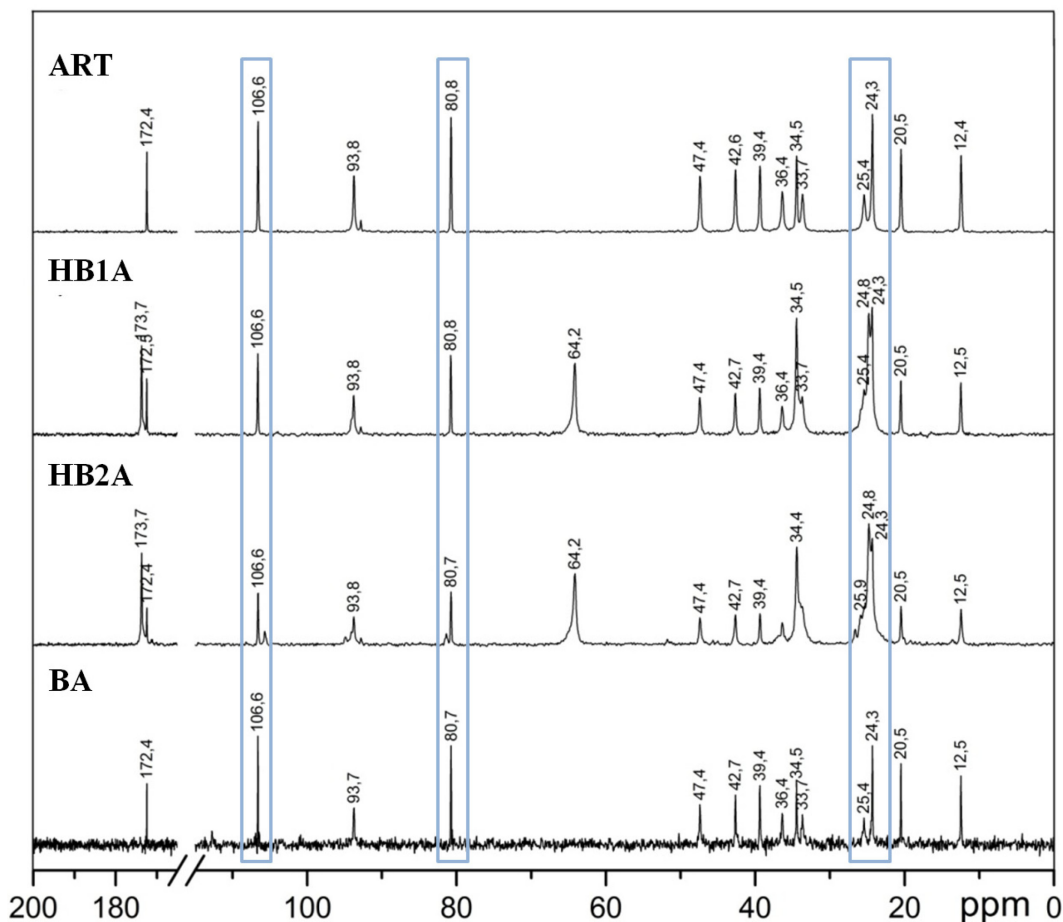


Figure 5.4: Solid-state  $^{13}\text{C}$ -NMR spectra of neat ART, HB1A, HB2A, and BA blends.

### 5.3.3 Thermogravimetric analysis (TGA)

The thermal stabilities of neat ART and its blends were investigated through TGA measurements, see Figure 5.5.

In Table 5.4 the onset temperature ( $T_{\text{onset}}$ ), the temperature at 5 % weight loss ( $T_{5\% \text{wt. loss}}$ ) and the temperature at maximum degradation rate, defined as the maximum of the weight loss derivative curves, ( $T_{\text{max. deg. rate}}$ ) are reported for 1.5HB16, 5HB30, and Boltorn samples. Instead, in Table 5.5,  $T_{\text{onset}}$ ,  $T_{5\% \text{wt. loss}}$ , and  $T_{\text{max. deg. rate}}$  for neat ART, HB1A, HB2A, and BA blends, are listed.

From  $T_{5\% \text{wt. loss}}$  values reported in the tables, it can be observed that the three polymers are much more thermally stable than the neat ART and, as a consequence, also the ART blends show temperature of starting degradation higher.



In the temperature range between 180 and 300 °C, the degradation peaks visible in the derivative TG traces of ART blends are related to the neat ART degradation. Instead the second higher degradation peaks located between 300 and 450 °C are relative to polyesters degradation.

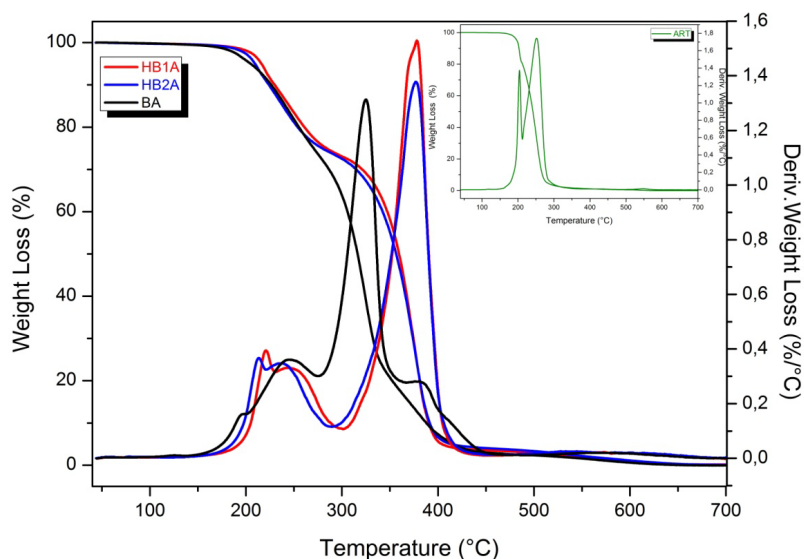


Figure 5.5: TG traces of HB1A, HB2A, and BA blends. Inset: TG trace of neat ART.

Since the degradation mechanism of ART endo-peroxide bridge can be associated to the degradation temperature of 204°C, synthesized HB polyesters increase the thermal stability of this molecule.

Table 5.4:  $T_{\text{onset}}$ ,  $T_{5\% \text{wt. loss}}$ , and  $T_{\text{max. deg. rate}}$  for 1.5HB16, 5HB30, and Boltorn samples.

	1.5HB16	5HB30	Boltorn
$T_{\text{onset}}$ (°C)	290	238	263
$T_{5\% \text{wt. loss}}$ (°C)	322	265	288
$T_{\text{max. deg. rate}}$ (°C)	401	391	338-387-418

Table 5.5:  $T_{\text{onset}}$ ,  $T_{5\% \text{wt. loss}}$ , and  $T_{\text{max. deg. rate}}$  for neat ART, 1.5HB16, 5HB30, Boltorn, HB1A, HB2A, and BA.

	Neat ART	HB1A	HB2A	BA
$T_{\text{onset}}$ (°C)	184	202	195	177
$T_{5\% \text{wt. loss}}$ (°C)	197	216	209	205
$T_{\text{max. deg. rate}}$ (°C)	204-252	220-245-378	213-236-376	196-244-324-386

### 5.3.4 Differential scanning calorimetry (DSC)

In order to study the thermal properties, DSC measurements were conducted on neat ART and its blends.

In Table 5.6, the melting and crystallization temperature ( $T_m$  and  $T_c$ , respectively), the heat of fusion and crystallization ( $\Delta H_m^I$ ,  $\Delta H_m^{II}$ , derived from the first and second heating scan, respectively, and  $\Delta H_c$ ) are reported.

**Table 5.6:**  $T_m$ ,  $T_c$ ,  $\Delta H_m^I$ ,  $\Delta H_m^{II}$ ,  $\Delta H_c$  of neat ART.

	$T_m$ (°C)	$T_c$ (°C)	$\Delta H_m^I$ (J/g)	$\Delta H_m^{II}$ (J/g)	$\Delta H_c$ (J/g)
<b>ART</b>	154	93	73	54	56

<sup>I</sup> values measured from the second first scan; <sup>II</sup> values measured from the second heating scan.

The neat ART used in this study has a sharp melting endothermic peak at 154 °C and a crystallization exothermic peak at 93 °C, as shown in Figure 5.6.

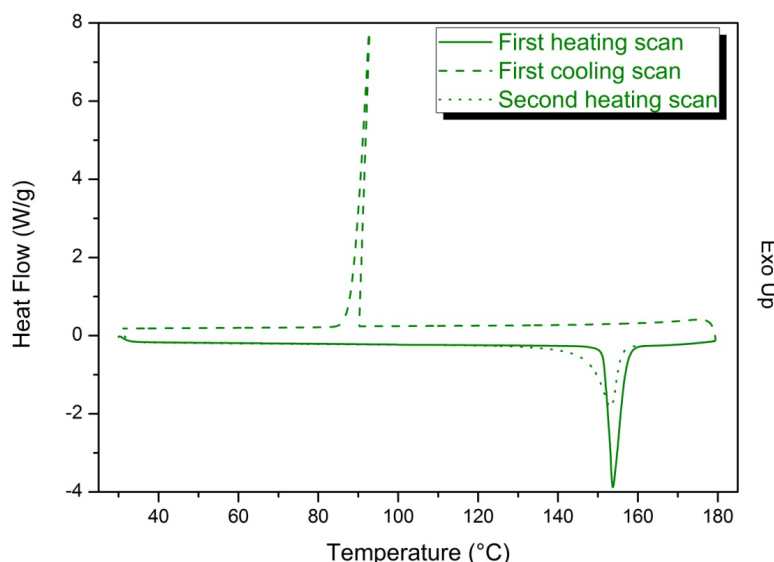


**Figure 5.6:** DSC trace of neat ART.

In Figure 5.7, it is worth noticing that in ART blends with synthesized HB polymers (H1A and H2A) only the melting peaks related to these HB polyesters are visible and a very broad endothermic band at about 115 °C, probably due to fusion of ART micro-crystals formed. During the cooling scan from 180 °C to 40 °C, no crystallization peak is visible and, even in subsequent heating ramp, any melting peak is present. It is particularly interesting to note that in the second heating scan the melting peaks characteristic of HB structures disappear as well as the broad endothermic band. We hypothesize that this thermal behavior is due to the amorphization of both ART and HB polymers.

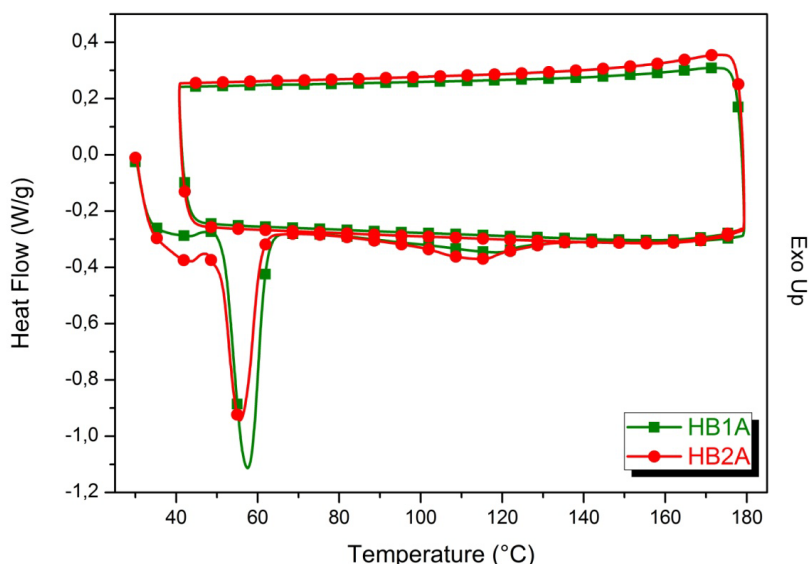


Figure 5.7: DSC traces of HB1A and HB2A blends.

In Figure 5.8 the DSC thermograms of ART blend with Boltorn is reported. Also in this picture it is visible a broad band at about 115 °C which disappears in the second heating scan and not lead to any crystallization form during cooling ramp. It is important remember that Boltorn, despite of synthesized HB species, is an amorphous polymer.

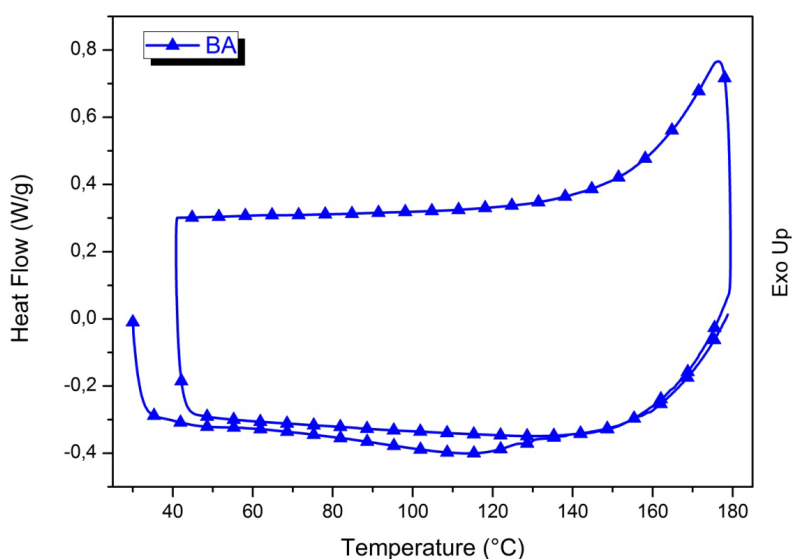


Figure 5.8: DSC trace of BA blend.

On ART blends, an isothermal analysis at 140 °C for 1 h was made to be sure that at a temperature close to  $T_m$ , ART does not reorganize and restructure into its crystalline form. The results are depicted in Figure 5.9 (ART blends with synthesized HB samples, HB1A and HB2A) and in Figure 5.10 (ART blend with commercial dendritic polymer, BA). It is clear from all thermograms that the isothermal process at 140 °C does not allow the ART crystals formation in the blends.

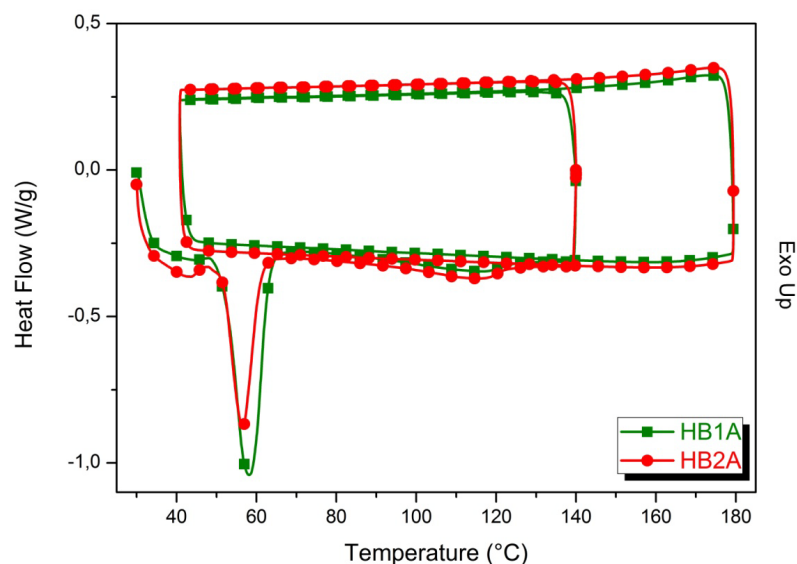


Figure 5.9: Isothermal DSC traces at 140 °C of HB1A and HB2A blends.

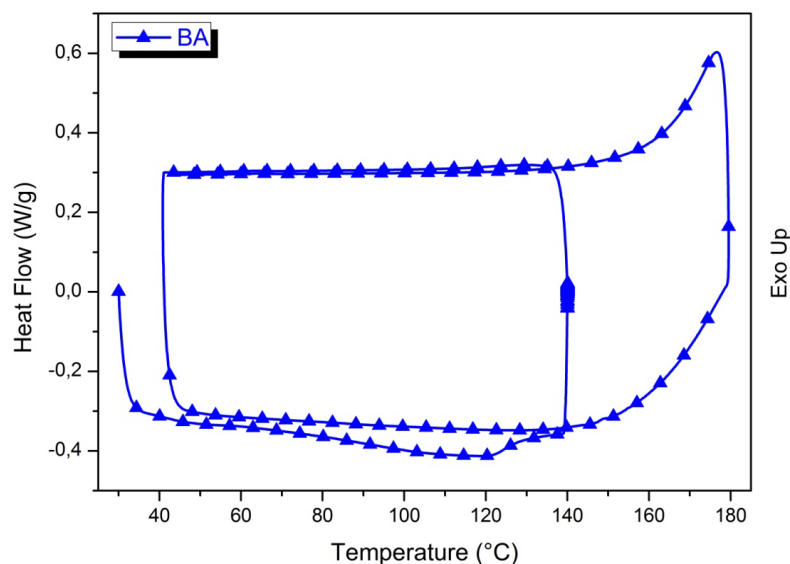
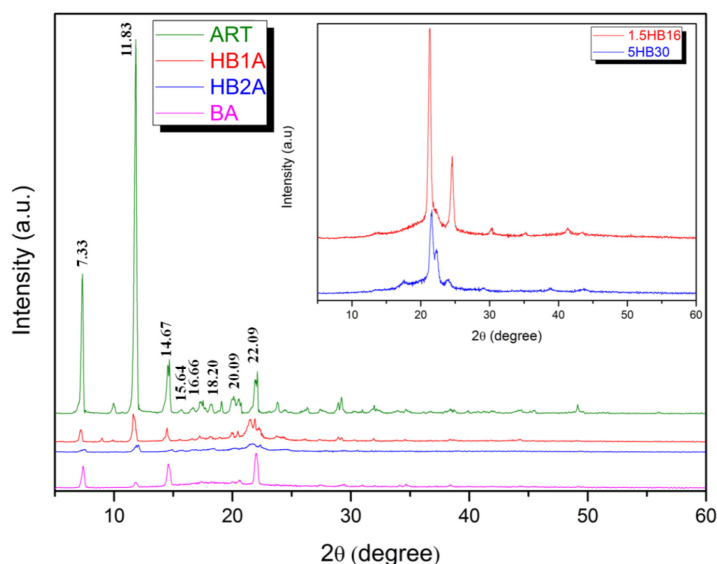


Figure 5.10: Isothermal DSC trace at 140 °C of BA blend.

### 5.3.5 Wide angle X-ray diffraction (WAXD)

The X-ray patterns of the neat ART, displayed in Figure 5.11, shows the presence of numerous distinct peaks at  $2\theta$  of 7.33 °, 11.83 °, 14.67 °, 15.64 °, 16.66 °, 18.20 °, 20.09 °, and 22.09 °, indicating the typical crystalline structures.<sup>26,34,35,36</sup> The peak appearing at a diffraction angle of  $2\theta$  at 11.83 ° is most prominent.

The X-ray diffraction patterns of ART blends show a drastic decrease in the peak intensities, which suggests in particular that ART loses its crystallinity, becoming amorphous in HB2A blend.



**Figure 5.11: XRD patterns of neat ART and ART blends. In the inset, XRD measurements of neat synthesized HB polyesters, 1.5HB16 and 5HB30.**

As a confirmation of this tendency to amorphization process, as also confirmed by DSC analyses previously discussed, the blends were heated to 140 °C and held at this temperature for 1 h. After this isothermal heating process, the blends were analyzed by means of ATR spectroscopy. The data show the complete amorphization of ART blends for all systems, synthesized and commercial.

### 5.3.6 Skin contact simulation

To simulate human skin surface, sebum formulation was prepared according approximately to literature.<sup>37</sup> Human sebum is a mixture of triglycerides, fatty acids, wax esters, squalene, cholesterol and cholesterol esters. The following percentage quantity of components was used:<sup>38</sup>

Squalene (16% -  $C_{30}H_{50}$ ), Tripalmitine (8% -  $C_{51}H_{98}O_6$ ), Oleic acid (10% -  $C_{18}H_{34}O_2$ ), Palmitic acid (7% -  $C_{16}H_{32}O_2$ ), Myristic acid (5% -  $C_{14}H_{28}O_2$ ), Cholesterol (4% -  $C_{27}H_{46}O$ ), Glycerol (50% -  $C_3H_8O_3$ ).

At normal skin temperature (skin surface temperature is 32 °C), sebum contains both a solid and a liquid phase. Preliminary studies were done on the sebum formulation in contact with neat ART and HB polyesters for 48 h at 37 °C. The relative ATR spectra are portrayed in Figure 5.12 in which also ART spectrum was displayed as reference.

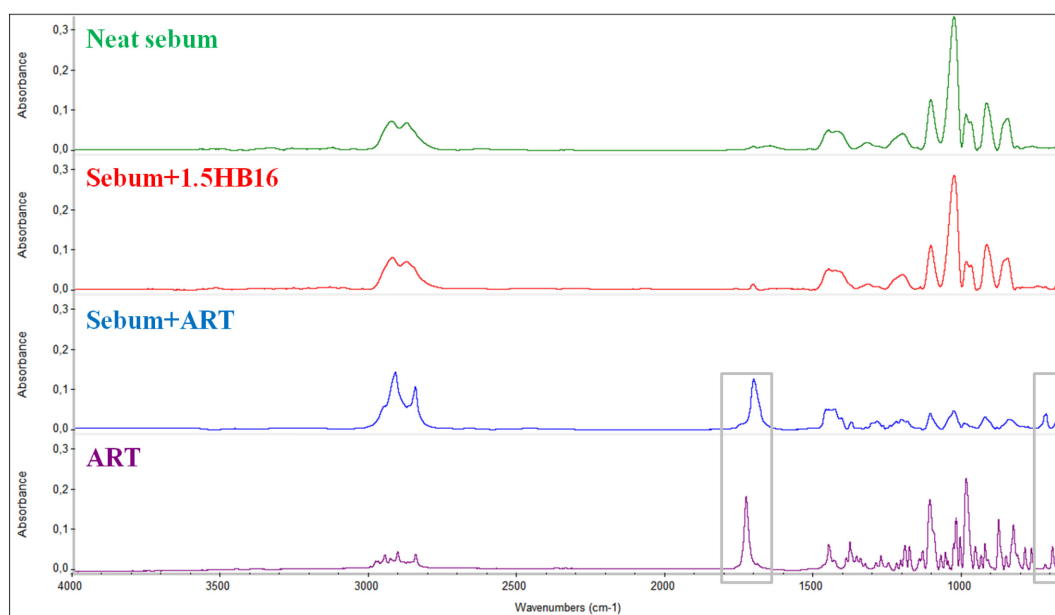


Figure 5.12: ATR spectra of neat sebum, sebum+1.5HB16, sebum+ART and ART as reference.

After the contact with HB samples, the sebum solution was analyzed and no trace of specific signals related to HB polyester is visible in the ATR spectrum. In the ATR spectrum of sebum in contact with ART, instead, the signal of carbonyl groups ( $C=O$ ) at  $1710\text{ cm}^{-1}$  and that related to the trioxanic ring at  $725\text{ cm}^{-1}$  are observable. This means that HB species do not dissolve in sebum formulation unlike what happens for ART molecules. The ART blends were pressed and dipped into sebum formulation for 48 h at  $37\text{ }^{\circ}\text{C}$ . The sebum left in contact with ART blends was then analyzed to be sure that ART dissolves and not remains entrapped into branched structure of HB polymers. The relative ATR spectra are reported in Figure 5.13.

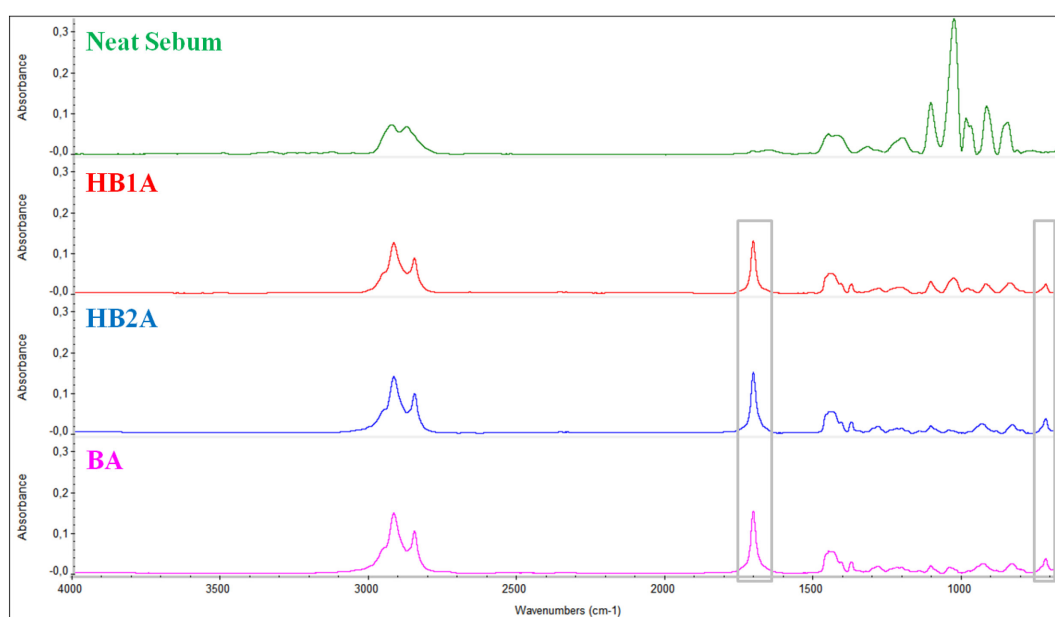


Figure 5.13: ATR spectra of sebum formulation in contact with ART blends.

From Figure 5.13, it is very interesting to note the presence of signal of carbonyl group ( $1710\text{ cm}^{-1}$ ) and that related to trioxanic ring of ART molecules in all blends, such as we have seen in ATR spectrum of sebum added with neat ART. This means that synthesized HB and dendritic polyesters besides to inhibit the ART crystallization, allow the release of ART in sebum formulation reproduced in our laboratories. This is an important preliminary study on the possibilities to create in future TDDS which contain ART.

**References**

1. Svensson, U. S. H.; Sandström, R.; Carlborg, Ö., *Drug Metab Dispos* 1999, 27, 227-232;
2. Thaithong, S.; Beale, G. H., *Bull World Health Organ* 1985, 63, 617-619;
3. Klayman, D. L., *Science* 1985, 228, 1049-1055;
4. Wu, W.-M.; Wu, Y.; Wu, Y.-L.; Yao, Z.-J.; Zhou, C.-M.; Li, Y.; Shan, F., *J Am Chem Soc* 1998, 120, 3316-3325;
5. Kapetanaki, S.; Varotsis, C., *FEBS Lett* 2000, 474, 238-241;
6. Cazelles, J.; Robert, A.; Meunier, B. C. R., *Acad Sci Paris, Chim* 2001, 4, 85-89;
7. Kannan, R.; Sahal, D.; Chauhan, V. S., *Chem Biol* 2002, 9, 321-332;
8. Eckstein-Ludwig, U.; Webb, R. J.; van Goethem, I. D. A.; East, J. M.; Lee, A. G.; Kimura, M.; O'Neill, P.M.; Bray, P.G.; Ward, S. A.; Krishna, S., *Nature* 2003, 424, 957-961;
9. Wu, Y., *Acc Chem Res* 2002, 35, 225-259;
10. Moles, P.; Oliva, M.; Safont, V. S., *J Phys Chem A* 2006, 110, 7144-7158;
11. Titulaer, H.; Zuidema, J.; Kager, P., *J Pharma Pharmacol* 1990, 42, 810-813;
12. Wong, J.; Yuen, K., *Int J Pharm* 2001, 227, 177-185;
13. Sahoo, N. G.; Kakran, M.; Li, L., *Mat Sci Eng C* 2011, 31, 391–399;
14. Navaratnam, V.; Mansor, S. M.; Sit, N. W.; Grace, J.; Li, Q.; Olliaro, P., *Clin Pharmacokinet* 2000, 39, 255–270;
15. Ashton, M.; Sy, N. D.; Huong, N. V.; Gordi, T.; Hai, T. N.; Huong, D. X.; Nieu, N. T.; Cong, L. D., *Clin Pharmacol Ther* 1998, 63, 482–493;
16. Stoughton, R. B.; *South Med J* 1962, 55, 1134–1138;
17. Kim, J. H.; Choi, H. K., *Int J Pharm* 2002, 236, 81–85;
18. Karavas, E.; Ktistis, G.; Xenakis, A., *Eur J Pharm Biopharm* 2006, 63, 103–114;
19. Ruan, L. P.; Yu, B. Y.; Fu, G. M., *J Pharm Biomed Anal* 2005, 38, 457–464;
20. Tantishaiyakul, V.; Kaewnopparat, N.; Ingkatawornwong, S., *Int J Pharm* 1996, 143, 59–66;
21. Sahoo, N. G.; Kakran, M.; Li, L.; Judeh, Z., *Powder Technology* 2010, 203, 277-287;
22. Nowak, D. M.; Lansbury, P. T., *Tetrahedron* 1998, 54, 319-336;
23. Sahoo, N. G.; Abbas, A.; Judeh, Z.; Li, C. M.; Yuen, K.-H., *J Pharm Sci* 2009, 98, 281-296;
24. Cilurzo, F.; Minghetti, P.; Casiraghi, A.; Tosi, L.; Pagani, S., *Eur J Pharm Biopharm* 2005, 60, 61-66;
25. Titulaer, H. A. C.; Zuidema, J.; Lugt, C. B., *Int J Pharm* 1991, 69, 83-92;



26. Lipp, R., *J Pharma Pharmacol* 1998, 50, 1343-1349;
27. Pattnaika, S.; Swaina, K.; Mallick, S.; Lin, Z., *Int J Pharm* 2011, 406, 106-110;
28. Kim, J. H.; Choi, H. K., *Int J Pharm* 2002, 236, 81-85;
29. Wong, J. W.; Yuen, K. H., *Drug Dev Ind Pharm* 2003, 29, 1035-1044;
30. Moroni, L.; Gellini, C.; Miranda, M. M.; Salvi, P. R.; Foresti, M. L.; Innocenti, M.; Loglio, F.; Salvietti, E., *J Raman Spectrosc* 2008, 39, 276–283;
31. Lawal, A.; Umar, R. A.; Abubakar, M. G.; Faruk, U. Z.; Wali, U., *J Pharm Biomed Sci* 2012, 24, 6-14;
32. Blasko, G.; Cordell, G. A., *J Nat Prod* 1988, 51, 1273-1276;
33. Zhan, J.-X.; Zhang, Y.-X.; Guo, H.-Z.; Han, L.-L.; Guo, D.-A., *J Nat Prod* 2002, 65, 1693-1695;
34. Shahzad, Y.; Shah, S. N. H.; Ansari, M. T.; Riaz, R.; Safdar, A.; Hussain, T.; Malik, M., *Chin Sci Bull* 2012, 57, 1685-1692;
35. Shi, Y.; Zhang, J.; Xu, S.; Dong, A., *J Biomat Sci: Polym Ed* 2012, 24, 551-564;
36. Sahoo, N. G.; Kakran, M.; Abbas, A.; Judeh, Z.; Li, L., *Advanced Powder Technology* 2011, 22, 458-463;
37. L'OREAL, *Composition cosmétique mimant le sebum, et utilisations*, Frenc Patent 2003, WO 03/037288 A2;
38. Carfagna, C.; Persico, P., *Macromol Symp* 2006, 245-246, 355-362.

## Chapter 6

### Conclusions

In this work, linear–hyperbranched hybrid polyesters (HB) were synthesized through a branching reaction between a tailored linear poly(butylene adipate) (PBA) pre-polymer ended with methyl ester groups and different molar percent of branching agent. The progress of reaction was followed by  $^1\text{H}$  and solid-state  $^{13}\text{C}$ -NMR and MALDI-TOF mass spectrometry (MALDI-TOF MS) tools, to obtain reliable knowledge about structure and chemical composition of either telechelic PBA pre-polymer and the final HB products, as a function of experimental parameters, such as time, temperature, and monomers molar ratio. All  $^1\text{H}$ -NMR spectra of HB samples displayed the same signals pattern (with a little variation of the relative signal intensities). The NMR analysis provided qualitative information on the formation of the HB samples, however, it was not possible to identify the structure and composition of their components. MALDI-TOF MS and SEC/MALDI-TOF MS analyses provided unequivocal information on the branched units and also on the end-groups present in the synthesized HB macromolecules. Mass spectra revealed that they were constituted by HB macromolecules and linear PBA oligomers with molar masses (MM) lower than 9'000 g/mol. Mass peaks corresponding to the HB macromolecules terminated only with methyl ester (i.e., species  $\text{IP}_n\text{A}_n$ ,  $\text{IP}_2\text{A}_n$ , and  $\text{IP}_3\text{A}_n$ ) could be unambiguously assigned to one on type of macromolecules; whereas peaks corresponding to HB species having hydroxyl groups (i.e., species  $\text{IP}_n\text{B}_n$ ,  $\text{IPC}_n$ ,  $\text{IPD}_n$ ,  $\text{IP}_2\text{B}_n$ ,  $\text{IP}_2\text{C}_n$ , etc) could be attributed to isobar structures. As expected, the mass spectra showed that HB macromolecules formed by more branched units linked together increased with increasing the amount of 1,1,1-tris(hydroxy methyl)propane (TMP) as branching agent, and the reaction time, while linear PBA chains decreased with increasing the amount of TMP in the feed and the progress of reaction. For lower molar percent of TMP (i.e., 1.5 mol %) and reaction time (i.e., 16 h) the transesterification reactions, which involved the (-OH) groups of TMP and the methyl ester (-OCH<sub>3</sub>) end-groups of the PBA prevailed; moreover, increasing the reaction time and the molar percent of TMP, the transesterification reactions, which engaged the ester inner groups occurred. HB macromolecules containing a cyclic branch inside the HB structure were revealed in the mass spectra of the synthesized HB samples using molar percent of TMP higher than 3 and longer period of

time. In these experimental conditions, the (inter and intra)-molecular transesterification reactions took place, leading to the formation of ether-containing HB species. The intermolecular transesterification and intermolecular transesterification side reactions could be responsible for the increase of the MMs with increasing reaction time. Absolute MMs were calculated by self-calibration curves built by SEC/MALDI-TOF MS analysis. The calculated values were lower than those calculated by conventional PS calibration method, indicating that the hydrodynamic volumes of PBA and HB samples were higher than those measured by linear PS of similar MMs.

The structure-to-thermal relationship was investigated through thermogravimetric analysis (TGA) and differential scanning calorimetry (DSC). The thermal behavior of HB systems change significantly, depending on the experimental conditions used during the synthesis and thus on their internal architecture. A better insight of this behavior may be achieved considering the general degradation mechanism of polyesters, occurring through two main degradation processes: a chain scission through a  $\beta$ -hydrogen transfer reaction, leading to vinyl ester and acid end-groups, and an intramolecular back-biting, leading to cyclic oligomers. In particular, the most stable samples were the linear methyl ester (-OCH<sub>3</sub>) terminated PBA as well as the poorly HB systems, 1.5HB16 and 3HB16, in which the primary cleavage process is a  $\beta$ -hydrogen transfer reaction, which generated a series of open-chain oligomers. As soon as the time of reaction increased, more complex but lower thermally stable HB systems (i.e. 1.5HB24 and 3HB24) formed, leading to short hydroxyl (-OH) terminated branches. These structures were thought to be the initiation site for easier degradation, as they would allow for back-biting on the main-chain and formation of cyclic oligomers. This explain why, increasing the reaction time, the HB systems were more prone to degradation than the less reacted ones. For more molar percent of TMP and prolonged reaction times, instead, ether units, cyclic branches and cross-linked portions, leading to the formation of interconnected TMP units, were generated. The presence of these species conferred very high thermal stability to the HB system (i.e 5HB44).

In order to evaluate the thermal behavior of HB systems, the linear PBA pre-polymer was considered as reference sample. PBA is characterized by a rather complex melting behavior, showing two types of polymorphic crystals. It is likely to state that polymorphism phenomena found in 1.5HB16 sample was related to the presence of long linear PBA units, making this HB sample much similar to linear systems for thermal behavior. It is worth noticing that the thermal behavior of HB systems was closely related to the evolution of chain architecture. It can be inferred that  $T_m$  and  $\Delta H$  values decreased

by increasing the reaction time. These results indicate that the formation of even more complex branched structures, such as cyclic and cross-linked moieties, affected the extent of ordered portions, leading to an increment of amorphous phase. Moving from PBA to HB samples, it seemed that as the branching reaction evolved, the branched fraction having a behavior similar to that of PBA was reduced, generating a HB structure less prone to crystallize. Summarizing, both reaction times and molar amounts of branching agent were key factors in determining the structural features of HB systems and thus their thermal behavior.

The crystallization, such as melting behaviors of polymers, were closely related to their chain architecture. All HB samples displayed peaks at 21.35 and 24.55° which are identical to the peak positions observed for the linear PBA sample, but at lower intensities. As expected, this reflects lower degree of crystallinity in HB samples with increasing HB structure. These results are in excellent agreement with their thermal properties determined by DSC and TGA results, previously discussed.

A procedure for achieving a significant inhibition of plasticizer migration without affecting thermal and mechanical properties was the blending of polyvinyl chloride (PVC) with polymeric plasticizers. Linear polymeric plasticizers are employed as an alternative or in addition to the usual monomeric plasticizers to provide flexibility, softness and lower modulus values and to maintain these characteristics after PVC compound exposure to severe use conditions or harsh environments. Because of their higher molecular weight and bulkiness their volatility and diffusivity is reduced compared to monomeric plasticizers. On the other hand, their use usually makes the material more difficult to process. Therefore, a manufacturing dilemma is to select the right molecular weight to use in order to satisfy the conflicting requirements of increased plasticizer retention and decreased manufacturing compatibility and processability. In the recent years, a growing interest has been shown also for more complex polymer architectures, HB polymers, as substitute of phthalate plasticizers, DOP, for PVC.

In this work HB poly(butylene adipate) sample (1,5HB16) was synthesized and used in blending with PVC. A linear commercial polyester (Palamoll) was also employed. The properties of PVC/polymeric plasticizers blends were studied and compared with those of PVC/DOP (R70) formulation. Thermal, structural, mechanical, dynamic-mechanical analyses and migration tests were performed on PVC/polyesters plasticized blends.

Since HB and Palamoll (PBA) were basically more stable upon heating, their presence in PVC increased blends thermal stability by about 40 °C, regardless of the polyesters amount used. Wide angle X-ray diffraction analysis (WAXD) was carried out to investigate the morphology of PVC/HB blends. The absence of the signal related to the semi-crystalline structure of 1.5HB16 sample in the blend, indicated that HB sample lost its structure when added to PVC. The blends resulted amorphous at any PVC/HB ratio, indicating good miscibility between the HB plasticizer and PVC matrix. Analogous information derives from the evaluation of glass transition temperatures ( $T_g$ ), since a single value was observed at each composition. The high miscibility between polyester and PVC is due to the hydrogen bonding between the carbonyl group of the ester and the  $\alpha$ -hydrogen next to the chlorine atom in PVC. Moreover, monotonic shift of transition temperatures toward low values were observed with addition of polymeric plasticizers. Comparing the samples containing the same amount of plasticizer, both linear and HB, each PVC/HB system showed a  $T_g$  value of about 10 °C higher than the corresponding PVC/PBA blend and R70 formulation. This was probably due to the complex architecture of HB macromolecules, which restricted the PVC chain mobility.

As for migration tendency, the polymeric plasticizers (PBA and 1.5HB16) were expected to have better migration stability compared to the monomeric one (DOP). The weight loss of the exudable flexible components was determined by measuring the weights of the samples at different aging times, i.e.  $t = 1, 4, 8, 15, 25$  and 30 days. As expected, HB containing system exhibited the lowest values of weight loss, which remain constant with the aging time, meaning that an efficient plasticizer retention was achieved by the use of highly branched poly(butylene adipate) sample.

In order to improve the toughness of epoxy resin, overcoming the limitations of traditional toughening agents, HB polymers have been proposed, since their compact structure resulted in low melt viscosities, even at high molecular weight due to a lack of restrictive inter-chain entanglements compared to their linear analogous polymers. The high density of functional end-groups on HB polymer surface offers the potential for tailoring their compatibility with the epoxy resin through conversion of HB terminal groups to chemically suitable moieties to form *in-situ* covalent bounds. As a result, HB polymers are promising candidates for modifying thermosets with minimal decrease in processability of the modified resins, such as unwanted great increase of viscosity, without affecting the resin glass transition temperature ( $T_g$ ) or sacrificing the thermal stability and storage

modulus. Some studies have been proposed dealing with the use of hydroxyl functionalized commercial HB polymers, namely Boltorn<sup>TM</sup>, acting as modifiers of toughening properties of epoxy resins.

The properties of a commercial one-part liquid epoxy system (Cycom), usually used in resin transfer moulding process (RTM), were studied in mixture with both commercial dendritic (Boltorn) and synthesized HB (5HB30) polyesters. Structural, thermal, rheological, dynamic-mechanical, morphological analyses and fracture toughness measurements were performed on Cycom/polyester toughening blends.

Being a commercial product, Cycom® 890 RTM formulation is not known. The cure of the neat epoxy resin was monitored by the disappearance of the epoxy vibration, which occurred at about  $909\text{ cm}^{-1}$ , attributed to the C-O deformation of the oxirane group, and the appearance of C-N stretch at approximately  $3300\text{ cm}^{-1}$ . It is interesting to note in ATR spectra of Cycom/polyester toughening polymers the presence of the peak related to the stretching of carbonyl group ( $\text{-C=O}$ ), typical of polyester species. This signal located at  $1735\text{ cm}^{-1}$  increased with increasing the content of polyesters in the epoxy resin-based blends. The ATR spectra showed that between the epoxy resin matrix and the polyesters added there were only physical and not chemical bonds.

TGA analysis confirmed that the increment in toughening content did not influence the stability of Cycom/ polyester blends, which showed a thermal degradation behavior very similar to neat Cycom despite the lower thermal stability of both polyester polymers used.

DSC analysis explained the thermal behavior caused by the loading effect of polyesters on the cure reaction of Cycom/blends. Boltorn induced a shift of the curing peak to lower temperatures with increasing the content of dendrimer in blends. The addition of Boltorn, having a highly branched flexible backbone with numerous primary hydroxyl groups, enhanced the reactivity of epoxy, resulting in a high degree of epoxy conversion. This can be interpreted in terms of intermolecular transition state. According to this mechanism, the strong hydrogen-bonding species, such as alcohol groups, stabilize the transition state, thus, encouraging the nucleophilic attack of the amine. Instead, the addition of 5HB30 sample did not affect the cure kinetics of the epoxy resin, suggesting that this synthesized polyester did not behave as cure catalyst. The heat of reaction was also influenced by the presence of Boltorn and 5HB30, since it increased with increasing the polymer content. Considering that the energy measured is related to the epoxy rings opening, the increment in the value of  $\Delta H_{\text{norm}}^*$  could be attributed to the polymers addition. The presence of these polyesters in the epoxy matrix prevented the cure reaction caused by viscosity effect,

hindering the motion of the reactive chain segments and requiring a larger amount of energy to complete the cure reaction.

The first requirement for a RTM resin is the attainment of low viscosity during the injection phase. In order to understand the effect of the addition of polyesters in epoxy resin, the uncured neat Cycom and epoxy resin-based blends, were studied in a parallel plate rheometer for 1 h at 80 and 100 °C. From the viscosity graphs of the neat Cycom and their blends, both polymeric systems, Boltorn and 5HB30, showed a decrease in viscosity blends. This decrease in viscosity blends was due to finely phase separation which caused a sort of slipping of the epoxy macromolecules on the polyester particles. Increasing the polymers content, the thermoplastic particles aggregated to each other generating agglomerates firmly attached to the epoxy matrix by hydrogen bonding causing the increment of viscosity blends. It is interesting to note that Cycom/Boltorn blends always exhibited viscosity values higher than Cycom/HB blends at the same polymeric additive content. This effect was due to the high concentration of polar groups (-OH) on the dendrimer shell that could give rise to hydrogen bonding able to catalyze the epoxy reaction, increasing the reaction rate.

The trend of  $T_g$ s, measured by dynamic-mechanical thermal analysis (DMTA) as maximum of  $\tan\delta$  curve, was used as an indirect tool to evaluate the extent of compatibility between epoxy resin matrix and polyesters. All blends showed a single  $T_g$ , index of a good miscibility, and this value gradually shifted to lower temperature with increasing concentration of polyester added. The good miscibility can be ascribed to the hydrogen bonding between the carbonyl groups (-C=O) of the esters and the hydroxyl groups (-OH) of the epoxy matrix. Low  $T_g$  was also attributed to the reduction of cross-linking density as a result of the dilution effect of the un-cross-linked, HB molecules. The decrease in  $\tan\delta$  peak temperature at higher concentration of HB polymers was related to the their dissolution into the epoxy resin matrix.

Fracture toughness tests of cured neat Cycom and epoxy resin-based blends were performed by using the single-edge-notch bending (SENB) method according to ASTM D 5045-99. The neat cycom resin is very brittle, with a  $K_{Ic}$  value of 0.318 MPa·m<sup>1/2</sup>. Cycom/Boltorn blends produced only a small improvement in the impact strength. C1B blend increases  $K_{Ic}$  value of 43% than neat Cycom. In Cycom/HB blends, instead, the  $K_{Ic}$  and  $G_{Ic}$  values gradually increased with increasing the content of 5HB30 up to 5 wt. % (C5H blend) but then rapidly dropped down for 10 wt. %. C5H blend showed an improvement of 90% of  $K_{Ic}$  value than neat Cycom. The addition of dendritic and HB



polyesters can remarkably improve the toughness of the epoxy resin because of the intramolecular defect of HB polymers, which can absorb much more energy while impacting. This was also visible in morphological observation in which the fracture surface of these blends after impact tests were investigated with SEM. The epoxy network clearly appeared as a smooth, glassy, fractured surface with cracks in different planes and without any sign of plastic deformation, and this accounts for its poor impact strength. In Cycom/HB blends, increasing the 5HB30 content, a particulate morphology in which the discrete HB-rich phases were dispersed in a continuous matrix of epoxy resin was obtained. In other words, the fracture surface of the modified networks consist of two phases: a globular HB particle dispersed in the continuous epoxy matrix. The increase of 5HB30 content produced a HB-rich phase with larger particle size distribution due to aggregation which caused increased adhesion to the epoxy matrix with an improved toughening effect. The SEM images of C5H blend showed “sea-island” structures, characteristics of rubber-modified epoxy resins. When phase separation occurred, the particles disperse efficiently as a fine structure and the HB systems interpenetrated the epoxy networks, improving the miscibility and the interface adhesion between HB polymers and epoxy matrix. This structure might inhibit the craze formation, absorbing great energy. In the case of C10H blend the elevated density of polyester particles promoted the craze propagation, because the continuity of the epoxy network was interrupted and the particles appeared as many points of discontinuity. In Cycom/Boltorn blends the aggregation of Boltorn molecules increased with increasing polymer content in epoxy matrix. This aggregation could not undergo plastic deformation, which resulted in a low impact strength. Moreover there were no cavitations because Boltorn particles were tightly enwrapped into epoxy matrix. This indicated that the good interfacial adhesion between Cycom matrix and Boltorn particles occurred due to the strong hydrogen bonding.

Since the discovery of the antimalarial properties of artemisinin, the natural remedy against fever in the old Chinese medicine, much effort has been made to investigate the structure-activity relationship in this molecule. Although ART has shown excellent permeability across the intestinal mucosa, it has low bioavailability due to poor aqueous solubility, which may lead to incomplete clearance of the malaria parasite, resulting in recurrence of malarial symptoms. The poor water solubility of ART could cause a number of negative clinical affects, such as high local drug concentrations at the sites of aggregate deposition,



which could be associated with local toxic effects, and decreased systemic bioavailability. Besides, ART is extensively metabolized by the liver, but oral bioavailability is low (32%). Transdermal drug delivery systems (TDDS) facilitates the passage of therapeutic of drug substances through the skin into the general circulation where they can have systemic effects, thus bypassing the hepatic first-pass effect. One of the major problem of ART is its crystallinity, which causes a reduction of solubility through the stratum corneum. To prevent the re-crystallization during the storage process, we have thought to use inhibitors or anti-nucleating agents. In fact, combining the drug with an amorphous or less crystalline polymer can change the degree of crystallinity and the polymorphic form of ART. As a result, it is possible to obtain less crystalline or more amorphous drug particles with enhanced solubility and increased bioavailability. In biomedical applications, HB polymers are widely used as drug delivery systems in recent years. The drugs are attached to HB structure through non-covalent bonding or are entrapped inside the nano-cavities of dendritic architecture. These drug delivery systems offer several advantages, such as enhancing the aqueous solubility and bioavailability of drugs, prolonging the circulation time, inducing the preferential accumulation at the tumor sites through the enhanced permeability and retention effect, and reducing the systemic side effects.

In our studies a commercial dendritic (Boltorn) and two synthesized (1.5HB16 and 5HB30) polyesters were used as crystallization inhibitors for the antimalarial drug. The ART blends were characterized by means of ATR and NMR spectroscopy to have structural indication about the existence of peroxide bridge, which is responsible for chemical activity of this antimalarial drug. Both ATR and NMR spectra revealed the presence of the specific signals related to the trioxanic ring (858, 883, 917, 928  $\text{cm}^{-1}$ ), index of the good blend preparation which did not alter the ART chemical structure and did not involve chemical bonds with HB or dendritic polymers.

The thermal degradation behavior of ART blends were measured by TGA. Since HB polyesters and Boltorn were basically more thermally stable, their presence in ART blends increased blends thermal stability by about 10°C.

The crystallinity of ART blends was studied by means of DSC and WAXD analysis. DSC thermograms showed in the first heating scan the melting peaks of HB polymers (Boltorn, instead, appears amorphous) and a very broad band at about 115 °C associated to the fusion of ART micro-crystals present in all ART blends. In the second heating scans, it was very interesting to note the complete amorphization of all systems, with the

disappearance of melting peak belonging to HB polymers. These results were also confirmed by WAXD measurements.

To analyze the possibilities to use these ART blends as TDDS, preliminary studies were made, simulating human skin surface through the preparation of sebum formulation. The ART blends were pressed and dipped into sebum formulation for 48 h at 37 °C. The sebum left in contact with ART blends was then analyzed by means of ATR spectroscopy. The ATR spectra show the presence of carbonyl signals ( $1735\text{ cm}^{-1}$ ) belonging to drug molecule in sebum come in contact with ART blends. This means that HB or dendrimer polymers not only inhibited the ART crystallization, but also allowed the release of ART in sebum formulations reproduced in our laboratories.

**List of Abbreviations**

A4F – Asymmetric flow field flow fractionation

Ac – Acetone

AFM – Atomic force microscopy

ART – Artemisinin

ASTM – American society for testing and materials

ATR – Attenuated total reflectance

BD – 1,4-Butanediol

CDCl<sub>3</sub> – Deuterated chloroform

CH<sub>3</sub>OH – Methanol

CHCl<sub>3</sub> – Chloroform

DB – Degree of branching

DC – Degree of cristallinity

DEHE – Di-2-ethyl hexyl phthalate

DGEBA – Diglycidyl ether of bisphenol A

DHCl – Dehydrochlorination

DMA – Dimethyl ester of adipic acid

DMAc – N,N-Dimethyl acetamide

DMF – N,N-Dimethyl formamide

DMSO – Dimeyhyl sulphoxide

DMSO-d<sub>6</sub> – Deuterated dimethyl sulphoxide

DMTA – Dynamic mechanical thermal analysis

DOP – Dioctyl phthalate

DRI – Differential refractive index

DSC – Differential scanning calorimetry

FTIR – Fourier transform infra-red

G<sub>ic</sub> – Critical strain energy release rate

HABA – 2(-4-Hydroxyphenylazo-)benzoic acid

HB – Hyperbranched

IPN – Interpenetrating polymer networks

K<sub>ic</sub> – Critical stress-intensity factor

MALDI-TOF MS – Matrix assisted laser desorption/ionization time of flight mass spectrometry

MALLS – Multi-angle laser light scattering

MM – Molar mass

M<sub>n</sub> – Number-average molar mass

M<sub>w</sub> – Weight-average molar mass

NMR – Nuclear magnetic resonance  
PBA – Poly(butylene adipate)  
PDI – Polydispersity index  
PMMA – Polymethyl methacrylate  
PS – Polystyrene  
PVC – Polyvinyl chloride  
ROMBP - Ring-opening multi-branching polymerization  
RTM – Resin transfer moulding  
SCROP – Self-condensing ring-opening polymerization  
SCVCP – Self-condensing vinyl copolymerization  
SCVP – Self-condensing vinyl polymerization  
SEC – Size exclusion chromatography  
SEM – Scanning electron microscopy  
SENB – Single-edge-notch bending  
TDDS – Transdermal drug delivery systems  
TFA – Trifluoro acetic acid  
 $T_g$  – Glass transition temperature  
TG – Thermogravimetric  
TGA – Thermogravimetric analysis  
THF – Tetrahydrofuran  
TIP – Titanium(IV)isopropoxide  
TMP – 1,1,1-Tris(hydroxy methyl)propane  
 $T_{room}$  – Room temperature  
 $V_e$  – Elution volume  
WAXD – Wide angle X-ray diffraction  
XRD – X-ray diffraction

---

**List of Equations**

$$\alpha_A = \frac{[A_t]}{[A_0]} \quad 1.1$$

$$DB_{Fréchet} = \frac{D + T}{D + L + T} \quad 1.2$$

$$DB_{Frey} = \frac{2D}{2D+L} \quad 1.3$$

$$g = \frac{\langle Rg^2 \rangle_{branched}}{\langle Rg^2 \rangle_{linear}} \quad or \quad g' = \frac{[\eta]_{branched}}{[\eta]_{linear}} \quad 1.4$$

$$g' \approx g^b \quad 1.5$$

$$Insoluble \text{ fraction wt. } \% = \frac{(W_{tg} - W_t)}{W_s} * 100 \quad 2.1$$

$$X_n = (I_{4.09}/4)/(I_{3.67}/6) + 1 \quad 2.2$$

$$M_n = X_n \cdot 200.2 \quad 2.3$$

$$\%mol_{(-OCH_3)} = (I_A + I_D + 1/2I_B)/(I_A + I_B + I_C + I_D) \quad 2.4$$

$$\%mol_{(-OH)} = (I_C + 1/2I_B)/(I_A + I_B + I_C + I_D) \quad 2.5$$

$$\log M_w = 8.005 - 0.147V_e + 3.213 \cdot 10^{-4}(V_e)^2 \quad 2.6$$

$$\log M_w = 18.18 - 1.0817V_e + 0.01308 (V_e)^2 \quad 2.7$$

---

$$\text{Extent of migration (\%)} = \frac{W_i - W_t}{W_i * y} * 100 \quad 3.1$$

$$K_{Ic} = \left( \frac{P}{BW^{1/2}} \right) f(x) \quad 4.1$$

$$f(x) = 6x^{1/2} \frac{[1.99 - x(1-x)(2.15 - 3.93x + 2.7x^2)]}{(1+2x)(1-x)^{3/2}} \quad 4.2$$

$$G_{Ic} = \frac{(1-v^2)K_{Ic}^2}{E} \quad 4.3$$

$$B, a, (W-a) > 2.5 (K_Q/\sigma_y)^2 \quad 4.4$$

$$1/T_{gb} = w_1/T_{g1} + w_2/T_{g2} \quad 4.5$$

---

**List of Figures**

Figure 1.1: Regular star polymer	5
Figure 1.2: Regular comb polymer	6
Figure 1.3: Dendrimer growth	6
Figure 1.4: Difference between dendrimer and HB structures	7
Figure 1.5: HB synthetic route (with focal unit, A) through polymerization of AB <sub>2</sub> monomers	8
Figure 1.6: HB synthetic route (without focal unit) through copolymerization of AB <sub>2</sub> monomers with B <sub>3</sub> core molecule	9
Figure 1.7: Mechanism of SCVP	10
Figure 1.8: Different type of units in HB polymers	16
Figure 2.1: MALDI-TOF mass spectra of PBA-9 (a) and PBA-1 (b) samples	40
Figure 2.2: SEC traces of PBA-9, 1.5HB16, and 1.5HB24 samples	42
Figure 2.3: Sections of the <sup>1</sup> H-NMR spectra of PBA-9 (A), 1.5HB16 (B), 3HB16 (C), 7HB16 (D), and 10HB16 (E) samples	44
Figure 2.4: Solid-state <sup>13</sup> C-NMR spectrum of 5HB44 sample	45
Figure 2.5: MALDI-TOF mass spectra of 1.5HB16 (a) and 1.5HB24 (b) samples. In the insets some enlarged sections of these spectra are reported	47
Figure 2.6: MALDI-TOF mass spectrum of 3HB16 sample	52
Figure 2.7: MALDI-TOF mass spectra of PBA-9 (a), 5HB16 (b), 5HB24 (c), 5HB30 (d) samples	55
Figure 2.8: SEC chromatogram and MALDI-TOF mass spectra of some fractions of 3HB16 sample	57
Figure 2.9: Enlarged sections of MALDI-TOF mass spectra of some fractions of 3HB16 sample: F45 (a), F39 (b), F33(c), F29 (d)	58
Figure 2.10: SEC chromatogram and MALDI-TOF mass spectra of some fractions of 3HB24§ sample	60
Figure 2.11: Enlarged sections of MALDI-TOF mass spectra of some fractions of 3HB24§ sample: F31 (a), F25 (b), F22(c), F16 (d)	61
Figure 2.12: TG traces of PBA-9, 5HB16, 5HB24, 5HB30, and 5HB44 samples. Inset: Detailed view of the curves in the temperature range between 250 and 400 °C	64

---

Figure 2.13: DSC curve of 1.5HB16 sample	65
Figure 2.14: DSC of PBA sample crystallized at three temperature regimes: (A) high-T, (B) intermediate-T, and (C) low-T. <sup>51</sup>	65
Figure 2.15: DSC curve of 1.5HB16 sample obtained after melt-crystallized at 27 °C	66
Figure 2.16: DSC curve of 1.5HB16 sample obtained after melt-crystallized at 32 °C	66
Figure 2.17: DSC curve of 1.5HB16 sample obtained after melt-crystallized at 29 °C	67
Figure 2.18: DSC traces of PBA-9, 5HB16, 5HB24, 5HB30, and 5HB44 samples measured from the second heating scan	68
Figure 2.19: DSC traces of PBA-9, 5HB16, 5HB24, 5HB30, and 5HB44 measured from the first cooling scan	69
Figure 2.20: XRD patterns of poly(butylene adipate) films after melt-crystallized at different temperatures. <sup>50</sup>	70
Figure 3.1: Migration test setup	80
Figure 3.2: TG curves of DOP, PBA and 1.5HB16 plasticizers	81
Figure 3.3: TG curves of PVC/DOP and PVC/PBA blends	82
Figure 3.4: TG curves of PVC/DOP and PVC/HB blends	82
Figure 3.5: XRD pattern of 1.5HB16 sample	83
Figure 3.6: XRD pattern of H70 blend	84
Figure 3.7: DMTA curves of PVC/DOP and PVC/PBA blends	85
Figure 3.8: DMTA curves of PVC/DOP and PVC/HB blends	85
Figure 3.9: Stress-strain curves of R70 (-■-), L70 (-●-), and H70 (-▲-) blends	86
Figure 3.10: Extent of migration (%) from flexible PVC sheets for PVC/DOP and PVC/PBA blends	88
Figure 3.11: Extent of migration (%) from flexible PVC sheets for PVC/DOP and PVC/HB blends	88
Figure 3.12: Extent of migration (%) for R70 (-■-), H70 (-●-), L70 (-▲-) blends	89
Figure 4.1: ATR spectra of cured and uncured neat Cycom	97



## List of Figures

---

Figure 4.2: ATR spectra of Boltorn, cured neat Cycom, and Cycom/Boltorn blends	98
Figure 4.3: ATR spectra of 5HB30, cured neat Cycom, and Cycom/HB blends	99
Figure 4.4: TG curves of Boltorn, neat Cycom, and Cycom/Boltorn blends	100
Figure 4.5: TG curves of 5HB30, neat Cycom, and Cycom/HB blends	100
Figure 4.6: Dynamical cure analysis for neat Cycom and Cycom/Boltorn blends	101
Figure 4.7: Dynamical cure analysis for neat Cycom and Cycom/HB blends	102
Figure 4.8: Steady shear viscosity of 5HB30, Boltorn, and PBA pre-polymer, used as reference, at 80 °C	103
Figure 4.9: Time sweep test for Cycom/Boltorn (a) and Cycom/HB (b) blends at 80 °C	104
Figure 4.10: Time sweep test for Cycom/Boltorn (a) and Cycom/HB (b) blends at 100 °C	104
Figure 4.11: DMTA curves of neat Cycom and Cycom/Boltorn blends	106
Figure 4.12: DMTA curves of neat Cycom and Cycom/HB blends	106
Figure 4.13: Effect of polymers loading on the $K_{Ic}$ for the neat Cycom and the epoxy resin-based blends	108
Figure 4.14: Effect of polymers loading on the $G_{Ic}$ for the neat Cycom and the epoxy resin-based blends	108
Figure 4.15: SEM images of the fracture surface under impact of the neat Cycom at 500X (a), and 2000X (b)	109
Figure 4.16: SEM images of fracture surface under impact of the C1H (a) and C3H (b) samples	110
Figure 4.17: SEM image of the fracture surface under impact of C5H sample	110
Figure 4.18: Particular of SEM images of C5H sample at 2000X (a) and 20000X (b)	111
Figure 4.19: SEM images of fracture surface under impact of C10H sample at 500 X (a) and 2000X (b)	111
Figure 4.20: SEM images of fracture surface under impact of C1B sample at 2000X	112
Figure 4.21: SEM images of the fracture surface under impact of C10B sample at 2000X (a and b) and 20000X (c)	113
Figure 5.1: Molecular structures of ART (1) with atomic numbering, 1,2,4-trioxane (2), $\gamma$ -valerolactone (3) and cyclohexane (4)	121

---

Figure 5.2: ATR spectra of neat ART, HB1A blend, and 1.5HB16 sample	123
Figure 5.3: ATR spectra of neat ART, BA blend, and Boltorn sample	123
Figure 5.4: Solid-state $^{13}\text{C}$ -NMR spectra of neat ART, HB1A, HB2A, and BA blends	125
Figure 5.5: TG traces of HB1A, HB2A, and BA blends. Inset: TG trace of neat ART	126
Figure 5.6: DSC trace of neat ART	127
Figure 5.7: DSC traces of HB1A and HB2A blends	128
Figure 5.8: DSC trace of BA blend	128
Figure 5.9: Isothermal DSC traces at 140 °C of HB1A and HB2A blends	129
Figure 5.10: Isothermal DSC trace at 140°C of BA blend	129
Figure 5.11: XRD patterns of neat ART and ART blends. In the inset, XRD measurements of neat synthesized HB polyesters, 1.5HB16 and 5HB30	130
Figure 5.12: ATR spectra of neat sebum, sebum+1.5HB16, sebum+ART and ART as reference	131
Figure 5.13: ATR spectra of sebum formulation in contact with ART blends	131

---

**List of Tables**

Table 2.1: Experimental synthesis condition, molar mass distributions and yields of synthesized tailored PBA pre-polymers and HB polyesters samples	33
Table 2.2: Structural assignments of peaks displayed in the MALDI-TOF mass spectra of PBA samples as reported in Figure 2.1	39
Table 2.3: Assignments of proton signals due to PBA oligomers and their end-groups, TMP unit, and TMP unit linked to PBA sequences as observed in $^1\text{H-NMR}$ spectra	43
Table 2.4: Assignments of carbon signals due to HB species as observed in $^{13}\text{C-NMR}$ spectrum of 5HB44 sample	45
Table 2.5: Structural assignments of peaks displayed in the MALDI mass spectra of HB samples	47
Table 2.6: Structural assignments of peaks displayed in the MALDI mass spectra of HB families, ether and cyclic units	49
Table 2.7: $T_{\text{onset}}$ , $T_{5\% \text{wt. loss}}$ and $T_{\text{max. deg. rate}}$ of PBA-9 and HB samples	62
Table 2.8: $T_m$ , $T_g$ , $T_c$ , $\Delta H_m$ and $\Delta H_c$ of PBA-9 and HB samples	67
Table 2.9: DC measured by X-ray diffractogram of PBA-9 and HB samples	71
Table 3.1: Flexible PVC-based formulations	78
Table 3.2: $T_{5\% \text{wt. loss}}$ and $T_{\text{max. deg. rate}}$ of plasticizers	81
Table 3.3: $T_{5\% \text{wt. loss}}$ and $T_{\text{max. deg. rate}}$ of PVC-based blends	82
Table 3.4: $T_g$ values of PVC-based blends	84
Table 3.5: Mechanical properties of PVC/PBA blends	86
Table 3.6: Mechanical properties of PVC/HB blends	86
Table 4.1: Epoxy resin-based blends	94
Table 4.2: Peak frequencies and tentative assignments for the spectrum of cured neat Cycom	98
Table 4.3: $T_{\text{onset}}$ , $T_{5\% \text{wt. loss}}$ , $T_{\text{max. deg. rate}}$ , and char yield for neat Cycom, Boltorn, 5HB30, and epoxy resin-based blends	99
Table 4.4: $T_{\text{onset}}$ , $T_{\text{max}}$ , $\Delta H$ , $\Delta H_{\text{norm}}^*$ for neat Cycom and epoxy resin-based blends	101
Table 4.5: Viscosity values of neat Cycom and epoxy resin-based blends	104

---

Table 4.6: DMTA values in terms of $E'$ , $T_g^{\text{DMA}}$ , $T_g^{\text{DSC}}$ and $T_g^{\text{Fox Eq.}}$ for neat Cycom and epoxy resin-based blends	106
Table 4.7: $K_{Ic}$ and $G_{Ic}$ for neat Cycom and epoxy resin-based blends	107
Table 5.1: ART blends	120
Table 5.2: Experimental ATR wavenumbers ( $\text{cm}^{-1}$ ) and vibrational assignment. In the assignment column, 2,3,4 refer to the molecular units as shown in Figure 5.1	122
Table 5.3: Assignments of carbon signals belonging to ART molecule as observed in solid-state $^{13}\text{C}$ -NMR spectrum	124
Table 5.4: $T_{\text{onset}}$ , $T_{5\% \text{wt. loss}}$ , and $T_{\text{max. deg. rate}}$ for 1.5HB16, 5HB30, and Boltorn samples	126
Table 5.5: $T_{\text{onset}}$ , $T_{5\% \text{wt. loss}}$ , and $T_{\text{max. deg. rate}}$ for neat ART, 1.5HB16, 5HB30, Boltorn, HB1A, HB2A, and BA	126
Table 5.6: $T_m$ , $T_c$ , $\Delta H_m^I$ , $\Delta H_m^{II}$ , $\Delta H_c$ of neat ART	127

**List of Schemes**

Scheme 2.1: Synthesis route of HB polyester samples	34
Scheme 2.2: Formation of anhydride groups, D <sub>n</sub>	40
Scheme 2.3: Transesterification reactions	52
Scheme 2.4: Transesterification reactions	53
Scheme 2.5: $\beta$ -hydrogen transfer mechanism	63
Scheme 2.6: Back-biting mechanism	63
Scheme 3.1: Synthesis route of 1.5HB16 sample	78
Scheme 4.1: Synthesis route of 5HB30 sample	93
Scheme 5.1: Synthesis route of HB samples	119